Rail Surface Geometry Defects and Track Settlement

M.D. Williams

B.E., Adelaide

Thesis presented for the degree of Master of Engineering Science

at the University of Adelaide

August 1994

Awarded 1995

CONTENTS

Declaration

This thesis contains no material which has been accepted for the award of any other Degree or Diploma in any University and to the best of my knowledge and belief contains no material previously published or written by another person except where due reference is made in the text.

I give consent to this copy of my thesis, when deposited in the University Library, being available for loan and photocopying.

Signed:

Date: 14/3/95

Acknowledgments

The author wishes to thank Mr L. Schmid from the Civil and Environmental Engineering Department at the University of Adelaide for his valued guidance and patience throughout this study, the Laboratory staff from the same department and staff from Australian National whose practical assistance made this work possible.

CHAPTER 1 INTRODUCTION

Railway operators throughout the world, whether they be a heavy haul, metro or mixed traffic system are striving to increase their operating parameters, such as speed, axle load, volume and on time running reliability, whilst minimising the total cost of maintenance. To assist with this process the maintenance and construction standards of the railway track need to be closely defined with accurate information being provided to management so that optimal solutions can be derived.

The track structure, that guides and supports railway vehicles, has a number of imperfections. The level of the resources that need to be applied to correct these are continually being subject to economic investigation to improve the return on a very costly capital infrastructure investment.

One of the large numbers of economic considerations that arise is the cost of maintaining vertical track geometry. Defects in vertical track geometry are an important factor to all railway authorities as one of the main contributors to the generation of vehicle vibrations. In the extreme these defects can lead to vehicle derailment, but are more commonly controlled because of the additional damage that they cause to track components and vehicles, as well as their effect on passenger comfort levels. It is the prediction, and control, of the rate of vertical track geometry deterioration that has been a dilemma ever since the commencement of railway operations.

Track geometry defects occur in both the lateral and vertical direction, and can cause force variation in both planes. Although there is coupling between the vertical and lateral forces, the majority of deterioration is in the vertical plane. As the scope of this study was to investigate vertical settlements and as the lateral forces are a second order consideration further analysis was not carried out into these. This limits the scope of the track that was investigated to being straight, and only considering vehicles that were not operating in the region of lateral instability.

Vertical defects consist of a number of differing wavelengths. These can be discrete steps, short wavelength corrugations (from 60mm up to 200mm), long wavelength deformations (up to 1 metre), track geometry defects (2 metres up to 60 metres) or design variations such as vertical curves. The discrete defects are placed in track predominantly during manufacture and installation, and deteriorate further due to impact loading, and alterations in residual stresses due to the work hardening of the running surface. With traffic these defects are believed to develop into longer wavelength faults that are of concern to vehicle ride. Because of this possible link between the discrete defects and deterioration rates, the study concentrated on their interrelationship.

Discrete defects cause increased damage to the rail, sleeper and ballast upon which the track is supported. The ballast deterioration shows itself in the compaction of the ballast due to the rearrangement of the ballast particles, as well as abrasion of the rock asperities. These then lead to the lowering of the track. Although general settlement occurs along the complete track length the effect of discrete defects is to cause loading variations and hence differential settlement. This results in longer wavelength defects being introduced into the track.

From the above discussion, it became the aim of this thesis to develop a quantitative tool, to assist in the rational assessment of tradeoffs between differing levels of track vertical geometry defects, and examine in some detail the effect that discrete vertical rail shape irregularities have on deterioration rates. Due to the characteristics of the track system there was a need to model some non linearities as these are of importance in the picture of track dynamics.

Investigation into existing models showed that they all needed varying degrees of modification to be used. This factor, together with the wish of the author to develop from first principles a dynamic model of the track structure, meant that a model was developed through the use of a commercially available general purpose simulation package.

The model was calibrated by in track field trials. Laboratory experiments were not utilised as early investigations revealed the extreme difficulties in generating enough force at the required frequency of application to those levels that exist in the track structure.

The thesis that follows reviews in the second chapter the previous work in the field, and the theoretical basis for this thesis, with the following chapters detailing the model developed, including modes of vibration and characteristics that have been assumed.

The research work was undertaken in three distinct phases;

1) Development of a mathematical model to simulate the dynamic behaviour occurring at the sleeper/ballast interface by the passage of a vehicle through discrete rail surface geometric defects.

2) Experimental work to confirm the model and provide numeric approximations to physical parameters.

3) Investigate the relationship between energy dissipation in ballast and the short term settlement of the track.

CHAPTER 2 THEORY

2.1 TRACK FORCES

In this chapter a review of the theory regarding railway track dynamics is undertaken, with the aim of highlighting the historic background and factors that other authors have considered to be important, and which need to be taken into account in the development of railway track models.

Track dynamics have been of concern to railway engineers ever since the first train ran on a railway track. As an example, Stokes [1] in 1849 (five years before a train ran in Australia) wrote a paper in response to a Royal Commission that was inquiring into the conditions observed by engineers in the use of iron in structures exposed to violent concussion and vibration.

It is known that static and dynamic forces generate stresses and strains on the track structure which lead to the breakdown of components, and changes in geometry leading to poor ride and further increases in loading. The forces which are generated at the wheel to rail interface are transmitted through the rail, rubber pad, sleeper, ballast and finally to the underlying formation.

If the track running surface was perfectly rigid, level and straight with the vehicle's suspension designed so that there would be no tendency towards lateral dynamic instability, the predictions of the stresses imposed on the track structure would be a simple case of statics.

If however the track has geometric deviations, both vertical and lateral, and the vehicle is unstable then the loading spectrum becomes very complex. The majority of track models developed such as those of Ahlbeck [2 3 4], Cai [5 6], Clark [7], Grassie [8 9 10], Hempelmann [11], Ishida [12], Jenkins [13], Lyon [14] and Newton [15] only consider the vertical interaction. Lateral effects are usually in the domain of vehicle stability models such as those of Williams [16] and Shelley [17]. Wanming [18] however does consider the combined lateral and vertical modes by the combination of separate vertical and lateral models.

As noted by Jenkins [13] the railway track and vehicle combination comprises heavy rigid wheels running on heavy rails. If the rail surface is not perfectly smooth there are generated variations in the forces that are applied to the track. Other forms of force increase due to lateral vehicle body and bogie motions such as hunting are also imposed on the track structure but due their secondary effect on vertical forces are not considered further in this research.

Jenkins [13] has identified five major causes of variations in the vertical force between the wheel and rail consisting of;

1. Isolated irregularities in the rail running surface which occur by default at joints and welds, and also by design at points and crossings.
2. Periodic irregularities such as corrugation on the rail surface or the repetitive effect of sleeper spacing.
3. Random variations of longitudinal profile (track top roughness).
4. Defects in the vehicle such as wheel flats and wheel eccentricity.
5. Random variations in sleeper support stiffness such as voids.

Lyon [14] has noted that the most severe loadings are of a transient nature and caused primarily by dipped joints, raised welds and wheel flats. Based on these impact loadings Lyon introduced into literature the concepts of the P1 force which is due to the initial impact, and the P2 force which is the subsequent vibration response of the unsprung mass on the track. Esveld [19] noted a 400% increase in force due to the impact arising from a six millimetre dip over a three metre span at 140 km hr^{-1}. Tunna [20] has extended this theory to include what he calls P1½ which is related to the movement of the rail and sleeper on the railpad.

Jenkins [13] and Lyon [14] note that at frequencies less than 10 Hz, dynamic loading is due almost entirely to variations in suspension forces caused by the vehicle body and bogie motions. The track system has a relatively small effect and may be modelled very simply. At intermediate frequencies of 20 to 100 Hz the track system plays a significant part in determining force levels while usually only the unsprung parts of the vehicle and its primary suspension have some influence. Finally at the high frequencies of 500 Hz to 2000 Hz encountered during impacts or impulsive loadings, the response is mainly dependent on the track and wheelset masses and the elasticity of the wheel to rail contact zone. Jeffs [21] notes that the passage of a train causes a complex load to be imposed on the track structure due to multiple wheel spacings, varying support conditions and the random nature of the load paths.

As this thesis is concerned with the vertical forces caused at discrete defects this dictates that high frequency effects need to be considered. However the vehicle can be considered at a much simpler level.

2.2 RAIL

In frequency domain models the rail is modelled as a continuous linear beam. The primary advantage of this type of model as noted by Grassie [9] is that the end effect of a finite length time domain model is eliminated. Grassie also models the rail as a Timoshenko beam.

Nonlinear, continuous support, time domain models such as used by Ahlbeck [2] model the rail using beam on elastic foundation methods combined with field measured parameters. Williams [16] utilises a linear beam on elastic foundation calculation for the modelling of vehicle interaction.

Discrete sleeper, time domain models can have a variety of lengths ranging from 40 bays as used by Cai [5] for the modelling of two wheelsets, to 20 bays as used by Clark [7] for a single wheel. These discrete support models can either have the rail modelled as a Euler or Timoshenko beam as used by Cai [5 6], Newton [15] and Hempelmann [11].

Newton [15] observes that discrete support models give a better estimate of the force levels and have the advantage of allowing individual sleeper forces, stresses and ballast reactions to be calculated. Hempelmann [11] also models the rail in this manner, whilst Dahlberg [22] notes that deflection shows vibration at approximately sleeper spacing (0.66 metres). Grassie [9] also notes the need to discretely model the rail masses because at high frequency vibrations (above 20 Hz) the wavelength of bending waves in the rail becomes compatible with the spacing between sleepers, so that a model which ignores the discrete support of the rail and the discrete mass of the sleepers is likely to be inadequate in some aspects.

Depending on the phenomena to be studied the track can be modelled with one rail, such as was done by Clark [7], Grassie [9] and Cai [5] for symmetric rail defects, or using two rails as was done by Ishida [12] when the defects are asymmetric or contained in one rail only.

Nodal forces for discrete models can be determined by finite element, stiffness coefficients or partial differential functions. The use of finite element coefficients such as described by Thomson [23] require that both the nodal vertical and rotational degrees of freedom be modelled. The stiffness coefficient method applies a unit displacement at each of the node points in turn to calculate the resultant force at all nodes. The rail stiffness matrix elements are input via influence factors which can be calculated for either Euler or Timoshenko beams. Partial differential equations are used by Clark [7] to model the rails as Timoshenko beams.

The finite element coefficient method enabled the development of the stiffness matrices and was found to be the most convenient for this study.

2.3 PADS

The rail and sleeper are separated by a cork rubber bonded pad with the rail secured to the sleeper by a steel elastic fastening system (Pandrol PR 401 in this instance). The pad used in the experimental phase is a 5mm thick cork bonded rubber pad designed as an impact attenuator (poor in this case) and a wear surface in order to protect the concrete sleeper. With concrete sleepered track Grassie [9] noted that this pad must be modelled.

Although the pad exhibits a number of strong nonlinearities, the energy absorbed by the pad as a proportion of the total energy lost in the system is small. It is for this reason that Cai [5 6] models the railpads as linear springs with viscous damping.

The nonlinearity of the pads makes any measurement difficult and Nashif [24] describes the various environmental factors that have an effect on the nonlinear behaviour such as temperature, loading frequency, cyclic dynamic strain (hysteresis), static preload and others.

Grassie [25] has divided rail pads into two distinct categories on which extensive tests were carried out to predict the characteristics when subjected to dynamic loading. These two types are the linear hard pads which have formed the largest proportion of pads to date and softer resilient pads that are designed to attenuate impact loads from the rail and which harden under load.

Clark [7] determined the pad stiffness and damping characteristics by the use of a quasi static response over six complete loading cycles. It was noted that the quasi static response is significantly different to a static laboratory test. This difference is also observed by Grassie [25] in comparisons of field and laboratory tests who notes that the experimental stiffness for the 5mm rubber pads was 250 MN m^{-1}. Maree [26] notes the difference between dynamic and static stiffness, which for a 10mm studded rubber pad rises from 37 to 66 MNm^{-1}

Nashif [24] lists several methods of determining damping including half power bandwidth, resonant response amplitude, Nyquist diagram, hysteresis loops, quadrature bandwidth and dynamic stiffness. Generally all of these methods measure the response at resonance except for the dynamic stiffness method which consists of an experimental analysis that can consist of a measured input force (impact) and a measured response. The data is analysed by a fast Fourier transform to give the receptance and phase angle for a wide range of frequencies.

Due to these complexities and the secondary nature on the final result a simple linear viscous damped pad is used in this study.

2.4 SLEEPERS

Prestressed concrete sleepers are shown by Clark [7], Ahlbeck [2], Grassie [10], Ford [27], Lucas [28] and Kohutek [29] to possess a number of vibration modes up to 1300 Hz thus demonstrating the need for the sleeper to be modelled as a flexible beam in order to capture significant vibration modes. This flexibility has been a problem with prestressed concrete sleepers which although strong can undergo brittle fracture in tension. Existing static designs of the sleepers indicated that they would have sufficient strength to survive for up to 50 years. Early in their life however cracking below the rail seat was occurring as noted by Ahlbeck [3].

The normal shape of a concrete sleeper is that it has a waisted section becoming thinner towards the centreline. Grassie [8] gives a formula to enable the effective flexural rigidity of a sleeper to be modelled as an equivalent uniform beam by the formula;

$$\frac{1}{EI} = \frac{1}{2E}\left(\frac{1}{I_1}+\frac{1}{I_2}\right)$$

where I_1 and I_2 are the flexural rigidities at the sleeper centre and at the railseat, and E is the Young's modulus of concrete.

Material damping of a concrete sleeper has also been shown by Ford [27] and Grassie [10] to be low and has not being included in the model.

2.5 BALLAST

Selig [30] and Grassie [10] define that the purpose of ballast is to enable transmission of load, and reduce the stresses that are applied to the subgrade, support sleepers, provide resilience to shock (or damping) whilst providing drainage of the track with minimal plastic deformation and allowing ease of maintenance.

Shenton [31] describes how the track foundation can be divided into 3 distinct layers, top ballast immediately below and around the sleepers, deep ballast and subsoil. It is the top ballast that is of the most interest in this study as it is the layer that is subjected to the highest stresses and is disturbed at regular intervals by traffic and maintenance activities.

O.R.E. [32] has identified that the deterioration of vertical geometry, cross level and alignment are due to the movement of the track in the ballast or formation. Other defects such as gauge widening are generally defined as track component material failures and are not further considered within this study. O.R.E. [32] and Shenton [31] describe that vertical geometry defects are the result in fact of differential settlement caused by local mechanical behaviour, the causes of which are

Variation in dynamic load along a section of track.

Out of straightness of the rail

Random variation in sleeper spacing

Variation in vertical elasticity

Heterogenous settlement of ballast

Heterogenous settlement of formation

Frederick [33] details experimental work that showed that settlement is linearly dependent on axle load and from this assumes that settlement depends linearly on sleeper soffit force, even if this force is partly caused by irregularities in the rail.

Frederick [34] claims that when a rail becomes distorted due to geometric manufacturing defects in the rail, welding misalignments and work hardening of the running surface that takes on a shape that generally is dipped at the rail weld, that shape will slowly impose itself on the measurable track profile by causing differential ballast settlement. After a period under traffic the unloaded shape of the rail will begin to appear in the track profile. Short (one metre) wavelength rail irregularities will be measurable even if the rail is on a level foundation. Medium (five metre) wavelength irregularities will only develop as the ballast compacts. Long (20 metre) wavelength rail irregularities will probably be insignificant. Reissberger [35] supports this by noting that short wavelengths track defects up to six metres are due to rail deformations and cannot be readily corrected by tamping.

Variation in the spacing of sleepers is caused either during installation or migration under traffic. This is also allied to any variation in elastic support of the sleepers, which alters the load distributed to each of them together with variations in the formation stiffness, which will effect the rates of settlement.

Experimental work reported by Lucas [28] showed that the settlement of ballast is related to both the number of loadings and pressure between sleeper and ballast. The effect of higher contact pressures at a joint is to produce a greater settlement compared with the adjacent track and the effect of the dipped joint is enhanced.

As ballast is a random assortment of irregularly shaped, sized and hardened stone, different samples will react differently under the same loading conditions and consequently settle at different rates. Generowicz [36] has listed that slip and reorientation of particles, local attrition of asperities and structural breakdown all lead to ballast settlement.

After routine maintenance of the track structure, loading by traffic causes settlement of the ballast. If this settlement is not uniform then faults in the track geometry develop. This settlement is rapid initially but becomes slower with time.

O.R.E. [32] has concluded that rapid deterioration after any maintenance operation is followed by a slower deterioration after a few weeks, and that this rate stays steady for a section of track. The quality of track is directly related to its initial level during construction and that deterioration might be proportional to the axle load. These results are supported by Shenton [31] who has also found that the rate of deterioration is related to the quality of the track before tamping work has been carried out on it. Esveld [19] has shown that tamping only reduces the level of this dip by a small fraction. To correct these types of defects an alternative technique is utilised where the rails are mechanically bent and then ground flat.

O.R.E. [32] notes that dynamic overloads and residual deformation can be identified as being the most important with there being much more variation between the rates of deterioration of nominally identical sections of track other than the variations due to construction, age etc.

Jeffs [21] notes that one of the causes of rapid settlement is due to impact loading where shockwaves physically displace the ballast particles while Sato [37] describes that high frequency vibration above 1000 Hz exists even in ballast. Wanming [18] notes that ballast acceleration leads to a speeding up in the ballast residual deformation. The outcome is a broad frequency and amplitude spectrum. Jeffs [21] discusses the effect of frequency on the settlement but reaches no conclusion.

Koffman [38] believes that the biggest problem facing the permanent way designer is not so much to change the resilience of the ballast and subsoil but rather to create a uniformity of resilience along the track.

Selig [30] notes that after tamping the resulting initial density is low and subsequent density changes result from train traffic and environmental factors. He notes also that permanent deformation results from volume reduction due to particle rearrangement, inelastic recovery, volume reduction due to particle breakdown and subgrade penetration.

During the settlement of the ballast there have been noted a number of features of the settlement rates. There is generally an initial phase that is characterised by a rapid period of settlement in linear form followed by the longer term settlement at a slower rate which Jeffs [21] has noted is independent of the initial conditions. During this longer term phase recompaction zones are often noted where the settlement rate can increase by a factor of eight for a short period. This shape has also been reported by Eisenmann [39], Ebershohn [40], Kearsley [41] who also concludes that some of the largest displacements occur after maintenance.

Jeffs [21] has used laboratory cyclic loading tests to assess the settlement characteristics of ballast due to maximum and minimum loads, ballast type, ballast grading and sleeper type although Generowicz [36] detailed that the fast rates of rise and fall of pressures under a sleeper with passing wheel loads were impossible to approximate in the laboratory. Jeffs [21] also states that ballast testing should be conducted under actual operating conditions but laboratory experiments were chosen over field trials due to cost and control concerns.

Jeffs [21] has also pointed out that in the ballast and subgrade there not only exists material nonlinearities but also geometric nonlinearities with the most important of these being voids below a sleeper. Thus an initial strain is imposed on the system for relatively little stress which is one of the problems with determining the actual track profile from what can be measured in an unloaded state. Jeffs [21] discusses that the reasons for this complexity are due to multiple wheel spacings, varying support systems and the random nature of the load paths.

Grassie [9] notes that the maintenance process and consequent tamping reduces both the stiffness and damping of the ballast with this effect also being reported by Cox [42] who has recorded a halving in ballast damping for well settled to tamped track. Selig [30] has noted that the resulting initial density is created by maintenance tamping and the subsequent density changes result from train traffic and environmental factors. Experience has shown that tamping does not produce a high degree of compaction.

Ballast damping consists of both geometric (or the spread of energy through an elastic half space) and material damping. For purposes of settlement rates it is the relative level of material damping that is critical. The problem occurs in that geometric damping is more predominant. Mair [43] noted that whilst mass and stiffness are in broad terms inherent characteristics of the track system, damping is not. Of the mathematical formulations available he believes that it is convenient to treat track damping as linear viscous. In principle the track damping may be estimated from the rate of decay of the free vibrations induced by a loaded impulse. This could be achieved by rolling a vehicle up a ramp and allowing it to drop back onto the rail. In practice this is seldom done since the system is usually heavily damped and a value of the damping parameter is adopted between 8 to 18% of critical damping.

Plunkett [44] on measurement of damping notes that one should take measurements under circumstances which closely resemble those for which the information is needed. Probably the simplest form of measurement is the decay rate and it should give reliable results if the data is carefully reduced.

Cai [5] models the formation and ballast as linear springs and dashpots. Janardanam [45] noted that ballast has both elastic and inelastic deformation properties. Tew [46] models the ballast and formation as a bilinear beam on elastic foundation approach. This bilinear shape has also been reported by Birks [47].

Static values of the track modulus according to Mair [48] cannot be used directly in the analysis of track vibrations under dynamic load as they have to be adjusted to give the dynamic modulus values. He observes that the dynamic modulus value can be up to 2.5 times the static value at a wheel load of 150 KN in the frequency range of 35–55 Hz with lower ratios at lighter wheel loads or frequencies outside of this range.

El–Sibaie [49] states that for a railway track structure, damping represents the energy dissipated below the rail surface due to the dynamic action of a moving wheel. The dissipation is due in part to the friction in the ballast and subballast.

2.6 FORMATION

Vibrations have been shown by Esveld [19] to be transmitted through the ground by either compression, shear or Rayleigh waves. As the distance from the vibration source increases, the wave energy decreases due to material and geometric damping. Vehas [50] supports this by noting that in an elastic half space energy is lost through geometric attenuation and damping.

The determination of the effective damping through the ground is difficult, although Miller [51] has calculated the three responses to a circular point source excitation force. Due to the uncertainties of the nature of ground vibrations and the need to measure these experimentally in combination with the aim to only to study the settlement contained within the ballast layer, then a detailed analysis of the formation is not justifiable.

2.7 VEHICLE

Considerable research has been undertaken into the dynamics of vehicles on tracks such as Williams [16] and Shelley [17], where track roughness and wheel rail interaction were noted as being important in the accurate modelling of vehicle dynamics.

Williams [16] in his work modelled an eight wheel, two bogie wagon in which he defined the critical parameters in some detail including masses and stiffness. Hooper [52] states that most metal spring suspensions can be modelled linearly and that friction damping may be approximated by viscous damping.

As noted by Jenkins [13] at intermediate frequencies (20 – 100 Hz) the track system plays a significant part in determining force levels while usually only the unsprung parts of the vehicle and its primary suspension have some influence. Mutton [53] notes that for a vehicle model to be applicable to the problem of dipped welds, that the effects of vehicle speed, primary suspension characteristics and effective unsprung mass must be incorporated.

Ahlbeck [2] models the wheel mass of the axle and directly attached weights as the unsprung mass . The axle is a mass with vertical and rotational degrees of freedom together with the first four axle bending modes based on a pinned – pinned Euler beam. The vehicle modelling is limited to the sideframe. Williams [16] assumes that side frames are able to rotate freely about the bolster. Grassie [8] notes that for high frequency dynamics the unsprung mass of a freight or passenger vehicle should be about 350kg whilst for a locomotive it is around 2000 kg.

2.8 HERTZIAN CONTACT

The connection between the track and vehicle can be modelled as a Hertzian nonlinear contact between two elastic bodies. Jenkins [13] notes that this contact force needs to be modelled, as when impacts or impulsive loadings occur, the response is mainly dependent on the track and wheelset masses, and the elasticity of the wheel to rail contact zone. Ishida [12] states that for irregularities less than 200mm in length, such as corrugations or discrete defects, the use of the non linear spring is more accurate than a simple linear spring. This method is also used by Ahlbeck [2 4], Cai [5], Clark [7], Lyon [14] and Poplawski [54].

Hertzian contact theory assumes, that the contacting surfaces between the wheel and the rail follow the classic Hertz theory on the contact of elastic solids as described by Johnson [55].

- The highly concentrated contact stresses are separate from the general stress within the two contacting bodies.
- The contact area must be small in relation to the dimensions of each body and the relative radii of curvature of the surfaces.
- The contact is frictionless so that only normal stresses are transmitted.

Mutton [53] indicates for the problem of dipped weld that the separation of the wheel and rail contact must be considered. Ahlbeck [2 4] has used 8% of critical damping and states that variations in the damping from 2% to 50% has little effect on the peak rail accelerations. Due to the small value of the energy loss in the contact point the Hertzian damping has been excluded from the model.

2.9 LITERATURE REVIEW OF MATHEMATICAL MODELLING

Ever since the start of railway operations there have been numerous models to analyse the dynamic response of the track structure. These have all come about due to the desire to increase the capacity of the track or increase its effective life whilst reducing the total cost of that structure either through sudden failure or rapid deterioration.

The main models in this field that are reviewed in this thesis are:

Beam on Elastic Foundation (Classic Models)	
British Rail	[7],[13]
Battelle Columbus Laboratories	[2],[3]
University of Cambridge	[9]
Canadian Institute of Guided Transport	[5]
Research Institute of Rail Vehicles, China	[18]

Brief details of these models will be discussed in section 2.11 together with two of these being further selected for the comparison with the model described in this paper in chapter five.

Track models have been developed in both the time and frequency domains with the track being considered as either two dimensional, where the rails, sleepers and formation are simple lumped masses, or three dimensional where the effect of these components along the track can be included as separate layers. The sleepers can be further considered as a single layer, or as discrete elements. Various levels of nonlinearity can also be included dependent on the complexity of the phenomena to be studied. The vehicle can extend from a very simple wheel element up to a highly complex vehicle model. Symmetric defects can be investigated by a half track model consisting of a single rail and half sleepers, whilst asymmetric defects require the modelling of the complete track structure.

Hooper [52] has described the various methods available for the analysis of the track structure including modal analysis, frequency response analysis and simulation all of which require a state variable description of the model. Wilson [56] lists the simulation techniques of step by step integration, frequency domain analysis, mode superposition analysis, response spectra analysis and impulse response analysis with Lyon [14] utilising convolution integrals. Of these methods the step by step integration method is suitable for nonlinear analysis and the complex discontinuous loading such as the wheel bouncing off the track.

Simulation involves the creation of a model of interest and subject it to a forcing function. The basis of simulation is to solve the system equation of motion at small increments of time to produce a trajectory in state space describing the variations of the state variables. Most methods for solving ordinary differential equations can be used. Runge Kutta methods have been successfully used by Williams [16], Clark [7], Ahlbeck [2] and Shelley [17].

The advantage of modelling using numerical integration techniques is that it permits the modelling of nonlinear parameters, examples of which are Hertzian contact between the wheel and rail when a linear stress strain relationship is replaced by a 2/3 power relationship, and also during periods of contact loss and the movement of the bogie over a time domain track model. Wilson [56] recommends that for non linear analysis the development of special purpose computer programs is justifiable.

The step by step simulation approach has been used by Clark [7], and recommended by Mutton [53] who states that the effect of actual weld dip profile and track support conditions must be incorporated. In addition the model must consider separation of the wheel/rail contact, and the nonlinear characteristics associated with many of the track and vehicle components. The method followed by Clark [7] is that the model consists of two discrete parts, being the track and vehicle models respectively, separated at the wheel to rail interface by non linear Hertzian contact springs.

As noted by Wilson [56] all structures have an infinite number of degrees of freedom when subjected to dynamic loading. The model described in chapter three has a limited number of degrees of freedom which enables it to capture the significant physical behaviour.

Newton [15] notes that one of the problems that occur by using a finite beam as an approximation to the infinite beam, which would be needed to represent the correct energy radiation conditions, is that the length of beam depends on the time for which the solution is required, as eventually the effects of reflections from the ends will become evident.

A number of simulation packages were investigated as to their suitability for the project. CAL 86 as described by Wilson [56] provides a linear step by step integration method, it was not used due to fixed time steps and the inability to model the wheel/rail interaction. DARE–P [57] is a FORTRAN based numeric integration routine and is an equation oriented continuous system simulation language. It utilises a state space variable format. It was not used due to the lack of availability of a PC based version.

MATLAB is a matrix analysis system with highly optimised numeric calculation routines. This package was selected for the final model development as it enabled the nonlinear analysis of the model, was of a high computing efficiency, and was readily available to the author. It has the added advantages of an in built graphics capability and signal processing routines.

2.10 OTHER MODELS

2.10.1 CLASSICAL MODELS

The "Classical" method can be defined as the beam on elastic foundation model as used by many researchers up until the advent of suitable computer power in the 1960's. Grassie [9] describes the conventional model of railway track for vertical motion as an infinite Euler beam, on a uniformly distributed damped elastic support, representing the ballast. The sleeper mass is assumed to be distributed uniformly along the track and lumped with the rail mass.

Grassie [9] also notes that there are two primary deficiencies with this approach, due to the existence of resilient railpads, which are now inserted between the rail and the sleeper, and the rail being discretely supported by sleepers, in which the pinned – pinned resonance of the rail between the sleepers becomes important at higher speeds given by

$$f = \left(\frac{\pi}{rl}\right)^2 * \sqrt{\frac{EIr}{mr}}$$

where; rl is the sleeper spacing.

mr is the mass of rail per metre.

EIr is the flexural rigidity of the rail.

Equation 2.2

To overcome these limitations and with the advent of high speed digital computers the following models are examples of those which have been developed over the past 30 years.

2.10.2 BRITISH RAIL

The British Rail model described in detail by Clark [7] and utilised in studies conducted by Shenton [31], Frederick [33] and Round [58], was designed primarily to investigate the effects of short wavelength corrugation defects (60mm in length) on the rail and sleepers.

This is a 20 bay symmetric half track model with discrete sleepers and utilises modal analysis. The sleepers and rail have vertical bending stiffness and inertia with the railpads that separate them being modelled discretely and sleepers supported on a uniform ballast layer. The track and vehicle linear systems are separated at the wheel to rail interface by a nonlinear Hertzian contact spring with fixed time steps being used in the calculation routine.

As part of the calibration process the parameters for the British Rail model were used in section 5.6 as a comparison to the model described in this thesis to check the predictions against published theoretical and experimental results.

2.10.3 IMPWHL

Battelle Columbus Division under Ahlbeck [2 3 4] has developed a vehicle and track interaction program over the past 15 years with the primary intention being to determine the peak loads under specific running surface geometry defects and to predict the vehicle and track component loads.

Impact at one wheel only is included with geometry inputs seen from the wheels reference, which result in a need for an asymmetric model about the track centreline. It has been assumed that forward motion has little effect on vehicle track response and there is limited vibration above the primary suspension.

Track parameters are derived from beam on elastic foundation theories and experimental results with the first four sleeper and axle bending modes modelled.

Ahlbeck also goes into some discussion about the effect of including rail bending as used by Clark [7] and why it was not included in the model. It is claimed that the modes are highly dependent on the positions of the adjacent wheels and thermal stresses due to longitudinal restraint of the rail and are difficult to determine.

The results from this model were selected for comparative analysis in section 5.7 with the analysis work undertaken in this study as it is based on differing track conditions to those existing on Australian and British railways.

2.10.4 GRASSIE " TRACK" MODEL

This linear frequency domain model developed by Grassie [8 9 10] is used to calculate the dynamic response of the model track and vehicle to a uniform sinusoidal irregularity between the wheel and rail. Shear deformation and rotational inertia are not included because their effects would preclude use in the analysis of the transcendental functions pertaining to the vibration of Euler beams. The track rests on a continuous two layer support.

2.10.5 CANADIAN INSTITUTE OF GUIDED TRANSPORT

This model described by Cai [5] is a half track, symmetric, time domain model that has two components consisting of the vehicle, which has two unsprung wheel masses with side frame mass and pitch inertia supporting a primary suspension, and the track, consisting of only one rail with 40 bays, linear damped rail pads, Timoshenko rail beam and discrete sleepers. The two components are separated by an undamped nonlinear Hertzian contact. The numeric calculation consists of a 4^{th} order Runge Kutta integration routine with adaptive time stepsize control.

2.10.6 RESEARCH INSTITUTE OF RAIL VEHICLES CHINA

Wanming [18] describes a model that has 10 vehicle and 43 track degrees of freedom that investigates the combined vertical and lateral interaction. Nonlinearities due to springs, friction damping, wheel rail contact and creep forces were modelled. In order to overcome a concern with the solution of high order differential equations Wanming used Newmark's method.

CHAPTER 3 THE MATHEMATICAL MODEL

3.1 PHILOSOPHY

It is with the background from the previous chapter from which the modelling described in this chapter was developed, including the techniques that were used, and some of their limitations. Other developments that had occurred around the world were taken into account, with the author being particularly drawn to the work of British Rail and the University of Cambridge.

As previously described there are two basic types of approach used in the solution of track vibration problems, being either in the time or frequency domain. The time domain approach was used in this research due to its ability to handle nonlinear and asymmetric models. The disadvantages of this approach are that the models take longer to calculate, have a finite length causing problems with end effects and need to converge for low frequency effects.

The numeric calculation method adopted permits the use of variable time steps that allows shorter time steps during high frequency vibrations.

A large number of nonlinearities exist in the track structure and an attempt to model all of them was felt to be beyond the scope of the research. Thus the nonlinearities of Hertzian contact and potential loss of wheel rail contact were selected.

The rails beam elements are modelled with vertical and rotational degrees of freedom. The use of a more complex Timoshenko beam which includes shear deformation was not utilised as the added complexity was not warranted, given simplifications with other parts of the model. In the modelling of the rail beam elements, two different solution techniques were trialled consisting of finite element, and unit displacement, methods. The finite element method was selected due to its convenience.

The flexibility of prestressed concrete sleepers is of importance in track dynamics as has been shown by various Australian and overseas studies. A simplified model of the sleeper was selected.

In this chapter the detailed characteristics of the model are discussed, with the reasons for the method selected, alternative methods and approaches being previously discussed in chapter two. The parameters used in the analysis, and the methods by which they were obtained, are discussed in more detail in chapter five which deals with parameter determination.

The model that has been developed consists of two discrete parts, they being the track and vehicle models respectively. The reasoning behind this division is that each part can be readily described by a relatively simple model in itself, but once the movement of the bogie along a section of track is desired to be modelled, then the modelling becomes complex. These two parts are separated at the four wheel to rail interfaces by nonlinear Hertzian contact springs. This model has a total of 194 degrees of degrees of freedom which enables it to capture the desired dynamic characteristics.

3.2 TRACK MODEL DESCRIPTION

3.2.1 RAIL

The rail between two sleepers was modelled as a Euler beam with equal lumped masses being positioned over each of the sleepers. Each node has a vertical and rotational degree of freedom as shown in figure 3.1 (note signs).

Finite element methods were employed to model the beam interaction between nodes. A requirement is that both the rail displacement and rail node rotation be known at the beginning of each time step in order that the nodal forces can be resolved. The stiffness matrix for one of the rail elements is shown in table 3.1.

Figure 3.1 Rail element degrees of freedom

	1	2	3	4
1	$12 (\frac{EI_{rail}}{rl^3})$	$-6 (\frac{EI_{rail}}{rl^2})$	$-12 (\frac{EI_{rail}}{rl^3})$	$-6 (\frac{EI_{rail}}{rl^2})$
2	$-6 (\frac{EI_{rail}}{rl^2})$	$4 (\frac{EI_{rail}}{rl})$	$6 (\frac{EI_{rail}}{rl^2})$	$2 (\frac{EI_{rail}}{rl})$
3	$-12 (\frac{EI_{rail}}{rl^3})$	$6 (\frac{EI_{rail}}{rl^2})$	$12 (\frac{EI_{rail}}{rl^3})$	$6 (\frac{EI_{rail}}{rl^2})$
4	$-6 (\frac{EI_{rail}}{rl^2})$	$2 (\frac{EI_{rail}}{rl})$	$6 (\frac{EI_{rail}}{rl^2})$	$4 (\frac{EI_{rail}}{rl})$

Table 3.1 Rail element stiffness matrix [23] 10.2-1

[rl = length of rail between sleepers, EI_{rail} = rail flexural rigidity]

The stiffness matrix shown in table 3.1 is then used in the normal finite element method to form a 46 by 46 rail stiffness matrix for each rail as shown in figure 3.2.

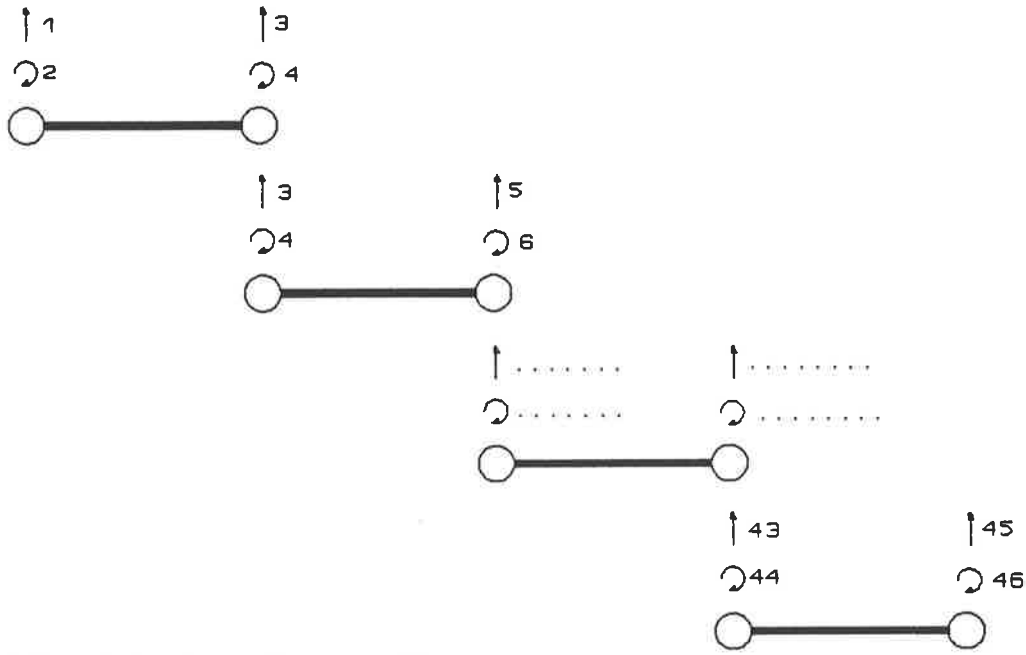

Figure 3.2 Rail element assembly

The rail is assumed to have constant linear physical characteristics of mass distribution and bending stiffness throughout the complete length of the model.

By knowing at the end of each time step the displacements and rotations of the rail nodes, it is possible to calculate the corresponding forces and moments acting at each node.

3.2.2 SLEEPERS

The prestressed concrete sleepers are modelled as discrete, flexible Euler beams. Thus shear deformation and rotary inertia associated with a Timoshenko beam element are ignored. Each sleeper has been modelled with a total of three nodes, one being under each of the two rails, and one on the centreline as shown in figure 3.3. The centreline node has both vertical and rotational degrees of freedom to model the first and second flexible bending modes as described by Ford [27]. These combine to give a total of four degrees of freedom per sleeper, permitting two rigid body and two bending modes.

The stiffness matrix for one of the sleepers is shown in table 3.2.

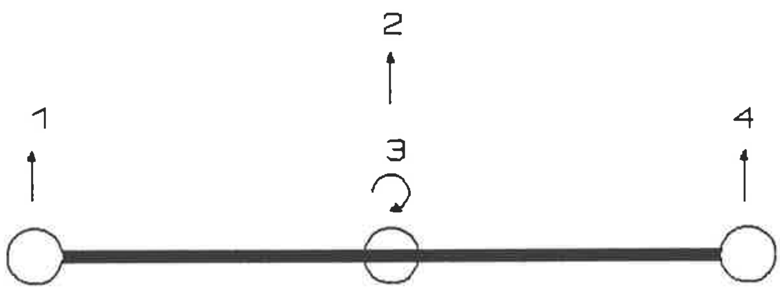

Figure 3.3 Sleeper degrees of freedom

	1	2	3	4
1	$3\ (\frac{EI_{sleeper}}{sl^3})$	$-3\ (\frac{EI_{sleeper}}{sl^3})$	$-3\ (\frac{EI_{sleeper}}{sl^2})$	0
2	$-3\ (\frac{EI_{sleeper}}{sl^3})$	$6\ (\frac{EI_{sleeper}}{sl^3})$	0	$-3\ (\frac{EI_{sleeper}}{sl^3})$
3	$-3\ (\frac{EI_{sleeper}}{sl^2})$	0	$6\ (\frac{EI_{sleeper}}{sl})$	$3\ (\frac{EI_{sleeper}}{sl^2})$
4	0	$-3\ (\frac{EI_{sleeper}}{sl^3})$	$3\ (\frac{EI_{sleeper}}{sl^2})$	$3\ (\frac{EI_{sleeper}}{sl^3})$

Table 3.2 Sleeper stiffness matrix

where sl = half effective sleeper length

$EI_{sleeper}$ = effective sleeper flexural rigidity

Although the sleeper has a variable cross section, for modelling purposes a method to determine an equivalent uniform beam element has been devised and is discussed in section 4.11.3. The material properties throughout the sleeper are assumed to be constant.

2.3 RAIL/SLEEPER PAD

The pad separating the sleeper and rail is treated as a linear stiffness/damper element and has the assumption that the pad can carry tension if rail uplift reaches a high enough value. The pad is held in a state of precompression by the action of the resilient fastenings.

The pad transmits the reaction from the rail, to and from, the sleeper and so is included in the equations of motion of the rails and sleepers.

3.2.4 BALLAST

The track structure is supported by ballast/formation springs that provide a linear reaction to the sleepers under each of the two outer nodes. Directly after tamping the sleeper is supported only beneath the rail seat. Support under the sleeper centre is deliberately avoided to minimise negative bending stress on the sleeper centreline.

3.2.5 TRACK MODEL

The two rails and 23 sleepers are combined into a track length of 24 bays between two fixed ends, and has a total of 184 degrees of freedom.

Figure 3.4 shows the cross section of the model at one sleeper and details the relationship between the rail and sleeper giving a total of eight nodes per sleeper location. The location of the rubber pad and the supporting ballast/formation element can also be seen.

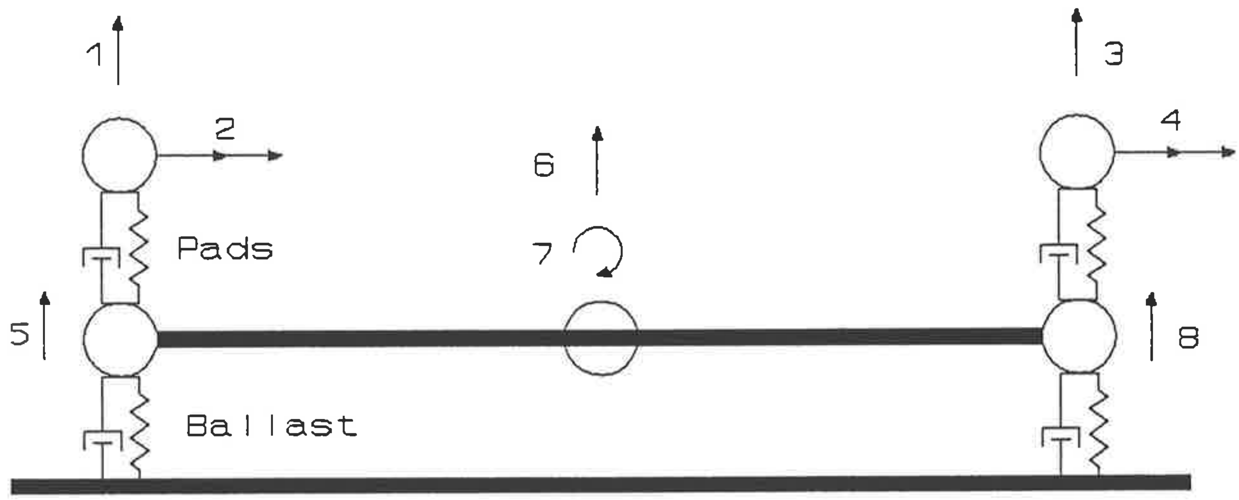

Figure 3.4 Track model cross section

Figure 3.5 shows the elevation of the model. The 23 sleeper locations can be clearly seen along with the 24 bays that form the total length. Shown here are only the 23 vertical degrees of freedom for one rail. As shown in figure 3.4 each of those bays has 8 degrees of freedom associated with it.

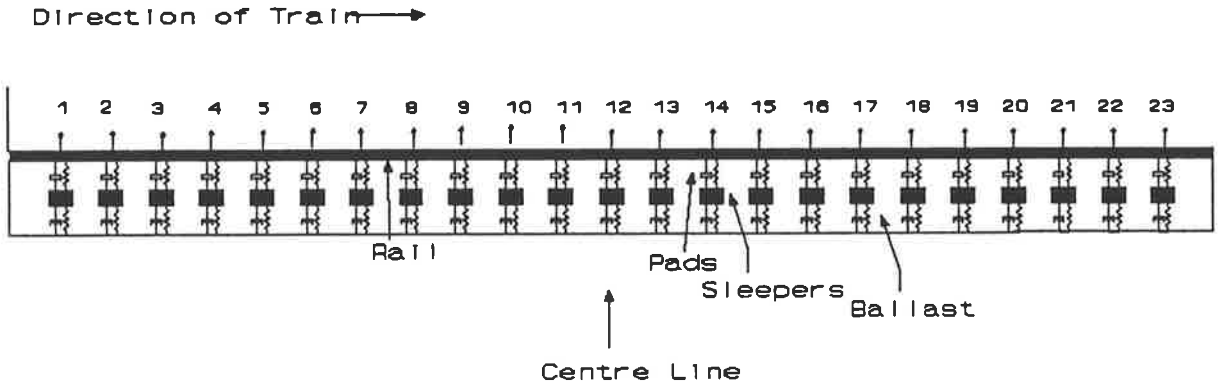

Figure 3.5 Track model longitudinal view

The movement of the vehicle is from the left to the right and care must be taken in the description of the rail surface geometric imperfection to ensure the correct direction is used. The rail defects are entered into the model as a variation away from a theoretically smooth surface.

3.2.6 MASS

The sleeper is not of a uniform cross section with the centre of the sleeper having less depth than under the rail seat area. The sleeper also projects outside of the rail and as such there is a larger distribution of mass towards the outer nodes as evident in figure 3.6. An estimate of the mass distributions at each of the three nodes is also shown. The centreline node rotary inertia was obtained from Meriam [59] Table C5 for a slender rod. The nodal mass for the centreline element was used along with an estimate of the node length of one third of the sleeper length. Section 5.4 details the sleeper bending modal analysis and the conclusions drawn from that analysis is that the mass distributions are reasonable. A more detailed analysis than that undertaken in this thesis would be required to confirm these results.

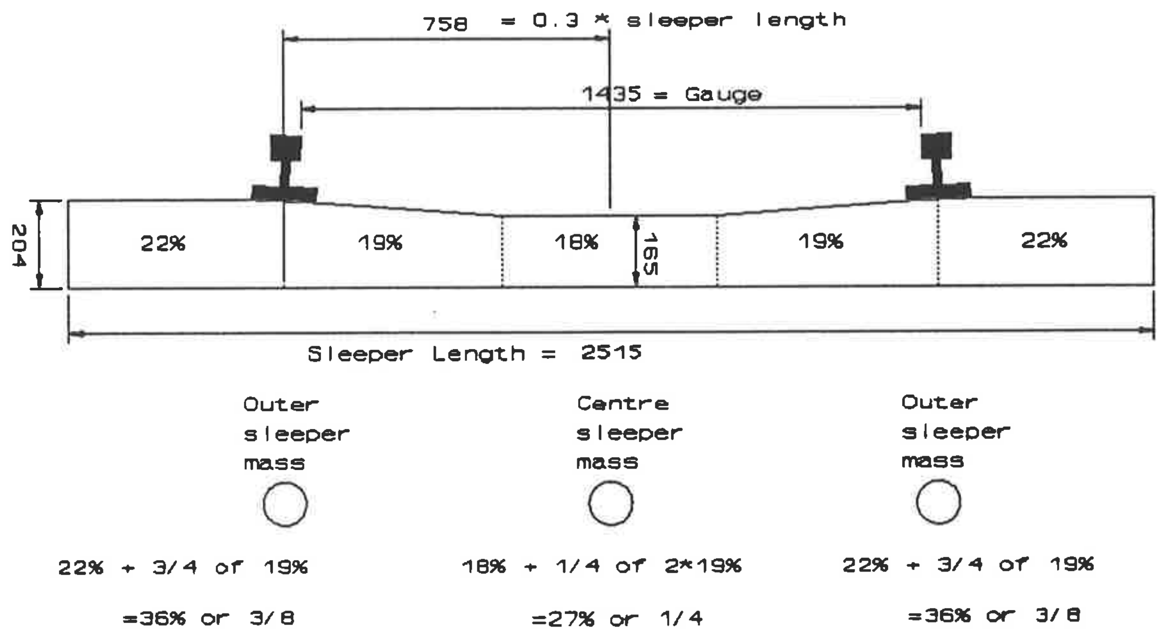

Fig 3.6 Sleeper mass distribution

Rail node masses were calculated on all of the rail mass being lumped above the sleeper node for that bay length.

At each of the nodes of interest the following mass elements have been used.

Element type	Mass
Rail vertical node	$lineal\ mass\ rail * rail\ node\ spacing$
Rail rotational node	$lineal\ mass\ rail * \frac{(rail\ node\ spacing)^2}{12}$
Sleeper vertical outer nodes	3/8 of total sleeper mass
Sleeper vertical central node	1/4 of total sleeper mass
Sleeper central rotational node	$\frac{\frac{1}{4} mass_{sleeper} * (0.33 * sleeper\ length)^2}{12}$

Table 3.3 Track nodal masses

The details described above are shown in figure 3.7 on a three dimensional schematic diagram for the complete track structure.

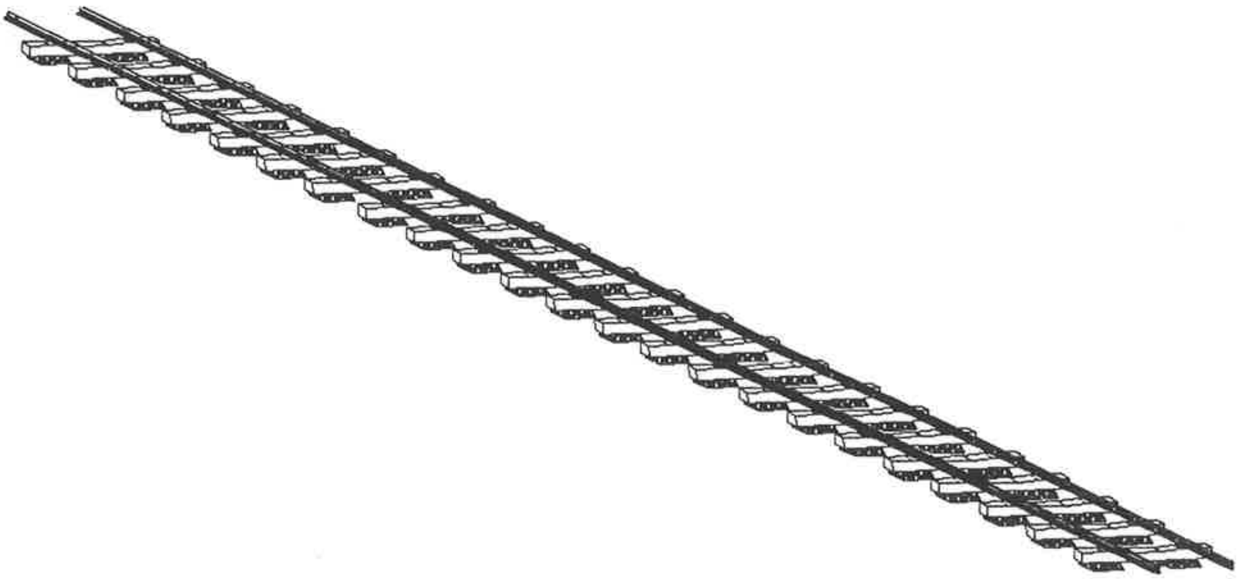

Figure 3.7 General track view

3.3 VEHICLE MODEL

The vehicle is modelled as a half vehicle consisting of half of a complete vehicle's body and one bogie. This contains 13 degrees of freedom. The body model is a considerably simplified model as compared to such models as SIMCAR [13] but is found to contain enough degrees of freedom to permit the modelling of its relationship to the track.

3.3.1 WHEELSETS

The two wheelsets consist of four degrees of freedom in the same plane as the sleepers as shown by figure 3.8.

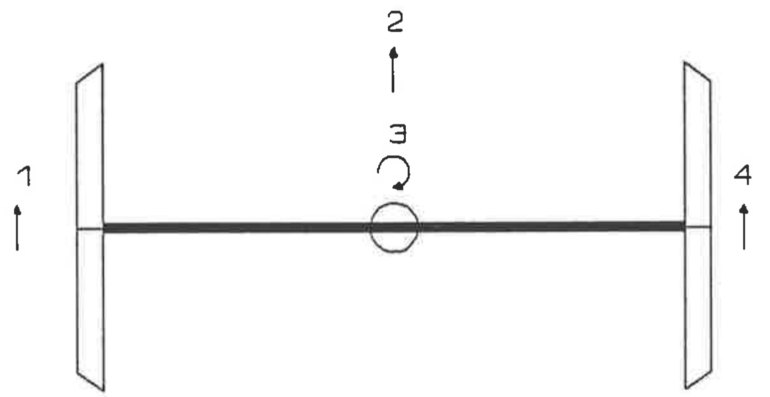

Figure 3.8 Axle degrees of freedom

The stiffness matrix for the wheel set is of the same form as for the sleeper as detailed in table 3.2 except that the effective sleeper flexural rigidity is replaced by the axle flexural rigidity, and the sleeper half length by the axle half length.

3.3.2 BOGIE FRAME

Above the wheelsets is the bogie frame, one type consists of two sideframes with no suspension separating it from the wheelsets that has vertical, and pitching degrees of freedom for each sideframe giving a total of four degrees of freedom as shown in figure 3.9. Above this, separated by the secondary suspension is the bolster. (A three piece bogie has two sideframes and one bolster).

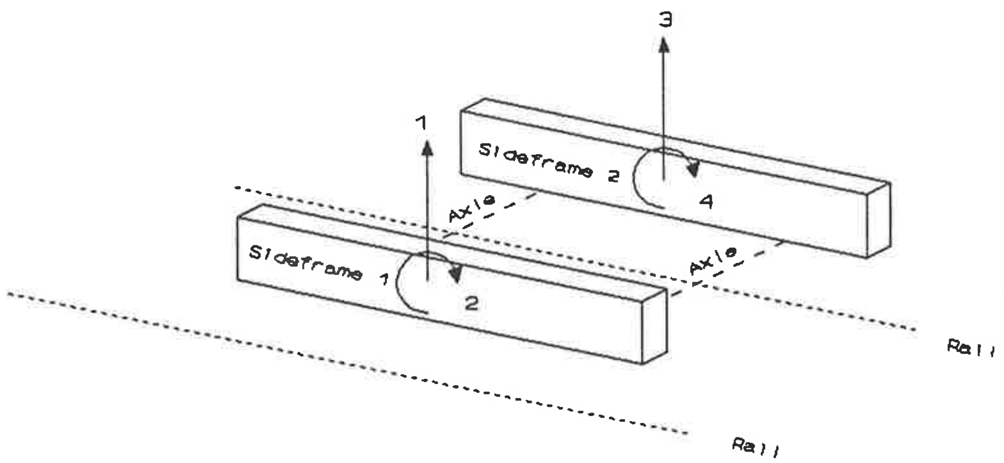

Figure 3.9   3 piece bogie degrees of freedom

The other sort of bogie is that shown in figure 3.10 which is a rigid type that has three degrees of freedom and separated from the wheelsets by primary suspension elements. Above the frame separated by the secondary suspension is the bolster.

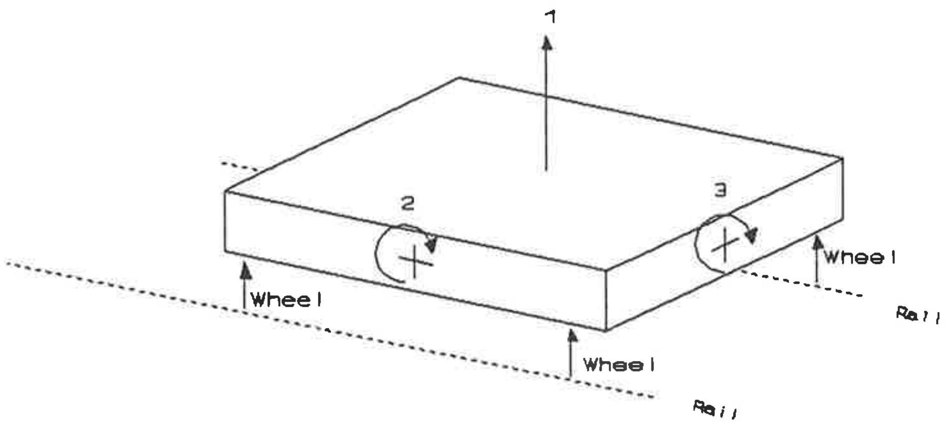

Figure 3.10 Primary suspension bogie degrees of freedom

3.3.3 BOGIE

The bogie is therefore made up of two wheelsets separated from the bogie by linear primary suspension elements, with the bogie being separated from the body by the secondary suspension.

Figure 3.11 shows a schematic view of the rigid bogie vehicle which details the relationship between the various components.

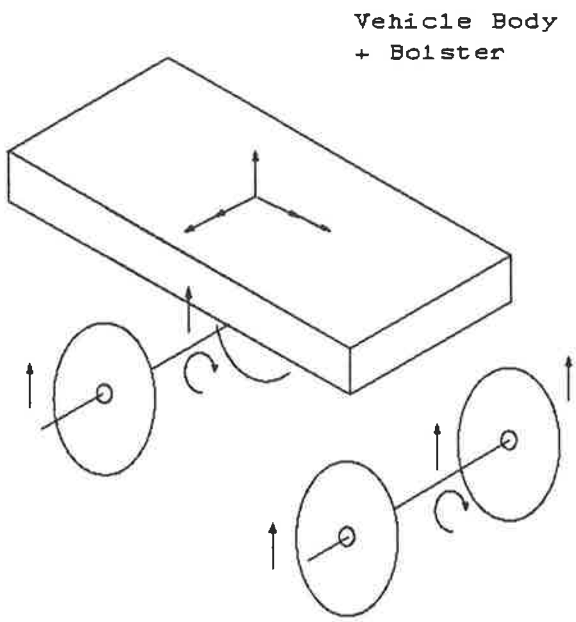

Figure 3.11 **Bogie model**

3.3.4 BODY

As only one bogie is being simulated the vehicle can be simplified to a half vehicle. Two degrees of freedom in the model (vertical and roll) allow the three vehicle rigid body degrees of freedom to be modelled (bounce, pitch and roll). These motions are however frozen, because although they are affected by the defect itself, they respond to long wavelength effects as detailed in section 3.7. Variations to both of these parameters can however be set in the initial conditions.

This primary suspension bogie vehicle has a total of 11 degrees of freedom with the three piece bogie vehicle having 12 degrees of freedom as shown in figure 3.12.

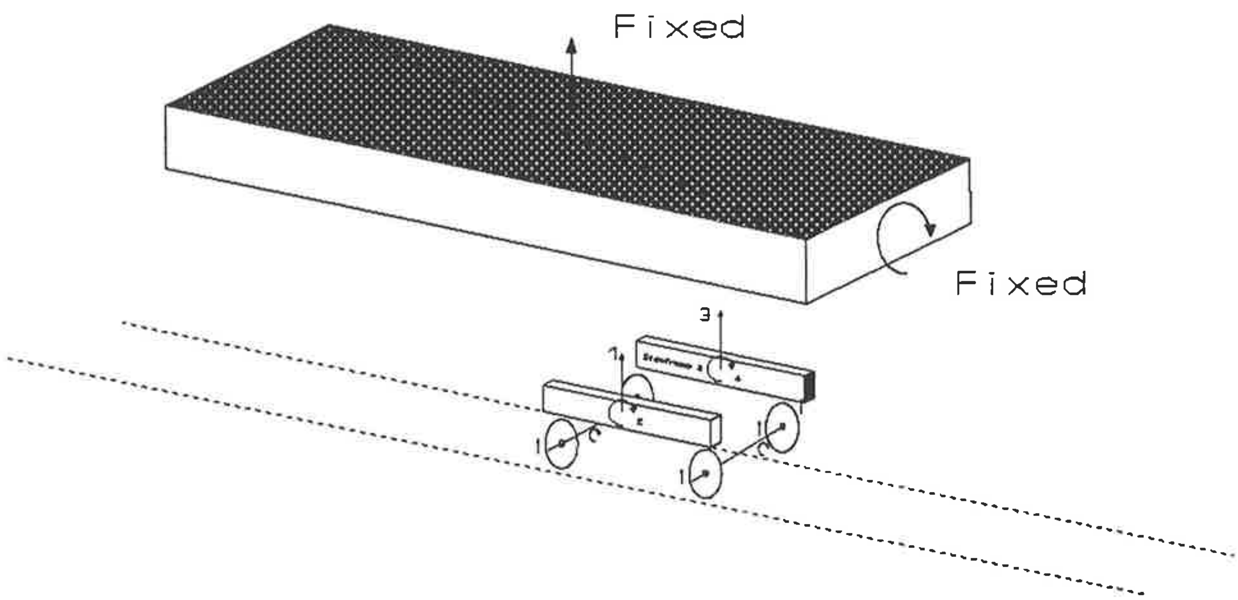

Figure 3.12 Vehicle model

3.4 CONTACT FORCE CALCULATION

This section describes in detail the method by which the forces connecting the wheels and rails are calculated and uses the method described by Lyons [14] which is reproduced here.

The first stage is to determine the Hertzian flexibility constant "C" which is dependent on readily measurable geometric or physical constants of the wheels and rails. A number of static input variables are required that are determined from well known physical and geometric parameters:

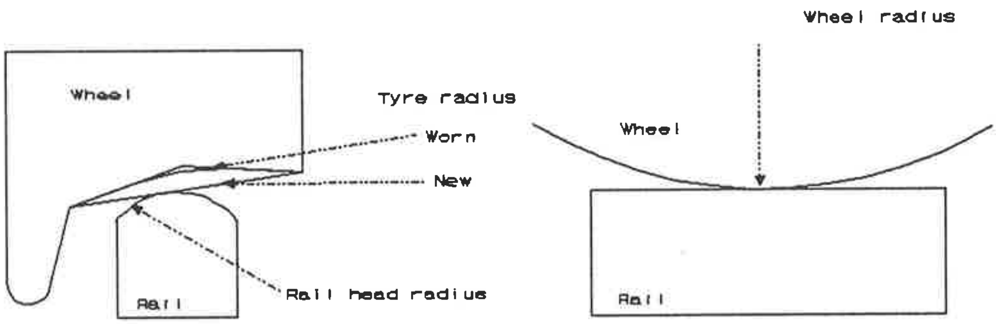

Figure 3.13 Wheel rail contact geometry

R2	= Cross sectional Head radius of rail	= 0.30m
R1	= Wheel radius	= 0.48m
R1'	= Tyre radius	= -0.7m for worn wheels or infinity for 1 in 20 coned wheel.

In the longitudinal direction the rail is assumed to have an infinite radius.

ϕ = angle of attack of wheelset relative to rail = 90°

(the angle formed between the plane containing the curvature 1/R1 on the wheel and the plane containing curvature 1/R2 on the rail)

E = Youngs modulus for rail steel = 2.1×10^{11} Nm^{-2}

(assumed same for wheel and rail)

μ = Poissons ratio = 0.3

(assumed same for wheel and rail)

$$C = \gamma\left(\frac{1}{(K^2\ \delta)}\right)^{\frac{1}{3}} \qquad = \textit{Hertzian flexibility}$$

where

$$:\delta = \frac{4}{\left(\frac{1}{R1}+\frac{1}{R1'}+\frac{1}{R2}\right)} \qquad :K=\frac{4}{3}\left(\frac{E}{(1-\mu^2)}\right)$$

$$\theta=\cos^{-1}\left(\frac{\delta}{4}\ \left(\left(\frac{1}{R1}-\frac{1}{R1'}\right)^2+\left(\frac{1}{R2}\right)^2+2\frac{\left(\frac{1}{R1}-\frac{1}{R1'}\right)}{R2}\cos(2\ \phi)\right)^{0.5}\right)$$

$$\gamma=0.57462\ +\ 0.034745\ \theta\ -\ 0.00021338\ \theta^2$$

The model then takes the flexibility "C" and applies the following formula

$$ContactForce\ =\ \left(\frac{\alpha}{C}\right)^{\frac{3}{2}}$$

where: α = indentation or compression at the wheel/rail interface.

To determine the contact force for each time step the location of the rail position at the point of contact needs to be defined which is done by the fitting of a cubic polynomial through the elevations and rotations at the two adjacent nodes. The method described by Thomson (10.2–2) [23] is used where

$$Rail\ Height = A(1) + A(2)\frac{loca}{rl} + A(3)(\frac{loca}{rl})^2 + A(4)(\frac{loca}{rl})^3$$

where (being careful of sign convention)

$A(1) = x(1)$

$A(2) = -rl * x(2)$

$A(3) = -3*x(1) + 2*rl*x(2) + 3*x(3) + rl*x(4)$

$A(4) = 2*x(1) - rl*x(2) - 2*x(3) - rl*x(4)$

Then using the wheel height which is estimated from the previous time step this enables the relative displacement between the rail at the contact point and the wheel to be calculated. The formula that is used is given by

$$\alpha = x_r - x_w - corrugation$$

where "corrugation" is the rail shape under investigation which is the height variation from an assumed perfect rail surface.

3.5 NUMERIC PROCEDURE

Three numeric analysis programs were investigated to ascertain which would be the most suitable for analysis of the model just described. They were DARE–P [57], CAL–86 [56] and MATLAB [60]. The selection of the program to be utilised was finally determined by the non availability of the DARE–P code for personal computers, and the difficulties with CAL–86 of having the vehicle model separated at the wheel rail interface from the track by the non linear Hertzian spring. MATLAB had also come into use with Australian National as a general analysis package and was found to be suitable for this type of modelling.

The MATLAB matrix analysis personnel computer based system with highly optimised numeric calculation routines, was used as it enabled the nonlinear analysis of the model. This model can be defined very concisely with this computer package and was chosen for its ease of use and computing capability.

Throughout the model description are references to programs with the extension M. These refer to the uncompiled program files. For further details on the program and the format that was utilised the reader is recommended to read both the sample listing contained in appendix one and the MATLAB users guide [60].

The following sections detail the numeric procedure that was used.

3.5.1 MODEL FORMAT

The model was developed in a state space format which is undertaken by rewriting each of the second order differential equations into two first order differential equations. This has the effect of doubling the number of simultaneous equations that need to be solved.

The numerical solution of the first order ordinary differential equations is made using adaptive time step control Runge Kutta methods based on Fehlberg 4^{th} or 5^{th} order pairs of formulas. This procedure is available as a standard subroutine in MATLAB and was only modified to permit the use of variables within the program and store the required final information.

The normal procedure is to run the model from time = 0 which corresponds to the trailing axle being at the edge of the model, and concluding once the trailing axle has reached node 20. The model can however be run with any starting value greater than zero, and an end value less than 25 bays minus the axle spacing. End effects however limit the accuracy of model runs towards the extremities.

3.6 MODEL ROUTINE

This section describes in detail the step by step operation of the model including the variables required.

3.6.1 FIXED PARAMETERS

The fixed parameters that are needed by the model are either input by the user, or calculated by the program before the commencement of the calculation routine. The criteria is that these variables will stay constant throughout the duration of the model run.

	Parameter type	Parameter	Symbol	Units
A	Geometry Parameters	Sleeper Spacing	rl	m
		Sleeper length	sl	m
		Axle spacing	axs	m
		Primary and secondary suspension spacing	pss & sss	m
B	Vehicle Speed		vel	km hr^{-1}
C	Material Stiffness	Rail flexural rigidity	EIr	N m^2
		Sleeper flexural rigidity	EIs	N m^2
		Axle flexural rigidity	EIa	N m^2
D	Spring Element Stiffness	Primary and secondary suspension	ksp & kss	N m^{-1}
		2 ballast elements to permit analysis of stiffness variation	kb1 & kb2	N m^{-1}
		Rail/Sleeper pads	kp	N m^{-1}
E	Mass	1/2 body + bolster	mv	kg
		Side frame/bogie	mb	kg
		Axle	ma	kg
		Wheels	mw	kg
		Rail mass/m	mr	kg
		Sleeper	ms	kg
F	Damping	Calculated as a Critical %		

Table 3.4 Fixed parameters

3.6.2 INITIAL CONDITIONS

The initial conditions as required by the user are then set dependent on the conditions to be modelled.

The nodal displacements and velocities of the rail nodes, sleeper nodes and wheels are normally set to zero as the transient response time of these elements is short. This also avoids the problem of the wheel being set at a level that either causes extremely high contact stresses, or is out of contact and therefore would be liable to bouncing.

The vehicle body vertical displacement is set at 50–150% of the static displacement calculated by the following formula;

$$\left(\frac{mv\ g}{2\ kss}+\frac{(mv+mb)\ g}{4\ ksp}\right)$$

This enables a variety of pseudo static loading conditions to be tested. The body can also have an initial roll angle to simulate uneven wheel loading conditions.

Bogie or sideframe vertical displacement can be adjusted to minimise the startup transient due to their medium wavelength response and the sensitivity of this on the final results.

To enable the model to run a number of control parameters need to be defined.

Start time	(generally zero or one bay)
Finish time	(generally 20 bays)
Screen trace control	(this enables monitoring of the run during calculation)

Accuracy of calculation routine normally 10^{-5} or a step size of 12mm.

3.6.3 CALCULATION ROUTINE

Once all of the above steps have been undertaken the main calculation can take place. The following steps are carried out for each time step, with iterations using various time steps occurring until the accuracy of the calculation is within the parameters contained in the run control parameters. The vehicle position along the length of the model is determined by the multiplication of the fixed velocity and the elapsed model time. The contact force at each of the four wheel to rail interfaces is then determined by the formula contained within section 3.4.

These contact forces are then distributed to adjacent rail nodes on a encastre beam allocation method as shown in figure 3.14 using the formula from Shigley [61] table A–12,15.

$$MX = \frac{Fv * loca * locb^2}{r\ l^2}$$

$$MY = \frac{-Fv * locb * loca^2}{r\ l^2}$$

$$FX = -Fv * locb^2\ \frac{3 * loca + locb}{r\ l^3}$$

$$FY = -Fv * loca^2\ \frac{3 * locb + loca}{r\ l^3}$$

Rail nodal forces are determined from rail deflection calculations using finite elements type calculations. Accelerations for all of the nodes are then calculated by the use of the Runge Kutta integration routine. The calculation is reiterated using varying time steps until within the accuracy required. The data for the time step completed is then stored temporarily, with the data required for post analysis being saved in files.

The vehicle is then moved forward a distance calculated by the speed multiplied by the time at the end of the calculation step. The model then continues the calculation steps until the model end time is reached.

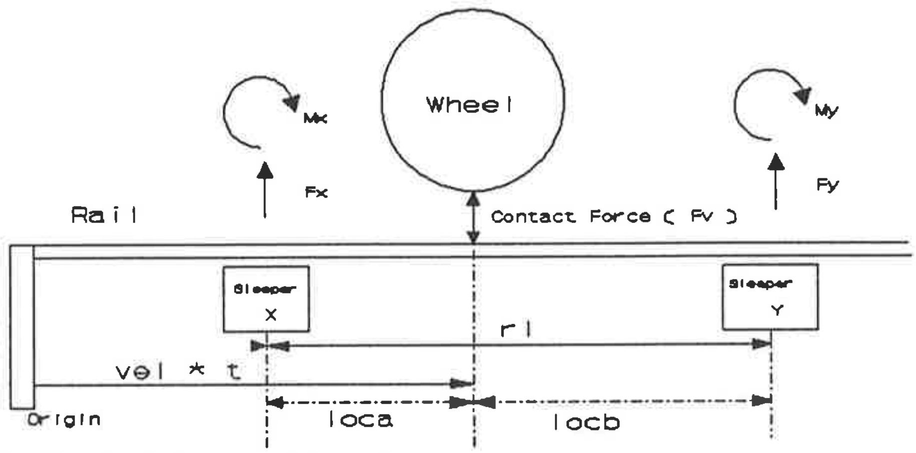

Figure 3.14 Contact force distribution

3.6.4 STORE MODEL RESULTS

At the completion of each step of the model a number of results are stored to permit the examination of the run and for post analysis of the results. These results are stored on numeric files.

1. Time at each iteration step
2. Contact force at leading right hand wheel.
3. Velocities of all nodes adjacent to damper elements.
4. Displacement of rail and sleeper nodes at sleeper 12.

3.7 STABILITY OF THE MODEL

The problems that confront a time domain model with a finite track length in comparison to a frequency domain continuous model, are the effect of the initial conditions on the final output results and the end effects due to displacement reflections. Even considering the problems the criteria for selecting the time domain approach was to enable modelling of variations along the track structure. Thus aspects of the stability of the model must be addressed.

There are a number of crucial components of the system which have the following frequency response characteristics which can be determined from the modal analysis contained within chapter five at a speed of 110 kmhr^{-1}:

Vehicle body	1–2 Hz	30–15 metre wavelength
Bogie	5–6 Hz	5–6 metre wavelength
Track	20 Hz	1–2 metres

These responses become important in a time domain model as the length of the track section modelled becomes highly dependent on the particular phenomena of interest. Thus a model of 24 bays length or 15 metres can only adequately consider responses that relate to the bogie and track. A model of greater length and hence complexity would be needed to model the effects due to the vehicle body. At these sorts of wavelengths a simple vehicle model also becomes questionable. To allow for the variations in vehicle vertical, pitch and roll movements the vertical and roll of the vehicle can be set at a fixed value. Although the movement of a vehicle through the defects considered in this thesis may occur the relative insensitivity to these short defects introduces to the authors belief only a small error in the final results.

Depending on the damping parameters any error in the initial conditions will have the differing effects on the time required to damp out the system. Figure 3.15 shows the model responses due to the initial conditions currently used.

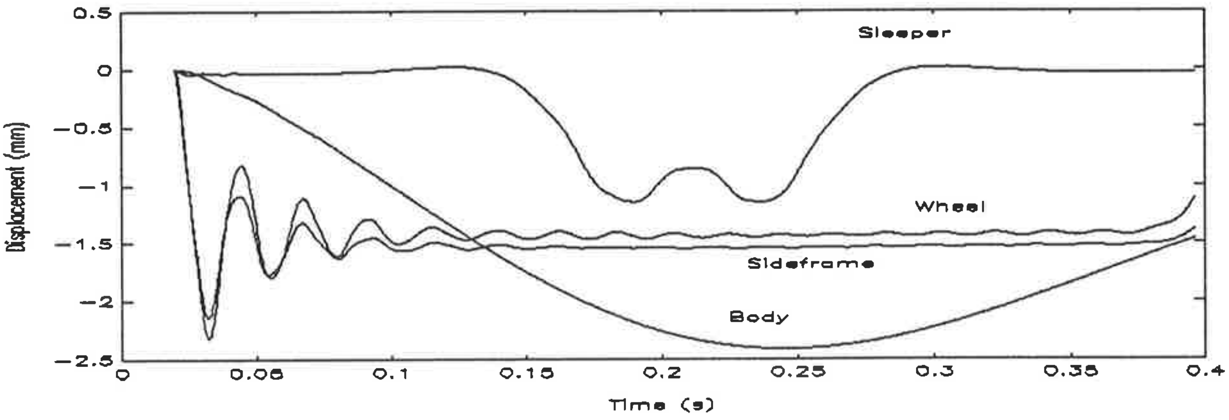

Figure 3.15 Model convergence

To allow for the effect of assumed initial conditions and the accuracy of the final energy outputs it is important that all transients are damped out by bay six or T = 0.13 seconds at 110 km/hr. As such the body motion has been fixed at a predetermined level thus removing the problem of the 1-2 Hz type of frequencies.

3.8 NUMERIC ACCURACY

The numeric accuracy of the model was tested from a range of 10^{-3} to 10^{-6} with the results as listed in table 3.5.

ACCURACY	BALLAST DAMPING @ SLEEPER 12 ($kNsm^{-1}$)	% improvement
10^{-3}	13.210	
10^{-4}	14.178	7.33 %
10^{-5}	14.199	0.15 %
10^{-6}	14.202	0.02 %

Table 3.5 Numeric accuracy

CHAPTER 4 EXPERIMENTAL WORK AND PARAMETER DETERMINATION

4.1 INTRODUCTION

This chapter describes the experimental work carried out to determine both the model parameters, and the effects of certain defects on the settlement rate of the track structure. The method of signal analysis and the determination of the field results are shown in some detail. The parameters used in the model runs are listed in section 4.11.6.

Dynamic measurements using vertically mounted accelerometers were undertaken due to the need to measure the high frequency response of the track structure under the action of moving vehicles. Accelerometers offered the wide frequency range and removed the need to provide a fixed reference point about which to measure the track vibration. Another advantage of the accelerometers was the ease in mounting and transportation compared to the equipment and facilities required for other forms of measurement. A number of alternative methods were also investigated such as displacement transducers and high speed film cameras, but these either proved not feasible to mount in such a position to provide an absolute reference (deeply piled rods in the case of displacement transducers), or vibration problems under traffic (when the high speed camera was used there were problems with ground vibration and a difficulty to sight the light pen marker on the target mounted on the rail). Thus this chapter details the experimental method that was used, and the signal processing undertaken to obtain an estimate of the tracks vertical displacement.

4.2 SITE DESCRIPTION

A site on the Trans Australia Railway (22 km north of Port Pirie in South Australia) was used to provide experimental data to assist with the validation of the model, and to provide settlement data of the track for the defects that were present. The test site selected was chosen because it has the typical Australian National track characteristics of being built with prestressed concrete sleepers at 666 mm spacing and 47 kgm^{-1} Australian Standard rail which had been continuously welded. It also had the ability to be able to accommodate test speeds of up to 140 $kmhr^{-1}$ and was on a straight section of track.

4.3 VEHICLES

The vehicles that are believed to cause the majority of the track damage can be categorised into three basic types, locomotives that have three axle bogies with 21 tonne axle loads, freight bogies without suspension elements from the axle to the bogies, which have axle loads ranging from 5 to 25 tonnes (three piece bogies), and bogies used for both freight and passenger vehicles that have suspension elements between the axle and bogie, with axle loads again ranging from 5 to 25 tonnes (primary suspension bogies).

Over the various test days the train consist was marshalled to provide a mixture of locomotives and vehicles. These consists are listed in appendix three. Of the vehicles used in the tests only a limited number were selected to provide data for the model validation. The vehicles selected were the GM class of locomotives, a primary suspension freight vehicle AQMH 4228 (which was kept at the same load throughout the tests) and a three piece bogie freight vehicle AQMH 4247 (with variable axle loads as listed in table 4.8). These three types of vehicles provided a range of loading conditions that could be used in the model analysis.

4.4 DYNAMIC MEASUREMENTS

Dynamic measurements were taken using high frequency vertical accelerometers placed on the rail foot or sleeper. By doubly integrating these results displacements of the track under load were obtained. These results are needed to allow calibration of the model through ballast stiffness adjustments.

The accelerometers were mounted directly onto the sleepers via an epoxy glue connector. They thus responded to the vibration of the sleeper over the full range of sensitivities of the accelerometer.

The raw experimental data was stored on two channels of an eight track analogue tape recorder, after passing from the accelerometers through the accelerometer amplifiers by cables, over a 300 metre distance.

4.5 STATIC TRACK MEASUREMENTS

Four track test sites were selected that provided three different types of vertical rail surface geometry defect types, and one site that had been machine ground to provide a location that was close to defect free to be used as a control.

Measurements without trains were taken of all the weld defect sites using a "Geissmar" profile measurement device that provides a plot over a 1.2 metre long rail section showing the deviation away from a fixed baseline onto a graphical hardcopy that can then be digitised. This provides the basic information to be used by the model to predict the dynamic action of the track structure.

A survey of the sites at each of the sleeper locations over ten sleepers either side of the defect, was undertaken to an accuracy of one mm, with these measurements being undertaken directly after lifting and tamping, but before any traffic had run over it and then four weeks later to determine the initial settlement. Data for the three sites that contained defects are shown in figure 4.1.

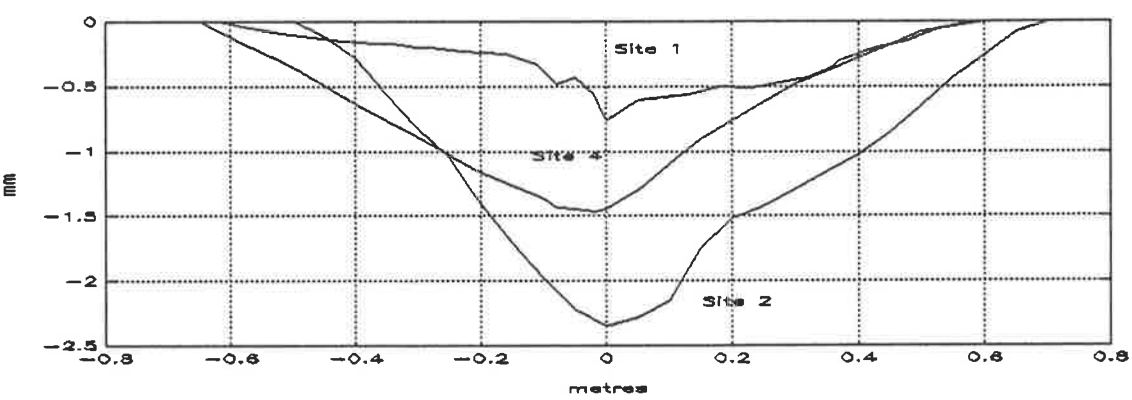

Figure 4.1 Test site weld shapes

4.6 MAXIMUM DISPLACEMENT

A number of tests were carried out with cork blocks sliding on vertical rods, welded to a steel baseplate, as shown in figure 4.2, that gave an estimate of the maximum rail deflection after the passage of a train. These were undertaken to provide an approximate estimate of the accuracy of the displacements derived from the accelerometers. A design limitation is that they sit on the ballast at the sleeper level, and thus move with the ballast with the result that they may not fully respond to the movement of the rail.

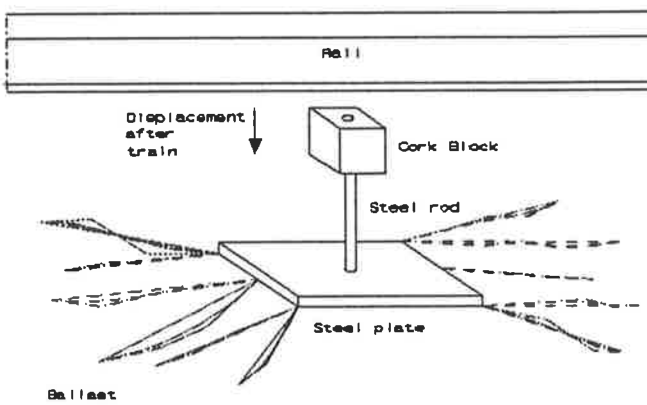

Figure 4.2 Cork block displacement

Another limitation is that they only give results for the maximum displacement for the complete train so that it is not possible to precisely determine which vehicle caused this maximum value. Given these limitations, they still give an estimate of the maximum deflections as a check on the double integration results.

RUN No	Speed	Site 1	Site 2	Site 3	Site 4
	Crawl	2.1 mm	2.1 mm		
	Passenger Train	2.0 mm	2.5 mm		
R 115	100 km/hr	2.3 mm	3.1 mm	1.1 mm	2.0 mm
R 116	110 km/hr	2.4 mm	3.0 mm	1.2 mm	2.2 mm
R 117	120 km/hr	2.4 mm	3.0 mm	1.2 mm	2.3 mm

Table 4.1 Cork block displacements

4.7 DIGITISATION

To extract the accelerometer data the personnel computer, digital signal processing system CTRAN [62] was used due to its availability to the author. Various data sampling rates were tried to ensure that the final rate used was greater than the Nyquist frequency, thus ensuring that the signal is fully represented by the digitised results. A rate of 32 000 Hz was chosen and as shown by a section of the digitised signal from one of the accelerometers in figure 4.3, the necessary sampling rate has been achieved.

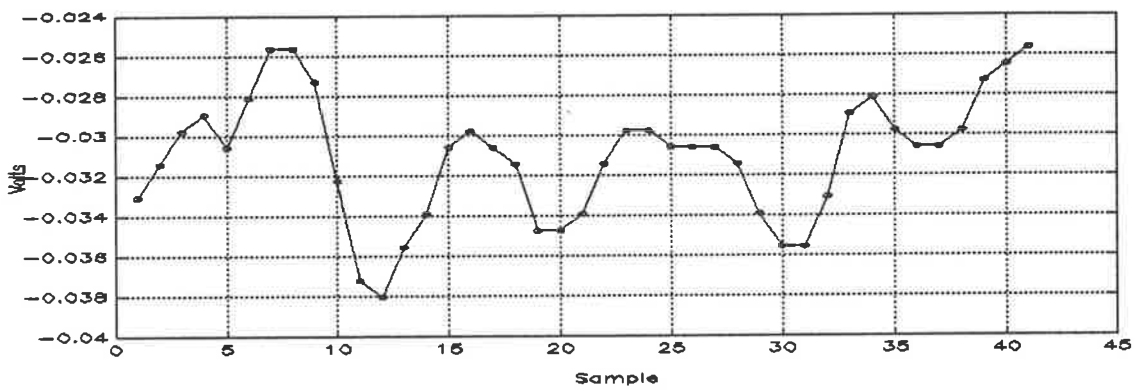

Figure 4.3 Sampling rate

With a typical length of 10 seconds for a run the data for one channel can be stored on a single 1.44 MB floppy disk. The file names for the data that have been digitised are listed in appendix three. This is the form in which the data are stored for the long term with the original analogue recordings being also retained for future analysis if required.

The next stage of the signal analysis involved the CTRAN software being used to extract certain sections of the data as required for further processing by MATLAB (generally 18 000 samples in length or 0.5 seconds). The sections selected are based on the capturing of either the lead or trailing bogies of the train or pairs of adjacent bogies from coupled vehicles through the length of the train itself. The listing is located in appendix three.

The disk containing the complete train run data can then be loaded and converted to MATLAB format by use of the CTRAN "Bounds" command over any of the first, last or intermediate pairs of bogies.

Limited number of runs were extracted to provide data for the calibration of the model. Sleeper vertical accelerations were extracted for work in this research as the parameter was the one that needed the most of the experimental work to help determine the effective ballast and formation stiffness. Only a limited number of vehicles were also used as their parameters were well known and defined. The vehicles used were the GM locomotives and vehicles AQMH 4228 and AQMH 4247. The list of each data run extracted are detailed in appendix three.

4.8 CALIBRATION

The accelerometer channels are calibrated by the transmission of a ±1.414 Volt signal from the acceleration amplifier, which is then recorded onto the analogue tape. This voltage is multiplied by the calibration factor to provide the conversion between volts and acceleration in ms^{-2} . Three sets of calibration factors were calculated for the different sets of data that had been extracted. Figures 4.4, 4.5 and 4.6 show a section of the calibration voltages sampled at 4 000 Hz.

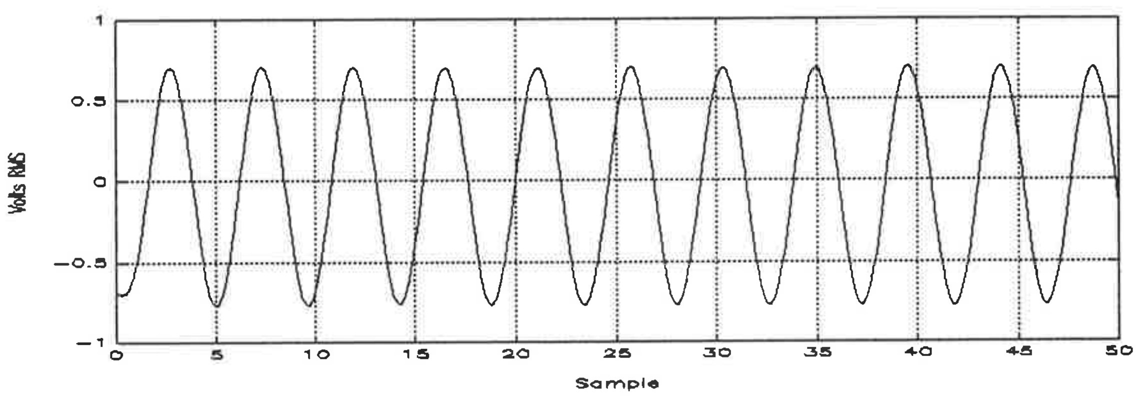

Figure 4.4 Run 67, ± 1.414 Volt signal recorded on tape

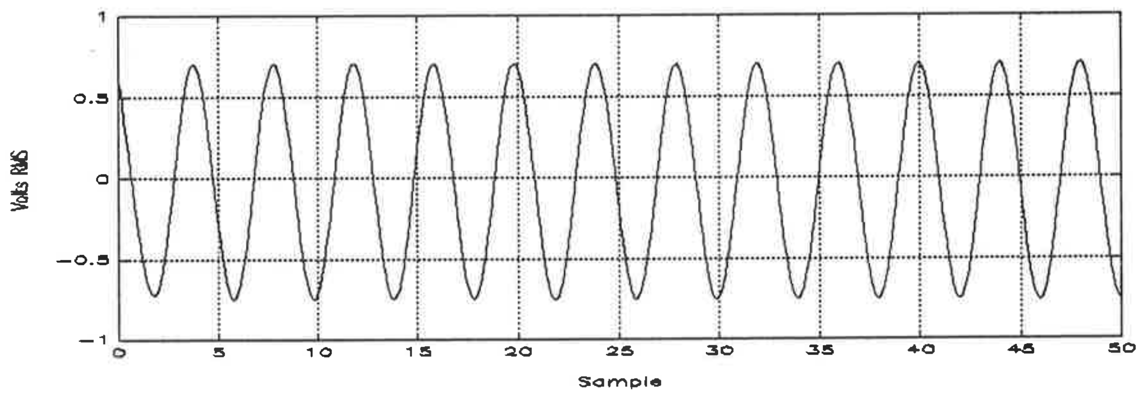

Figure 4.5 Run 85, ± 1.414 Volt signal recorded on tape

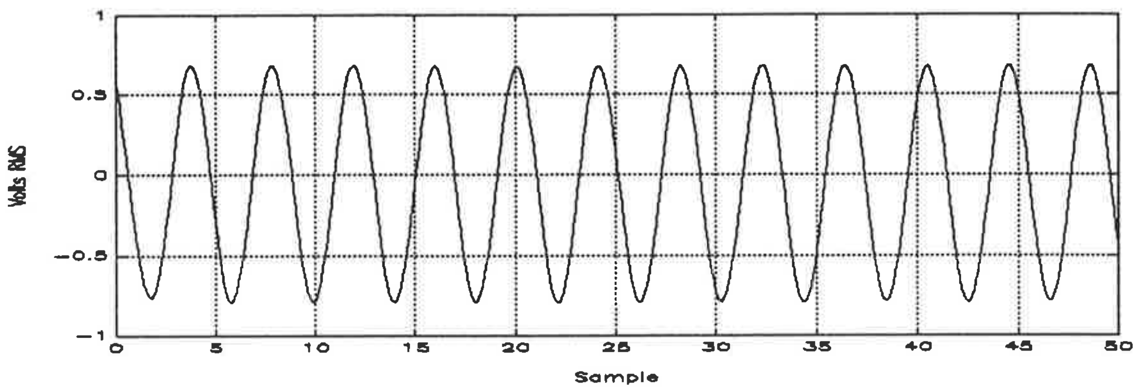

Figure 4.6 **Run 112, ± 1.414 Volt signal recorded on tape**

Positive and negative peak voltages from each of these plots have been extracted and listed in table 4.2. Utilising the known accelerometers manufacturers calibration factors and amplification factor (x1000) enables a conversion factor from volts to acceleration to be obtained as shown in table 4.2 using the formula;

$$\mathit{Calibration\ factor} = 1000 * \frac{2 * 1.414}{\mathit{difference}} * \mathit{accelerometer\ factor}$$

RUN	Max +ve voltage	Max -ve voltage	Difference	Accelerometer factor (manufacturers)	CALIBRATION FACTOR
R67	0.6925	-0.7705	1.463	0.9987	1930
R85	0.7128	-0.7542	1.467	0.9987	1925
R112	0.6803	-0.7949	1.475	0.9987	1930

Table 4.2 **Calibration data**

4.9 PROCESSING

The MATLAB software that was used for the model runs is again utilised to doubly integrate the raw acceleration signals into displacement plots. This has been done through a MATLAB program called FFTINT2.M and has been written to carry out the following calculation stages that digitally convert data from a raw acceleration result (volts) to displacement (metres).

The sections that follow show how the signal at each stage of the process is converted. This example is for run R97Z which is vehicle AQMH 4228 at a speed of 110 km/hr. The method of double integration is based on the comments by Lynn [63] in the discussion of digital filters that the magnitudes and phases of various frequency components may be adjusted in accordance with the desired filter characteristics, and the filtered time domain signal evaluated by inverse transformation. Lynn [63] (page 179) also details how a single integrator in the frequency domain is

$$H(s) = \frac{1}{s} \quad \text{where} \quad s = j\omega$$

thus a double integrator is given by. $\dfrac{1}{-\omega^2}$

This relationship is also noted by Thomson [23] [14 1.1-6] who says that displacement and acceleration are related in harmonic motion by the formula

$$\ddot{x} = -\omega^2 x$$

which rearranged gives

$$x = \frac{\ddot{x}}{-\omega^2}$$

4.9.1 The raw digitised acceleration data from disk (which is stored as a two column matrix with time and voltage readings) is loaded into the computers memory. As the time steps are constant, the actual recorded times are discarded and a single vector of voltages remains.

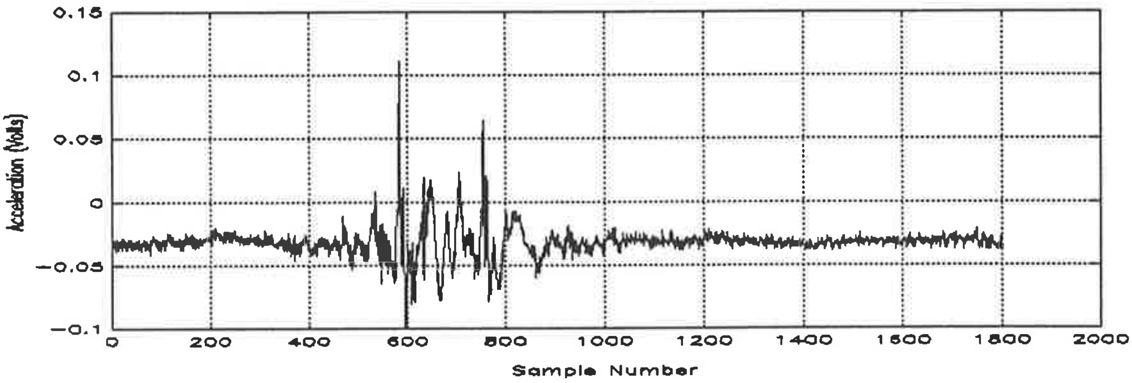

Figure 4.7 Raw voltage signal

4.9.2. The voltage is then multiplied by the calibration factor, as previously determined in section 4.8, from the ± 1.414 Volt signal input into the tape recorder from the acceleration amplifiers.

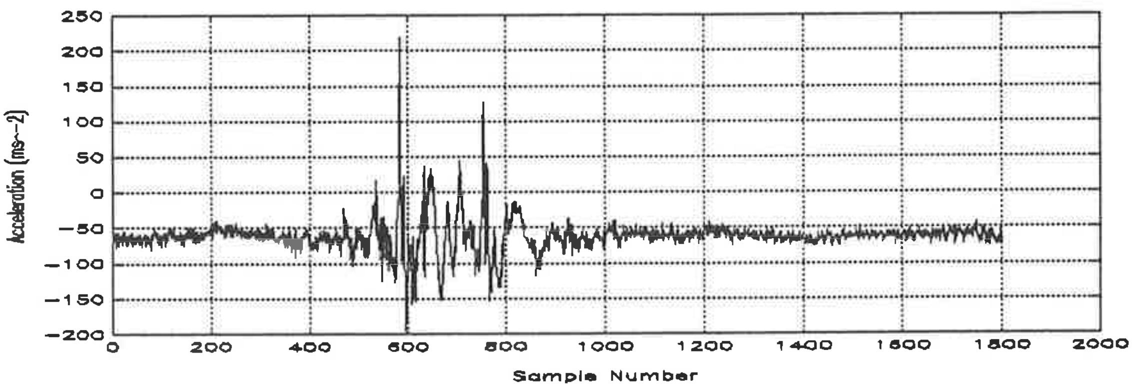

Figure 4.8 Raw acceleration data

4.9.3. The end points of the data is then adjusted to zero to eliminate any end step, and consequent error, when the leading and trailing zeros are added in section 4.9.6.

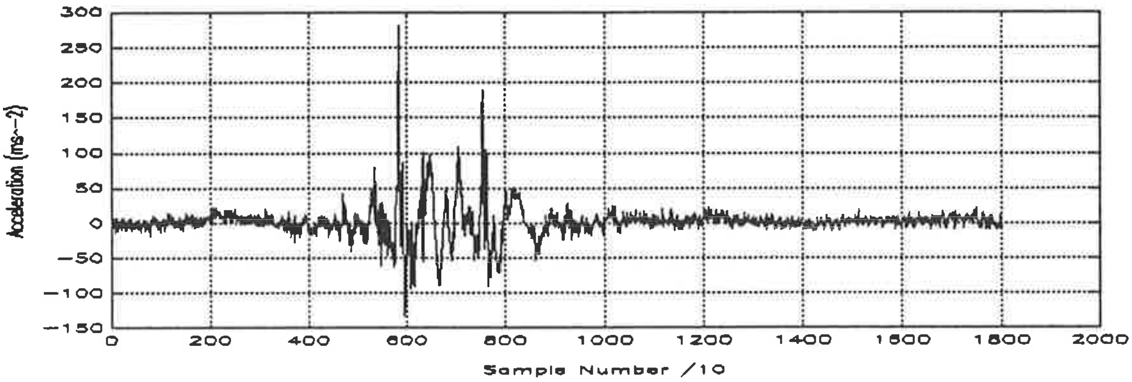

Figure 4.9 Zero corrected accelerated data

4.9.4. A Hanning window 2000 points long is created. This window is used to smooth the transitions. The Hanning window is a series of digits starting at zero, reaching a peak of one and trailing off again to zero.

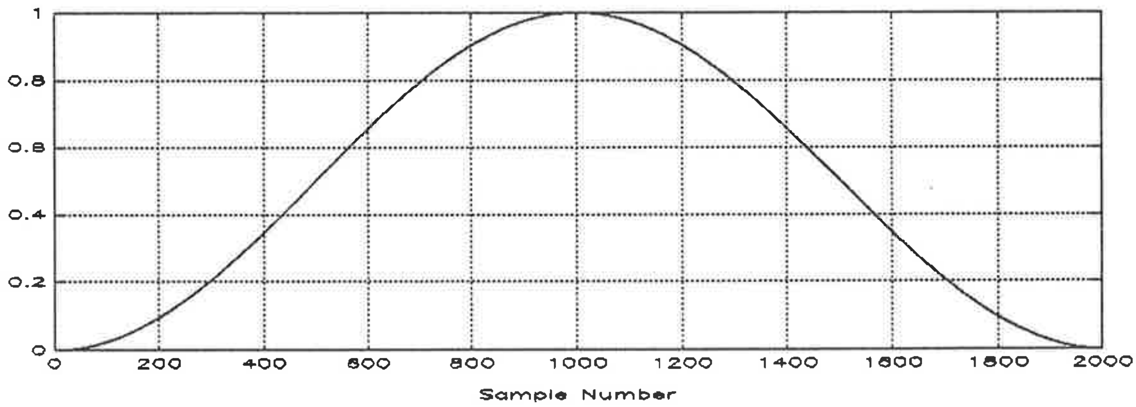

Figure 4.10 Hanning window

4.9.5. A longer window that is sufficient to cover the signal section of interest is then created. The leading tail of the Hanning window already determined, is followed by a string of ones of the required length followed by the trailing tail of the Hanning window. Each end of the window is set to zero.

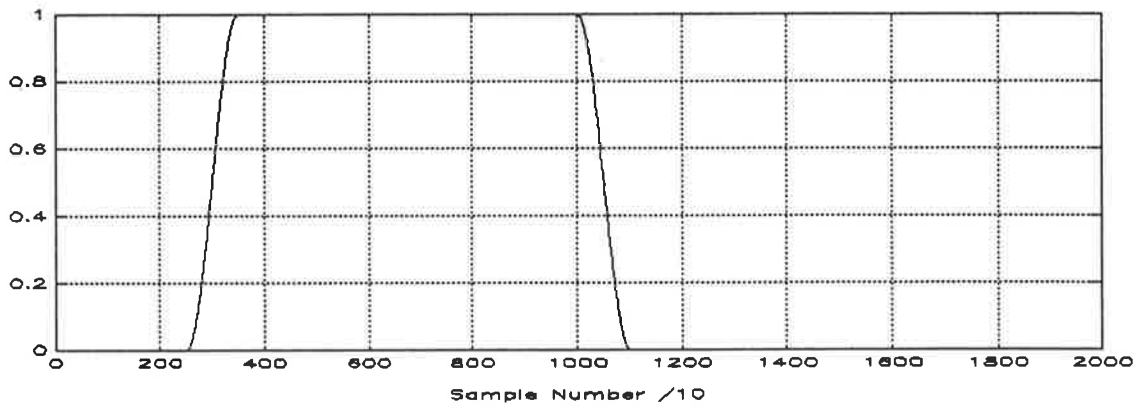

Figure 4.11 Total window

4.9.6. The signal is then multiplied by the window and has tails of zero's added to each end of the data so that an efficient fast Fourier transform analysis can be performed (This signal is 32,768 or 2^{15} points long)

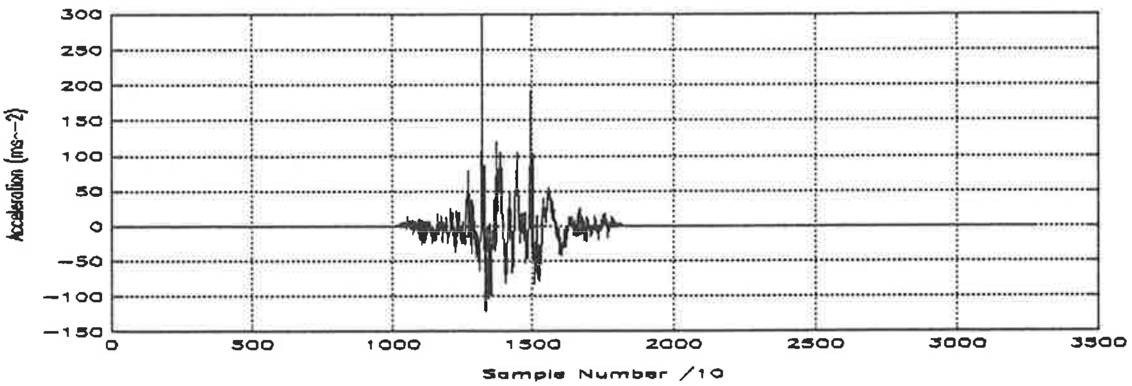

Figure 4.12 Windowed acceleration data

4.9.7. Fast Fourier transform the data in one block. The complete block is needed as the signal is non repetitive and so cannot be broken into smaller components.

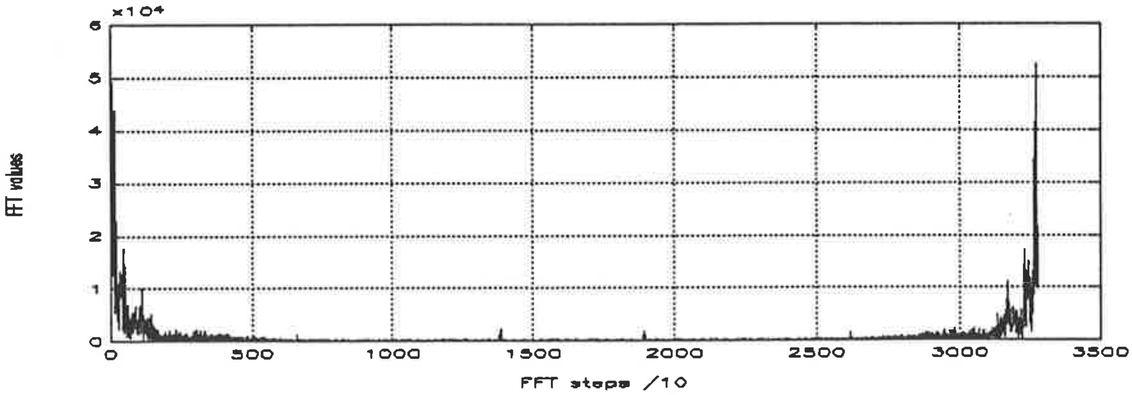

Figure 4.13 Raw frequency spectra

4.9.8. The frequency for each fast Fourier transform step is then calculated.

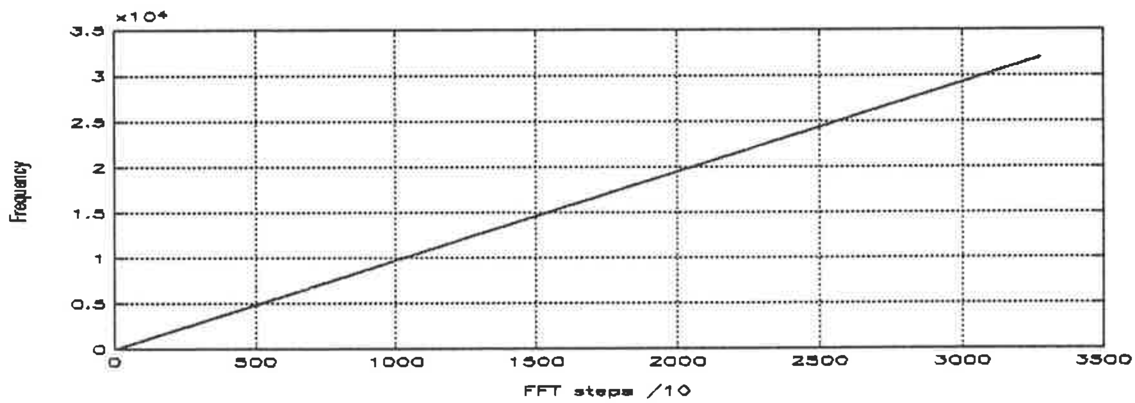

Figure 4.14 Frequency steps

4.9.9. Remove the DC drift from signal by setting first frequency value to zero.

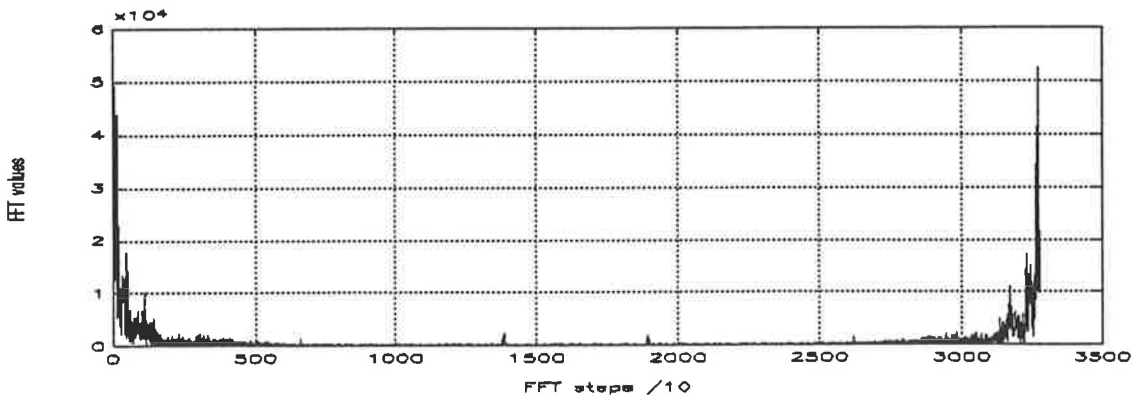

Figure 4.15 Frequency spectra (DC drift removed)

4.9.10. Divide each fast Fourier transform step by the negative squared frequency, to convert to displacement.

4.9.11. Remove 1st fast Fourier transform point which is now infinite (it has been divided by zero frequency)

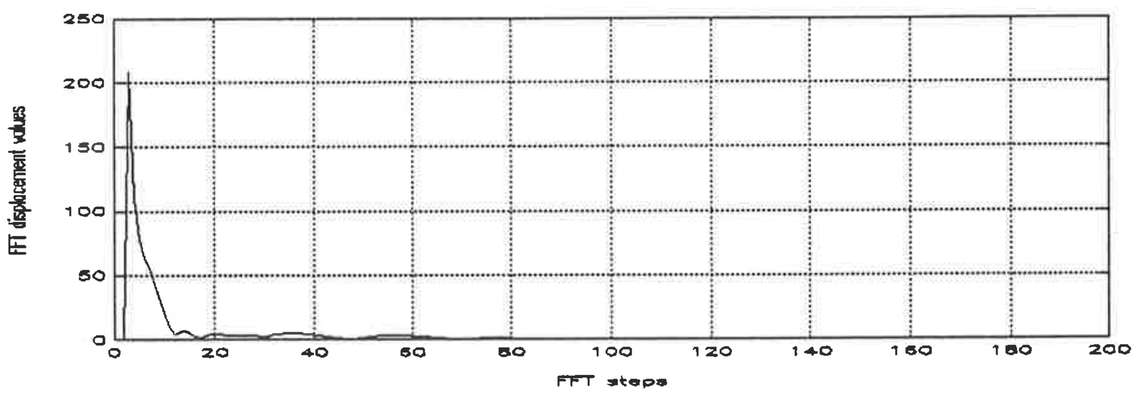

Figure 4.16 Displacement frequency spectrum

4.9.12. Calculate the inverse fast Fourier transform to recreate the displacement time history.

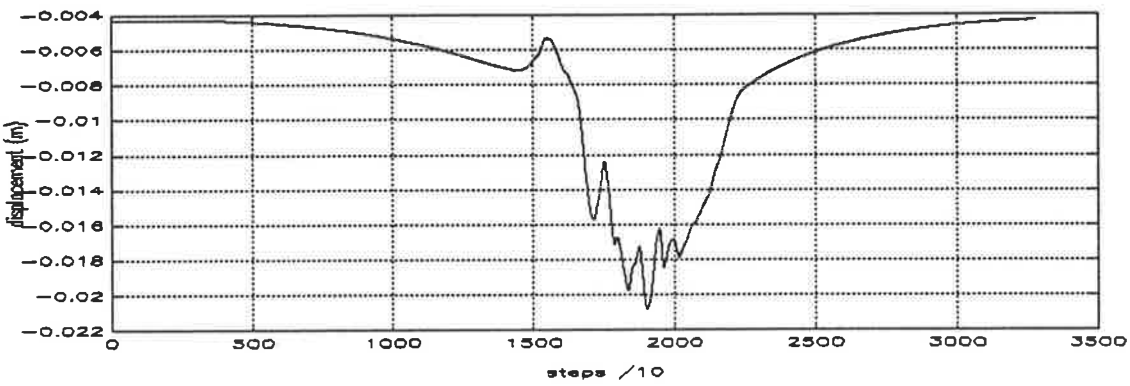

Figure 4.17 Raw displacement

4.9.13. Filter the result using a 4[th] order Butterworth filter to remove low frequency drift of the final signal.

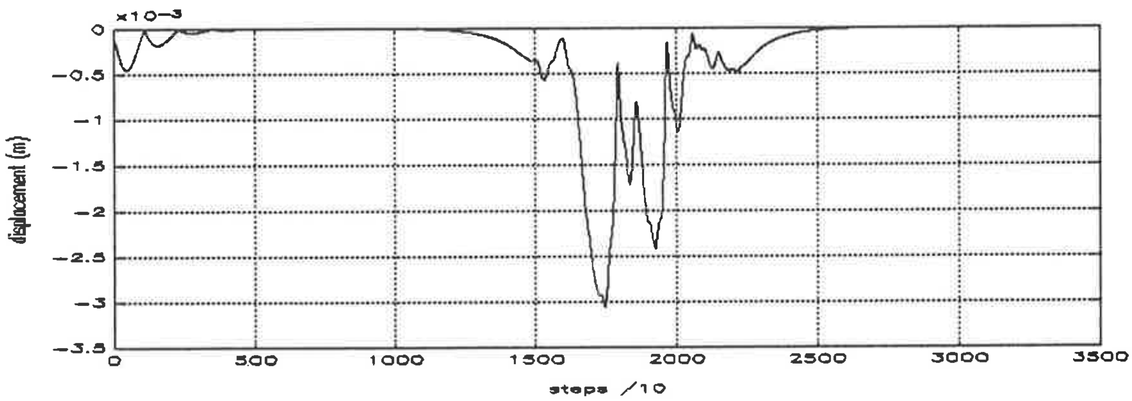

Figure 4.18 Filtered displacement

4.9.14. Plot the results detailing run number, vehicle type, speed and location. (all experimental results analysed are shown in appendix four)

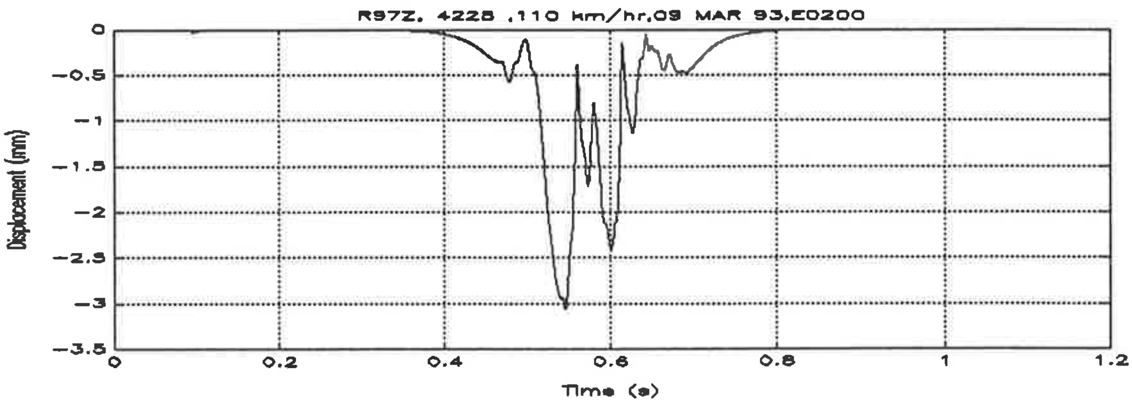

Figure 4.19 Final graph

4.10 COMPARISON OF RESULTS

The maximum displacement results as determined from the above analysis, were then plotted to permit the comparison of alternative runs shown in figures 4.20 to 4.27. As found by other authors there can be a considerable scatter of the results for seemingly identical conditions.

A possible explanation why the following variations that have not been determined experimentally could include vehicle body oscillations and hence variations in vertical force, or variations in the wheel locations across rail head with corresponding different effective defect sizes.

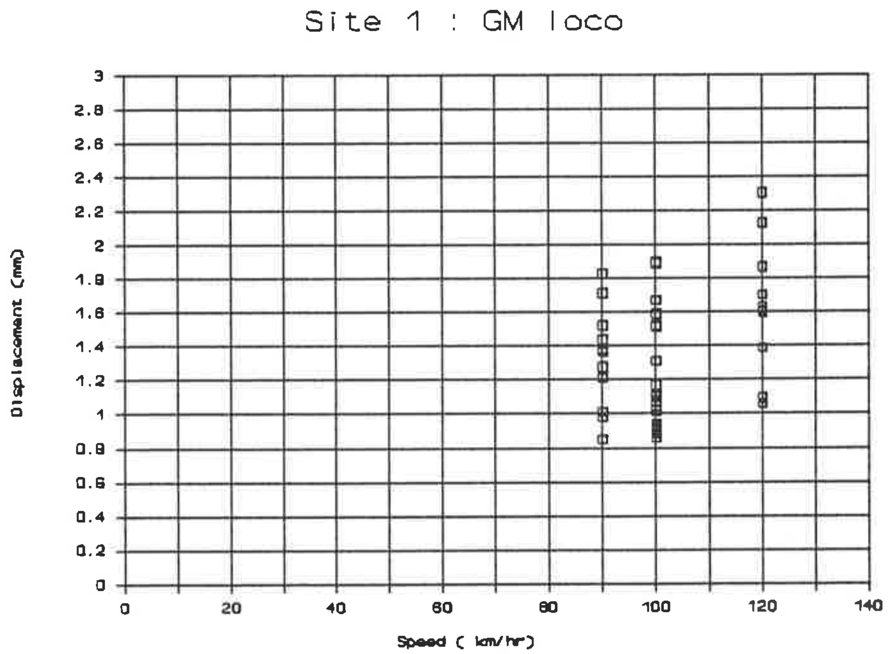

Figure 4.20 Speed/displacement, site 1, GM loco

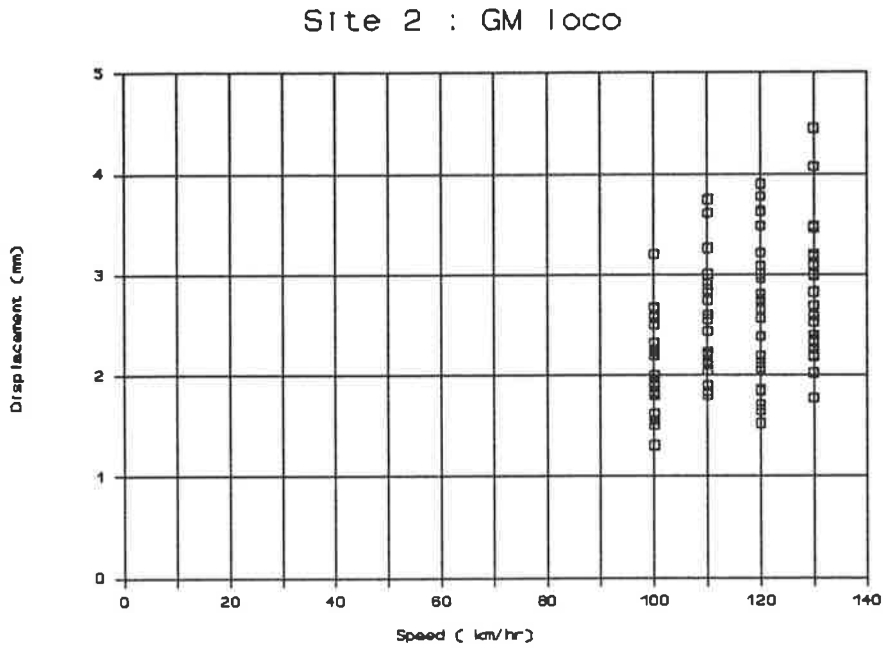

Figure 4.21 Speed/displacement, site 2, GM loco

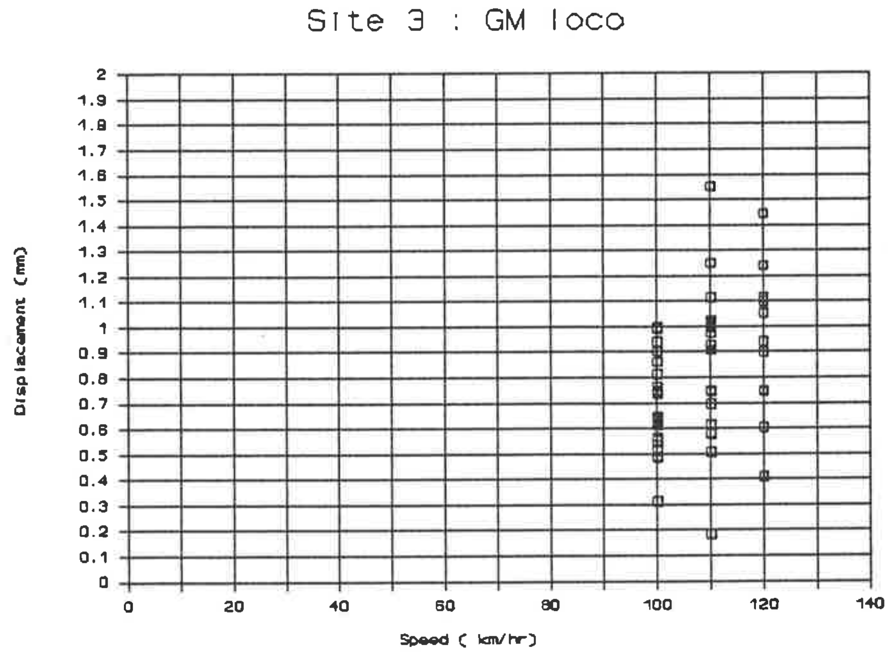

Figure 4.22 Speed/displacement, site 3, GM loco

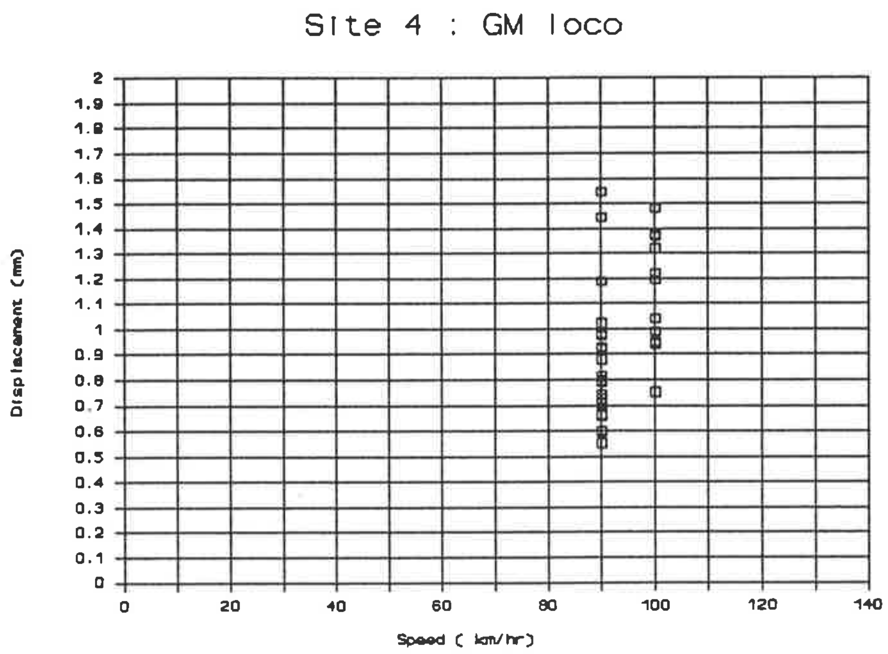

Figure 4.23 Speed/displacement, site 4, GM loco

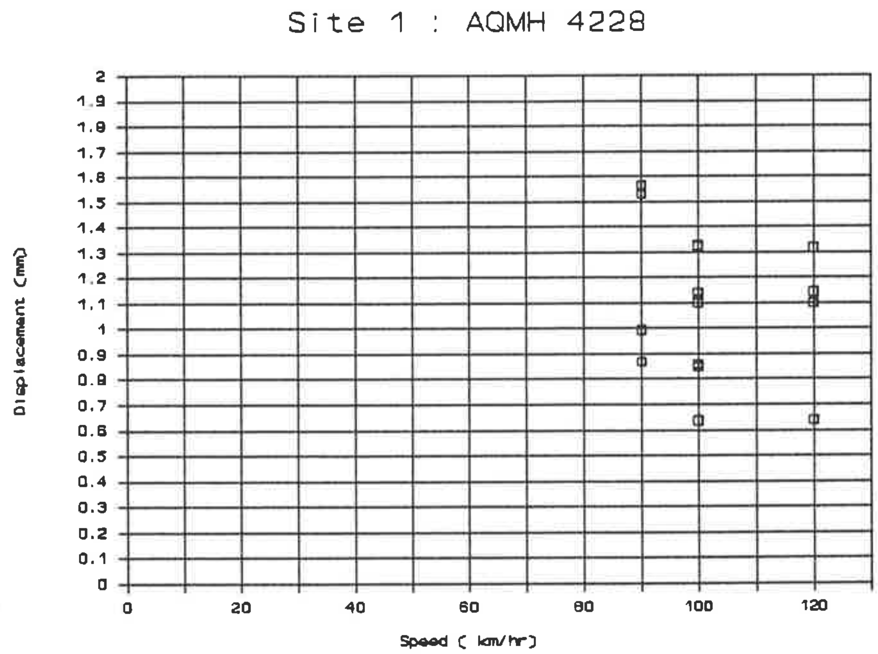

Figure 4.24 Speed/displacement, site 1, AQMH

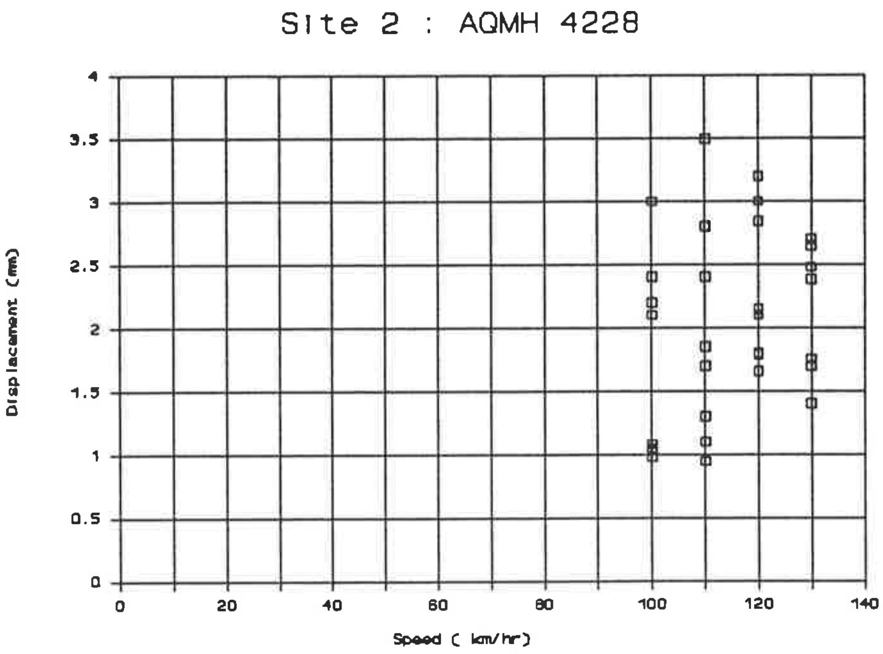

Figure 4.25 Speed/displacement, site 2, AQMH

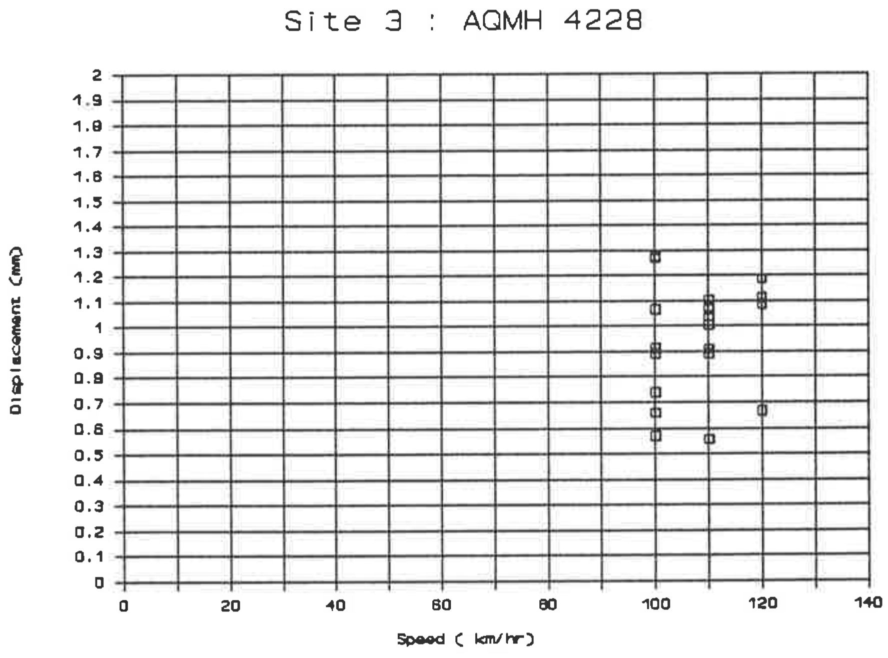

Figure 4.26 Speed/displacement, site 3, AQMH

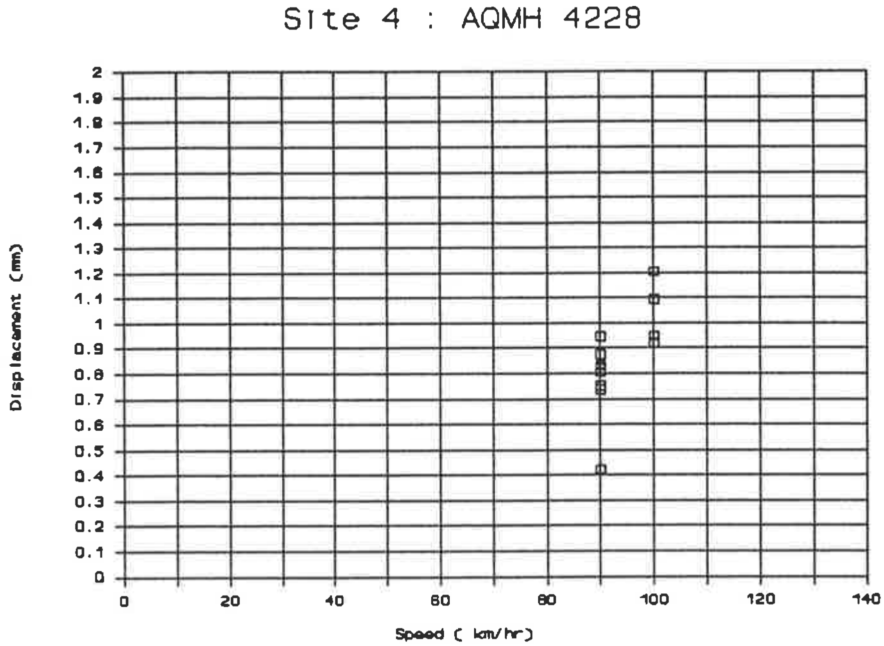

Figure 4.27 Speed/displacement, site 4, AQMH

The results that are used to proceed into the parameter determination phase as estimated from the above graphs are, for a speed of 110 $kmhr^{-1}$ shown in table 4.3.

	SITE 1	SITE 2	SITE 3	SITE 4
GM locomotive	2.0 mm	3.3 mm	1.2 mm	1.5 mm
AQMH 4228	1.3 mm	2.8 mm	1.1 mm	1.2 mm
CORK BLOCK	2.4 mm	3.0 mm	1.2 mm	2.2 mm

Table 4.3 Test site displacements

The maximum displacement from the cork block devices are shown to increase the confidence in the results obtained from the double integration.

4.11 TRACK PARAMETER DETERMINATION

The parameters for use within the model come from primarily two different types of sources, previously well defined physical parameters from design drawings, manufacturers data or literature reference's in addition to experimentally derived values. The reference values are usually not site dependent and are assumed for this study to be linear in nature. The more difficult parameters are those which are highly dependent on local conditions and can only be ascertained from experimental results.

4.11.1 RAILS

The rail parameters used are those defined by AS 1085, part one, 1981, page 11, for 47 kgm^{-1} Australian Standard rail. The losses due to wear on the top surface are assumed to be minimal and thus no correction for this potential error has been included. This factor would need to be allowed for in areas of significant rail material loss, but not in the situations studied.

Mass per linear metre = 47 kg

Young Modulus = 207 GPa

Second Moment of Area = $15.41*10^{-6}$ m^4

Therefore flexural rigidity (EI_r) = 3.19 MNm^2

4.11.2 RAIL TO SLEEPER PAD

The rail and sleeper are separated by a rubber pad, although this is highly nonlinear it has an assumed linear stiffness and damping detailed in section 2.3.

As the pad is modelled as a spring and damper element the mass of the pad itself is ignored. Grassie [25] has determined that for well compacted ballast, the tracks dynamic behaviour is little affected by railpad damping. In support of this claim it is well understood that the damping of the 5 mm cork bonded rubber pads used in the test are of a low energy absorbance type and have little effect on the total track energy loss.

Under laboratory conditions the stiffness of a 10mm composite pad has been estimated by Grassie to be 125 MNm^{-1} therefore for a 5 mm pad this stiffness would double to 250 MNm^{-1}. Other work by Grassie on rail pad stiffness gives results such as pad stiffness of 280 MNm^{-1} and corresponding pad damping of 63 $KNm^{-1}s$.

The typical pads that are in use on Australian National and those that were used in the test sections are 5 mm in thickness and as such can be modelled as a spring having twice the stiffness of a 10 mm pad or equal to 250 MNm^{-1}.

4.11.3 SLEEPERS

For prestressed concrete sleepers there is a variability in section size along the length of the sleeper between the rail seat at its greatest depth, waisting down to the centreline. This variation had been shown in section 3.2.6. A uniform section sleeper is required to permit simplification of the numeric routines. The method discussed by Grassie [8] is used, in which he has determined that for the typical Australian National prestressed concrete sleepers used (designated CR2) in the test site, that an equivalent uniform flexural rigidity can be estimated from;

$$\frac{1}{EI}=\frac{1}{2E}\left(\frac{1}{I_1}+\frac{1}{I_2}\right)$$

where I_1 and I_2 are the moments of inertia of the non uniform sleeper at the railseat and centre respectively. For the CR2 design parameters of;

E = 43 GPa

EI_1 = 2.70 MNm^2

EI_2 = 7.71 MNm^2;

this results in the effective flexural rigidity being equal to 4.00 MNm^2.

4.11.4 TRACK STIFFNESS

Track stiffness is an area where experimental work needed to be undertaken due to the wide variety of values that exist in reality, primarily due to the variable geotechnical nature of the ballast and formation. The method used was to run the model with all of the known parameters and vary the track stiffness until the value of the displacement agreed with that determined experimentally, as determined in section 4.10. The results are shown graphically in figure 4.28, the results shown as circles and a linear plot drawn through them with an estimate of the linear stiffness.

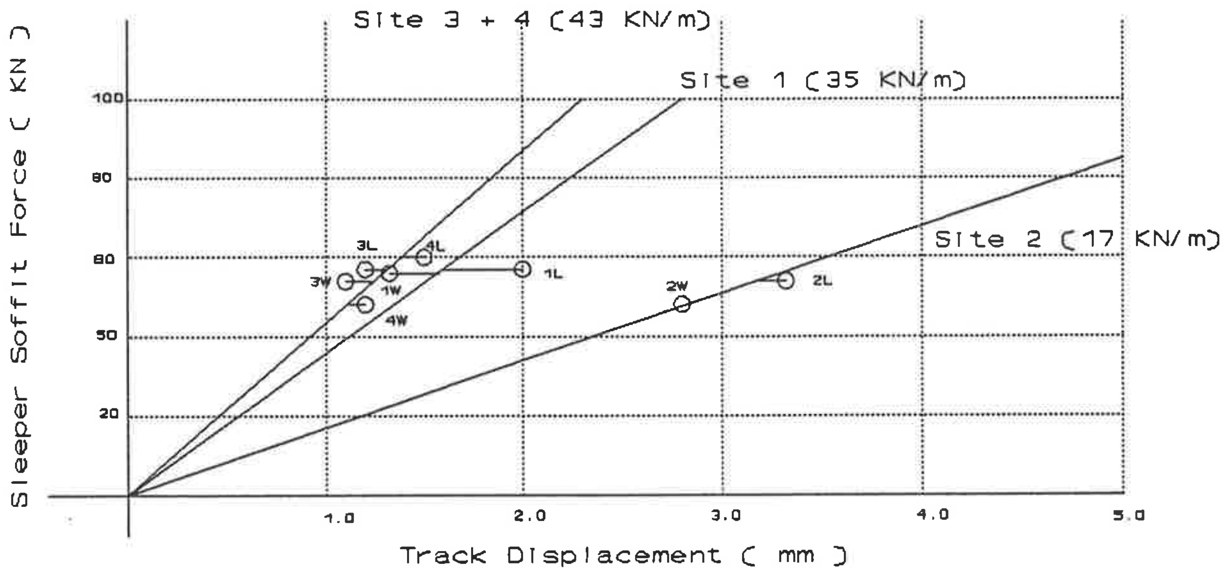

Figure 4.28 Ballast displacement/force

To ensure that the values derived from the experimental work are within the accepted range of values, the following table shows values as having being previously determined by other authors. Note that the results need to be modified to 40% of the value if the model was of the beam on elastic foundation type.

Author	Reference	Stiffness MNm^{-1}
Jenkins	13	average conditions 50 high level 94
Grassie	9	72
Ishida	12	20
Lyon	64	104
Shugu	65	68 – 83

Table 4.4 Track stiffness

Due to the relatively thin layer of ballast which exists on Australian National tracks it was expected that the values obtained will be at the lower end of the stiffness range. The range that has been obtained of between 17 and 43 MNm^{-1} is thus acceptable as it falls within the range quoted by Ishida and Jenkins.

4.11.5 TRACK DAMPING

Mair [43] states that "In principle the track damping may be estimated from the rate of decay of the free vibrations induced by a loaded impulse. This could be achieved by rolling a vehicle up a gradual ramp on a rail surface and allowing it to drop back onto the rail. In practice this is seldom done since the system is usually heavily damped and a value of the damping parameter is adopted between 8 to 18% of critical damping" for an equivalent viscous damper.

The closest that this effect could occur was if the track started vibrating under circumstances that were not being driven by a wheel. This could conceivably occur when the wheel bounces and loses contact. A study of the time histories of the acceleration readings revealed that this phenomena could have occurred at least twice over the period of the trials.

In the following two examples, time histories are shown over a series of three positive and three negative peaks. The logarithmic decrement curve is estimated for the upper and lower series of peaks.

For experimental run R76 it can be seen that by investigating the voltage pattern as shown in figure 4.29

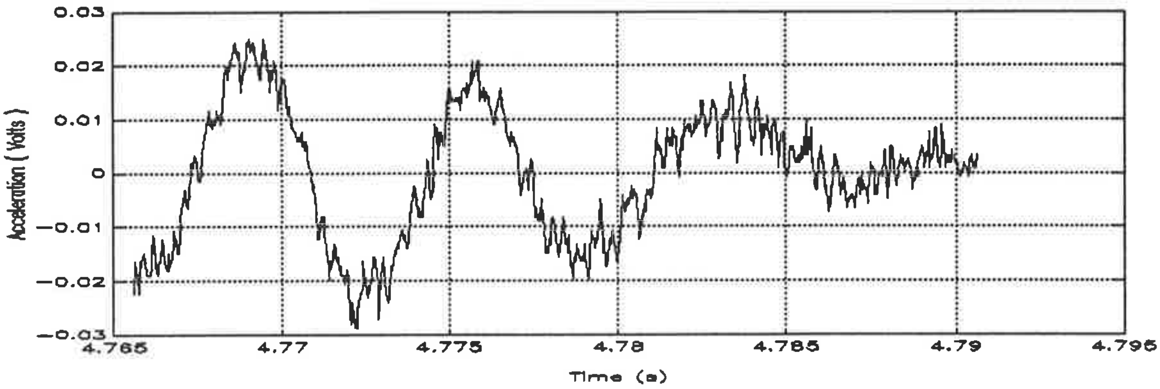

Figure 4.29 Damping run 76

and by utilising the equation for logarithmic decrement of;

$$\delta = \frac{1}{n} \log_{10} \left(\frac{X_0}{x_n}\right)$$

then a damping coefficient can be estimated at

	Upper	Lower
1st Peak voltage (X_o)	0.0240	-0.0208
3rd Peak voltage (X_2)	0.0101	-0.0050
Decrement %	19%	30%

Table 4.5 Damping run 76

and for run 67 given the following experimental result;

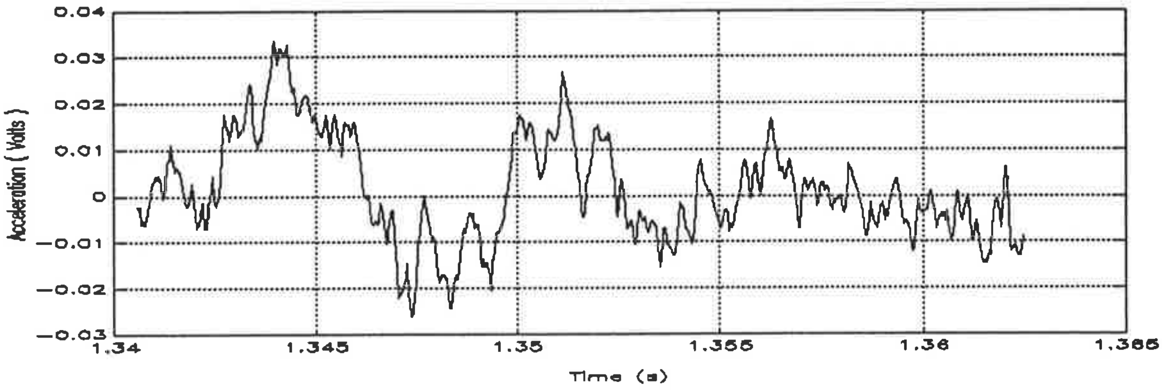

Figure 4.30 Damping run 67

	Upper	Lower
1st Peak voltage (X_0)	0.0257	-0.0189
3rd Peak voltage (X_2)	0.0093	-0.0060
Decrement %	22%	25%

Table 4.6 Damping coefficient run 67

The average of these decrements is 24% which is the value that is used in the model which equates, for a track stiffness of 43 MNm^{-1}, and mass of 31 kg for rail and 143 kg for the ½ sleeper mass to a damping constant of 42 $kNsm^{-1}$.

These results can be compared to the literature results shown in table 4.7 (note again that the continuous models are corrected by a factor of 0.4).

Author	Reference	Damping ($kNsm^{-1}$)
Jenkins	13	52
Grassie	9	33
Ishida	12	60
Lyon	64	300
Cox	42	50 tamped, 100 well settled

Table 4.5 Damping factors

where the result obtained of 42 $kNsm^{-1}$ falls in the range quoted by Jenkins and Grassie.

4.11.6 TRACK SUMMARY

In summary the following track parameters are used in the model for all of the vehicle types.

mr = 47 kgm^{-1}

ms = 292.6 kg

EIr = 3.19 MNm^2

EIs = 4.00 MNm^2

kp = 250 MNm^{-1}

cp = 20% of critical

kb = Site 1 35 MNm^{-1}

Site 2 17 MNm^{-1}

Site 3/4 43 MNm^{-1}

cb = 24% of critical

4.12 VEHICLE DATA

There are three basic types of vehicle that are modelled in this study. Figure 4.31 shows the schematic diagram for a locomotive which has three axles per bogie. The bogie is heavy and the three wheelsets are also heavy due to the contribution of the traction motors.

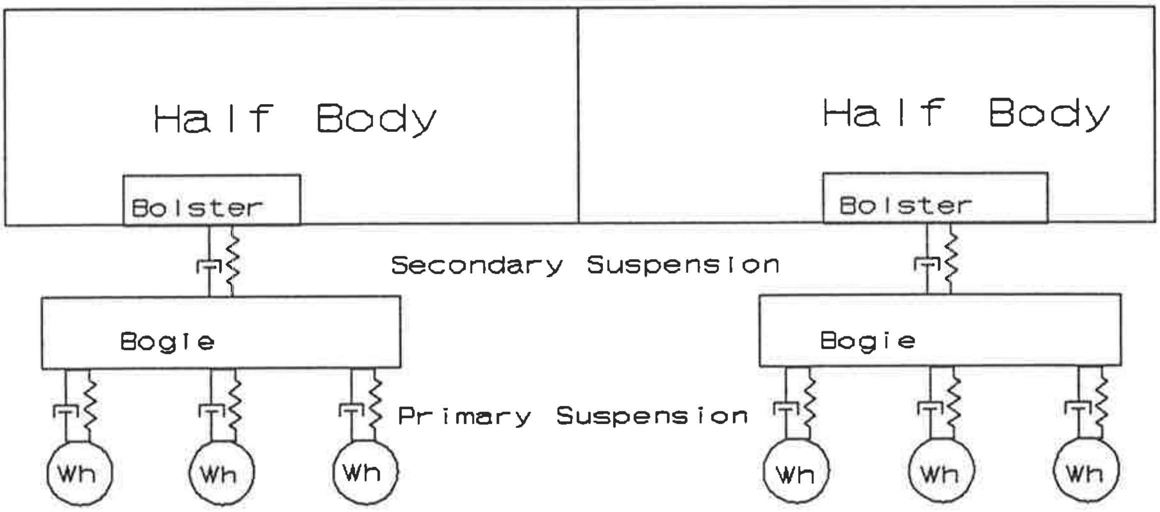

Figure 4.31 Locomotive Schematic Diagram

The locomotive is modelled however in a simplified form similar to that for a primary suspension bogie which is shown in figure 4.32. Although the parameters for mass are different an equivalent model is derived that permits the analysis of the locomotives.

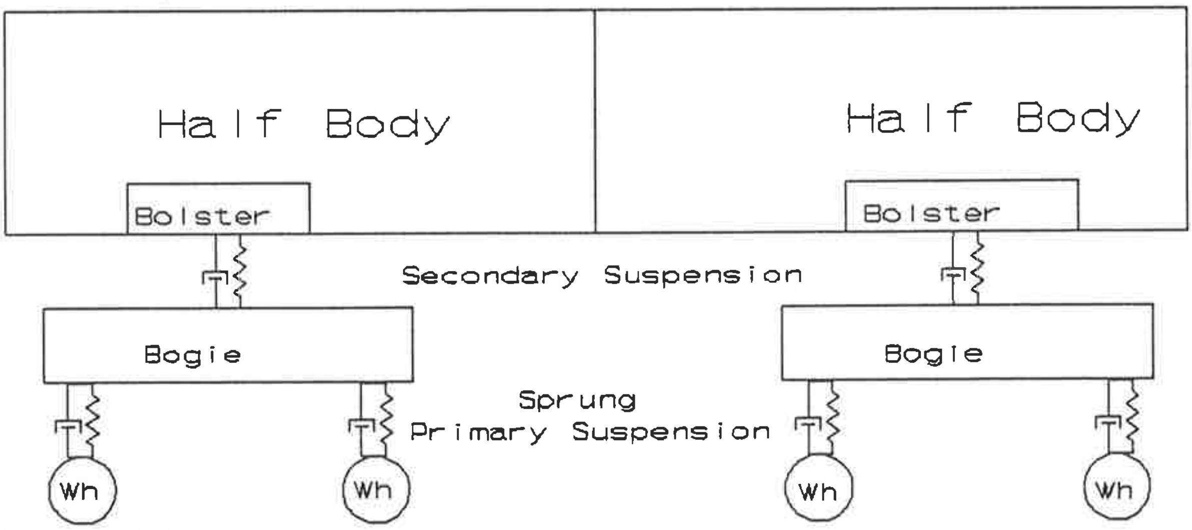

Figure 4.32 Primary suspension bogie

The third type is the three piece bogie which is characteristic of most freight bogies now in existence in Australia today. The differences between the above two bogie type of vehicles and these is that instead of a single piece bogie the two wheelsets are separated by two sideframes which are independent of each other. No suspension is placed between the wheelsets and sideframes, but for modelling purposes a very stiff spring is included. The main suspension comes from the springs held in the sideframes which support the bolsters and hence the remainder of the vehicle.

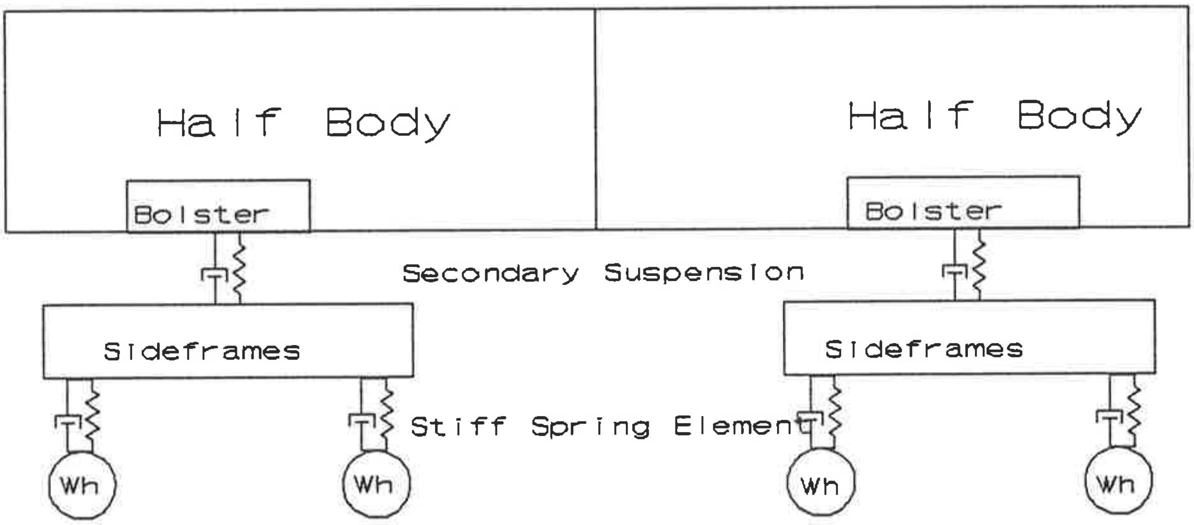

Figure 4.33 3 piece bogie

The known physical parameters are listed in table 4.8 and come from design and literature data for the relevant vehicle type. The data shown here is well defined and was not verified by experiment.

Vehicle	mv Mass Half Body +Bolster	mb Mass Bogie or Sideframe	mu Wheel Mass	ma Mass Axle	axs Wheel Spacing	Bogie Centres
LOCOMOTIVES						
GM Loco	31.6 T *29.1 T*	15.86 T *10.58 T*	1600 kg	282 kg	2.007 m	10.363 m
3 PIECE BOGIES						
Freight Wagon 3 Piece Bogie EMPT / 14 TAL / 21 TAL	8.3 T 24.7 T 38.7 T	2x360kg [16]	380 kg	282 kg	1.753 m	14.935 m
PRIMARY SUSPENSION	BOGIES					
Primary Suspension 19 TAL Bogie AQMH 4228	34.7 T	1212 kg	380 kg	282 kg	1.753 m	14.935 m

Table 4.8 Vehicle physical parameters

Note: Masses in Italics are a two axle equivalent used in the model.

Table 4.9 shows the data on stiffness and damping factors which is less well defined but however is still extracted from data discussed in the literature.

Vehicle	ks Primary Suspension Stiffness	cs Primary Suspension Damping as % of critical	kss Secondary Suspension Stiffness	css Secondary Suspension Damping as % of critical	Ela Axle bending stiffness
LOCOMOTIVES					
GM Loco	2.5 MNm^{-1}	20%	2.4 MNm^{-1}	20%	12.5 MNm^{-2}
3 PIECE BOGIES					
Freight Wagon 3 Piece Bogie	1000 MNm^{-1}	20%	3.1 MNm^{-1} ref [15]	20%	12.5 MNm^{-2}
PRIMARY SUSPENSION	BOGIES				
Primary Suspension Bogie	3.3 MNm^{-1}	20%	8.0 MNm^{-1}	20%	12.5 MNm^{-2}

Table 4.9 Vehicle stiffness and damping parameters

CHAPTER 5 ENERGY ANALYSIS AND MODEL VALIDATION

In this chapter a number of techniques were used to validate the model, and provide a method by which the final results can be obtained. As a means to determine the correlation between energy loss predictions, and the settlement of the track an energy analysis calculation routine was developed.

Section 5.3 explains the model validation that was undertaken which used modal analysis, comparison between the model's and experimental power spectral densities, and finally comparison to other authors published experimental results.

5.1 BALLAST/FORMATION ENERGY LOSS

Part of the analysis work is the estimation of the energy loss through the ballast damping elements. This is calculated by firstly estimating the ballast damping by

$$24\%\ \ of\ \ 2\ \sqrt{BallastStiffness\ (\ 0.5\ mass_{sleeper}\ +\ mass_{rail\ node})}$$

(see page 86 for estimation of %)

The mean energy loss per time step is given by

$$Ballast\ Damping\ \frac{(Velocity_{N}^{2}+\ Velocity_{N+1}^{2})}{2}$$

The energy loss per time step is then equal to the Time Step by Mean Energy Loss.

Figure 5.1 shows the cumulative energy loss by an the 12th ballast element in the central section of the model. The energy absorbed by one sleeper end during the passage of a single bogie is approximately 2.9 Joules.

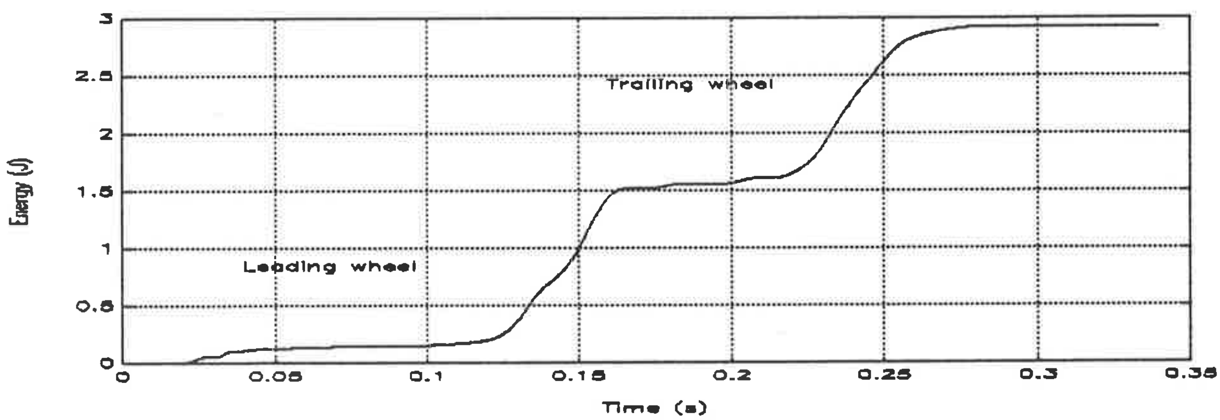

Figure 5.1 **Ballast cumulative energy loss**

The correlation between the energy lost and the settlement is based on the assumption that all of the bogies can be linearly superimposed. As shown in figure 5.2 the interaction between the closest spaced bogies (3.24 metres between the trailing wheel of the lead bogie and the leading wheel of the trailing bogie or 0.1 seconds at 120 km hr^{-1}) is insignificant.

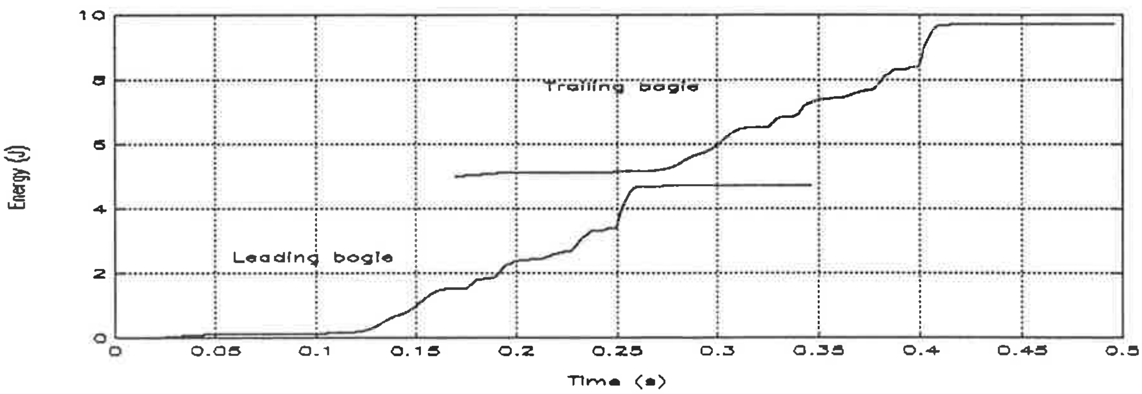

The model can be run a number of times with the various defects to show the effect of the defects on the energy dissipated, and thus provide a method to correlate the energy loss with the settlement rate. Figure 5.3 shows the effect of the defect size where three model runs were made using the same shaped defect scaled up using no defect, ½ defect and a full size defect on the sleeper preceding the defect. This clearly shows the relationship between defect size and energy loss.

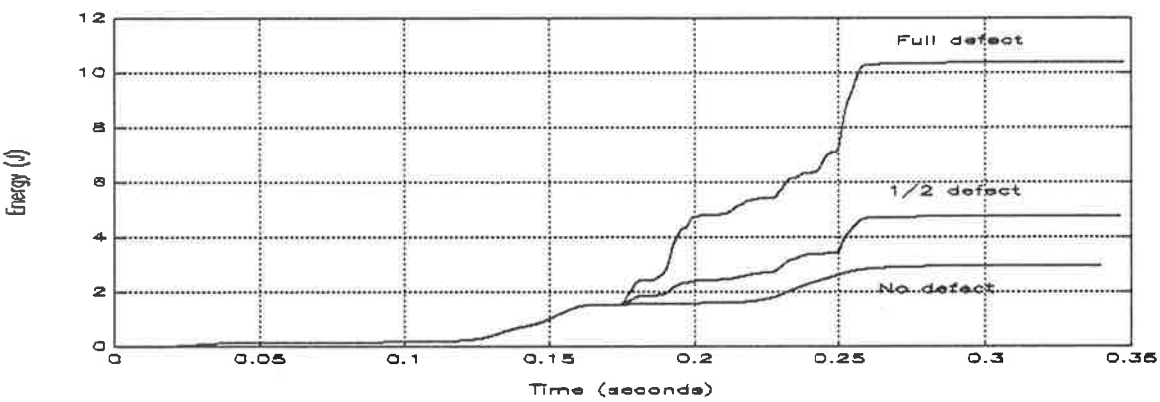

Figure 5.3 **Ballast energy loss**

5.2 MODEL VALIDATION

The model that has been previously discussed in chapter three is validated by two processes to enhance the confidence in the models predictive capabilities. The first of these involves the undergoing of a modal analysis to determine if it adequately models the vibration modes of concern. Secondly by comparison of the experimental and model power spectral densities and thirdly by comparing model results with the work by other researchers the validity of the model to other conditions can be ascertained. This also allows the limitations of the model to be determined. For this third part of the validation two examples are presented.

The modal analysis method that has been used to determine the undamped track and vehicle natural frequencies, and mode shapes, is by the use of eigenvalues and eigenvectors utilising an analysis method available as a subroutine of MATLAB. There is an added advantage through the use of the modal analysis techniques in the modelling routine in that it ensures that clerical errors in the formation of the stiffness and mass matrices are eliminated by the visual inspection of the graphical presentation of the eigenvectors.

The modal analysis performed included a check on the sensitivity of the model to alterations in the number of sleepers that are incorporated. This is due to the end effects of having a fixed length model as previously discussed in chapter three on the model itself. The sleeper modes of vibration were also checked as literature is available for comparison.

5.3 MODAL ANALYSIS OF TRACK LENGTH

The number of sleeper bays in the model will influence the natural modes of the track as a whole and a point needs to be determined where the influence of additional nodes becomes insignificant.

Using the Eigenvalue method model track lengths of 20 to 28 sleepers were analysed. In this analysis the bogie is positioned in the centre of the track and the wheel to rail Hertzian contact spring is linear.

Table 5.1 details the results from the modal analysis with the number of bays and the model name that was used for the analysis. The mode shapes corresponding to the results for the 24 bay model are shown in appendix two.

	FREQUENCY Hz				
Mode Number	20 sleepers	22 sleepers	24 sleepers	26 sleepers	28 sleepers
1	1.5	1.5	1.5	1.5	1.5
2	2.6	2.6	2.6	2.6	2.6
3	17.2	17.2	17.2	17.2	17.2
4	25.5	25.5	25.5	25.5	25.5
5	28.8	28.8	28.8	28.8	28.8
6	36	36	36	36	36
7	40	40	40	40	40
8	44	44	44	44	44
9	48	48	48	48	48
10	49	48	48	48	48
11	49	49	48	48	48
12	56	52	52	50	50
13	56	56	52	50	50
14	65	59	59	57	54
15	65	64	59	57	54
16	67	65	64	64	62
17	67	67	64	64	62
18	73	68	68	65	64
19	73	70	68	65	64
20	75	73	70	68	66

Table 5.1 Modal analysis

The change in the frequency for the different modes levels out at 24 bays and although there is still a variation with increasing model length the change is not of sufficient magnitude to warrant lengthening the model for this reason. For this reason the length of the track model was set at 24 bays. A longer model would be desirable but extensions increase the computing time for decreasing levels of accuracy improvement.

5.4 SLEEPER VIBRATION MODAL ANALYSIS

To check that the sleeper masses and stiffness matrices are correct a modal analysis on the sleeper as an isolated body was undertaken. This was again through the MATLAB eigenvector program (subroutine SLPVIB.M) which gave the following results for the four degree of freedom element. As a comparison the analysis undertaken by Ford [27] is presented, which was made on New South Wales prestressed concrete sleepers, together with results reported by Ahlbeck [2] for USA prestressed concrete sleepers and Clark [7] for British Rail sleepers.

MODE	Frequency (½ sleeper length = 0.95 m)	Description	Ford [50]	Ahlbeck [2]	Clark [7]
1	0	Rigid Body			
2	0	Rigid Body			
3	114 Hz	1st bending	113 Hz	108 Hz	220 Hz
4	346 Hz	2nd bending	343 Hz	333 Hz	
5	–	3rd bending	664 Hz	633 Hz	630 Hz

Table 5.2 Sleeper modal analysis

The first two modes have zero frequency response as they are the rigid body vertical and rotational modes. Clark does not show any results for the second bending mode as his model is symmetric. Given the above limitation of the third and higher vibration modes being absent from the model the response as shown above is acceptable. This extension to higher modes can be made as part of any further study but was not pursued any further at this stage.

5.5 VEHICLE DEGREES OF FREEDOM

The vehicle is modelled in a relatively simple manner with the bogie being the most complex part. With increasing complexity it is possible to add additional modes which tend to be at the lower end of the frequency spectrum. These consist of all the body vibrations (body roll, yaw, pitch) as well as deflections of the sideframes etc.

The vertical and roll modes of the body were included in the modal analysis but as shown in table 5.1 have wavelengths, at 110 km hr^{-1}, of 30 and 18 rail bays of 0.66 metres in length respectively. To accurately model the effects of these two modes there would be a need to extend the model to at least three times this distance to permit damping of any transients. As these modes are also excited by much longer wavelengths than are under consideration in this research then these two modes are fixed in the model.

For the above reason the body degrees of freedom were fixed. To allow for imbalances in the force being applied by the body to the bogie initial conditions for body height and roll angle can be set.

5.6 BRITISH RAIL MODEL COMPARISON

The British Rail model described in detail by Clark [7] is used as the first of the two comparative models that were used to assess the validity of the model. The availability of both experimental and model time histories was the primary reason for selection. The advantage also exists in that the defect type is different to that studied in this research.

The British Rail model consists of a 20 bays and utilises modal analysis. It was designed primarily to investigate the effects of short wavelength corrugation defects (60mm in length) on the rail and sleepers. The characteristics of the model are:

- Sleepers are discrete.
- Symmetric across track (½ track model).
- Primarily linear, however with non linear Hertzian contact.
- Sleepers are modelled as flexible beams.
- Sleepers and rail have vertical bending stiffness and inertia.
- Railpads.
- Sleepers supported on a uniform ballast layer.
- Two linear systems separated at the wheel/rail interface by a nonlinear Hertzian contact spring.
- Fixed time steps.

As part of the calibration process for the model the parameters for the British Rail model were used to check the results of this model against published theoretical and experimental results.

The parameters used are;

Unsprung mass	380 kg
Axle mass	280 kg (not BR but from Ahlbeck)
Body mass	18430 kg
Vehicle speed	37.5 ms^{-1} (135 km hr^{-1})

Suspension stiffness is not given but derived based

on a maximum spring deflection of 20 mm = 2.260 MNm^{-1}

Track stiffness	46.6 MNm^{-1}
Pad stiffness	250 MNm^{-1}
Rail Bending	4.86 MNm^2
Sleeper bending	3.75 MNm^2
Axle stiffness	12.5 MNm^2

Corrugation amplitude	0.115 mm (½ depth)
Corrugation pitch	60 mm

Contact stiffness	BR	4.56×10^{-7}
Contact stiffness	Program	4.38×10^{-7}

The results shown in figures 5.4 to 5.6 show some differences. which are explained by the alternative format of the models with the primary one being the inclusion in the British Rail model of higher frequency modes of vibration in the sleeper. At the critical points however the model agrees with the experimental results obtained.

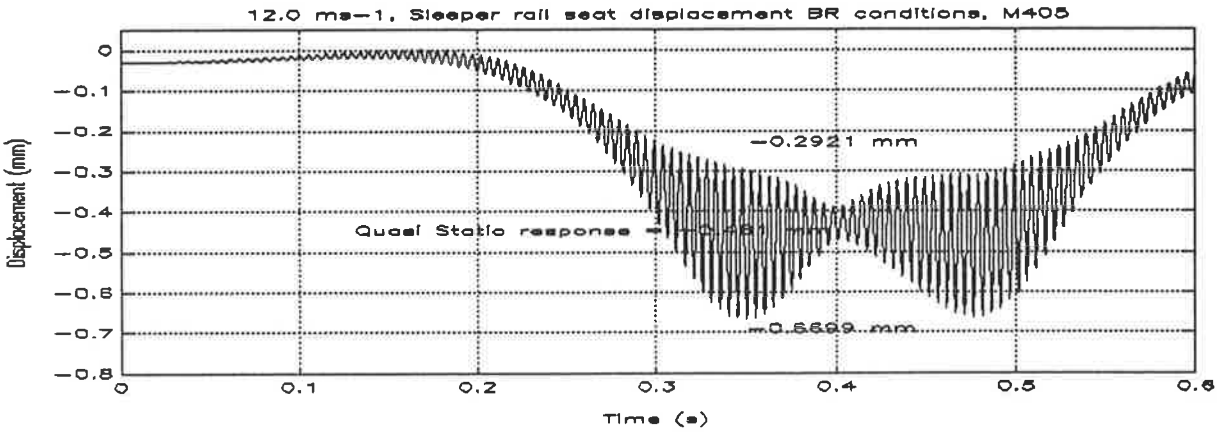

Figure 5.4 **Sleeper rail seat displacement**

The results of the sleeper displacement at the rail seat at 12 ms^{-1} can be compared to figure 11 in Clark's paper [2] which shows the sleeper end displacement.

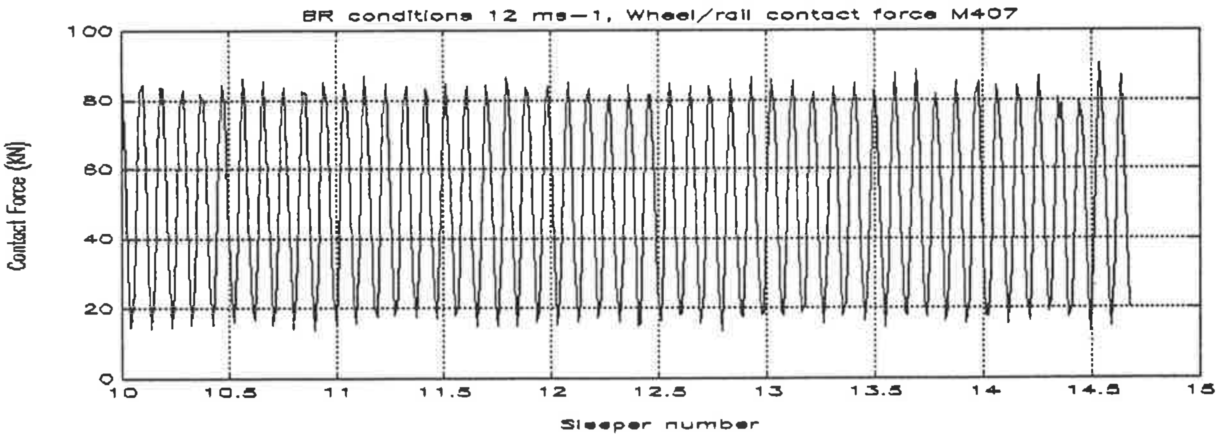

Figure 5.5 **Wheel rail contact force**

The contact force diagram as shown in Figure 5.5 shows the force that exists between the wheel and rail at a speed of 12 ms^{-1}. The results are in close agreement with the British Rail results shown in Figure 10 of Clark's paper [7]. The agreement exists in the magnitude of the contact force however the effect of higher contact forces existing over the sleeper are not evident.

Figure 5.6 shows a number of model runs were undertaken at different speeds and matched against the experimental results reported by Clark [7].

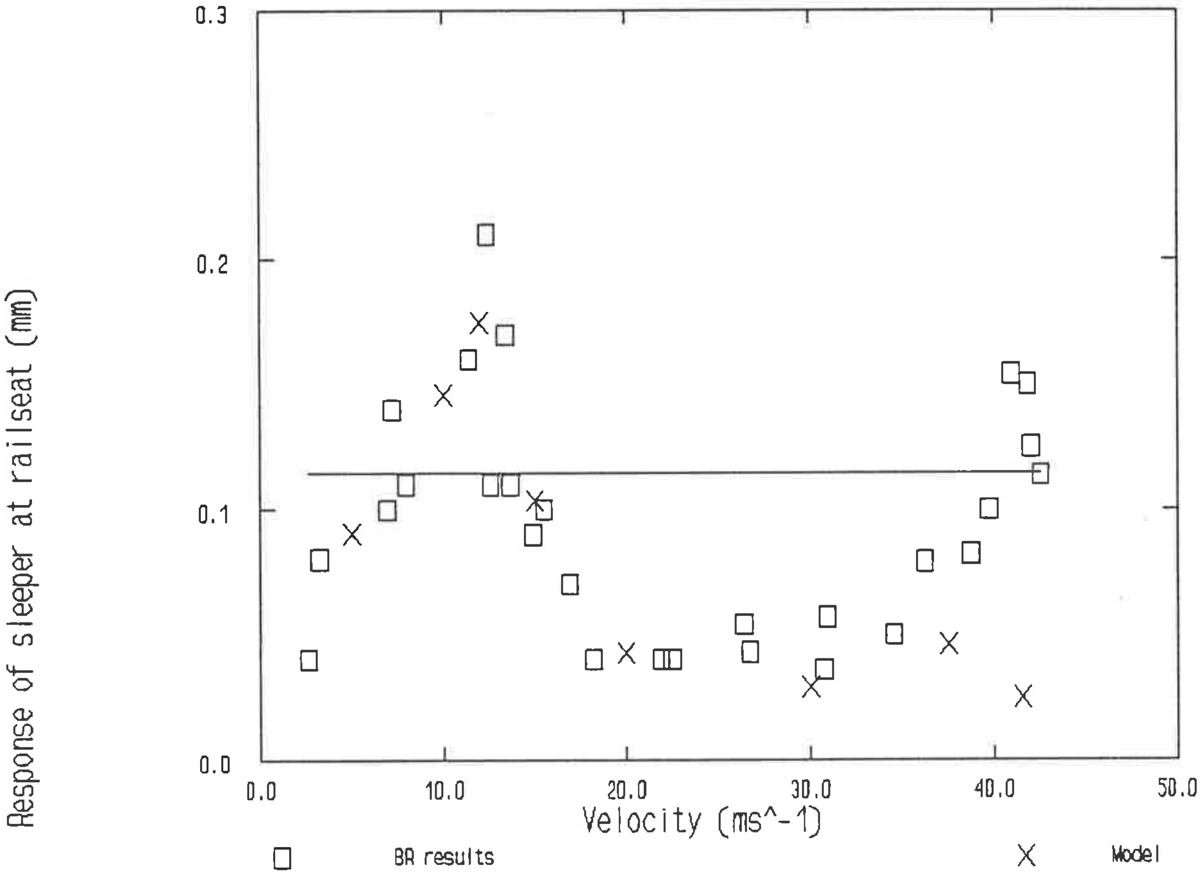

Figure 5.6 **Experimental vs model prediction**

Close agreement is evident from the first peak but not with the second peak which corresponds to a frequency of 700 Hz. The reason for this anomaly is the modelling by Clark of higher sleeper frequencies than was undertaken in this research (table 5.2).

5.7 IMPWHL MODEL COMPARISON

The second case study examined was that of the model developed by the Battelle Columbus Division under Ahlbeck who has developed this vehicle/track interaction program over the past 15 years. This model was selected as it is based on differing track conditions to those existing on Australian and British railways but also having the availability of the defect shape, all of the physical parameters and the final result.

The primary intention of Ahlbeck's model [2 3 4] is to determine the peak loads under specific running surface geometry defects and from this to predict the vehicle and track component loads. The work was driven by concerns on the North East corridor in the US where high speed trains operate on concrete sleepered track. The effect of wheel flats and rail geometry errors is to cause failure of the sleepers. Some of the assumption contained within Ahlbeck's model are

- Impact at one wheel only with the resulting need for a nonsymmetric model about the track centreline.
- Forward motion has little effect on vehicle track response.
- Limited vibration above the primary suspension.
- Track parameters derived from beam on elastic foundation theories and experiment results.
- Geometry inputs are seen from the wheels reference.
- First four sleeper bending modes are included.
- First four axle transverse bending modes included.

Ahlbeck also goes into some discussion about the effect of including rail bending as used by Clark [7] and why it was not included in the model. The reason it is claimed is that the modes are highly dependent on the positions of the adjacent wheels and thermal stresses due to longitudinal rail restraint. The results from this analysis are examined by running the model with the wheel burn defect shown in Ahlbeck figure 12 [4] with the result as shown in figure 5.7.

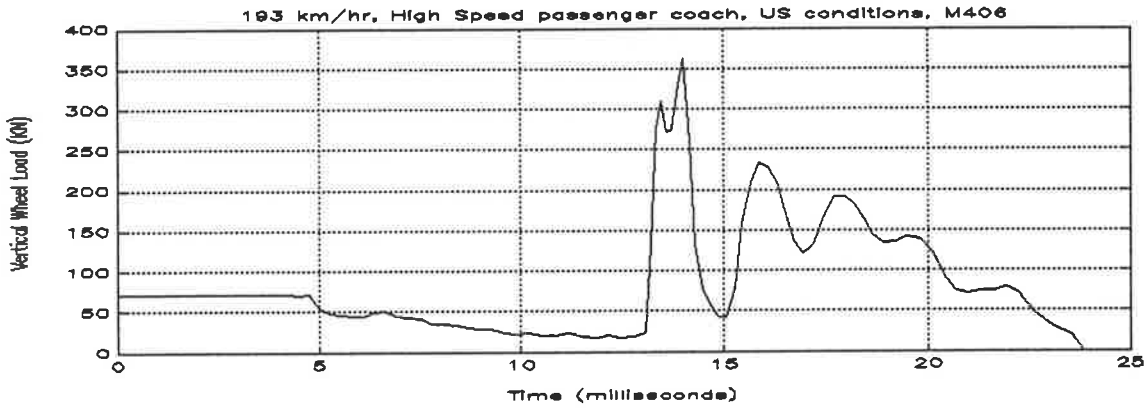

Figure 5.7 Wheel/rail contact force US conditions

This result can be compared then to Ahlbeck's figure 13 [4] reproduced in figure 5.8. where he predicts that there will be a peak load with his model of 294 kN (not 194 kN as printed in the paper).

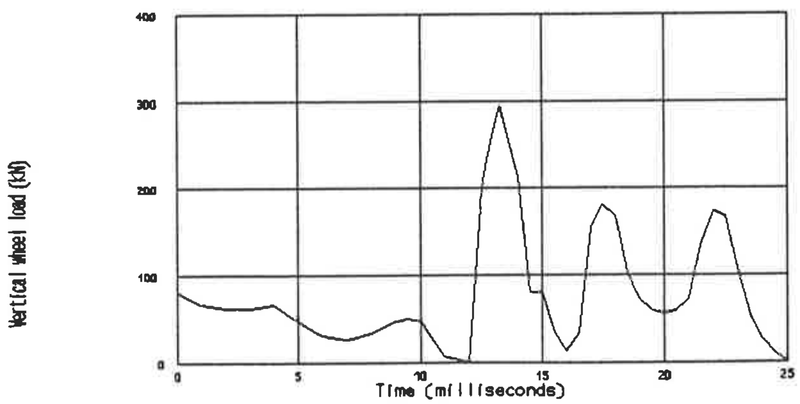

Figure 5.8 Wheel/rail contact force US conditions from Ahlbeck [4] (Figure 13)

CHAPTER 6 SETTLEMENT AND ENERGY LOSS ANALYSIS

6.1 INTRODUCTION

Using the methodology detailed in chapter five, an estimate is made of the energy loss through a number of defects, to investigate the relationship between the total energy absorbed by the ballast and formation, against the track settlement obtained from survey results.

A total of 72 results are presented with the following characteristics having being investigated.

1. Train Speeds of 60, 80, 100 and 120 km hr^{-1}.

2. Three piece bogies with axle loads of 5.8 Tonnes (empty vehicle), 14 Tonnes and 21 Tonnes.

3. Defect type consisting of perfect rail surface and three field dips on one rail only (sites one, two and four).

4. As the track was single line operation the effect of vehicles passing over the sites in both directions needs to be taken into account. Thus all the above model runs were undertaken for both directions.

The model in all cases was run over a total of 20 bays or 13.2 metres with the relevant defect at the centre of the track.

6.2 TRACK SETTLEMENT

Track settlement measurements were undertaken by survey methods of the unloaded track profile. Levels were taken at sleeper intervals for ±10 sleepers from the centreline prior to the track being disturbed, directly after the track had been lifted and tamped and after 21 and 63 days of traffic.

The data was reduced to show the settlement in figures 6.1 to 6.4. These show the rapid settlement phase of the track which is generally equal for each of the sites. The formation of the original track shape is also becoming evident, however it should be noted that site two had the weld profile lifted and ground in between the 21 day and 63 day readings. This shows the elimination of the dip profile.

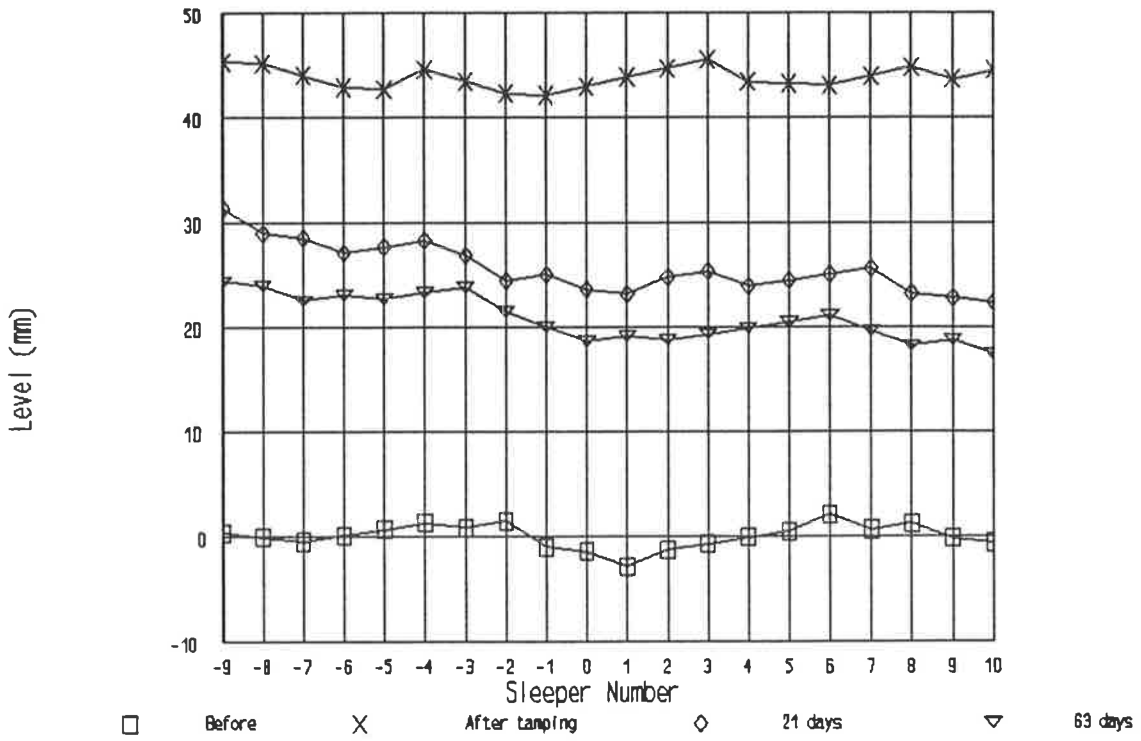

Figure 6.1 Site 1 settlement

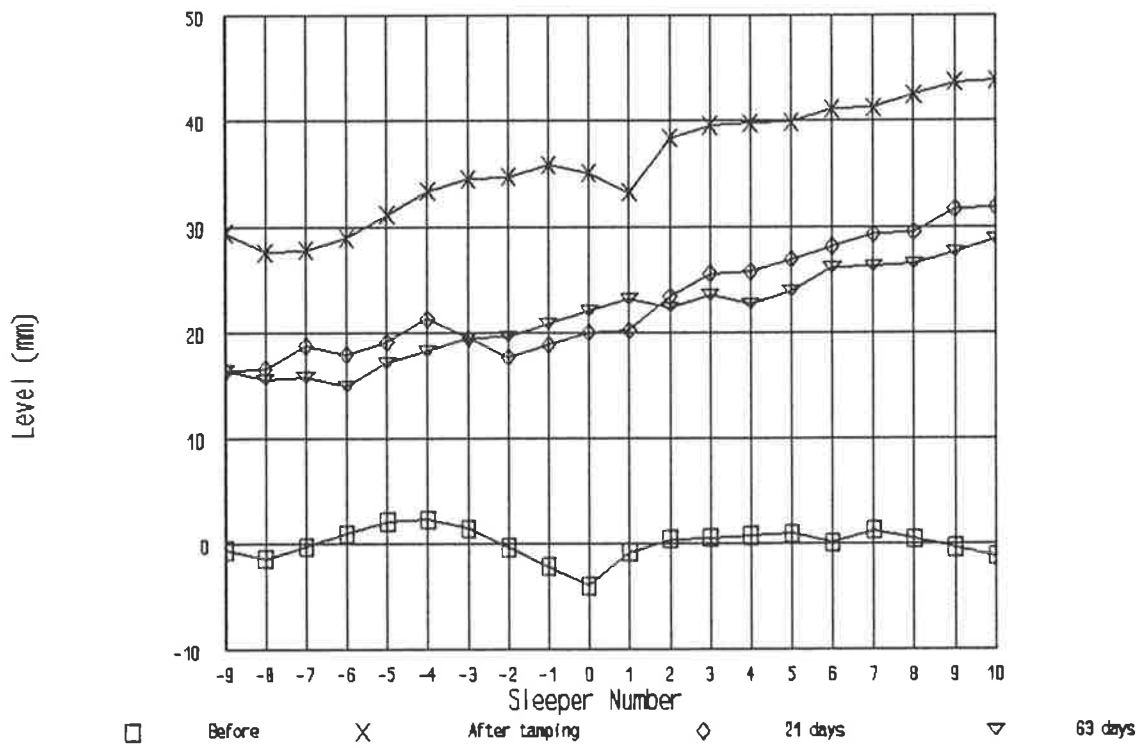

Figure 6.2 Site 2 settlement

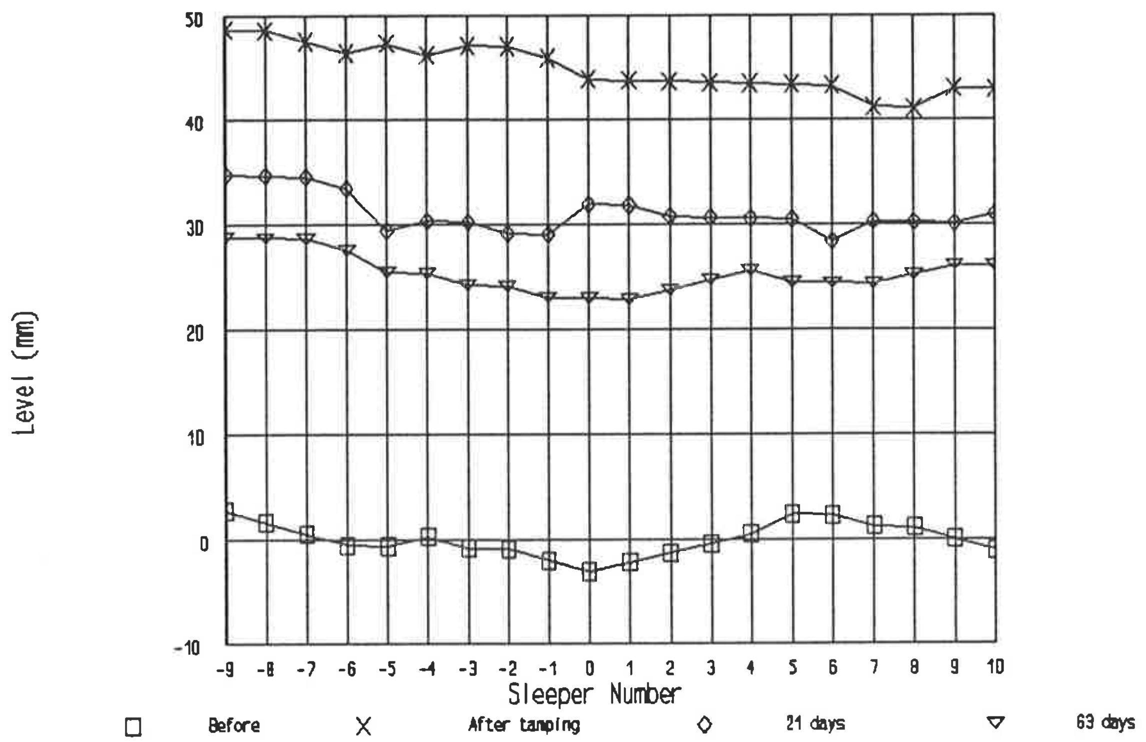

Figure 6.3 Site 3 settlement

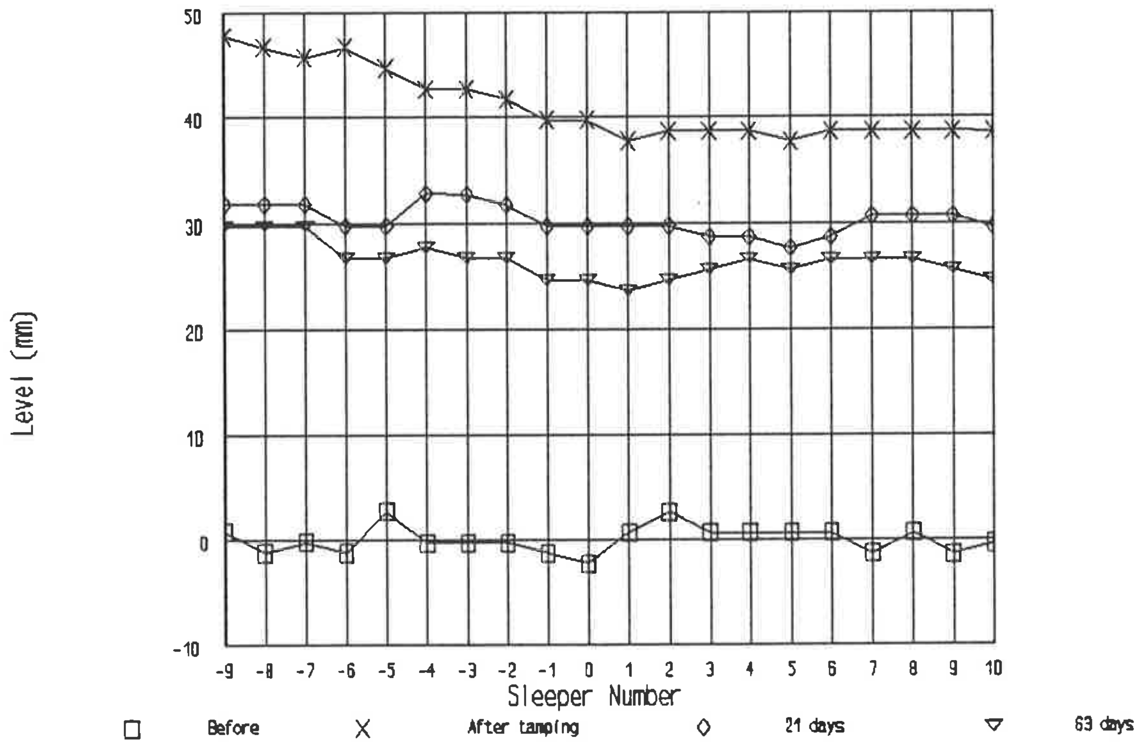

Figure 6.4 Site 4 settlement

Further analysis of these results was made to predict the differential settlement of the track at the defect compared to the surrounding track as shown in figure 6.5. This is due to the assumption that the absolute level of the track is not the primary problem, but the differential settlement which leads to rough riding of vehicles and increased load on the track and vehicles.

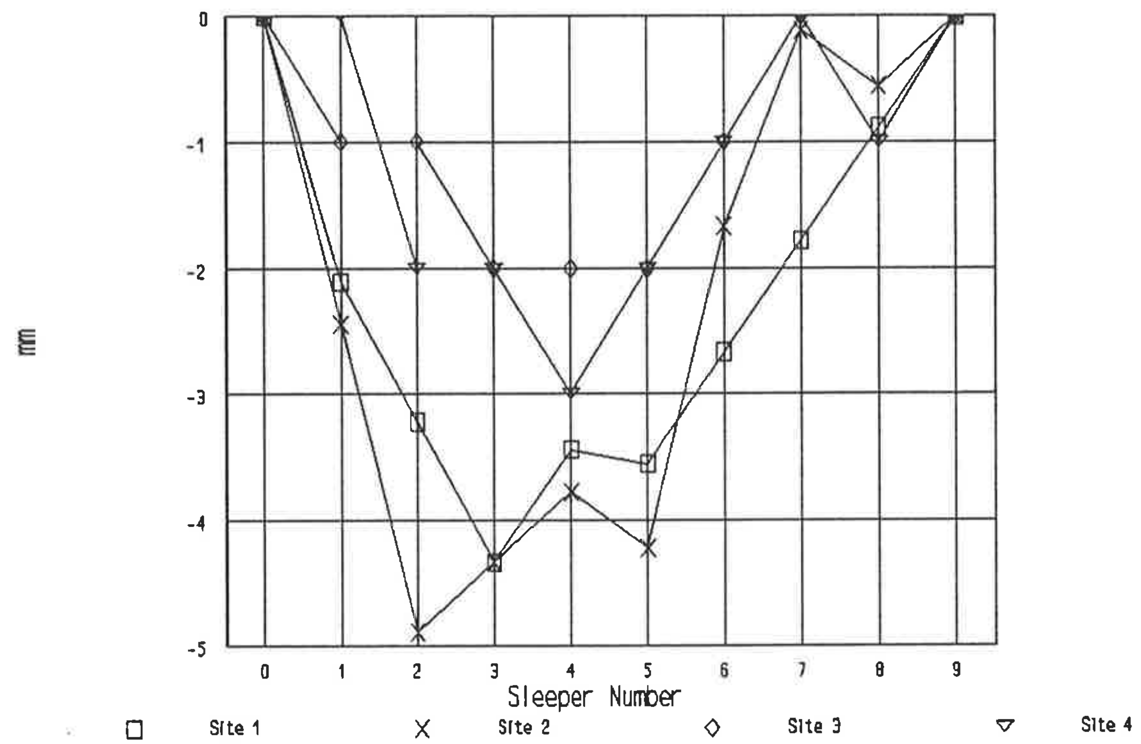

Figure 6.5 Differential settlement

6.3 BALLAST ENERGY LOSS

The energy absorbed by the track is not just confined to the sleeper adjacent to the defect itself, but as shown in figure 6.6 is spread over a number of sleepers. It is hypothesised that if the track settlement is related to the energy absorbed the track will form a shape that follows closely that shown in the energy diagram. The results for the sleeper energies are extracted and stored in tabular form for analysis.

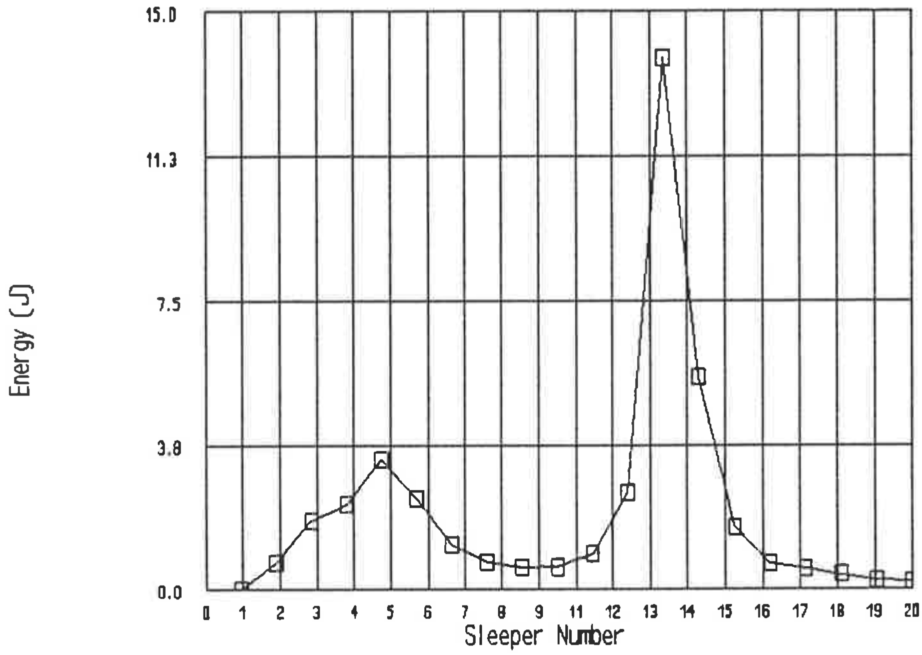

Figure 6.6 Total ballast energy loss : Site 1

The spectrum for the vehicles that were travelling over the site was estimated from data available through the Australian National train information monitoring system. The results for a four week period during which the settlement results were obtained is shown in table 6.1 as a loading spectrum of the number of bogies at the various speed, axle load and direction.

	WESTBOUND			EASTBOUND		
SPEED AXLE LOAD	5.8 tonne	14 tonne	21 tonne	5.8 tonne	14 tonne	21 tonne
80 km hr^{-1}	1046	4534	1395	3238	3238	720
100 km hr^{-1}	651	2820	868	1969	1969	438
120 km hr^{-1}	0	480	0	0	48	0

Table 6.1 Vehicle density spectrum

There is difference in the tonnage being hauled in the westbound and eastbound directions due to the commodity flows that operate on this corridor. From this information the speed and axleload combinations were multiplied by the energy predictions per bogie, to give an estimate of the total energy absorbed by the ballast over the complete site. The model was run a total of 72 times. The results were then tabulated into a matrix format.

The results for each site, which totals eight runs per site are then summed for the number of bogies that actually ran over the site, to give a total energy absorbed result. For sites one and four the results are after 63 days while site two was after only 21 days. the peaks due to the initial transient response are eliminated from the following graphs.

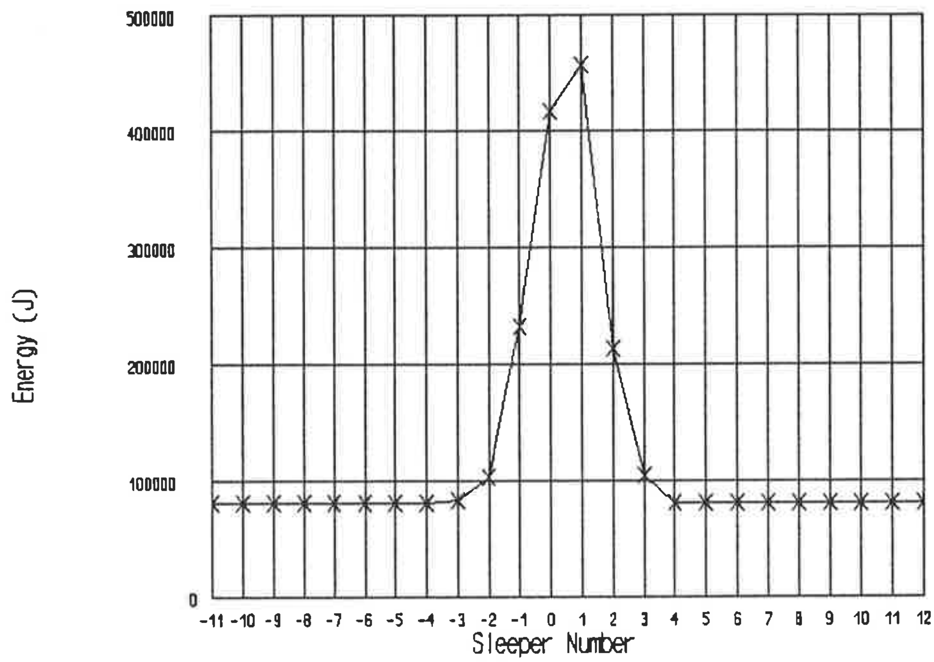

Figure 6.7 Site 1 cumulative energy loss

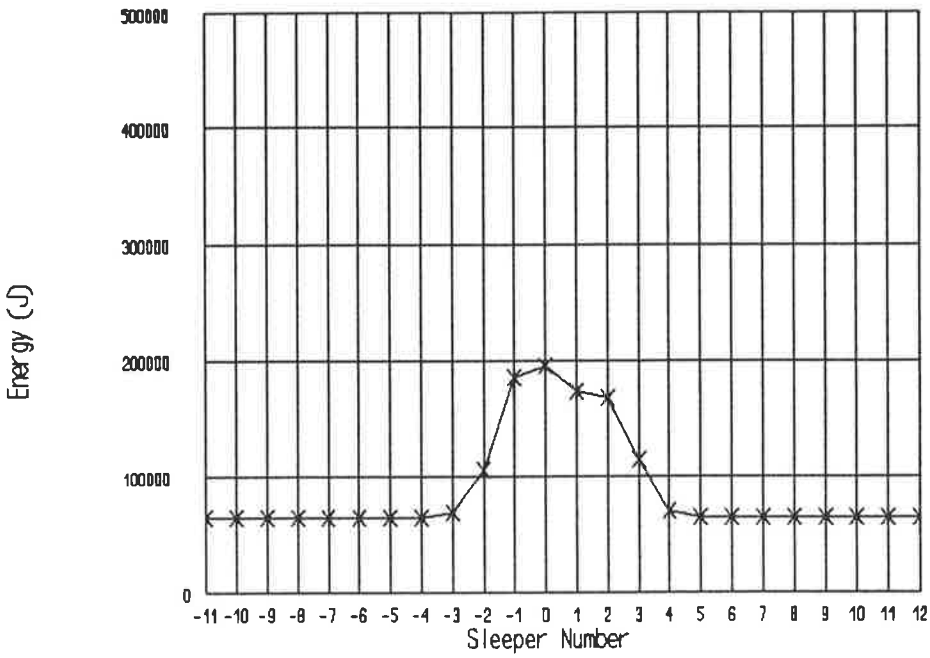

Figure 6.8 Site 2 cumulative energy loss

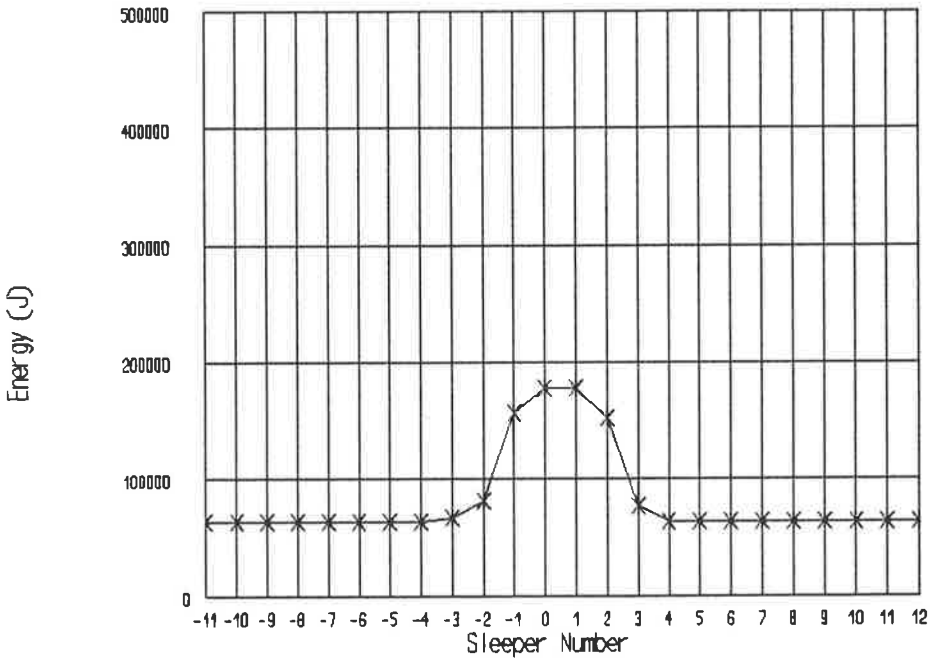

Figure 6.9 Site 4 cumulative energy loss

These results are then plotted as values on the X axis in figure 6.10 against the settlement curves from figures 6.1 to 6.4 in the Y axis. This shows the correlation between settlement and energy absorption.

Linear regression line

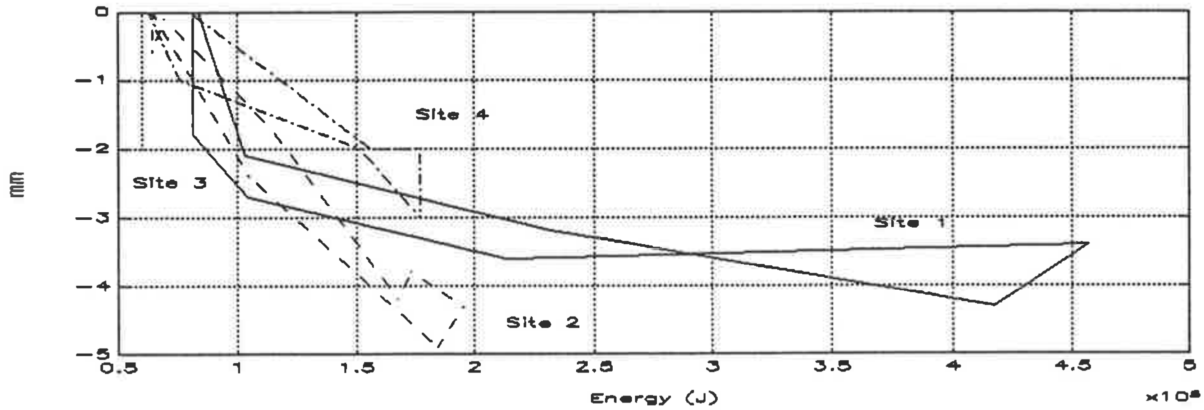

Figure 6.10 Settlement and energy loss

The linear regression curve shown in figure 6.10 for sites two and four give a differential settlement rate of 23.8 mm per MJ of energy lost by the damper. The results for site one have a different characteristic shape that indicates a lesser dependence on the energy which indicates that the differential shape will stabilise after a relatively short period of time.

6.3 SLEEPER ENERGY SENSITIVITY

These peak energy loss results are plotted onto the figures 6.11 to 6.13 so that direct comparisons can be made between differing configurations of axle loads, speeds, defect sites and direction.

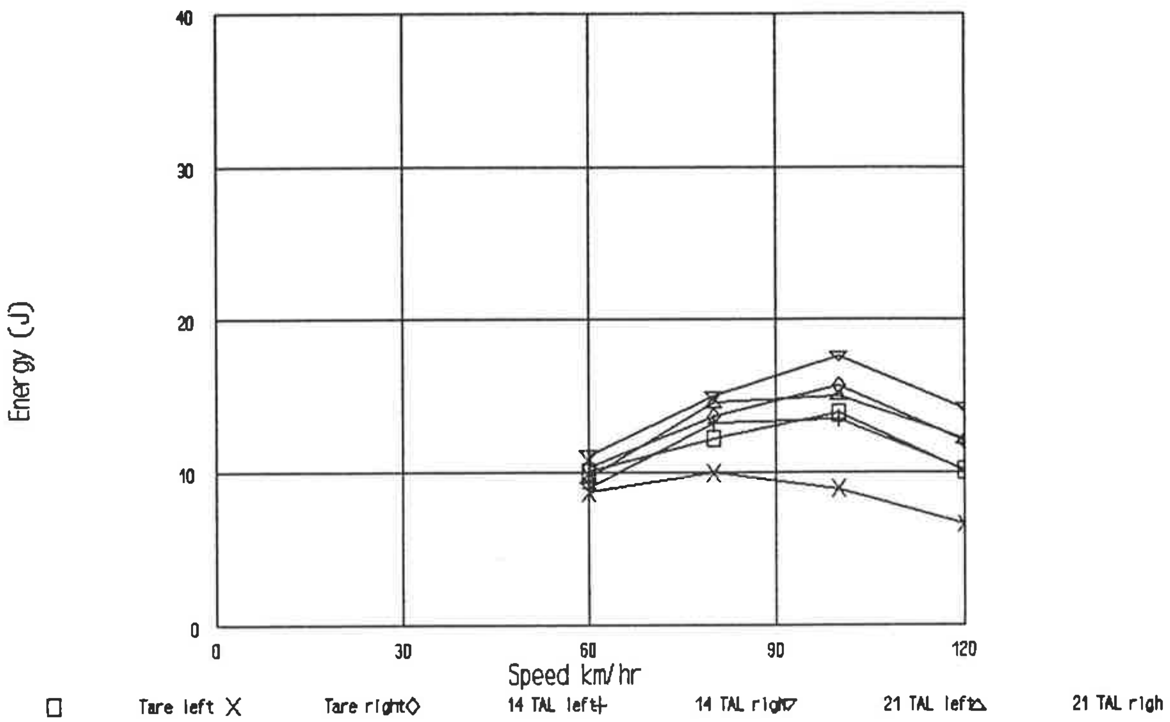

Figure 6.11 Site 1 energy loss

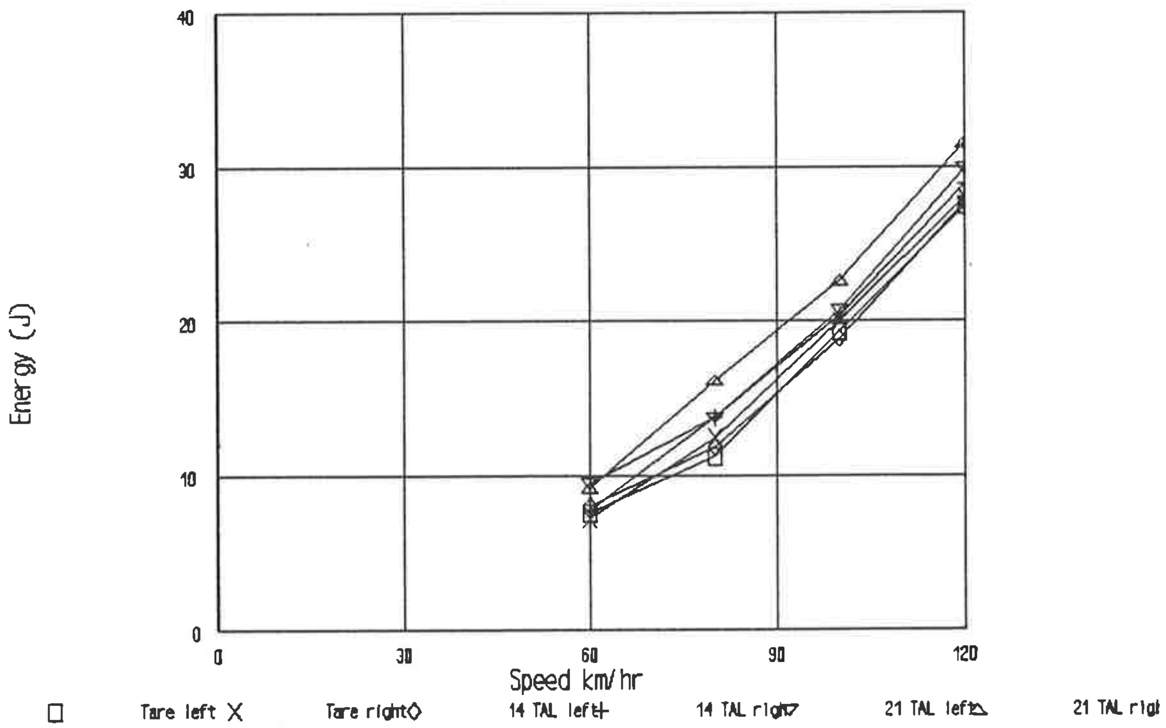

Figure 6.12 Site 2 energy loss

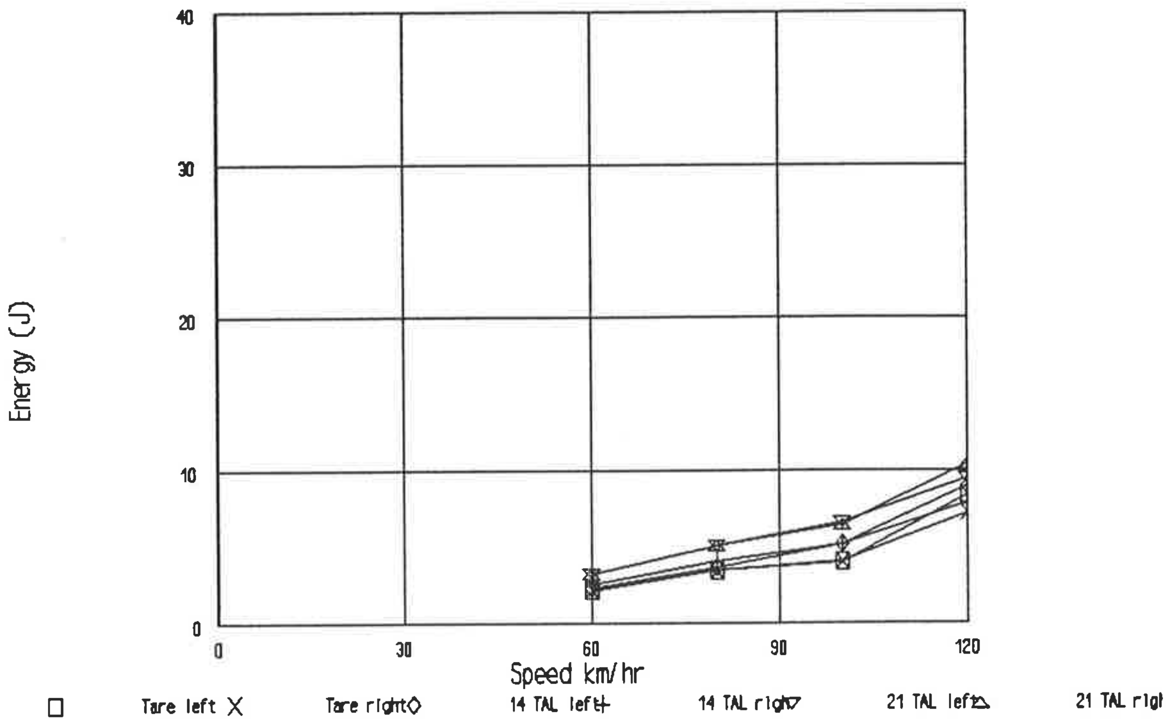

Figure 6.13 Site 4 energy loss

As can be seen from figures 6.11 to 6.13 the results are generally highly site sensitive. The nonlinearity of the system becomes evident from the results of site one which show a peak loading at 100 km hr^{-1}. This result does not appear in either of the other two sites. The insensitivity of the results to direction indicate that the defects studied were nearly symmetric.

CHAPTER 7 OBSERVATIONS AND CONCLUSIONS

A number of conclusions will be drawn from the work carried out during this study. The main conclusions that arise are

1. There is a correlation between the energy absorbed by the track and the rate of settlement of the ballast.

2. Rail surface defects can have a significant effect on the damage and energy cost of running a railway and with the assistance of dynamic models, planners will be better able to quantify their cost and as such provide economic measures to correct them.

3. Track dynamics can be predicted by suitable numeric modelling that is available on PC based systems.

4. Nonlinear modelling must become an important part of future dynamic analysis, and effort will be required to determine nonlinearities that occur within the vehicle and track systems.

Experimental results are difficult to obtain due to the high frequency responses of the track components. This difficulty was overcome in the most part by the use of high frequency accelerometers. The method of double integration shows a great promise although work needs to be done to validate this method. If it can be fully developed however it would enable detailed measurements to be undertaken at relatively low cost and high portability.

Modelling using the MATLAB software proved to be successful and enabled a complex model to be run on a PC. Optimisation of the code was relatively easy and with increased computer power would enable larger models to be developed. As with all time domain models the run time is long and generally required overnight processing with typical models running for two to three hours.

Careful analysis of the traffic mix that includes both the loading spectrum and direction needs to be made because it is very rare that a defect is symmetric which may lead to significantly differing results for the same site.

Rail Surface Geometry Defects and Track Settlement

M.D. Williams

B.E., Adelaide

Thesis presented for the degree of Master of Engineering Science

at the University of Adelaide

August 1994

APPENDICES

APPENDIX 1 COMPUTER CODE

The following computer code listings are presented in this appendix. The routines are;

TRCRV033.M and TRCKV033.M	Mathematical model
TRENG3.M	Sleeper energy analysis
FFTINT2.M	Signal analysis
TREIG4.M	Modal analysis

All of these routines are written in the MATLAB language and reference should be made to the users guide for further understanding of the program operation.

Appendix 1.1 TRCRV033.M

```
clear;
pack;
%*************************************************
%
%    Rail track model with moving vehicle load
%    3 piece bogie model
%
%    24 bay model with double rails
%
%    TRCRV033.M
%
%
%     Version 33
%    M. Williams  20 FEB 94
%*************************************************
clg;
tol=1.0e-5;   % accuracy of ode45m calculation
g=9.81;       % gravitational acceleration constant

%%%%%%%% GEOMETRY PARAMETERS %%%%%%%%%%%%%%%%

rl=0.66;      % sleeper node spacing (m)
sl=1.9/2;     % sleeper length (m)
axs=1.753;     % axle spacing (m)
pss=2.1;      % primary suspension spacing (m)
sss=2.1;      % secondary suspension spacing (m)
vel=100/3.6;   % speed of vehicle  (m.s^-1)
del=0.000115;  % corrugation half depth (m)
lam=0.06;     % wavelength of defect(m)
%%%%%%%%%%%%%%%%%% STIFFNESS PARAMETERS %%%%%%%%%
Elr=3.19e+6;  % rail flexural rigidity (Nm^2)
Els=4.00+6;   % sleeper flexural rigidity (Nm^2)
Ela=12.5e+6;  % axle flexural rigidity (Nm^2)
rstf=Elr/(rl^3);

%%%%%%%%%%%%%%%%%% MASS PARAMETERS  %%%%%%%%%%%%%
mv=8300;      % mass of vehicle body + bolster (kg)
mb=360;       % mass of side frame (kg)
ma=566;       % axle mass (kg)
mu=380;       % unsprung mass of wheel  (kg)
mr=47*rl;     % nodal mass of rail (kg/m)
ms=292.6;     % mass of sleeper (kg)
```

```
%%%%%%%%%%%%%%%%% STIFFNESS PARAMETERS %%%%%%%%%%
kss=3.1e6;  % secondary suspension stiffness (N/m)
ks=1000e6;  % primary suspension stiffness (N/m)
kb=35e6;    % ballast stiffness (N/m)
kp=250e6;   % pad stiffness     (N/m)

%%%%%%%%%%%%%%%%%% DAMPING PARAMETERS %%%%%%%%%%%%%
css=0.2*2*sqrt(kss*mv/2);    % secondary suspension damping (Ns/m)
cs=0.2*2*sqrt(ks*mb/2);      % primary suspension damping (Ns/m)
cb=0.2*2*sqrt(kb*(ms/2+mr));% ballast damping   (Ns/m)
cp=0.2*2*sqrt(kp*mr);        % pad damping       (Ns/m)
ca=0.2*2*sqrt(EIr/rI*mr);    % Rail rotation material damping
%%%%%%%%%%%%%%%%%%%%%%%%%%%%%%%%%%%%%%%%%%%%%%%%%%%%%%%

%
%       HERTZIAN CONTACT CALCULATIONS
%
R1=0.505;                % Wheel radius (m)
R1d=inf;                 % Tyre radius  (m)
R2=0.3;                  % Rail head radius (m)
Phi=90;                  % Angle of attack  (degrees)
E=2.1e11;                % Youngs modulus
Pr=0.3;                  % Poissons ratio
crit=0.1;                % damping percentage of critical
delta=4/(1/R1 + 1/R1d +1/R2);
Kbar= 4/3*(E/(1-Pr^2));
theta=abs(360/(2*pi)*acos(delta/4*sqrt((1/R1-1/R1d)^2 ...
    +(1/R2)^2 +2*(1/R1-1/R1d)*cos(2*Phi*(2*pi)/360))));
Gamma=0.57462 + 0.034745*theta - 0.00021338*(theta^2);

kh=Gamma*(1/(Kbar^2*delta))^(1/3);      % Contact flexibility

%%%%%%%%%%%%%%%%%%%%%%%%%%%%%%%%%%%%%%%%%%%%%%%%%%%%%%%
%
%       INITIAL CONDITIONS
%
X0(1:398)=zeros(1,398);  % Initialise parameters
X0(393)=-mv*g/(2*kss);   % Initial body displacement


%%%%%%%%%%%%%%%%%%%%%%%%%%%%%%%%%%%%%%%%%%%%%%%%%%%%%%%
%
%           RUN CONTROL PARAMATERS
%
T0=1*rl/vel;   % start time of simulation run
Tf=18*rl/vel;  % finish time
trace=1;       % trace=1 for time step solutions to be displayed

clear disp;
pack;



%
%    Call routine which contains state variables
%
[xdot,T,X1]=ode45('trckv033',T0,Tf,X0,tol,trace);
%
%    Save the variables required to file
%
save S33b xdot X1 T
```

Appendix 1.2 TRCKV033.M

```
% Lumped mass railway track vibration model
%
% M Williams
%
% This model is a two rail model 24 bays
%
% 3 piece bogie model
%
%  TRCKV033.M
%
%  20 FEB 94
%
function xdot=trckv033(t,x,IV,IV2);% Name of routine
%================================================================
% INPUT VARIABLES
%
vel=IV(1);  % vehicle velocity (ms^-1)
ks=IV(2);   % vehicle primary suspension
cs=IV(3);   % vehicle suspension damping
kb=IV(4);   % ballast spring constant
del=IV(6);  % corrugation 1/2 depth
lam=IV(7);  % corrugation wavelength
rl=IV(8);   % rail length between nodes
mv=IV(9);   % mass of vehicle
mr=IV(10);  % mass of rail node
rstf=IV(11); % bending stiffness of rail
mu=IV(12);  % unsprung mass of wheel
ms=IV(13);  % mass of sleeper
kp=IV(14);  % pad spring constant
cp=IV(15);  % pad damping
kh=IV(16);  % hertzian contact stiffness
crit=IV(17); % hertzian contact damping critical %
EIr=IV(18); % rail bending stiffness

ma=IV2(1);  % mass of axle
EIa=IV2(2); % axle bending stiffness
sl=IV2(3);  % sleeper length
EIs=IV2(4); % sleeper bending stiffness
axs=IV2(5); % axle spacing
g=9.81;
kss=IV2(6); % secondary suspension stiffness
css=IV2(7); % secondary suspension damping
mb=IV2(8);  % bogie mass
pss=IV2(9);
sss=IV2(10);
ca=IV2(11); % axle material damping
```

```
%=========================================================
%    RAIL SURFACE DEFECT SHAPE
%%%%%%%%%%%%%%%%%%%%%%%%%%%%%%%%%%%%%%%%%%%%%%%%%%%%%%%%%%%%%%%%%%
% 1)   GEISMAR rail profile measurement machine
%             with centreline dip @ 5.5rl
%
          corr1=[-20          0
            -0.62+12.2*rl    0
            -0.57+12.2*rl   -0.000050
            -0.52+12.2*rl   -0.0000933
            -0.47+12.2*rl   -0.0001167
            -0.42+12.2*rl   -0.0001500
            -0.37+12.2*rl   -0.0001667
            -0.34+12.2*rl   -0.0001667
            -0.30+12.2*rl   -0.0002000
            -0.28+12.2*rl   -0.0001967
            -0.23+12.2*rl   -0.0002333
            -0.16+12.2*rl   -0.0002500
            -0.11+12.2*rl   -0.0003333
            -0.08+12.2*rl   -0.0004833
            -0.05+12.2*rl   -0.0004333
            -0.02+12.2*rl   -0.0005667
            -0.00+12.2*rl   -0.0007667
            0.05+12.2*rl   -0.0006000
            0.13+12.2*rl   -0.0005667
            0.18+12.2*rl   -0.0005000
            0.23+12.2*rl   -0.0005167
            0.32+12.2*rl   -0.0004333
            0.36+12.2*rl   -0.0004167
            0.37+12.2*rl   -0.0002667
            0.43+12.2*rl   -0.0002000
            0.48+12.2*rl   -0.0001500
            0.53+12.2*rl   -0.0000500
            0.58+12.2*rl    0
            20          0];

          corr2=[-20          0
            -0.50+12.2*rl    0
            -0.45+12.2*rl   -0.000110
            -0.40+12.2*rl   -0.000285
            -0.35+12.2*rl   -0.000551
            -0.30+12.2*rl   -0.000817
            -0.25+12.2*rl   -0.001044
            -0.20+12.2*rl   -0.001405
            -0.15+12.2*rl   -0.001709
            -0.10+12.2*rl   -0.001975
            -0.05+12.2*rl   -0.002222
             0.00+12.2*rl   -0.002354
            0.05+12.2*rl   -0.002279
             0.10+12.2*rl   -0.002146
             0.15+12.2*rl   -0.001747
             0.20+12.2*rl   -0.001519
             0.25+12.2*rl   -0.001424
             0.30+12.2*rl   -0.001291
             0.35+12.2*rl   -0.001158
             0.40+12.2*rl   -0.001025
             0.45+12.2*rl   -0.000854
             0.50+12.2*rl   -0.000656
             0.55+12.2*rl   -0.000437
             0.60+12.2*rl   -0.000266
             0.65+12.2*rl   -0.000076
             0.70+12.2*rl    0
             20             0];
```

```
corr4=[20          0
  0.65+12.2*rl    0
  0.60+12.2*rl   -0.000167
  0.50+12.2*rl   -0.000350
  0.40+12.2*rl   -0.000633
  0.30+12.2*rl   -0.000883
  0.20+12.2*rl   -0.001166
  0.15+12.2*rl   -0.001267
  0.10+12.2*rl   -0.001367
  0.08+12.2*rl   -0.001433
  0.05+12.2*rl   -0.00145
  0.02+12.2*rl   -0.001467
   0.00+12.2*rl   -0.001467
  -0.05+12.2*rl   -0.001300
  -0.10+12.2*rl   -0.001100
  -0.15+12.2*rl   -0.000900
  -0.20+12.2*rl   -0.000767
  -0.30+12.2*rl   -0.000483
  -0.40+12.2*rl   -0.000283
  -0.50+12.2*rl   -0.000083
  -0.60+12.2*rl    0
  -20              0];

xc1=table1(corr1,vel*t+axs);   % call up table to determine variation
xc2=0;                        % wheel 2
xc3=table1(corr1,vel*t);       % wheel 3
xc4=0;                        % wheel 4
%%%%%%%%%%%%%%%%%%%%%%%%%%%%%%%%%%%%%%%%%%%%%%%%%%%%%%%%%%%%%%

%   2)   PERFECT TRACK ie no rail shape irregularity
%
%%%%xc1=0;xc2=0;xc3=0;xc4=0; % set rail defects to zero
%
%=====================================================
%
% CALCULATE NODAL FORCES CAUSED BY WHEEL RAIL HERTZIAN CONTACT
%
Fx(46)=0;                % Initialise vector
Mx(46)=0;                % Initialise vector
kb(10:16:362)=kb*ones(1,23);

kb(16:16:368)=kb(10:16:362);    % Ballast stiffness initialisation

cb(10:16:362)=0.18*2*sqrt(kb(10:16:362)*(mr+ms/2));  % ballast damping
cb(16:16:368)=0.18*2*sqrt(kb(16:16:368)*(mr+ms/2));
%%%%%%%%%%%%%%%%%%%%%%%%%%%%%%%%%%%%%%%%%%%%%%%%%%%%%%%%%%%%%%

zz=fix((vel*t+axs)/rl)+1;      % bay number of wheel
loca=vel*t+axs-(zz-1)*rl;locb=rl-loca; % wheel position in bay

A(1)=    x(16*(zz-1)-15);              % Cubic polynomial constants
A(2)=                  -rl*x(16*(zz-1)-13);
A(3)= -3*x(16*(zz-1)-15)+2*rl*x(16*(zz-1)-13)+3*x(16*zz-15)+rl*x(16*zz-13);
A(4)=  2*x(16*(zz-1)-15)-  rl*x(16*(zz-1)-13)-2*x(16*zz-15)-rl*x(16*zz-13);

P1=A(1)+A(2)*loca/rl+A(3)*(loca/rl)^2+A(4)*(loca/rl)^3;
     % Solve cubic polynomial of rail ht at contact pt
```

```
dw1=P1+xc1-x(369);  % contact approach (+ve if in contact)
   if dw1> 0;Fv1=(dw1/kh)^(3/2);  % If wheel in contact, Hertz force
   elseif dw1<=0;Fv1=0;end;       % Loss of wheel contact force = 0
Mx(zz*2-3)= Fv1*loca*locb^2/(rl^2);      % Moment at previous node
Mx(zz*2-1)=-Fv1*locb*loca^2/(rl^2);      % Moment at next node
Fx(zz*2-3)=-Fv1*locb^2*(3*loca+locb)/(rl^3);% Vertical force at previous node
Fx(zz*2-1)=-Fv1*loca^2*(3*locb+loca)/(rl^3);  % Vertical force at next node

A(1)=x(16*(zz-1)-11);              % Repeat for opposite wheel
A(2)=-rl*x(16*(zz-1)-9);
A(3)=-3*x(16*(zz-1)-11)+2*rl*x(16*(zz-1)-9)+3*x(16*zz-11)+rl*x(16*zz-9);
A(4)=2*x(16*(zz-1)-11)-rl*x(16*(zz-1)-9)-2*x(16*zz-11)-rl*x(16*zz-9);
P2=A(1)+   A(2)*loca/rl+   A(3)*(loca/rl)^2+   A(4)*(loca/rl)^3;
dw2=P2+xc2-x(375);
   if dw2> 0;Fv2=(dw2/kh)^(3/2);
   elseif dw2<=0;Fv2=0;end;
Mx(zz*2-2)=Fv2*loca*locb^2/(rl^2);
Mx(zz*2)=-Fv2*locb*loca^2/(rl^2);
Fx(zz*2-2)=-Fv2*locb^2*(3*loca+locb)/(rl^3);
Fx(zz*2)=-Fv2*loca^2*(3*locb+loca)/(rl^3);
%
zz=fix((vel*t)/rl)+1;
loca=vel*t-(zz-1)*rl;locb=rl-loca;

A(1)=x(16*(zz-1)-15);
A(2)=-rl*x(16*(zz-1)-13);
A(3)=-3*x(16*(zz-1)-15)+2*rl*x(16*(zz-1)-13)+3*x(16*zz-15)+rl*x(16*zz-13);
A(4)=2*x(16*(zz-1)-15)-rl*x(16*(zz-1)-13)-2*x(16*zz-15)-rl*x(16*zz-13);
P3=A(1)+A(2)*loca/rl+A(3)*(loca/rl)^2+A(4)*(loca/rl)^3;
dw3=P3+xc3-x(377);
   if dw3> 0;Fv3=(dw3/kh)^(3/2);
   elseif dw3<=0;Fv3=0;end;
Mx(zz*2-3)=Fv3*loca*locb^2/(rl^2);
Mx(zz*2-1)=-Fv3*locb*loca^2/(rl^2);
Fx(zz*2-3)=-Fv3*locb^2*(3*loca+locb)/(rl^3);
Fx(zz*2-1)=-Fv3*loca^2*(3*locb+loca)/(rl^3);


A(1)=x(16*(zz-1)-11);
A(2)=-rl*x(16*(zz-1)-9);
A(3)=-3*x(16*(zz-1)-11)+2*rl*x(16*(zz-1)-9)+3*x(16*zz-11)+rl*x(16*zz-9);
A(4)=2*x(16*(zz-1)-11)-rl*x(16*(zz-1)-9)-2*x(16*zz-11)-rl*x(16*zz-9);
P4=A(1)+A(2)*loca/rl+A(3)*(loca/rl)^2+A(4)*(loca/rl)^3;
dw4=P4+xc4-x(383);
   if dw4> 0;Fv4=(dw4/kh)^(3/2);
   elseif dw4<=0;Fv4=0;end;
Mx(zz*2-2)=Fv4*loca*locb^2/(rl^2);
Mx(zz*2)=-Fv4*locb*loca^2/(rl^2);
Fx(zz*2-2)=-Fv4*locb^2*(3*loca+locb)/(rl^3);
Fx(zz*2)=-Fv4*loca^2*(3*locb+loca)/(rl^3);
%
%
```

```
%
%==========================================================================
%  NODAL FORCES DUE TO BEAM DEFLECTION
%
%  NEGATIVES OF STIFFNESS MATRICIES ( 4 BLOCKS )
%
%  permits calculation of nodal forces due to the deflections and rotations
%  of the rail beam.
%
stiff1=[-24 12 0 0 0 0 0 0 0 0 0 0 0 0 0 0 0 0 0 0 0 0 0
 12 -24 12 0 0 0 0 0 0 0 0 0 0 0 0 0 0 0 0 0 0
 0 12 -24 12 0 0 0 0 0 0 0 0 0 0 0 0 0 0 0 0 0
 0 0 12 -24 12 0 0 0 0 0 0 0 0 0 0 0 0 0 0 0 0
 0 0 0 12 -24 12 0 0 0 0 0 0 0 0 0 0 0 0 0 0 0
 0 0 0 0 12 -24 12 0 0 0 0 0 0 0 0 0 0 0 0 0 0
 0 0 0 0 0 12 -24 12 0 0 0 0 0 0 0 0 0 0 0 0 0
 0 0 0 0 0 0 12 -24 12 0 0 0 0 0 0 0 0 0 0 0 0
 0 0 0 0 0 0 0 12 -24 12 0 0 0 0 0 0 0 0 0 0 0
 0 0 0 0 0 0 0 0 12 -24 12 0 0 0 0 0 0 0 0 0 0
 0 0 0 0 0 0 0 0 0 12 -24 12 0 0 0 0 0 0 0 0 0
 0 0 0 0 0 0 0 0 0 0 12 -24 12 0 0 0 0 0 0 0 0
 0 0 0 0 0 0 0 0 0 0 0 12 -24 12 0 0 0 0 0 0 0
 0 0 0 0 0 0 0 0 0 0 0 0 12 -24 12 0 0 0 0 0 0
 0 0 0 0 0 0 0 0 0 0 0 0 0 12 -24 12 0 0 0 0 0
 0 0 0 0 0 0 0 0 0 0 0 0 0 0 12 -24 12 0 0 0 0
 0 0 0 0 0 0 0 0 0 0 0 0 0 0 0 12 -24 12 0 0 0
 0 0 0 0 0 0 0 0 0 0 0 0 0 0 0 0 12 -24 12 0 0
 0 0 0 0 0 0 0 0 0 0 0 0 0 0 0 0 0 12 -24 12 0
 0 0 0 0 0 0 0 0 0 0 0 0 0 0 0 0 0 0 12 -24 12
 0 0 0 0 0 0 0 0 0 0 0 0 0 0 0 0 0 0 0 12 -24 12 0
 0 0 0 0 0 0 0 0 0 0 0 0 0 0 0 0 0 0 0 0 12 -24 12
 0 0 0 0 0 0 0 0 0 0 0 0 0 0 0 0 0 0 0 0 0 12 -24];

stiff2=rl*[0 -6 0 0 0 0 0 0 0 0 0 0 0 0 0 0 0 0 0 0 0 0 0
 6 0 -6 0 0 0 0 0 0 0 0 0 0 0 0 0 0 0 0 0 0
 0 6 0 -6 0 0 0 0 0 0 0 0 0 0 0 0 0 0 0 0 0
 0 0 6 0 -6 0 0 0 0 0 0 0 0 0 0 0 0 0 0 0 0
 0 0 0 6 0 -6 0 0 0 0 0 0 0 0 0 0 0 0 0 0 0
 0 0 0 0 6 0 -6 0 0 0 0 0 0 0 0 0 0 0 0 0 0
 0 0 0 0 0 6 0 -6 0 0 0 0 0 0 0 0 0 0 0 0 0
 0 0 0 0 0 0 6 0 -6 0 0 0 0 0 0 0 0 0 0 0 0
 0 0 0 0 0 0 0 6 0 -6 0 0 0 0 0 0 0 0 0 0 0
 0 0 0 0 0 0 0 0 6 0 -6 0 0 0 0 0 0 0 0 0 0
 0 0 0 0 0 0 0 0 0 6 0 -6 0 0 0 0 0 0 0 0 0
 0 0 0 0 0 0 0 0 0 0 6 0 -6 0 0 0 0 0 0 0 0
 0 0 0 0 0 0 0 0 0 0 0 6 0 -6 0 0 0 0 0 0 0
 0 0 0 0 0 0 0 0 0 0 0 0 6 0 -6 0 0 0 0 0 0
 0 0 0 0 0 0 0 0 0 0 0 0 0 6 0 -6 0 0 0 0 0
 0 0 0 0 0 0 0 0 0 0 0 0 0 0 6 0 -6 0 0 0 0
 0 0 0 0 0 0 0 0 0 0 0 0 0 0 0 6 0 -6 0 0 0
 0 0 0 0 0 0 0 0 0 0 0 0 0 0 0 0 6 0 -6 0 0
 0 0 0 0 0 0 0 0 0 0 0 0 0 0 0 0 0 6 0 -6 0
 0 0 0 0 0 0 0 0 0 0 0 0 0 0 0 0 0 0 6 0 -6
 0 0 0 0 0 0 0 0 0 0 0 0 0 0 0 0 0 0 0 6 0 -6 0
 0 0 0 0 0 0 0 0 0 0 0 0 0 0 0 0 0 0 0 0 6 0 -6
 0 0 0 0 0 0 0 0 0 0 0 0 0 0 0 0 0 0 0 0 0 6 0];
```

```
stiff3=rl*[0 6 0 0 0 0 0 0 0 0 0 0 0 0 0 0 0 0 0 0 0 0 0
 -6 0 6 0 0 0 0 0 0 0 0 0 0 0 0 0 0 0 0 0 0 0 0
 0 -6 0 6 0 0 0 0 0 0 0 0 0 0 0 0 0 0 0 0 0 0 0
 0 0 -6 0 6 0 0 0 0 0 0 0 0 0 0 0 0 0 0 0 0 0 0
 0 0 0 -6 0 6 0 0 0 0 0 0 0 0 0 0 0 0 0 0 0 0 0
 0 0 0 0 -6 0 6 0 0 0 0 0 0 0 0 0 0 0 0 0 0 0 0
 0 0 0 0 0 -6 0 6 0 0 0 0 0 0 0 0 0 0 0 0 0 0 0
 0 0 0 0 0 0 -6 0 6 0 0 0 0 0 0 0 0 0 0 0 0 0 0
 0 0 0 0 0 0 0 -6 0 6 0 0 0 0 0 0 0 0 0 0 0 0 0
 0 0 0 0 0 0 0 0 -6 0 6 0 0 0 0 0 0 0 0 0 0 0 0
 0 0 0 0 0 0 0 0 0 -6 0 6 0 0 0 0 0 0 0 0 0 0 0
 0 0 0 0 0 0 0 0 0 0 -6 0 6 0 0 0 0 0 0 0 0 0 0
 0 0 0 0 0 0 0 0 0 0 0 -6 0 6 0 0 0 0 0 0 0 0 0
 0 0 0 0 0 0 0 0 0 0 0 0 -6 0 6 0 0 0 0 0 0 0 0
 0 0 0 0 0 0 0 0 0 0 0 0 0 -6 0 6 0 0 0 0 0 0 0
 0 0 0 0 0 0 0 0 0 0 0 0 0 0 -6 0 6 0 0 0 0 0 0
 0 0 0 0 0 0 0 0 0 0 0 0 0 0 0 -6 0 6 0 0 0 0 0
 0 0 0 0 0 0 0 0 0 0 0 0 0 0 0 0 -6 0 6 0 0 0 0
 0 0 0 0 0 0 0 0 0 0 0 0 0 0 0 0 0 -6 0 6 0 0 0
 0 0 0 0 0 0 0 0 0 0 0 0 0 0 0 0 0 0 -6 0 6 0 0
 0 0 0 0 0 0 0 0 0 0 0 0 0 0 0 0 0 0 0 -6 0 6 0
 0 0 0 0 0 0 0 0 0 0 0 0 0 0 0 0 0 0 0 0 -6 0 6
 0 0 0 0 0 0 0 0 0 0 0 0 0 0 0 0 0 0 0 0 0 -6 0];


stiff4=rl^2*[-8 -2 0 0 0 0 0 0 0 0 0 0 0 0 0 0 0 0 0 0 0 0 0
 -2 -8 -2 0 0 0 0 0 0 0 0 0 0 0 0 0 0 0 0 0 0 0 0
 0 -2 -8 -2 0 0 0 0 0 0 0 0 0 0 0 0 0 0 0 0 0 0 0
 0 0 -2 -8 -2 0 0 0 0 0 0 0 0 0 0 0 0 0 0 0 0 0 0
 0 0 0 -2 -8 -2 0 0 0 0 0 0 0 0 0 0 0 0 0 0 0 0 0
 0 0 0 0 -2 -8 -2 0 0 0 0 0 0 0 0 0 0 0 0 0 0 0 0
 0 0 0 0 0 -2 -8 -2 0 0 0 0 0 0 0 0 0 0 0 0 0 0 0
 0 0 0 0 0 0 -2 -8 -2 0 0 0 0 0 0 0 0 0 0 0 0 0 0
 0 0 0 0 0 0 0 -2 -8 -2 0 0 0 0 0 0 0 0 0 0 0 0 0
 0 0 0 0 0 0 0 0 -2 -8 -2 0 0 0 0 0 0 0 0 0 0 0 0
 0 0 0 0 0 0 0 0 0 -2 -8 -2 0 0 0 0 0 0 0 0 0 0 0
 0 0 0 0 0 0 0 0 0 0 -2 -8 -2 0 0 0 0 0 0 0 0 0 0
 0 0 0 0 0 0 0 0 0 0 0 -2 -8 -2 0 0 0 0 0 0 0 0 0
 0 0 0 0 0 0 0 0 0 0 0 0 -2 -8 -2 0 0 0 0 0 0 0 0
 0 0 0 0 0 0 0 0 0 0 0 0 0 -2 -8 -2 0 0 0 0 0 0 0
 0 0 0 0 0 0 0 0 0 0 0 0 0 0 -2 -8 -2 0 0 0 0 0 0
 0 0 0 0 0 0 0 0 0 0 0 0 0 0 0 -2 -8 -2 0 0 0 0 0
 0 0 0 0 0 0 0 0 0 0 0 0 0 0 0 0 -2 -8 -2 0 0 0 0
 0 0 0 0 0 0 0 0 0 0 0 0 0 0 0 0 0 -2 -8 -2 0 0 0
 0 0 0 0 0 0 0 0 0 0 0 0 0 0 0 0 0 0 -2 -8 -2 0 0
 0 0 0 0 0 0 0 0 0 0 0 0 0 0 0 0 0 0 0 -2 -8 -2 0
 0 0 0 0 0 0 0 0 0 0 0 0 0 0 0 0 0 0 0 0 -2 -8 -2
 0 0 0 0 0 0 0 0 0 0 0 0 0 0 0 0 0 0 0 0 0 -2 -8];

F1=rstf*[x(1:16:353) x(5:16:357) ]'*stiff1 ...
   +rstf*[x(3:16:355) x(7:16:359) ]'*stiff2; % rail vert force due to displacements

F2=rstf*[x(1:16:353) x(5:16:357) ]'*stiff3 ...
   +rstf*[x(3:16:355) x(7:16:359)]'*stiff4; % rail rotational force due
                                           % to displacements
```

```
%==========================================================================
%         SET STATE VARIABLES
%
xdot(1:2:395)=x(2:2:396);        % Velocity

%%           TRACK

xdot(2:16:354)=(Fx(1:2:45)+F1(1,:) ...
           +kp*(x(9:16:361) -x(1:16:353))' ...
           +cp*(x(10:16:362)-x(2:16:354))')/mr-g;     % RAIL NODE 1

xdot(4:16:356)=(Mx(1:2:45)+F2(1,:))/(mr*rl^2/12);    % RAIL ROT NODE 1

xdot(6:16:358)=(Fx(2:2:46)+F1(2,:) ...
           +kp*(x(15:16:367)-x(5:16:357))' ...
           +cp*(x(16:16:368)-x(6:16:358))')/mr-g;     % RAIL NODE 2

xdot(8:16:360)=(Mx(2:2:46)+F2(2,:))/(mr*rl^2/12);    % RAIL ROT NODE 2

xdot(10:16:362)=(-kp*(x(9:16:361)-x(1:16:353))' ...
            -kb(10:16:362).*x(9:16:361)' ...
            -cp*(x(10:16:362)-x(2:16:354))' ...
            -cb(10:16:362).*x(10:16:362)' ...
            -3*Els/(sl^3)*(x(9:16:361)-x(11:16:363))' ...
            +3*Els/(sl^2)*x(13:16:365)')/(3*ms/8)-g; % SLEEPER OUTER NODE 1 (3/8 mass)

xdot(12:16:364)=(3*Els/(sl^3))*(x(9:16:361)+x(15:16:367)-2*x(11:16:363))' ...
            /(ms/4)-g;              % SLEEPER INNER NODE   ( 1/4 mass)

xdot(14:16:366)=(3*Els/(sl^2)*(x(9:16:361)-x(15:16:367))' ...
           -6*Els/(sl)*x(13:16:365)')/(3/8*ms*sl^2/12); % SLEEPER ROT NODE

xdot(16:16:368)=(-kp*(x(15:16:367)-x(5:16:357))' ...
            -kb(16:16:368).*x(15:16:367)' ...
            -cp*(x(16:16:368)-x(6:16:358))' ...
            -cb(16:16:368).*x(16:16:368)' ...
            -3*Els/(sl^3)*(x(15:16:367)-x(11:16:363))' ...
            -3*Els/(sl^2)*x(13:16:365)')/(3*ms/8)-g;  % SLEEPER OUTER NODE 2

%
%           VEHICLE
%
xdot(370)=(Fv1-ks*(x(369)-x(385)+axs/2*x(387)) ...
          -cs*(x(370)-x(386)+axs/2*x(388)) ...
          -3*Ela/(sl^3)*(x(369)-x(371)) ...
          +3*Ela/(sl^2)*x(373))/mu-g;                % WHEEL 1

xdot(372)=(3*Ela/(sl^3)*(x(369)-2*x(371)+x(375)))/ma-g; % AXLE 1 VERT

xdot(374)=(3*Ela/(sl^2)*(x(369)-x(375)) ...
       -6*Ela/(sl^2)*x(373))/(ma*sl^2/12);            % AXLE 1 ROT

xdot(376)=(Fv2-ks*(x(375)-x(389)+axs/2*x(391)) ...
          -cs*(x(376)-x(390)+axs/2*x(392)) ...
          -3*Ela/(sl^3)*(x(375)-x(371)) ...
          -3*Ela/(sl^2)*x(373))/mu-g;                 % WHEEL 2
```

```
%   Second axle set
%
xdot(378)=(Fv3-ks*(x(377)-x(385)-axs/2*x(387)) ...
            -cs*(x(378)-x(386)-axs/2*x(388)) ...
         -3*Ela/(sl^3)*(x(377)-x(379)) ...
         +3*Ela/(sl^2)*x(381))/mu-g;                  % WHEEL 3


xdot(380)=(3*Ela/(sl^3)*(x(377)-2*x(379)+x(383)))/ma-g; % AXLE 2 VERT

xdot(382)=(3*Ela/(sl^2)*(x(377)-x(383)) ...
        -6*Ela/(sl^2)*x(381))/(ma*sl^2/12);            % AXLE 2 ROT

xdot(384)=(Fv4-ks*(x(383)-x(389)-axs/2*x(391)) ...
            -cs*(x(384)-x(390)-axs/2*x(392)) ...
        -3*Ela/(sl^3)*(x(383)-x(379)) ...
        -3*Ela/(sl^2)*x(381))/mu-g;                    % WHEEL 4

%   SIDEFRAMES

xdot(386)=(-ks*(2*x(385)-x(369)-x(377)) ...
         -cs*(2*x(386)-x(370)-x(378)) ...
         -kss*(x(385)-x(393)) ...
         -css*(x(386)-x(394)) )/mb-g;                  % SF1 VERT

xdot(388)=(-ks*axs/2*(2*x(387)*axs/2+x(369)-x(377)) ...
         -cs*axs/2*(2*x(388)*axs/2+x(370)-x(378)) ...
          )/(mb*(axs^2)/12);                   % SF1 PITCH

xdot(390)=(-ks*(2*x(389)-x(375)-x(383)) ...
         -cs*(2*x(390)-x(376)-x(384)) ...
         -kss*(x(389)-x(393)) ...
         -css*(x(390)-x(394)) )/mb-g;                  % SF2 VERT

xdot(392)=(-ks*axs/2*(2*x(391)*axs/2+x(375)-x(383)) ...
         -cs*axs/2*(2*x(392)*axs/2+x(376)-x(384)) ...
         )/(mb*(axs^2)/12);                    % SF2 PITCH

xdot(394)=0;   %   BODY VERT  ( FIXED )

xdot(396)=0;   %   BODY ROLL  ( FIXED )


%
%     Contact force for the wheel number 1
%
xdot(397)=xdot(186);
xdot(398)=xdot(185);             %  Required for contact force calculation
xdot=xdot';                 %  Transpose vector
return;
```

Appendix 1.3 TRENG3.M

```
clear;
pack;
%
%   ANALYSIS OF ENERGY AT SLEEPER
%
%   M.Williams August 1993
%
load sa_100;  % load file
rl=0.66;      % set node length
ms=282;       % sleeper mass
mr=47*rl;     % rail mass
kb=17e6;      % ballast/foundation stiffness

cb=0.24*2*sqrt(kb*(ms/2+mr)); % ballast stiffness
LL=length(T)-90;
tstep1=T(2:LL)-T(1:LL-1);
BD1=(xdot(1:LL-1,48:70).^2+xdot(2:LL,48:70).^2)'/2*cb;
BAD=tstep1*ones(1,23).*BD1';
cBAD=cumsum(BAD);
sload=cBAD(length(cBAD),1:23)  % printout results
```

Appendix 1.4 FFTINT4.M

```
clear;
pack;
%
%     FFTINT2.M
%
%     DOUBLE INTEGRATION ROUTINE TO ANALYSE SLEEPER DISPLACEMENT
%
%     M.Williams 29 Jan 92
%
[A,B]=butter(4,15/16000,'high');
        % calculate coefficients for Butterworth filter

F1=2;    % start freq
F2=1;    % decimate step

load R95X;              % Load input file

a2=1955*(accel(:,2));    % Scale function
W2=hanning(2000);        % Set window function
W3=[zeros(1,8000) W2(1:1000)' ones(1,14000-9000) ...
   W2(1001:2000)' zeros(1,length(a2)-15000)]; % Total window

b1=a2(1);b2=a2(length(a2));
step=(b1-b2)/length(a2);
for ii=1:length(a2);
   CF(ii)=-b1+step*ii;
end;
a3=a2+CF';       % Adjust zero level of signal
a4=[zeros(1,(32768-length(a2))/2) (a3.*W3')' zeros(1,(32768-length(a2))/2)]';
             % Window data and add zero tails to each end to create 32768 pt
             % signal for efficient FFT processing
```

```
f2=fft(a4);                    % FFT of signal
N2=length(f2);
T2=32000*(0:N2-1)/N2;  % Calculate frequency steps
f2dc=f2;
f2dc(1:F1)=zeros(1,F1);  % remove DC drift from signal

dispf2=[f2dc(1:F1)' (f2dc(F1+1:length(f2dc))./ ...
         (2*pi*T2(F1+1:length(f2dc)).^2)')'];
% Convert acceleration to displacement by dividing by freq ^2
disp2z=ifft(dispf2);                % Inverse Fourier Transform
disp2=filtfilt(A,B,disp2z);          % Filter data

Td2=length(disp2);
Tdd2=1/(32000/F2)*[1:Td2]*length(f2)/length(dispf2);
plot(Tdd2(3000:10:length(Tdd2)),-1000*abs(disp2(3000:10:length(disp2))));

grid,xlabel('Time (s)'),ylabel('Displacement (mm)')
title('R95X, 4247 ,130 km/hr,09 MAR 93,E0200')
pause
return
```

Appendix 1.5 TREIG4.M

```
clear;
pack;
%*****************************************************************************
%
%  MODAL ANALYSIS ROUTINE
%
%
% 24 bay model with two rails
%     %    TREIG4.M
%
%
%     Version 31
%    M. Williams 30 AUG 93
%*******************************************************
clg;
rl=0.66;    % sleeper bay length ( node spacing) (m)
g=9.81;

Elr=3.19e+6;    % Rail bending stiffness
Els=4.00e+6;    % Sleeper bending stiffness
Ela=12.5e+6;    % Axle bending stiffness
rstf=Elr/(rl^3);
sl=1.5/2;      % half sleeper length
axs=1.8;       % axle spacing (m)
pss=2.1;       % primary suspension spacing
sss=2.1;       % secondary suspension spacing
%
% % % % % % % % % % % % % % % % % %     M A S S   P A R A M E T E R S
%%%%%%%%%%%%%%%%%%%%%%%%%%%%%%%%%%%%%%%%%%%%%%%%%%
mv=34700;    % mass of vehicle body  (kg)
mb=1212;    % mass of bogie (kg)
mu=380;     % unsprung mass of wheel  (kg)
mr=47*rl;   % nodal mass of rail (kg/m)
ms=292.6;   % mass of sleeper (kg)
ma=282;     % axle mass
%%%%%%%%%%%%%%%%%% STIFFNESS PARAMETERS %%%%%%
kss=2.4e6;    % secondary suspension
ks=2.5e6;    % primary suspension stiffness
kb=17e6;     % ballast stiffness (N/m)
kp=250e6;    % pad stiffness    (N/m)
kh=1.21e9;   % hertzian contact stiffness
%
r1=[(1:8:161)];
s1=[(5:8:165)];
l1=[1:21];
%=====================================================
%
% Calculate stiffness and mass matrices
%
%%%%%%%%%%%%%%%%%%%%%%%%%%%%%%%%%%%%%%%%%%%%%%%%%%%%%%%%
ST(9, 1)= 12*rstf;
ST(9, 2)=-6*rl*rstf;
ST(9, 9)=-24*rstf-kp;
ST(9,13)= kp;
ST(9,17)= 12*rstf;
ST(9,18)= 6*rl*rstf;
```

```
ST(10, 1)= 6*rl*rstf;
ST(10, 2)=-2*rl^2*rstf;
ST(10,10)=-8*rl^2*rstf;
ST(10,17)=-6*rl*rstf;
ST(10,18)=-2*rl^2*rstf;

ST(11, 3)=12*rstf;
ST(11, 4)=-6*rl*rstf;
ST(11,11)=-24*rstf-kp;
ST(11,16)=kp;
ST(11,19)=12*rstf;
ST(11,20)=6*rl*rstf;

ST(12, 3)= 6*rl*rstf;
ST(12, 4)=-2*rl^2*rstf;
ST(12,12)=-8*rl^2*rstf;
ST(12,19)=-6*rl*rstf;
ST(12,20)=-2*rl^2*rstf;

ST(13, 9)= kp;
ST(13,13)=-kp-kb-3*Els/(sl^3);
ST(13,14)= 3*Els/(sl^3);
ST(13,15)= 2*Els/(sl^2);

ST(14,13)= 3*Els/(sl^3);
ST(14,14)=-6*Els/(sl^3);
ST(14,16)= 3*Els/(sl^3);

ST(15,13)= 2*Els/(sl^2);
ST(15,15)=-2*Els/(sl^2);
ST(15,16)=-2*Els/(sl^2);

ST(16,11)=kp;
ST(16,16)=-kp-kb-3*Els/(sl^3);
ST(16,14)= 3*Els/(sl^3);
ST(16,15)=-2*Els/(sl^2);

M(12,20)=0;
M(9,9)=mr;
M(10,10)=mr*rl^2/12;
M(11,11)=mr;
M(12,12)=mr*rl^2/12;
M(13,13)=ms/4;

M(14,14)=3/8*ms;

M(15,15)=0.25*ms*sl^2/12;

M(16,16)=ms/4;
```

```
ST1=[          ST(9:16,9:20) zeros(8,172)
            ST(9:16,:) zeros(8,164)
    zeros(8,8)  ST(9:16,:) zeros(8,156)
    zeros(8,16) ST(9:16,:) zeros(8,148)
    zeros(8,24) ST(9:16,:) zeros(8,140)
    zeros(8,32) ST(9:16,:) zeros(8,132)
    zeros(8,40) ST(9:16,:) zeros(8,124)
    zeros(8,48) ST(9:16,:) zeros(8,116)
    zeros(8,56) ST(9:16,:) zeros(8,108)
    zeros(8,64) ST(9:16,:) zeros(8,100)
    zeros(8,72) ST(9:16,:) zeros(8, 92)
    zeros(8,80) ST(9:16,:) zeros(8, 84)
    zeros(8,88) ST(9:16,:) zeros(8, 76)
    zeros(8,96) ST(9:16,:) zeros(8, 68)
    zeros(8,104) ST(9:16,:) zeros(8, 60)
    zeros(8,112) ST(9:16,:) zeros(8, 52)
    zeros(8,120) ST(9:16,:) zeros(8, 44)
    zeros(8,128) ST(9:16,:) zeros(8, 36)
    zeros(8,136) ST(9:16,:) zeros(8, 28)
    zeros(8,144) ST(9:16,:) zeros(8, 20)
    zeros(8,152) ST(9:16,:) zeros(8, 12)
    zeros(8,160) ST(9:16,:) zeros(8,  4)
    zeros(8,168) ST(9:16,1:16)        ];

%%%%%%%%%%%%%%%%%%%%%%%%%%%%%%%%%%%%
M1=[          M(9:16,9:20) zeros(8,172)
            M(9:16,:) zeros(8,164)
    zeros(8,8)  M(9:16,:) zeros(8,156)
    zeros(8,16) M(9:16,:) zeros(8,148)
    zeros(8,24) M(9:16,:) zeros(8,140)
    zeros(8,32) M(9:16,:) zeros(8,132)
    zeros(8,40) M(9:16,:) zeros(8,124)
    zeros(8,48) M(9:16,:) zeros(8,116)
    zeros(8,56) M(9:16,:) zeros(8,108)
    zeros(8,64) M(9:16,:) zeros(8,100)
    zeros(8,72) M(9:16,:) zeros(8, 92)
    zeros(8,80) M(9:16,:) zeros(8, 84)
    zeros(8,88) M(9:16,:) zeros(8, 76)
    zeros(8,96) M(9:16,:) zeros(8, 68)
    zeros(8,104) M(9:16,:) zeros(8, 60)
    zeros(8,112) M(9:16,:) zeros(8, 52)
    zeros(8,120) M(9:16,:) zeros(8, 44)
    zeros(8,128) M(9:16,:) zeros(8, 36)
    zeros(8,136) M(9:16,:) zeros(8, 28)
    zeros(8,144) M(9:16,:) zeros(8, 20)
    zeros(8,152) M(9:16,:) zeros(8, 12)
    zeros(8,160) M(9:16,:) zeros(8,  4)
    zeros(8,168) M(9:16,1:16)        ];

%%%%%%%%%%%%%%%%%%%%%%%%%%%%%%%%%%%%
% Vehicle
%
M1(153+32,153+32)=mu;
M1(154+32,154+32)=ma;
M1(155+32,155+32)=ma*sl^2/12;
M1(156+32,156+32)=mu;

M1(157+32,157+32)=mu;
M1(158+32,158+32)=ma;
M1(159+32,159+32)=ma*sl^2/12;
M1(160+32,160+32)=mu;
```

```
M1(161+32,161+32)=mb;
M1(162+32,162+32)=mb*axs^2/12;
M1(163+32,163+32)=mb*sss^2/12;
M1(164+32,164+32)=mv;
M1(165+32,165+32)=mv*sss^2/12;

%######################################################

ST1(153+32,81+16)=kh/2;
ST1(153+32,89+16)=kh/2;
ST1(81+16,153+32)=kh/2;
ST1(89+16,153+32)=kh/2;
ST1(81+16,81+16)=ST1(81+16,81+16)-kh/2;
ST1(89+16,89+16)=ST1(89+16,89+16)-kh/2;

ST1(153+32,153+32)=-12*Ela/(sl^3)-kh-ks;
ST1(153+32,161+32)=ks;
ST1(153+32,162+32)=-ks*axs/2;
ST1(153+32,163+32)=ks*pss/2;
ST1(153+32,154+32)=12*Ela/(sl^3);
ST1(153+32,155+32)=+6*Ela/(sl^2);

ST1(154+32,153+32)=12*Ela/(sl^3);
ST1(154+32,154+32)=-2*12*Ela/(sl^3);
ST1(154+32,156+32)=12*Ela/(sl^3);

ST1(155+32,153+32)= 6*Ela/(sl^2);
ST1(155+32,155+32)=-8*Ela/sl;
ST1(155+32,156+32)=-6*Ela/(sl^2);

ST1(156+32,83+16)=kh/2;
ST1(156+32,91+16)=kh/2;
ST1(83+16,156+32)=kh/2;
ST1(91+16,156+32)=kh/2;
ST1(83+16,83+16)=ST1(83+16,83+16)-kh/2;
ST1(91+16,91+16)=ST1(91+16,91+16)-kh/2;

ST1(156+32,156+32)=-12*Ela/(sl^3)-kh-ks;
ST1(156+32,161+32)=ks;
ST1(156+32,163+32)=-ks*pss/2;
ST1(156+32,162+32)=-ks*axs/2;
ST1(156+32,154+32)=12*Ela/(sl^3);
ST1(156+32,155+32)=-6*Ela/(sl^2);

ST1(157+32,57+16)=kh/2;
ST1(157+32,65+16)=kh/2;
ST1(57+16,157+32)=kh/2;
ST1(65+16,157+32)=kh/2;
ST1(57+16,57+16)=ST1(57+16,57+16)-kh/2;
ST1(65+16,65+16)=ST1(65+16,65+16)-kh/2;

ST1(157+32,157+32)=-12*Ela/(sl^3)-kh-ks;
ST1(157+32,161+32)=ks;
ST1(157+32,162+32)=ks*axs/2;
ST1(157+32,163+32)=ks*pss/2;
ST1(157+32,158+32)=12*Ela/(sl^3);
ST1(157+32,159+32)=+6*Ela/(sl^2);

ST1(158+32,157+32)=12*Ela/(sl^3);
ST1(158+32,158+32)=-2*12*Ela/(sl^3);
ST1(158+32,160+32)=12*Ela/(sl^3);
```

```
ST1(159+32,157+32)= 6*EIa/(sl^2);
ST1(159+32,159+32)=-8*EIa/sl;
ST1(159+32,160+32)=-6*EIa/(sl^2);

ST1(160+32,59+16)=kh/2;
ST1(160+32,67+16)=kh/2;
ST1(59+16,160+32)=kh/2;
ST1(67+16,160+32)=kh/2;
ST1(59+16,59+16)=ST1(59+16,59+16)-kh/2;
ST1(67+16,67+16)=ST1(67+16,67+16)-kh/2;

ST1(160+32,160+32)=-12*EIa/(sl^3)-kh-ks;
ST1(160+32,161+32)=ks;
ST1(160+32,162+32)=ks*axs/2;
ST1(160+32,163+32)=-ks*pss/2;
ST1(160+32,158+32)=12*EIa/(sl^3);
ST1(160+32,159+32)=-6*EIa/(sl^2);

ST1(161+32,161+32)=-4*ks-2*kss;
ST1(161+32,153+32)=ks;
ST1(161+32,156+32)=ks;
ST1(161+32,157+32)=ks;
ST1(161+32,160+32)=ks;
ST1(161+32,164+32)=2*kss;

ST1(162+32,162+32)=-4*ks*axs/2;
ST1(162+32,153+32)=-ks*axs/2;
ST1(162+32,156+32)=-ks*axs/2;
ST1(162+32,157+32)=ks*axs/2;
ST1(162+32,160+32)=ks*axs/2;

ST1(163+32,163+32)=-4*ks*pss/2-2*kss*sss/2;
ST1(163+32,153+32)=ks*pss/2;
ST1(163+32,156+32)=-ks*pss/2;
ST1(163+32,157+32)=ks*pss/2;
ST1(163+32,160+32)=-ks*pss/2;
ST1(163+32,165+32)=2*kss*sss/2;

ST1(164+32,164+32)=-2*kss;
ST1(164+32,161+32)=2*kss;

ST1(165+32,165+32)=-2*kss*sss/2;
ST1(165+32,163+32)=2*kss*sss/2;

Z1=ones(165+32,1);
Z2=diag(Z1);
[v1,a1]=eig(ST1/M1,Z2);          % Eigenvector routine
[a,k]=sort(diag(a1));
v=v1(:,k);
natf=sqrt(abs(a))/(2*pi);        % Natural frequencies
return
```

APPENDIX 2 MODAL ANALYSIS RESULTS

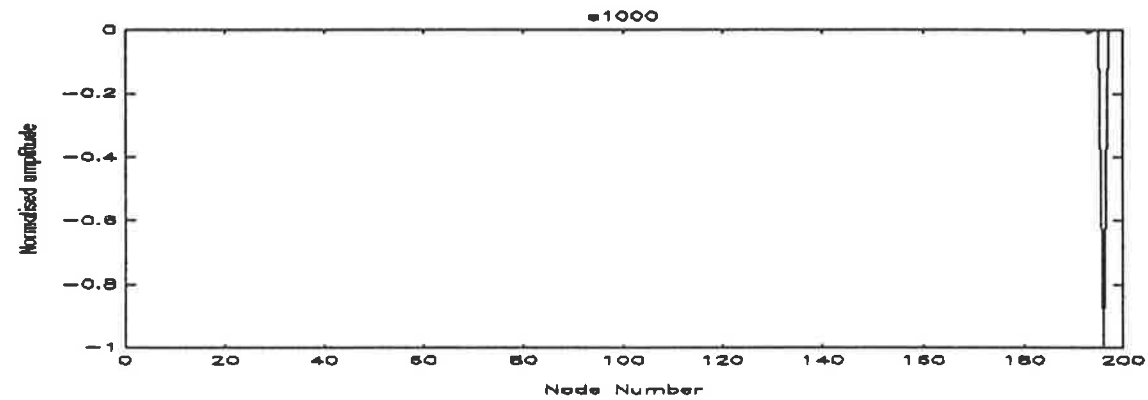

Figure A2.1 Mode 1, 1.5 Hz, Body vertical bounce

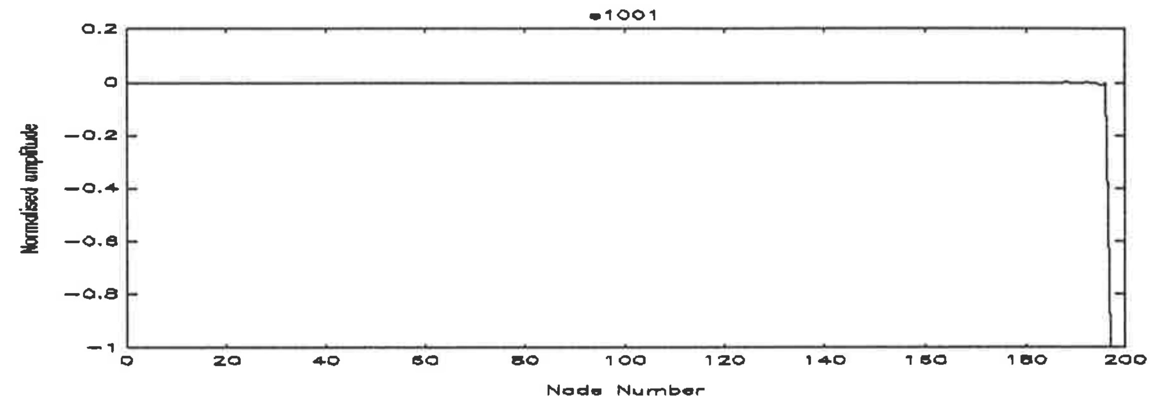

Figure A2.2 Mode 2, 2.6 Hz, Body roll

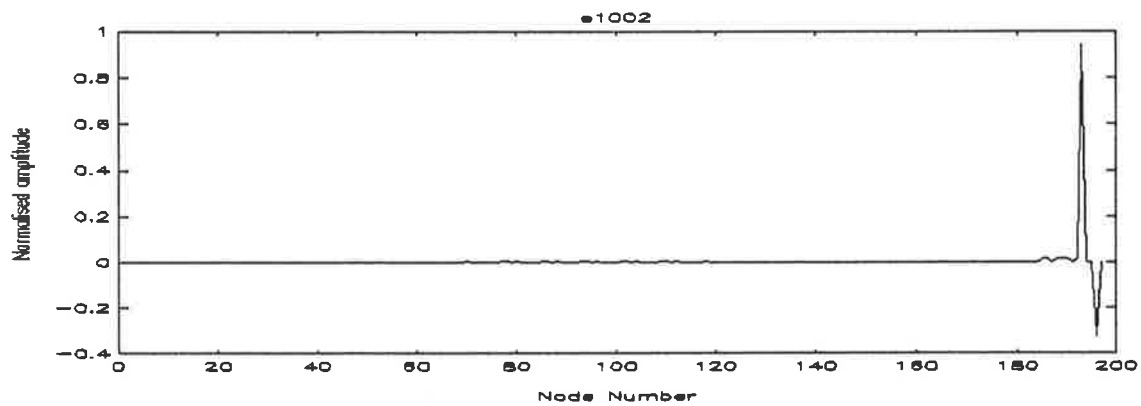

Figure A2.3 Mode 3, 17,2 Hz, Bogie bounce

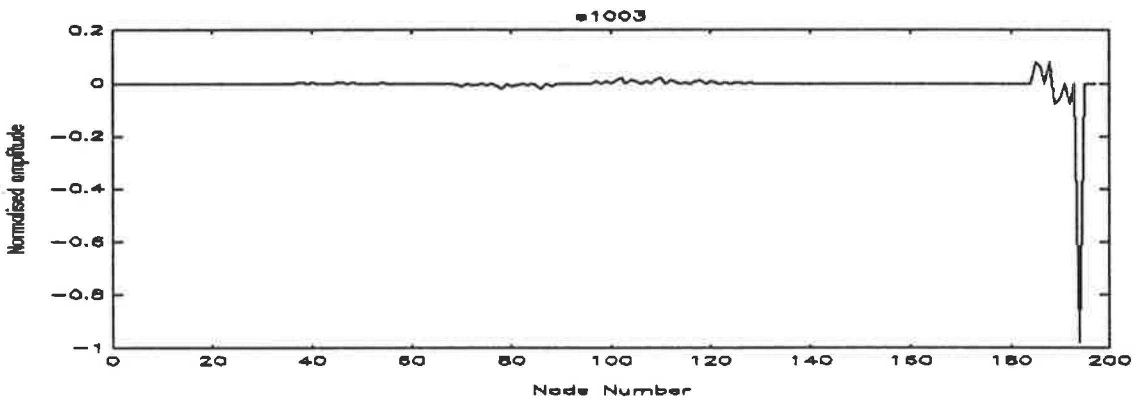

Figure A2.4 Mode 4, 25.5 Hz, Bogie pitch

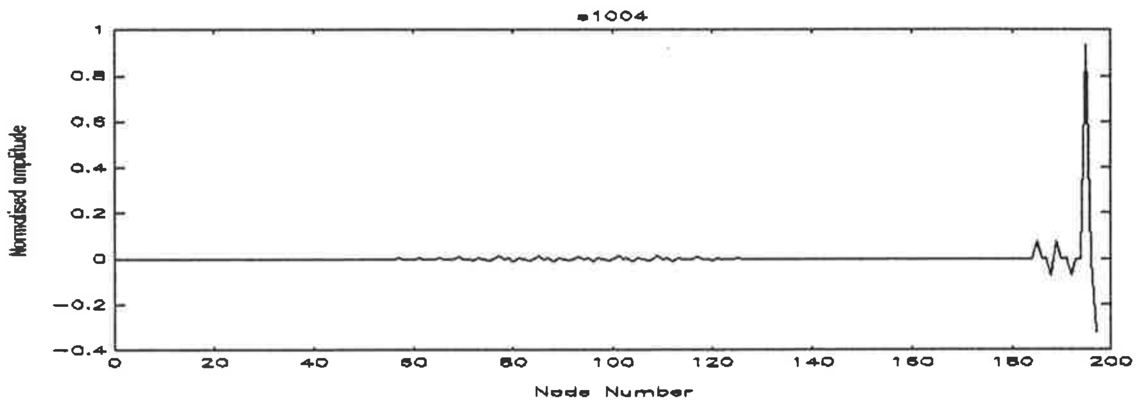

Figure A2.5 Mode 5, 28.8 Hz, Bogie roll

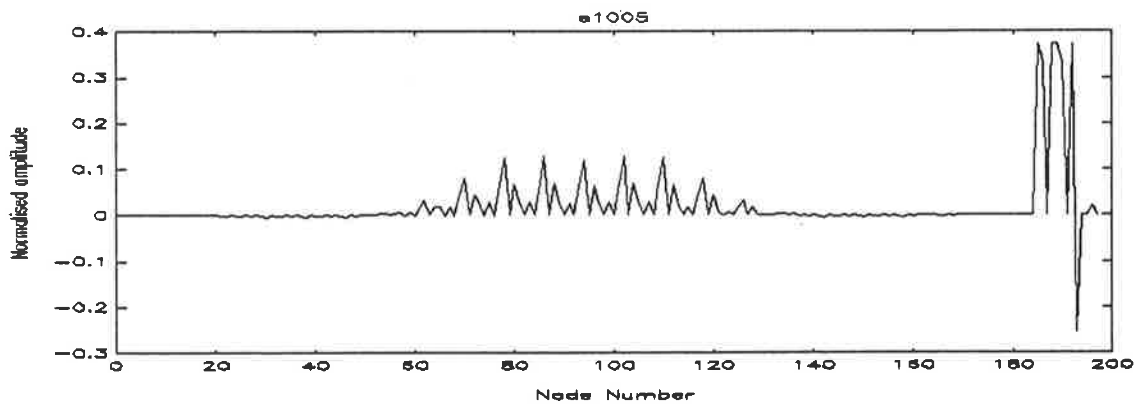

Figure A2.6 Mode 6, 36 Hz, Track forced, Symetric

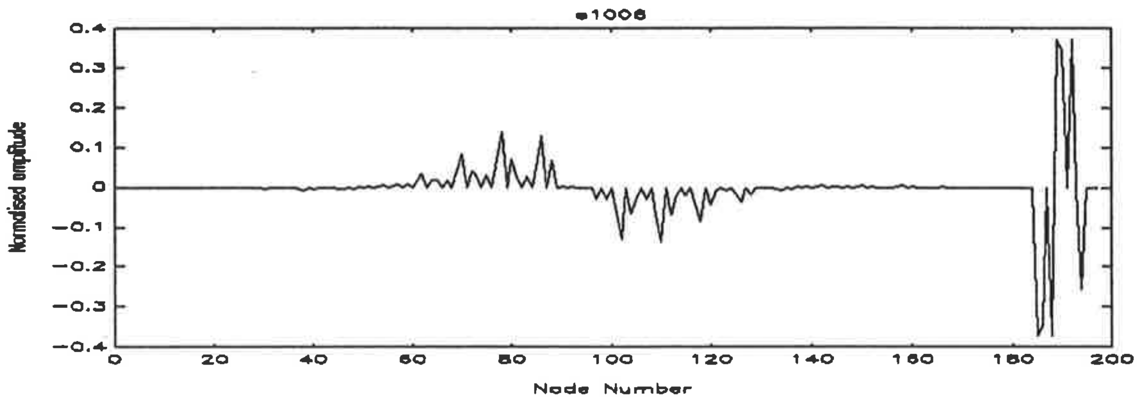

Figure A2.7 Mode 7, 40 Hz, Track forced, asymetric

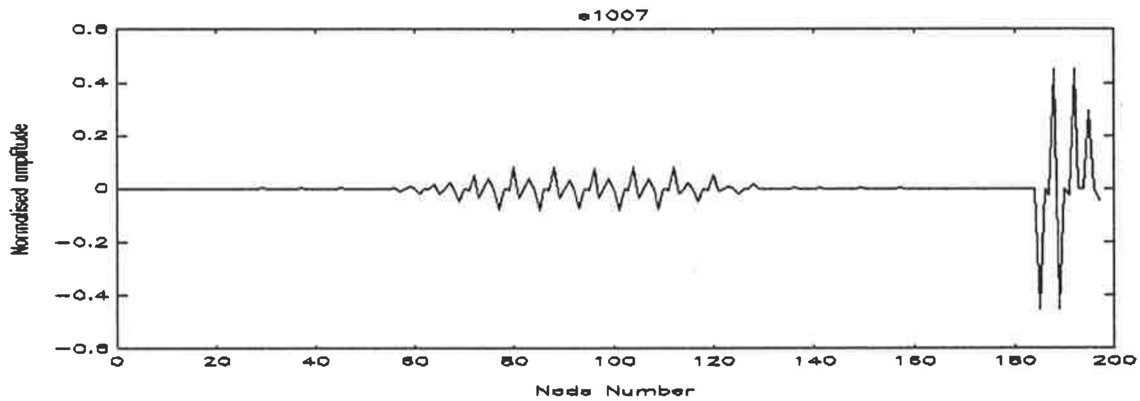

Figure A2.8 Mode 8, 44 Hz, Track forced asymetric

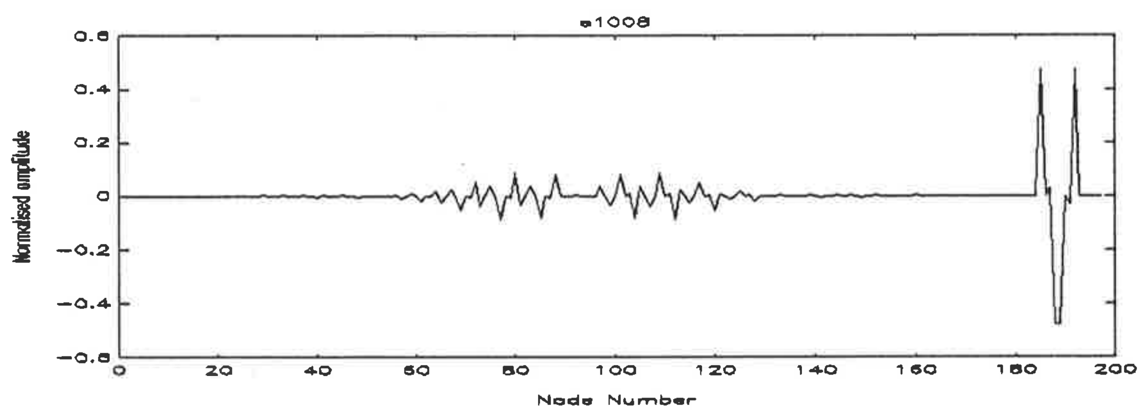

Figure A2.9, Mode 9, 48 Hz, Track forced, asymetric

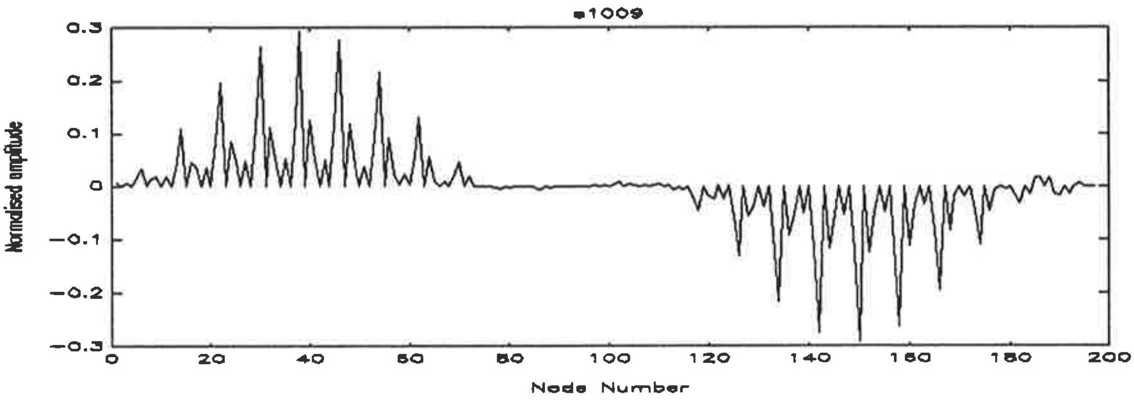

Figure A2.10 Mode 10, 48 Hz, Track free, symetric

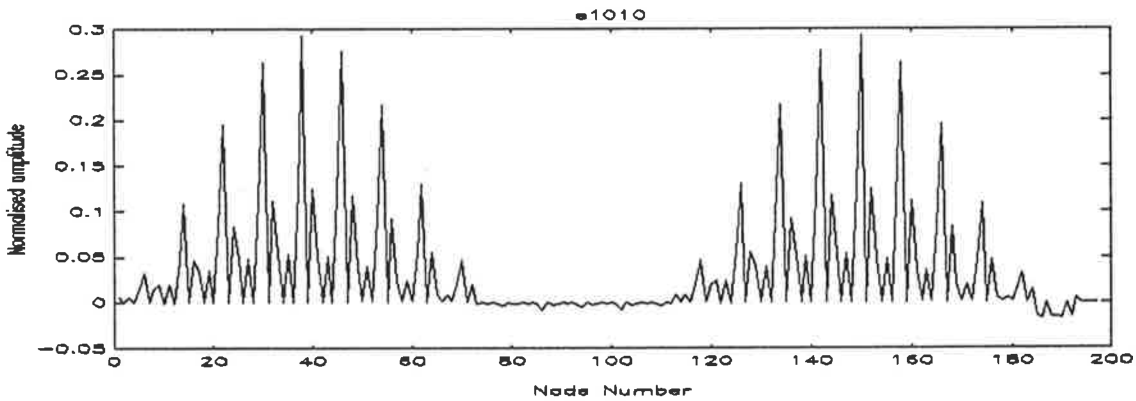

Figure A2.11 Mode 11, 48 Hz, Track free, symetric

APPENDIX 3 EXPERIMENTAL LOG

In this appendix the details of the test runs that were performed are listed. These lists show initially the vehicle consist with the axle loads of the vehicles of interest. Following these are the actual test runs undertaken which detail where to find the results on the tape recorder for post analysis, the estimated speed of the test and the location of the accelerometers on the track.

Shaded block shows data subsequently extracted and used in further analysis.

Test 1 06 Nov 1990

Vehicle consist

Vehicle identification number	Vehicle total mass	Individual axle load
GM46	116 Tonnes	19.3 Tonnes
GM47	116 Tonnes	19.3 Tonnes
CL 7	128 Tonnes	21.3 Tonnes
AZSY 1086		
AZTP 400		
AQMF 2778		
AQMF 2371		
AQMF 4240		
AQMF 2742		
AQMH 4247	25 Tonnes	4.5 Tonnes
AQMH 4228	69.7 Tonnes	17.43 Tonnes

TEST RUNS

Run Number	Data tape number	Tape Count of run start	Speed of test	Transducer A1 Tape channel 15	Transducer A2 Tape channel 16	
67	PG4	280	Calibration	S1 1VRMS	S1 1VRMS	
69	PG4	320	100	S1 Rail before dip	S1 Rail after dip	
70	PG4	337	110	"	"	
71	PG4	355	120	"	"	
72	PG4	371	130	"	S1 Rail @ 2 bays before dip	
73	PG4	391	130	"	"	
74	PG4	407	110	"	Not used	
75	PG4	425	100	"	S1 Sleeper @ CL	
76	PG4	444	100	S1 Rail Before dip	S1 Sleeper @ rail foot before dip	
77	PG4	461	90	"	"	
78	PG4	481	80	S1 Sleeper CL	"	
79	PG4	504	70	"	"	
80	PG4	527	60	"	"	
81	PG4	553	100	S1 Rail before dip	"	
82	PG4	568	120	"	"	

Test 2 13 Nov 90

Vehicle consist

Vehicle identification number	Total vehicle mass	Individual axle load
GM 43	116 Tonnes	19.3 Tonnes
GM 44	116 Tonnes	19.3 Tonnes
DL 37		
AZSY 1086		
AZTP 400		
AQMF 2778		
AQMF 2371		
AQMF 4274		
AQMF 4240		
AQMF 2742		
AQMH 4247	23 Tonnes	5.8 Tonnes
AQMH 4228	69.7 Tonnes	17.43 Tonnes

TEST RUNS

Run number	Data Tape number	Tape count of run start	Speed of test run	Transducer A1 Tape channel 15	Transducer A2 Tape channel 16	
85	PG4	1080	CAL	1 VRMS	1 VRMS	
87	"	1134	60	S2 Rail	S2 Sleeper	
88	"	1151	70	"	"	
89	"	1166	80	"	"	
90	"	1180	90	"	"	
91	"	1192	100	"	"	
92	"	1204	110	"	"	
93	"	1214	120	"	"	
94	"	1224	130	"	"	
95	"	1236	130	"	"	
96	"	1247	120	"	"	
97	"	1258	110	"	"	
98	"	1270	100	"	"	
99	"	1282	90	"	"	
100	"	1296	80	"	"	
101	"	1311	70	"	"	
102	"	1329	60	"	"	

Test 3 15 Nov 90

Vehicles

Vehicle identification number	Total vehicle mass	Individual axle load
GM 45	116 Tonnes	19.3 Tonnes
GM 37	116 Tonnes	19.3 Tonnes
601	116 Tonnes	18.6 Tonnes
AZSY 1086		
AZTP 400		
AQMF 2778		
AQMF 2371		
AQMF 4274		
AQMF 4240		
AQMF 2742		
AQMH 4247		
AQMH 4228	69.7 Tonnes	17.43 Tonnes
AQJY 18 (5 pack = 6 bogies)		

Test Runs

Run number	Data tape number	Tape count at run start	Speed of test run	Transducer A1 Tape channel 15	Transducer A2 Tape channel 16	
112	PG6	290	CAL	S3 Rail	S3 Sleeper	
115	"	377	100	"	"	
116	"	399	110	"	"	
117	"	420	110	"	"	
118	"	438	120	"	"	
119	"	460	100	"	"	
120	"	482	90	S4 Rail	S4 Sleeper	
121	"	508	80	"	"	
122	"	541	60	"	"	
123	"	560	90	"	"	
124	"	579	100	"	"	

Test 4 29 Nov 90

Test Consist

Vehicle identification number	Total vehicle mass	Individual axle load
GM 37	116 Tonnes	19.3 Tonnes
GM 35	116 Tonnes	19.3 Tonnes
AL 22		
AZSY 1086		
AZTP 400		
AQMF 2778		
AQMF 2371		
AQMF 4274		
AQMF 4240		
AQMF 2742		
AQMF 4247	76 Tonnes	19 Tonnes
AQMH 4228	69.7 Tonnes	17.43 Tonnes
AVEP 129		

Test Runs

Run number	Data tape number	Tape count at run start	Speed of test run	Transducer A1 Tape channel 15	Transducer A2 Tape channel 16
146	PG6	713	60	S2 Sleeper @ rail foot	S2 Sleeper @ centreline
147	"	734	70	"	"
148	"	753	80	"	"
149	"	769	90	"	"
150	"	785	100	"	"
151	"	801	110	"	"
152	"	816	120	"	"
153	"	828	130	"	"
154	"	842	120	"	S2 Sleeper @ 1/4 point
155	"	860	100	"	"
157	"	955	CAL	1 VRMS	1 VRMS

DIGITISED DATA LISTING

From the above tables the runs of interest were extracted via a analogue to digital converter through the software package CTRAN.

The following tables detail the blocks of data necessary to enable the double integration routine to give the displacement results.

The numbers contained within the tables are the start and end of the acceleration record of interest (in 1000^s). This information is used by CTRAN to extract the information of interest and output it in a form suitable to the post processing by the MATLAB software.

SITE 1

Run Number		76S		77S		81S		82S	
Speed		100		90		100		120	
lead GM46	B	10	30	0	18	0	17	25	45
GM46 GM47	D	30	58	18	50	17	39	45	65
GM47 CL7	F	58	86	50	81	39	60	65	85
CL7 1086	H	86	110	81	109	60	81	85	102
1086 400	J	110	133	109	134	81	98	102	118
400 2778	L	133	158	134	163	98	118	118	136
2778 2371	N	158	186	163	196	118	142	136	157
2371 4240	P	186	217	196	230	142	166	157	178
4240 2742	R	217	244	230	264	166	188	178	198
2742 4247	T	244	275	264	296	188	211	198	218
4247 4228	V	275	306	296	329	211	235	218	239
4228	X	306	337	329	363	235	266	239	270

RUN Number		91S		92S		93S		94S		95S		96S		97S		98S	
Speed		100		110		120		130		130		120		110		100	
Lead GM43	B	36	53	30	47	35	52	18	35	60	77	27	44	38	55	26	43
GM 43 GM44	D	50	75	47	68	52	71	35	52	77	94	44	60	55	72	43	62
GM44 DL37	F			68	90	71	90	52	71	94	110	60	77	72	90	62	82
DL37 1086	H			90	109	90	108	71	87	110	126	77	92	90	106	82	100
1086 400	J			109	126	108	123	87	101	126	139	92	105	106	120	100	116
400 2778	L			126	146	123	141	101	118	139	155	105	120	120	136	116	133
2778 2371	N			146	169	141	162	118	137	155	172	120	139	136	155	133	154
2371 4247	P			169	193	162	184	137	156	172	190	139	156	155	175	154	175
4247 4240	R			193	215	184	204	156	174	190	208	156	174	175	194	175	196
4240 2742	T			215	238	204	224	174	194	208	225	174	192	194	212	196	216
2742 4247	V	275	299	238	261	224	245	194	213	225	243	192	209	212	231	216	237
4247 4228	X	293	313	261	284	245	265	213	231	243	261	209	227	231	250	237	258
4228	Z	318	336	284	302	265	283	231	249	261	279	227	245	250	268	258	276

Calibration factor = 1955

SITE 3 and SITE 4

SITE		S 3										S 4					
RUN Number		115S		116S		117S		118S		119S		120S		123S		124S	
Speed		100		110		110		120		100		90		90		100	
lead GM45	B	37	55	65	85	28	48	10	30	15	31	1	20	25	45	28	46
GM45 GM37	D	55	78	85	105	48	68	30	49	31	54	20	45	45	70	46	68
GM37 601	F	78	98	105	125	68	88	49	67	54	73	45	69	70	93	68	90
601 1086	H	98	118	125	142	88	104	67	83	73	92	69	89	93	112	90	108
1086 400	J	118	135	142	157	104	119	83	98	92	111	89	109	112	134	108	125
400 2778	L	135	155	157	174	119	136	98	115	111	129	109	131	134	156	125	145
2778 2371	N	155	178	174	198	136	158	115	136	129	154	131	157	156	179	145	167
2371 4274	P	178	202	198	220	158	179	136	157	154	176	157	182	179	207	167	191
4274 4240	R	202	228	220	242	179	200	157	175	176	201	182	208	207	232	191	213
4240 2742	T	228	248	242	261	200	221	175	195	201	223	208	233	232	258	213	236
2742 4247	V	248	274	261	281	221	241	195	215	223	246	233	259	258	284	236	257
4247 4228	X	274	296	281	305	241	264	215	237	246	270	259	287	284	310	257	282
4228 18 (1)	Z	296	319	305	320	264	282	237	255	270	291	287	308	310	333	282	300
18(2)	ZB	319	332	320	338	282	295	255	266	291	304	308	324	333	348	300	314
18(3)	ZD	332	346	338	351	295	309	266	280	304	318	324	340	348	366	314	329
18(4)	ZF	346	362	351	364	309	320	280	292	318	333	340	356	366	382	329	343
18(5)	ZH	362	376	364	376	320	333	292	304	333	347	356	372	382	397	343	357
18(6)	ZJ	376	390	376	388	333	349	304	320	347	364	372	390	397	415	357	370

					4228	4228
Run Number	Speed (km hr^{-1})	Output File	Window from	Window to	Displacement (mm)	Displacement (mm)
R76X	100	E0316	2 000	17 000	0.8583	0.8491
R77X	90	E0317	6 000	20 000	0.8675	1.5664
R81X	100	E0318	3 000	15 000	1.0986	0.6354
R82X	120	E0319	2 000	15 000	0.6381	1.3173

					4247	4247	4228	4228
Run Numbe r	Speed (km hr^{-1})	Output File	Window from	Window to	Displ (mm)	Displ (mm)	Displ (mm)	Displ (mm)
R76V	100	E0320	5 000	25 000	0.6595	0.8621	1.1164	1.3208
R77V	90	E0321	7 000	20 000	0.9934	0.7374	0.9934	1.5299
R81V	100	E0322	7 000	20 000	1.2942	1.4689	1.3267	1.1397
R82V	120	E0323	4 000	17 000	1.0830	1.041	1.1443	1.0896

					GM46	GM46	GM46
Run Numbe r	Speed (km hr^{-1})	Output File	Window from	Window to	Displ (mm)	Displ (mm)	Displ (mm)
R76B	100	E0349	6 000	18 000	0.9097	1.022	1.111
R77B	90	E0350	5 000	16 000	1.0115	1.385	1.218
R81B	100	E0351	7 000	15 000	1.892	1.674	1.592
R82B	120	E0352	10 000	19 000	2.308	1.609	1.628

					GM46	GM46	GM46	GM47	GM47	GM47
Run Number	Speed (km hr^{-1})	Output File	Window from	Window to	Displ (mm)	Displ (mm)	Displ (mm)	Displ (mm)	Displ (mm)	Displ (mm)
R76D	100	E0353	3 000	25 000	0.919	0.858	0.904	1.169	1.016	0.937
R77D	90	E0354	4 000	28 000	1.714	1.364	1.277	0.983	1.831	1.211
R81D	100	E0355	2 000	20 000	1.014	1.046	1.514	1.310	1.075	1.522
R82D	120	E0356	2 000	18 000	1.090	1.057	1.057	1.387	2.130	1.870

					GM47	GM47	GM47
Run Number	Speed (km hr^{-1})	Output File	Window from	Window to	Displ (mm)	Displ (mm)	Displ (mm)
R76F	100	E0357	2 000	12 000	0.900	0.916	0.885
R77F	90	E0358	2 000	14 000	0.851	1.436	1.521
R81F	100	E0359	1 500	10 000	0.932	1.897	1.105
R82F	120	E0360	1 500	9 000	1.598	1.095	1.703

					4247	4247	4228	4228
Run Number	Speed (km hr^{-1})	Output File	Window from	Window to	Displ (mm)	Displ (mm)	Displ (mm)	Displ (mm)
R91X	100	E0244	5 000	17 000	1.628	1.912	0.978	1.049
R92X	10	E0245	7 000	17 000	1.278	1.562	0.948	1.099
R93X	120	E0246	5 000	15 000	1.943	1.231	1.653	1.790
R94X	130	E0247	5 000	14 000	1.540	1.978	1.755	2.384
R95X	130	E0248	4 000	14 000	1.931	2.221	2.648	2.480
R96X	120	E0249	5 000	14 000	1.238	2.107	2.145	2.846
R97X	110	E0250	5 000	14 000	1.489	2.181	1.851	2.403
R98X	100	E0251	5 000	16 000	2.149	1.825	1.038	1.082

					GM43	GM43	GM43	GM44	GM44	GM44
Run Number	Speed (km hr^{-1})	Output File	Window from	Window to	Displ (mm)	Displ (mm)	Displ (mm)	Displ (mm)	Displ (mm)	Displ (mm)
R91D	100	E0252	5 000	23 000	–	1.876	2.194	1.501	1.609	1.552
R92D	110	E0253	2 000	19 000	3.258	3.000	2.555	2.147	2.129	1.835
R93D	120	E0254	1 100	17 000	2.122	2.655	2.754	1.520	1.840	2.068
R94D	130	E0255	2 000	16 000	3.107	2.182	3.480	2.822	2.529	2.022
R95D	130	E0256	2 000	15 000	4.440	4.074	2.325	2.988	3.171	2.253
R96D	120	E0257	1 100	14 000	3.774	3.622	3.083	2.738	3.632	3.215
R97D	110	E0258	1 100	15 000	2.555	3.611	2.748	2.230	2.849	2.820
R98D	100	E0259	2 000	18 000	–	2.571	2.670	1.802	1.931	1.817

					GM44	GM44	GM44
Run Number	Speed (km hr^{-1})	Output File	Window from	Window to	Displ (mm)	Displ (mm)	Displ (mm)
R91F	100	E0361	3 000	13 000	2.257	2.232	1.990
R92F	110	E0362	1 100	11 000	2.183	2.853	2.198
R93F	120	E0363	1 100	10 000	2.192	2.564	2.381
R94F	130	E0364	2 000	9 000	3.000	1.773	2.687
R95F	130	E0365	1 100	8 000	2.591	3.462	2.351
R96F	120	E0366	1 100	9 000	2.961	3.896	3.479
R97F	110	E0367	1 100	9 000	2.433	3.743	2.037
R98F	100	E0368	1 100	10 000	2.320	1.840	2.663

					EMPT	EMPT
Run Number	Speed (km hr^{-1})	Output File	Window from	Window to	Displ (mm)	Displ (mm)
R91V	100	E0228	5 000	9 000	1.236	1.381
R92V	110	E0229	13 000	17 000	1.501	1.253
R93V	120	E0230	11 000	16 000	1.928	1.999
R94V	130	E0231	10 000	14 000	1.914	2.054
R95V	130	E0232	10 000	14 000	2.092	1.882
R96V	120	E0233	9 000	13 000	2.720	2.552
R97V	110	E0234	10 000	14 000	2.545	2.463
R98V	100	E0235	11 000	16 000	2.068	2.549

					4228	4228
Run Number	Speed (km hr^{-1})	Output File	Window from	Window to	Displ (mm)	Displ (mm)
R91Z	100	E0201	5 500	11 500	1.7	1.3
R92Z	110	E0202	6 000	12 000	1.8	2.1
R93Z	120	E0203	5 000	11 000	1.7	1.4
R94Z	130	E0204	4 000	11 000	2.7	1.7
R95Z	130	E0205	3 000	10 000	3.2	3.0
R96Z	120	E0206	4 000	10 000	3.5	2.8
R97Z	110	E0200	3 500	10 000	3.0	2.4
R98Z	100	E0207	5 000	10 000	2.2	2.1

					GM	GM	GM
Run Number	Speed (km hr^{-1})	Output File	Window from	Window to	Displ (mm)	Displ (mm)	Displ (mm)
R91B	100	E0209	6 000	15 000	2.1	1.8	1.9
R92B	110	E0210	6 000	15 000	1.7	1.9	1.7
R93B	120	E0211	7 000	16 000	2.4	3.1	2.2
R94B	130	E0212	9 000	15 000	2.2	3.2	2.2
R95B	130	E0213	9 000	16 000	3.0	2.8	2.8
R96B	120	E0214	8 000	17 000	2.6	3.0	2.9
R97B	110	E0208	7 000	16 000	3.2	2.6	2.2
R98B	100	E0215	7 000	15 000	1.3	2.5	2.5

					400	400
Run Number	Speed (km hr$^{-1)}$	Output File	Window from	Window to	Displ (mm)	Displ (mm)
R91J	100	E0369	9 000	16 000	2.2	2.8
R92J	110	E0370	8 000	15 000	2.6	3.1
R93J	120	E0371	7 000	13 000	3.1	2.5
R94J	130	E0372	7 000	12 000	3.1	4.2
R95J	130	E0373	6 000	11 000	2.9	3.4
R96J	120	E0374	7 000	11 000	3.5	4.2
R97J	110	E0375	7 000	12 000	3.3	3.7
R98J	100	E0376	7 000	13 000	2.8	3.7

					400	400
Run Number	Speed (km hr$^{-1)}$	Output File	Window from	Window to	Displ (mm)	Displ (mm)
R91L	100	E0377	2 000	9 000	2.6	2.4
R92L	110	E0378	2 000	9 000	2.8	3.2
R93L	120	E0379	2 000	7 000	1.9	2.7
R94L	130	E0380	1 500	7 000	2.6	2.6
R95L	130	E0381	1 100	6 000	2.7	4.0
R96L	120	E0382	2 000	7 000	2.4	3.1
R97L	110	E0383	1 500	7 000	3.0	4.4
R98L	100	E0384	1 500	7 000	2.8	3.0

					GM45	GM45	GM45
Run Number	Speed (km hr$^{-1)}$	Output File	Window from	Window to	Displ (mm)	Displ (mm)	Displ (mm)
R115B	100	E0301	8 000	17 000	0.311	0.484	0.552
R116B	110	E0302	9 000	19 000	–	–	–
R117B	110	E0303	10 000	19 000	–	–	–
R118B	120	E0304	9 000	19 000	0.749	1.239	1.115
R119B	100	E0305	6 000	15 000	0.813	0.611	0.646

					GM45	GM45	GM45	GM37	GM37	GM37
Run Number	Speed (km hr$^{-1)}$	Output File	Window from	Window to	Displ (mm)	Displ (mm)	Displ (mm)	Displ (mm)	Displ (mm)	Displ (mm)
R115D	100	E0306	3 000	20 000	0.639	0.566	0.621	0.742	0.675	0.861
R116D	110	E0307	3 000	18 500	1.013	0.187	0.584	0.577	0.617	0.507
R117D	110	E0308	2 500	18 000	1.001	1.550	1.250	0.973	0.697	1.115
R118D	120	E0309	2 000	17 000	0.900	0.941	1.445	0.746	0.408	0.603
R119D	100	E0310	2 000	20 000	0.941	0.989	0.629	0.903	0.748	0.996

					4247	4247	4228	4228
Run Number	Speed (km hr^{-1})	Output File	Window from	Window to	Displ (mm)	Displ (mm)	Displ (mm)	Displ (mm)
R115X	100	E0311	2 000	20 000	0.647	0.672	0.578	0.739
R116X	110	E0312	2 000	20 000	1.270	1.497	1.003	1.042
R117X	110	E0313	2 000	20 000	1.047	1.090	0.910	1.105
R118X	120	E0314	2 000	20 000	0.757	0.995	0.666	1.187
R119X	100	E0315	2 000	20 000	0.972	0.933	0.913	1.268

					4228	4228	18	18
Run Number	Speed (km hr^{-1})	Output File	Window from	Window to	Displ (mm)	Displ (mm)	Displ (mm)	Displ (mm)
R115Z	100	E0324	10 000	22 000	1.065	0.660	0.976	0.869
R116Z	110	E0325	4 000	15 000	0.556	1.065	0.962	1.349
R117Z	110	E0326	4 000	16 000	0.891	0.891	0.675	0.778
R118Z	120	E0327	8 000	17 000	1.086	1.111	1.371	1.292
R119Z	100	E0328	5 000	17 000	1.278	0.891	1.186	1.213

					GM37	GM37	GM37
Run Number	Speed (km hr^{-1})	Output File	Window from	Window to	Displ (mm)	Displ (mm)	Displ (mm)
R115F	100	E0329	1 000	11 000	–	–	–
R116F	110	E0330	2 000	11 000	1.026	0.928	0.995
R117F	110	E0331	1 000	11 000	0.908	0.748	0.745
R118F	120	E0332	1 000	10 000	1.099	1.117	1.053
R119F	100	E0333	1 000	12 000	0.511	0.735	0.487

SITE 4

					GM45	GM45	GM45
Run Number	Speed (km hr^{-1})	Output File	Window from	Window to	Displ (mm)	Displ (mm)	Displ (mm)
R120B	90	E0334	7 000	18 000	0.921	0.791	0.667
R123B	90	E0335	7 000	17 000	0.797	0.972	0.813
R124B	100	E0336	7 000	17 000	0.985	1.319	–

					GM45	GM45	GM45	GM37	GM37	GM37
Run Number	Speed (km hr^{-1})	Output File	Window from	Window to	Displ (mm)	Displ (mm)	Displ (mm)	Displ (mm)	Displ (mm)	Displ (mm)
R120D	90	E0337	2 000	23 000	0.797	0.879	1.022	0.934	0.590	0.553
R123D	90	E0338	2 000	23 000	0.752	0.664	0.746	1.445	1.546	1.189
R124D	100	E0339	2 000	21 000	1.374	0.940	0.990	1.040	1.218	0.751

					GM37	GM37	GM37
Run Number	Speed (km hr^{-1})	Output File	Window from	Window to	Displ (mm)	Displ (mm)	Displ (mm)
R120F	90	E0340	1 500	12 000	0.928	0.660	0.981
R123F	90	E0341	1 500	12 000	0.707	0.601	0.974
R124F	100	E0342	2 000	11 000	1.673	1.481	1.193

					4247	4247	4228	4228
Run Number	Speed (km hr^{-1})	Output File	Window from	Window to	Displ (mm)	Displ (mm)	Displ (mm)	Displ (mm)
R120X	90	E0343	6 000	20 000	0.502	0.678	0.806	0.422
R123X	90	E0344	5 000	20 000	0.840	0.886	0.817	0.753
R124X	100	E0345	5 000	19 000	1.180	0.600	0.920	0.949

					4228	4228
Run Number	Speed (km hr^{-1})	Output File	Window from	Window to	Displ (mm)	Displ (mm)
R120Z	90	E0346	5 000	11 000	0.946	0.735
R123Z	90	E0347	5 000	12 000	0.831	0.874
R124Z	100	E0348	5 000	10 000	1.093	1.203

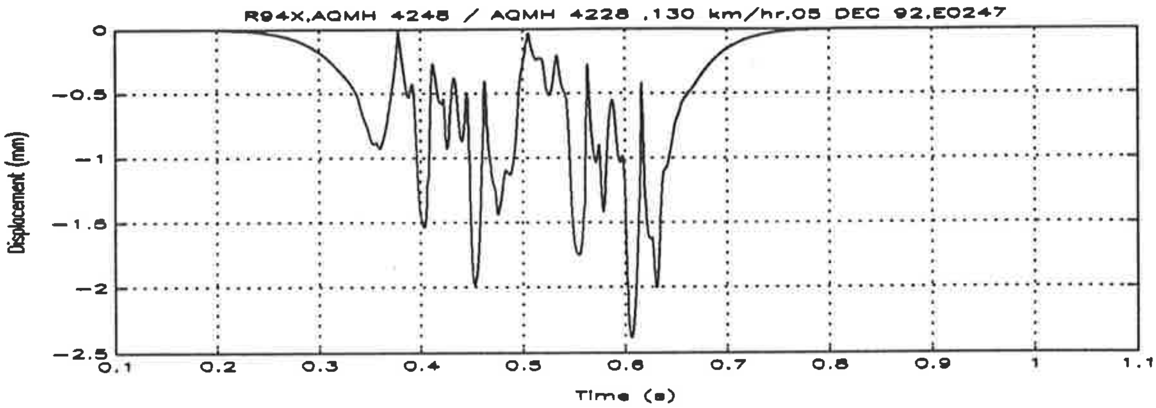
R94X,AQMH 4248 / AQMH 4228 ,130 km/hr,05 DEC 92,E0247
Displacement (mm)
Time (s)

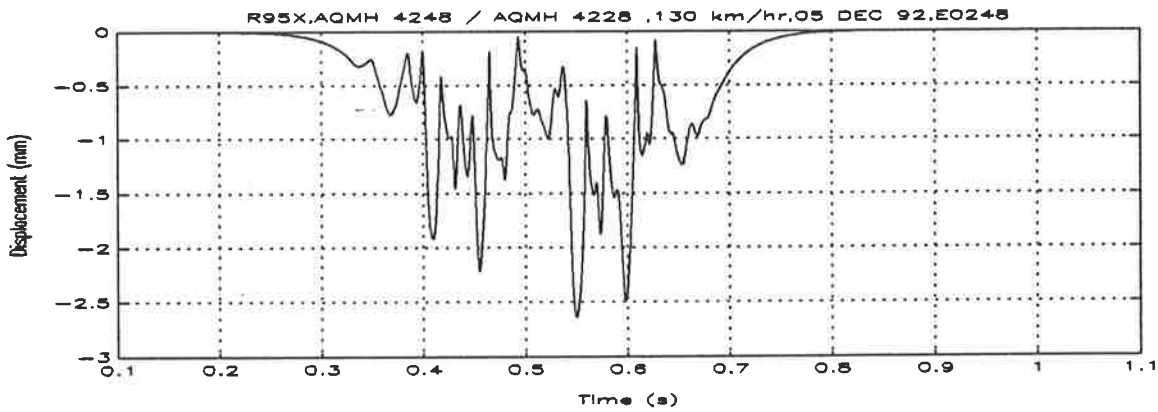
R95X,AQMH 4248 / AQMH 4228 ,130 km/hr,05 DEC 92,E0248
Displacement (mm)
Time (s)

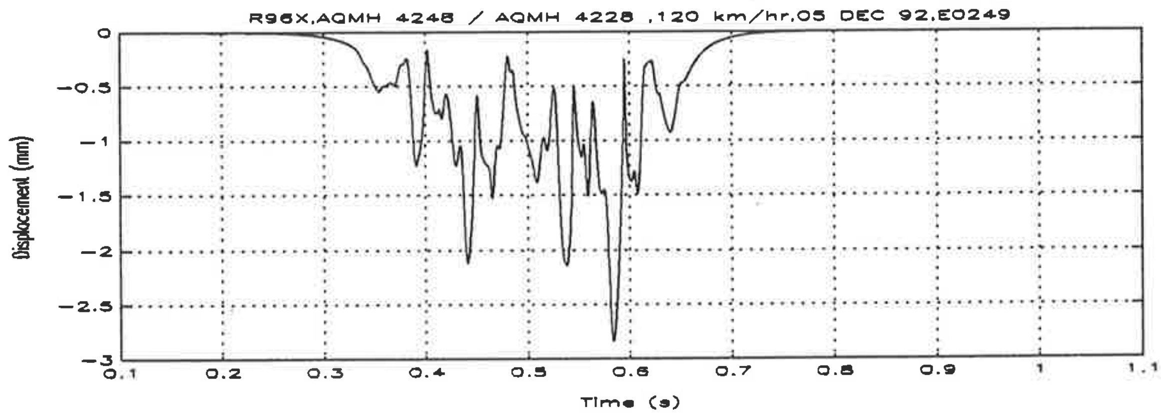
R96X,AQMH 4248 / AQMH 4228 ,120 km/hr,05 DEC 92,E0249
Displacement (mm)
Time (s)

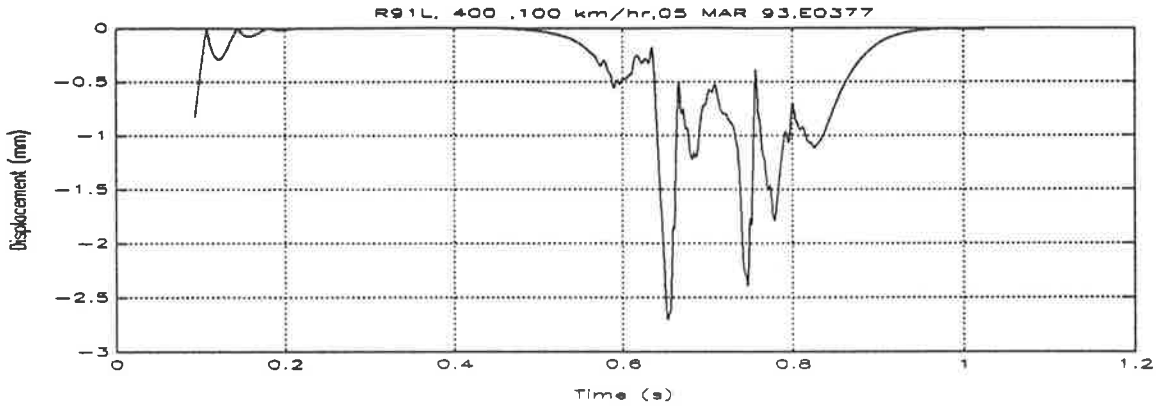
R91L, 400 ,100 km/hr,05 MAR 93,E0377
Displacement (mm)
Time (s)

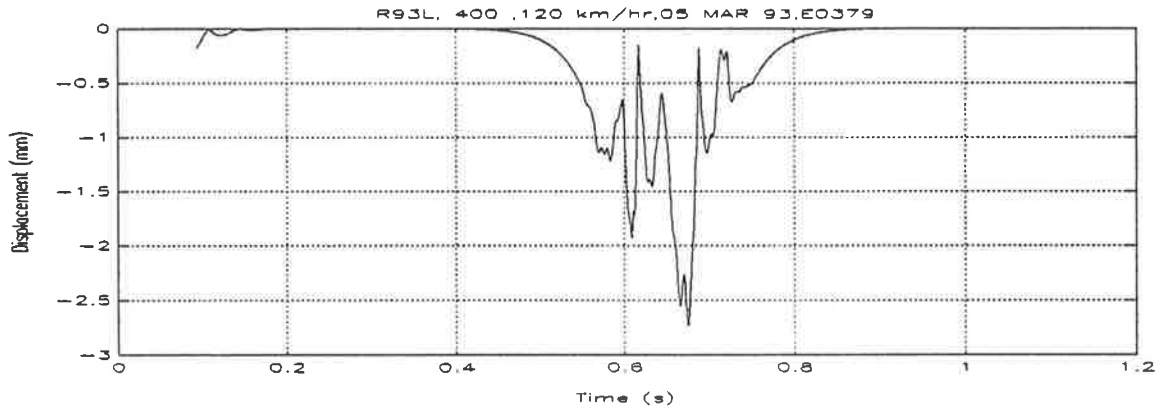
R93L, 400 ,120 km/hr,05 MAR 93,E0379
Displacement (mm)
Time (s)

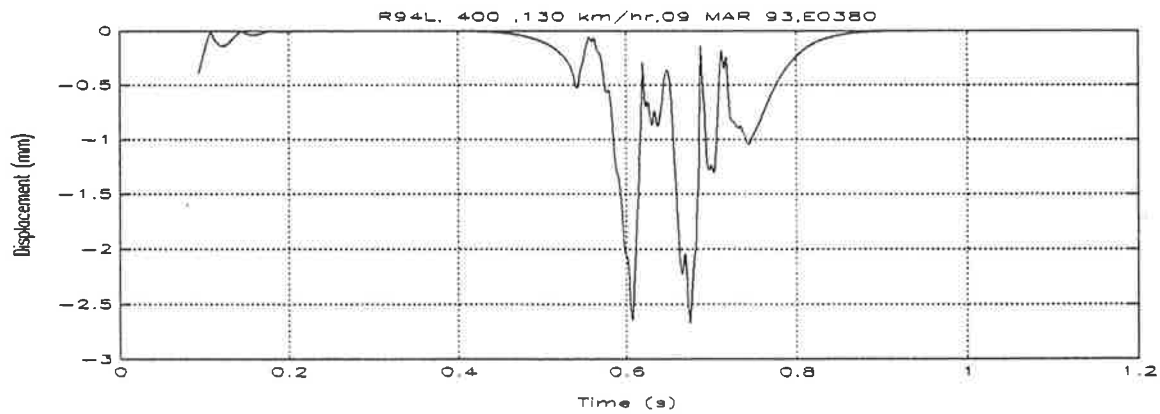
R94L, 400 ,130 km/hr,09 MAR 93,E0380
Displacement (mm)
Time (s)

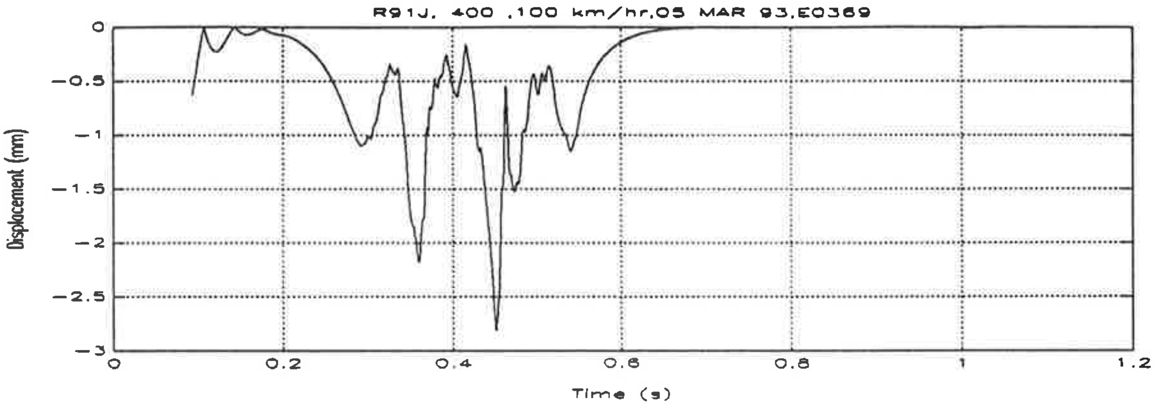
R91J, 400 ,100 km/hr,05 MAR 93,E0369
Displacement (mm)
Time (s)

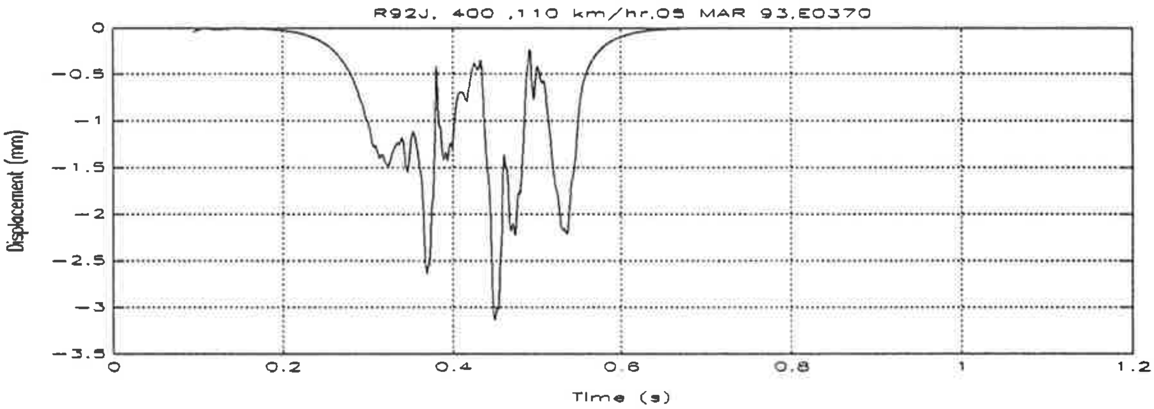
R92J, 400 ,110 km/hr,05 MAR 93,E0370
Displacement (mm)
Time (s)

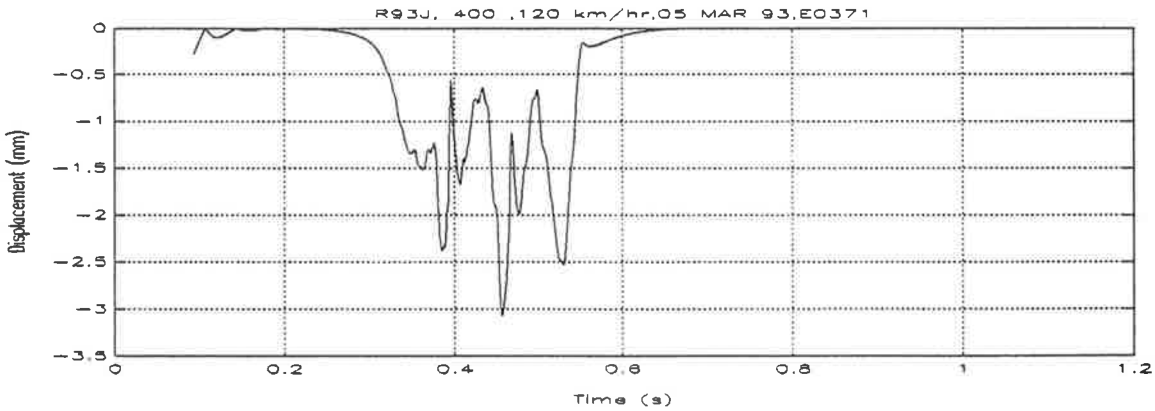
R93J, 400 ,120 km/hr,05 MAR 93,E0371
Displacement (mm)
Time (s)

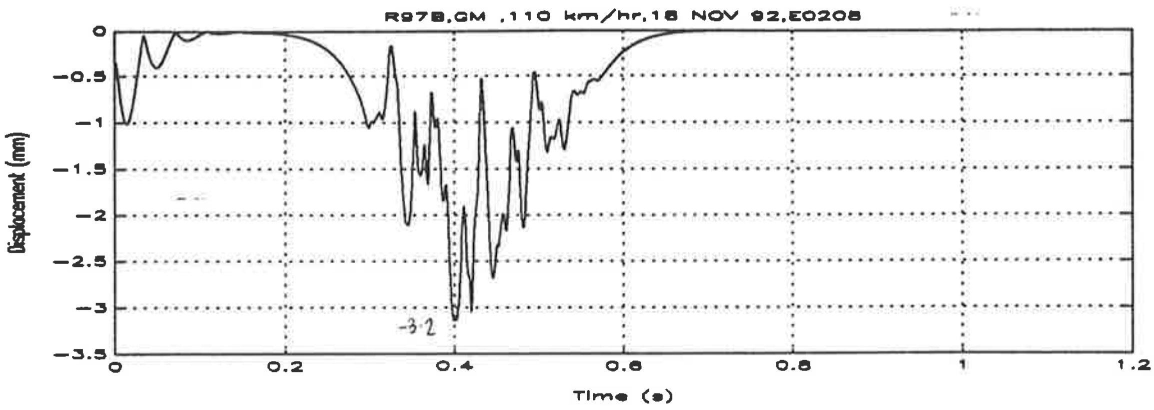
R97B,GM ,110 km/hr,18 NOV 92,E0208
Displacement (mm)
Time (s)
-3·2

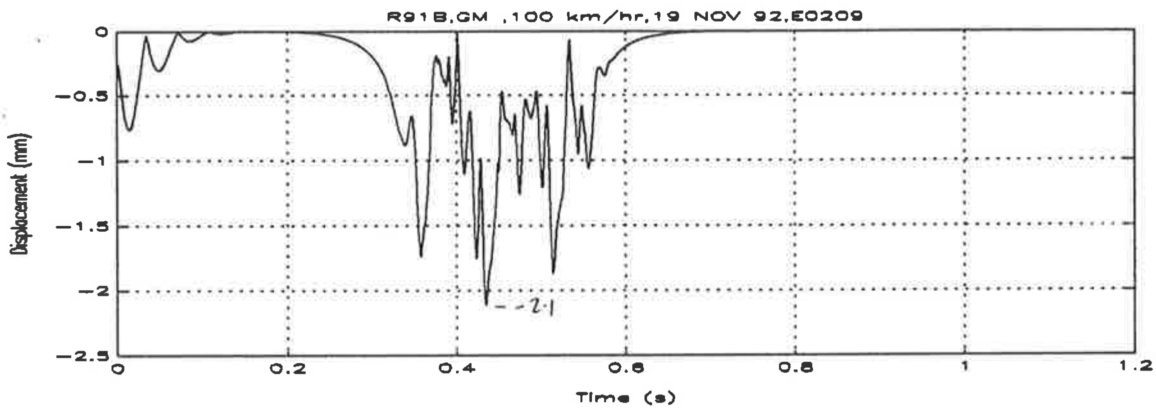
R91B,GM ,100 km/hr,19 NOV 92,E0209
Displacement (mm)
Time (s)
-2·1

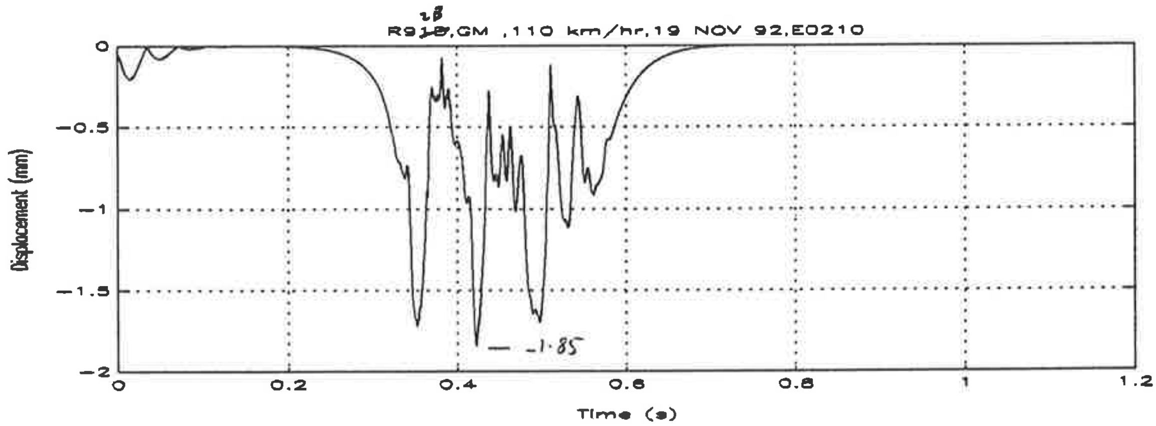
R9~~1B~~ 2B,GM ,110 km/hr,19 NOV 92,E0210
Displacement (mm)
Time (s)
-1·85

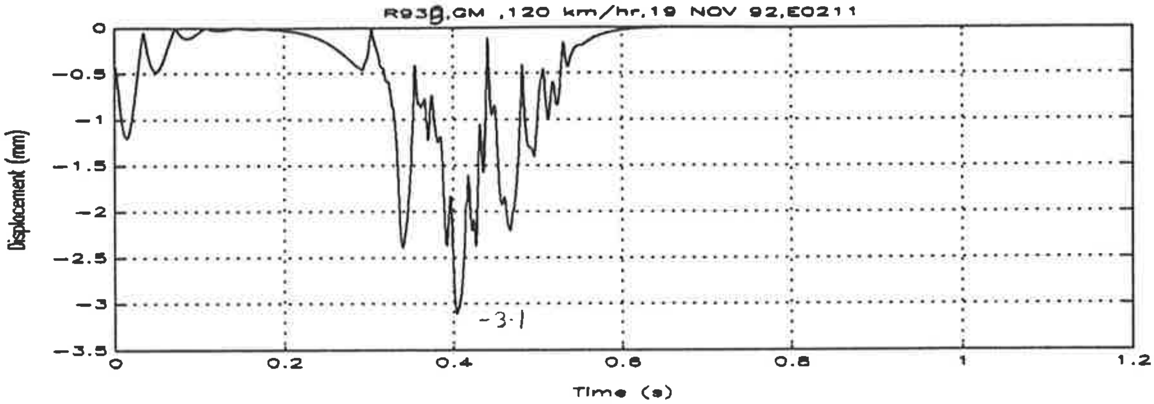

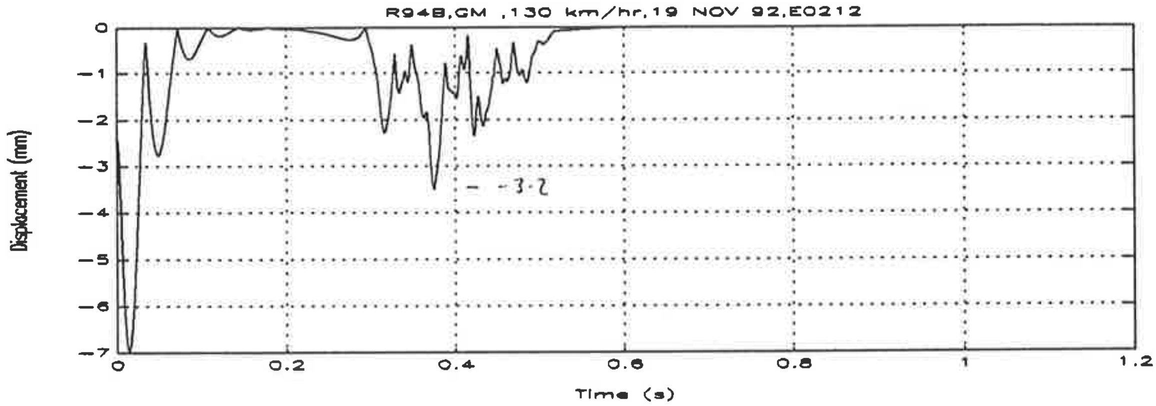

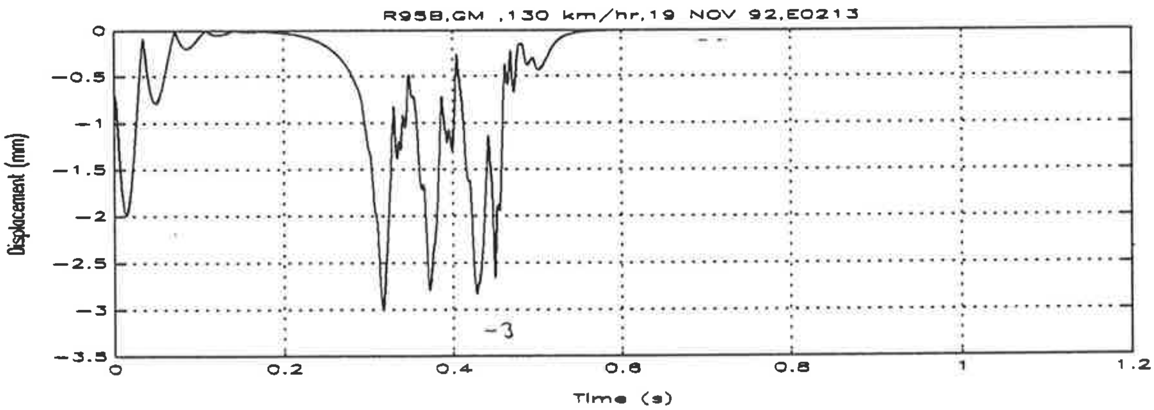

$\bar{x} = 2.74$

$SD = 0.527$

1.85
2.1
2.5
3.0
3.0
3.1
3.2
3.2

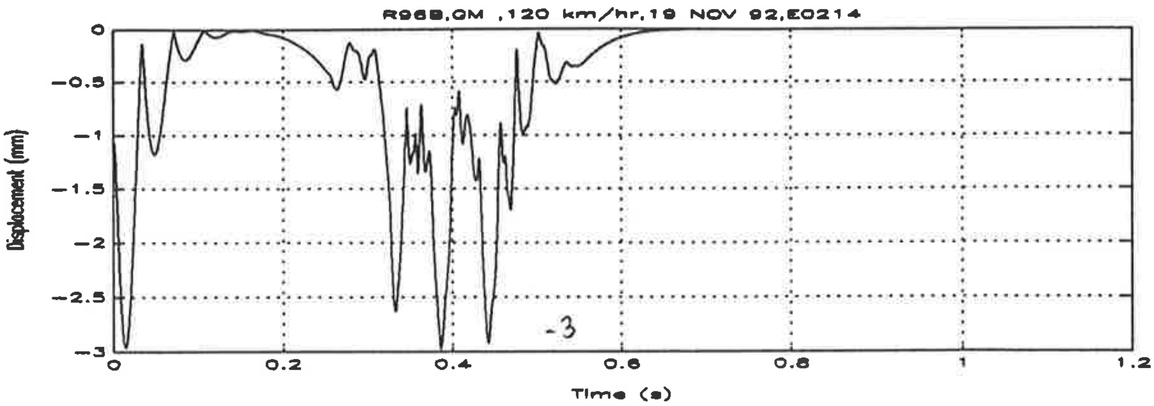
R968.GM ,120 km/hr,19 NOV 92,E0214
Displacement (mm)
0
-0.5
-1
-1.5
-2
-2.5
-3
0
0.2
0.4
0.6
0.8
1
1.2
Time (s)
-3

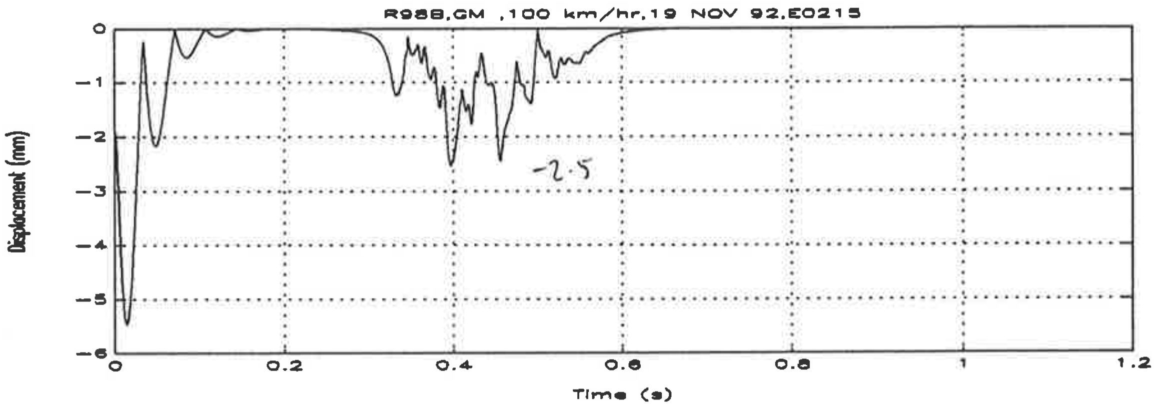
R988.GM ,100 km/hr,19 NOV 92,E0215
Displacement (mm)
0
-1
-2
-3
-4
-5
-6
0
0.2
0.4
0.6
0.8
1
1.2
Time (s)
-2.5

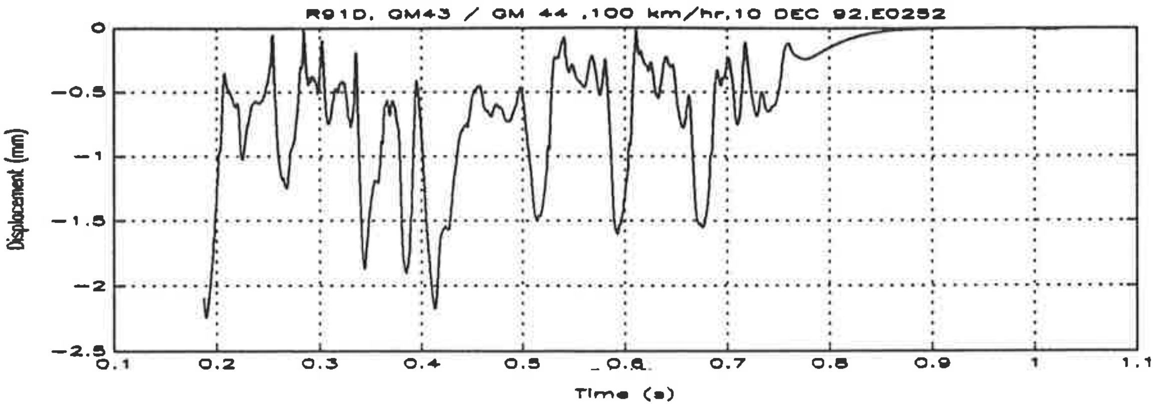
R91D, GM43 / GM 44 ,100 km/hr,10 DEC 92,E0252
Displacement (mm)
Time (s)

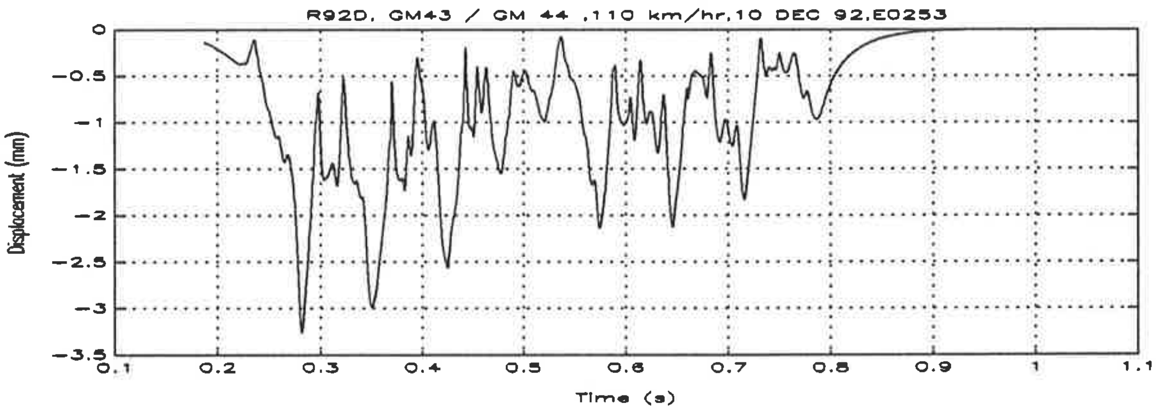
R92D, GM43 / GM 44 ,110 km/hr,10 DEC 92,E0253
Displacement (mm)
Time (s)

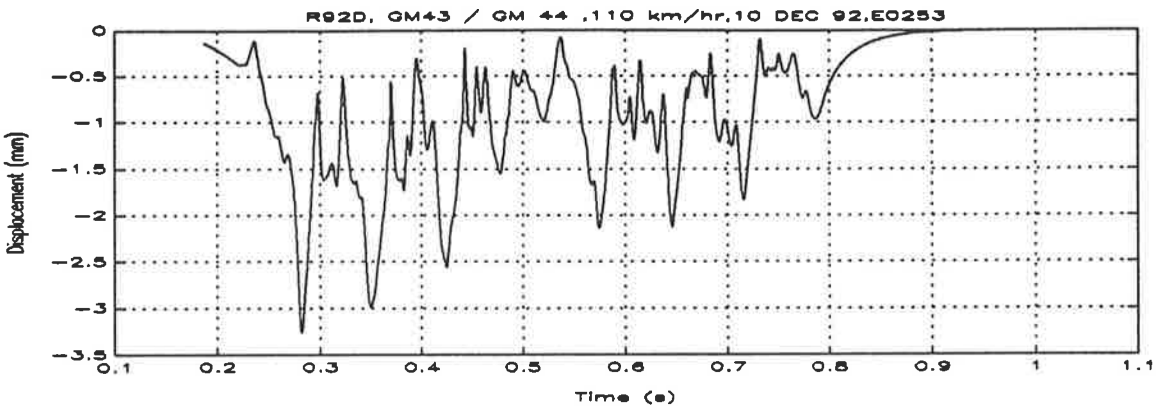
R92D, GM43 / GM 44 ,110 km/hr,10 DEC 92,E0253
Displacement (mm)
Time (s)

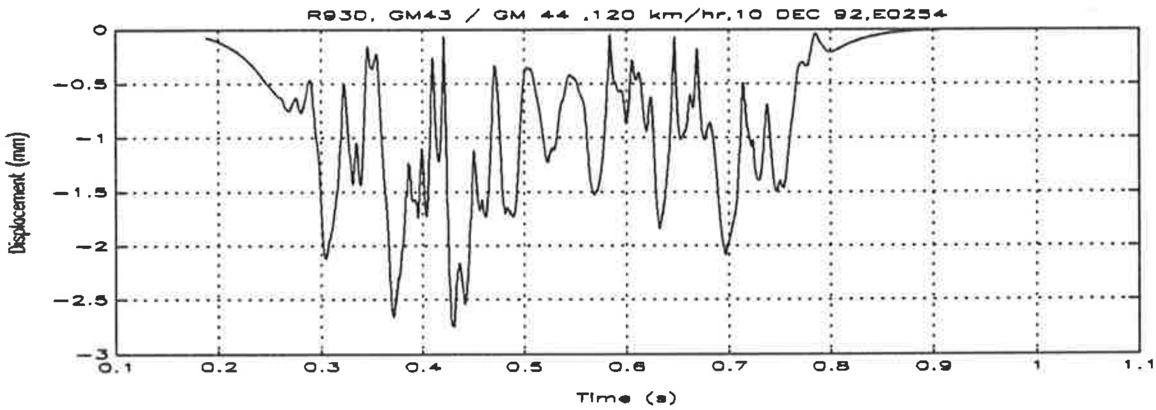
R93D, GM43 / GM 44 ,120 km/hr,10 DEC 92,E0254
Displacement (mm)
Time (s)

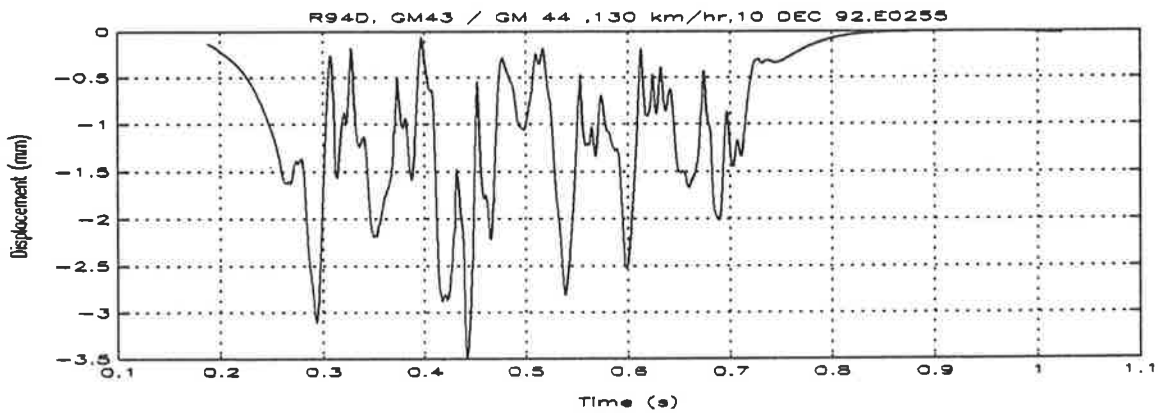
R94D, GM43 / GM 44 ,130 km/hr,10 DEC 92,E0255
Displacement (mm)
Time (s)

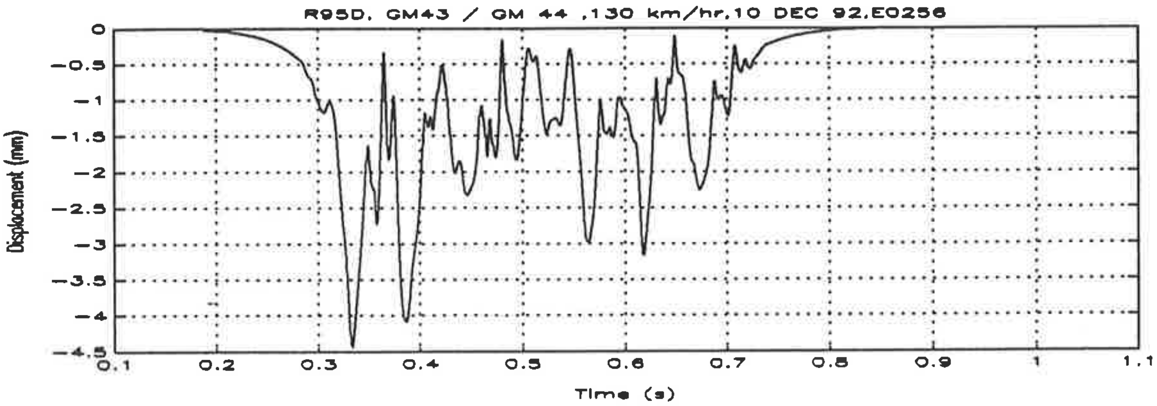

R95D, GM43 / GM 44 ,130 km/hr,10 DEC 92,E0256
Displacement (mm)
Time (s)

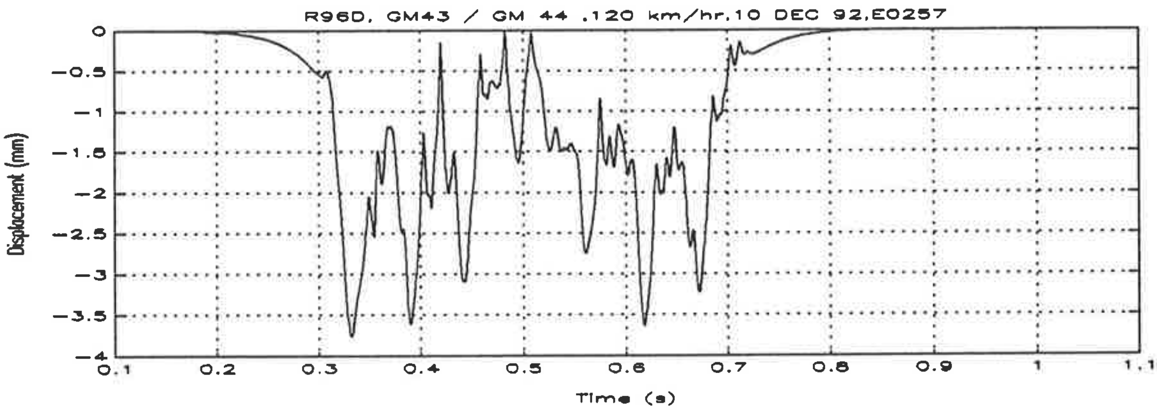

R96D, GM43 / GM 44 ,120 km/hr,10 DEC 92,E0257
Displacement (mm)
Time (s)

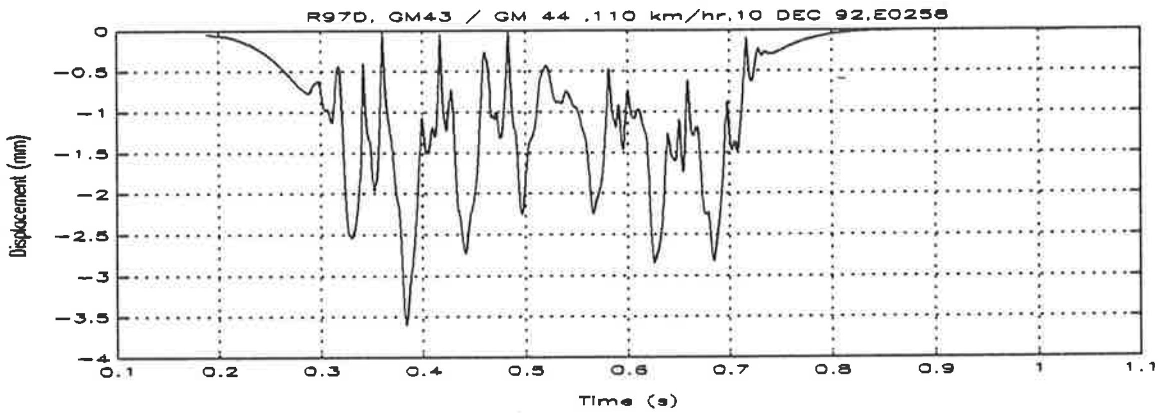

R97D, GM43 / GM 44 ,110 km/hr,10 DEC 92,E0258
Displacement (mm)
Time (s)

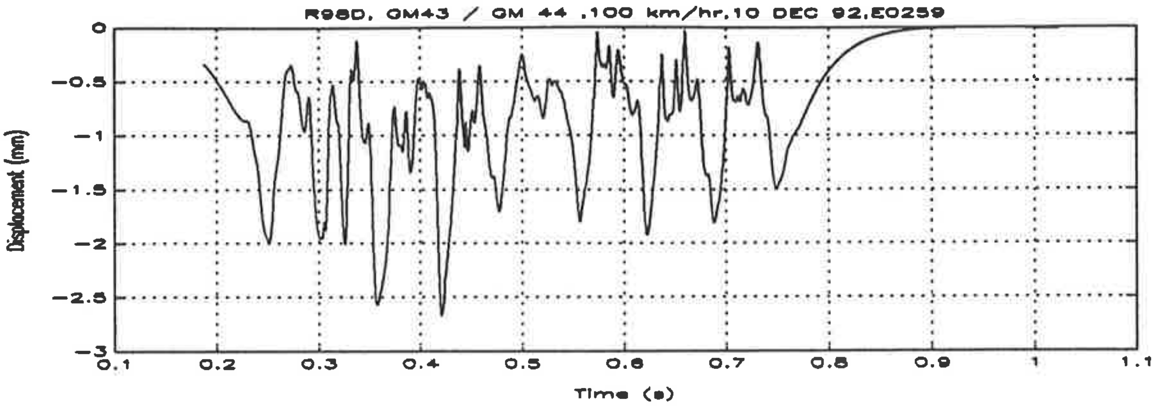

R98D, GM43 / GM 44 ,100 km/hr,10 DEC 92,E0259
Displacement (mm)
0
-0.5
-1
-1.5
-2
-2.5
-3
0.1
0.2
0.3
0.4
0.5
0.6
0.7
0.8
0.9
1
1.1
Time (s)

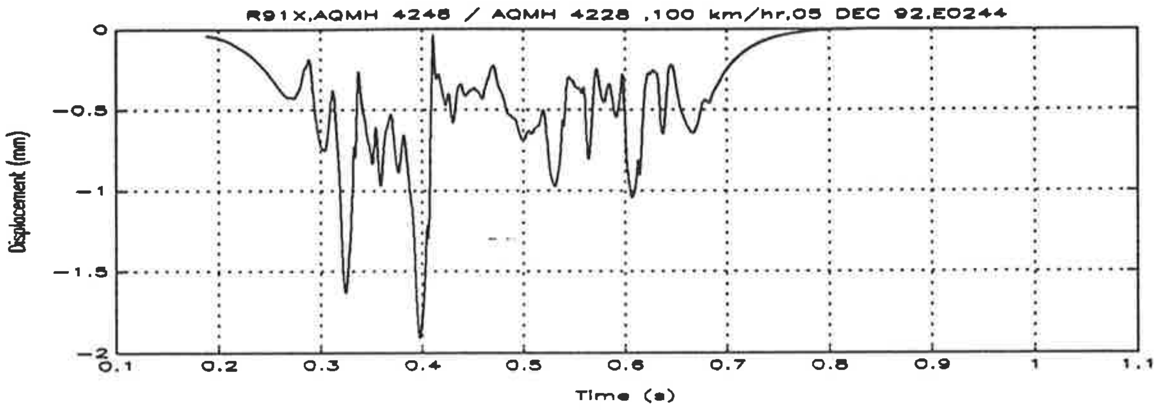
R91X,AQMH 4248 / AQMH 4228 ,100 km/hr,05 DEC 92,E0244
Displacement (mm)
Time (s)
0
-0.5
-1
-1.5
-2
0.1
0.2
0.3
0.4
0.5
0.6
0.7
0.8
0.9
1
1.1

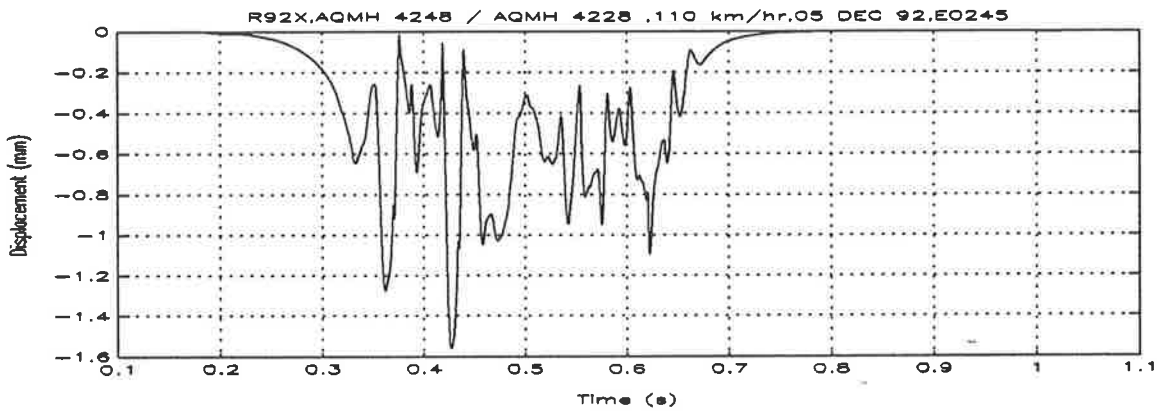
R92X,AQMH 4248 / AQMH 4228 ,110 km/hr,05 DEC 92,E0245
Displacement (mm)
Time (s)
0
-0.2
-0.4
-0.6
-0.8
-1
-1.2
-1.4
-1.6
0.1
0.2
0.3
0.4
0.5
0.6
0.7
0.8
0.9
1
1.1

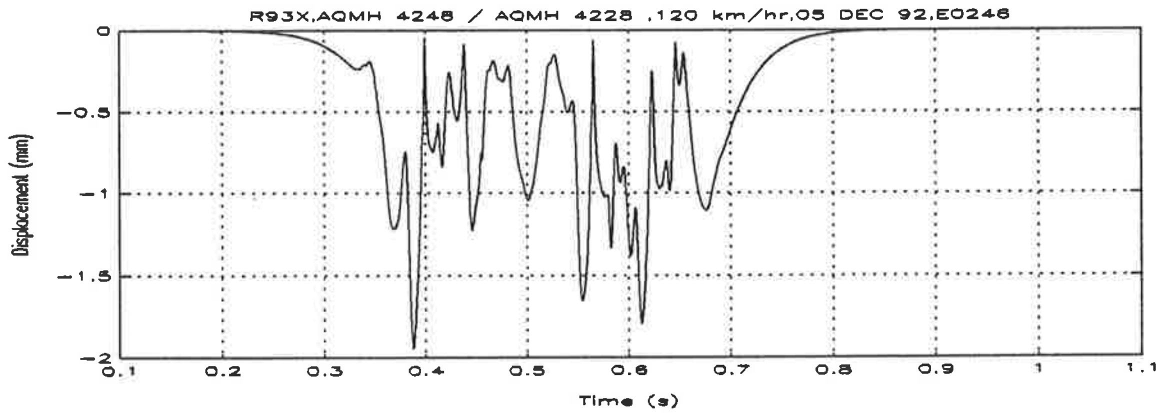
R93X,AQMH 4248 / AQMH 4228 ,120 km/hr,05 DEC 92,E0246
Displacement (mm)
Time (s)
0
-0.5
-1
-1.5
-2
0.1
0.2
0.3
0.4
0.5
0.6
0.7
0.8
0.9
1
1.1

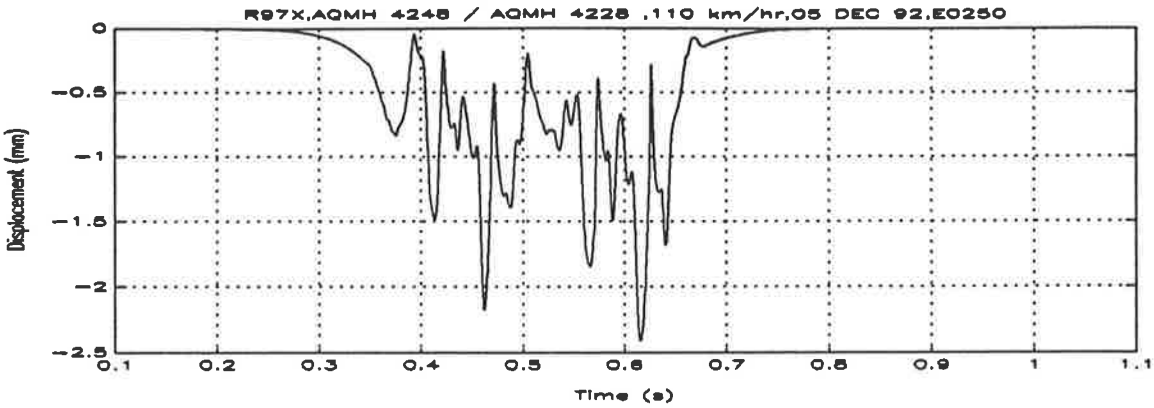
R97X,AQMH 4248 / AQMH 4228 ,110 km/hr,05 DEC 92,E0250
Displacement (mm)
Time (s)
0
-0.5
-1
-1.5
-2
-2.5
0.1
0.2
0.3
0.4
0.5
0.6
0.7
0.8
0.9
1
1.1

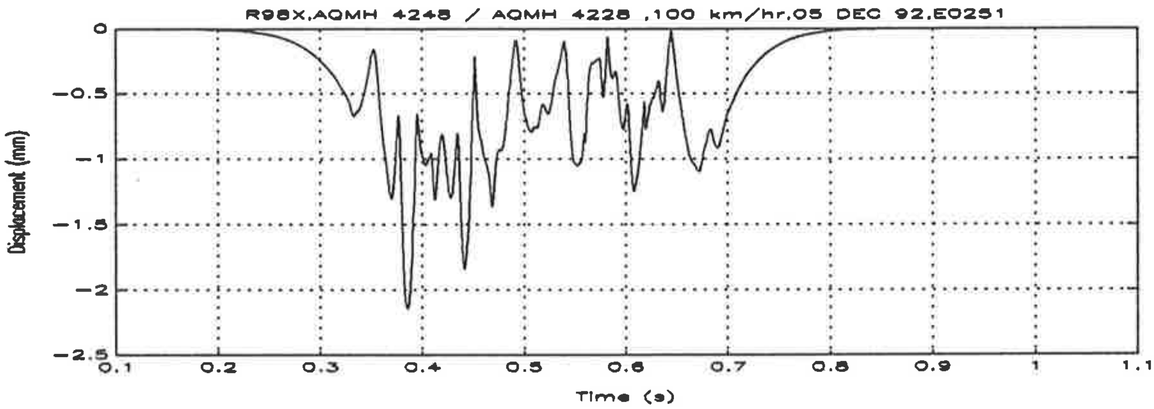
R98X,AQMH 4248 / AQMH 4228 ,100 km/hr,05 DEC 92,E0251
Displacement (mm)
Time (s)
0
-0.5
-1
-1.5
-2
-2.5
0.1
0.2
0.3
0.4
0.5
0.6
0.7
0.8
0.9
1
1.1

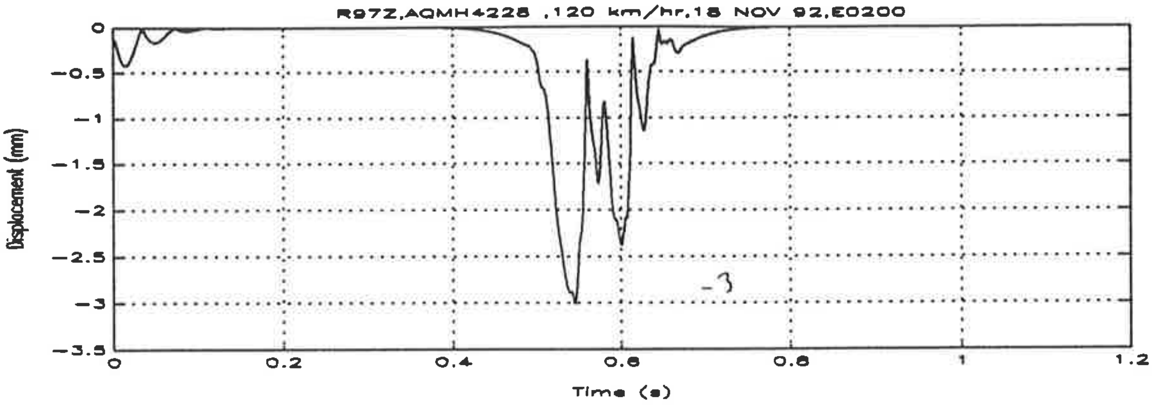
R97Z,AQMH4228 ,120 km/hr,18 NOV 92,E0200
Displacement (mm)
Time (s)
-3

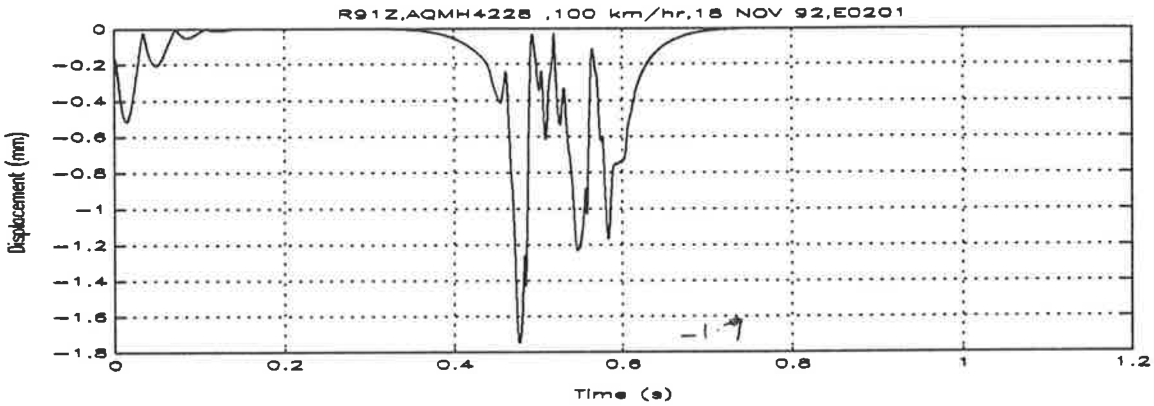
R91Z,AQMH4228 ,100 km/hr,18 NOV 92,E0201
Displacement (mm)
Time (s)
-1.7

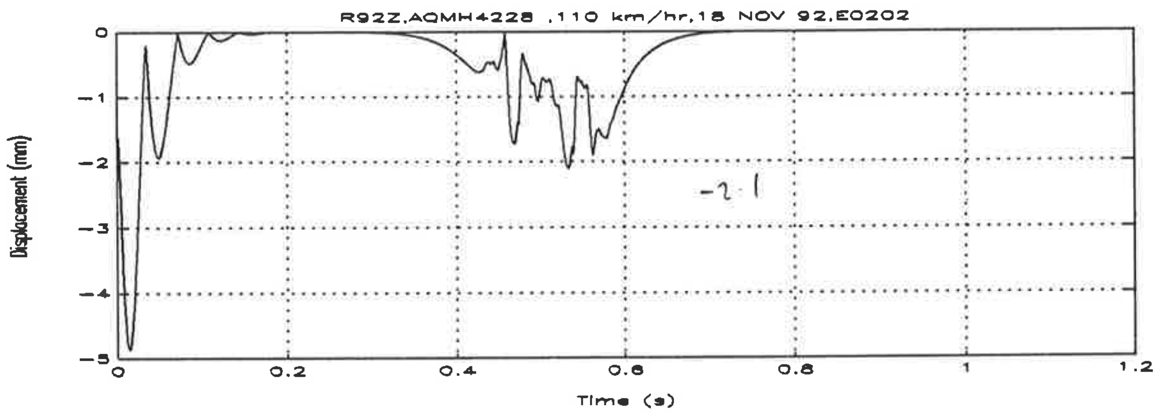
R92Z,AQMH4228 ,110 km/hr,18 NOV 92,E0202
Displacement (mm)
Time (s)
-2.1

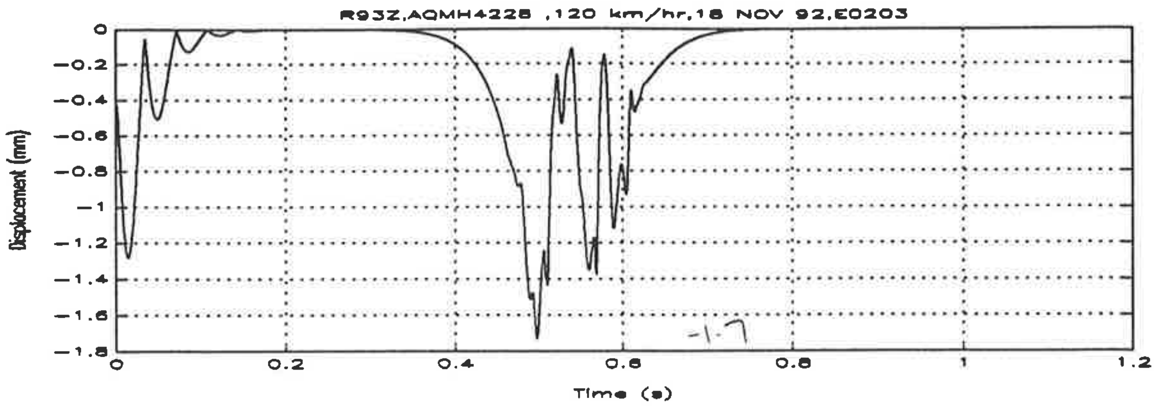
R93Z,AQMH4228 ,120 km/hr,18 NOV 92,E0203
Displacement (mm)
Time (s)
-1.7

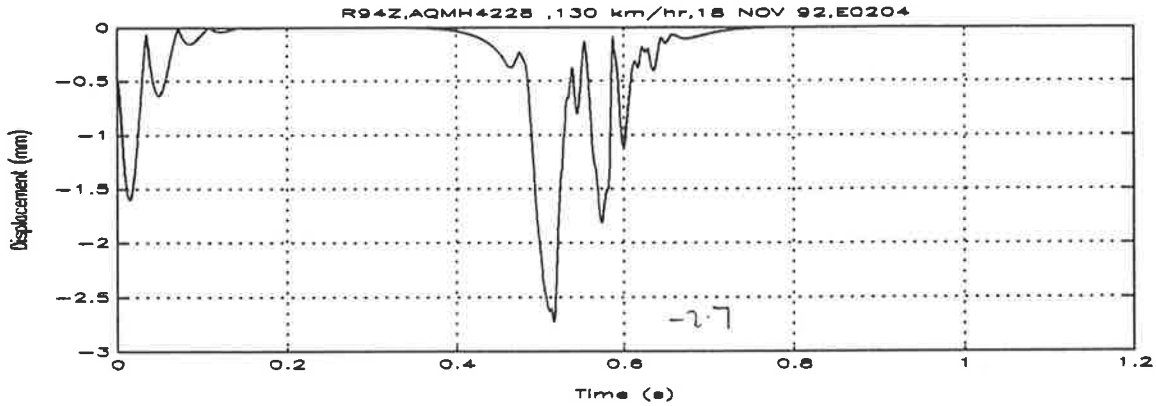
R94Z,AQMH4228 ,130 km/hr,18 NOV 92,E0204
Displacement (mm)
Time (s)
-2.7

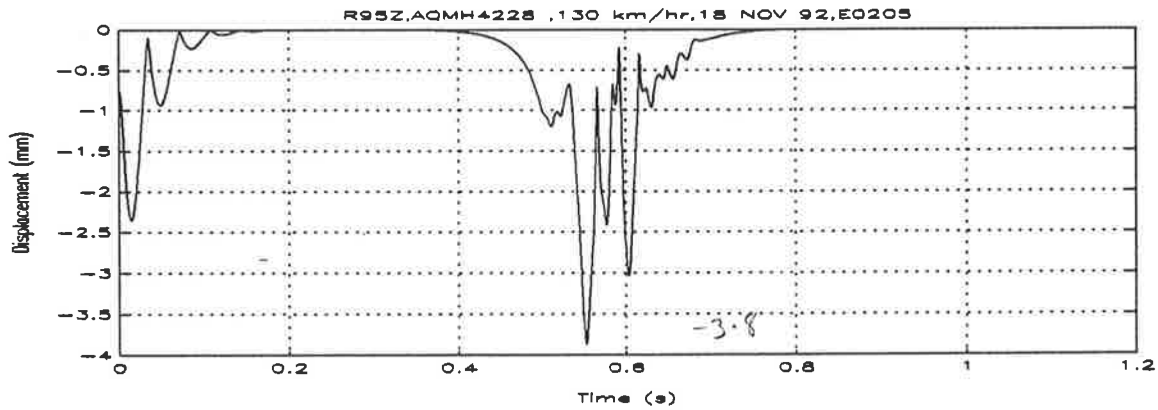
R95Z,AQMH4228 ,130 km/hr,18 NOV 92,E0205
Displacement (mm)
Time (s)
-3.8

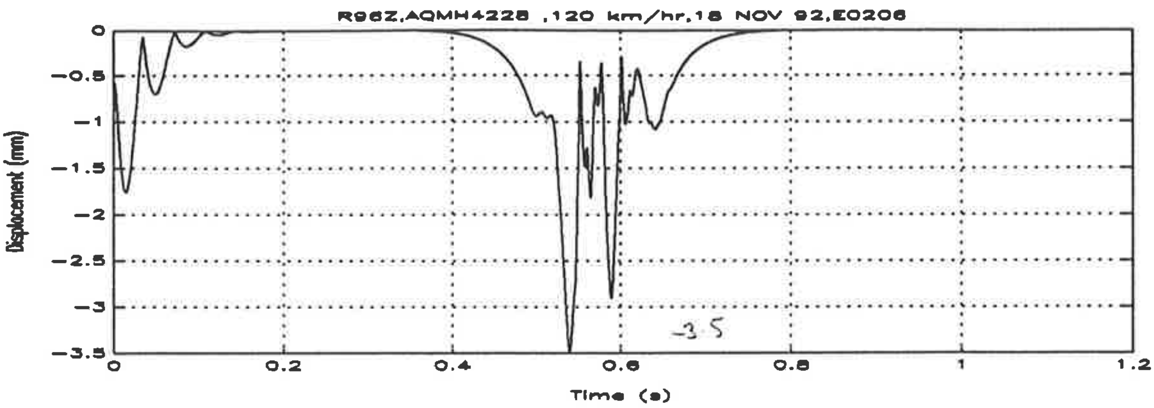

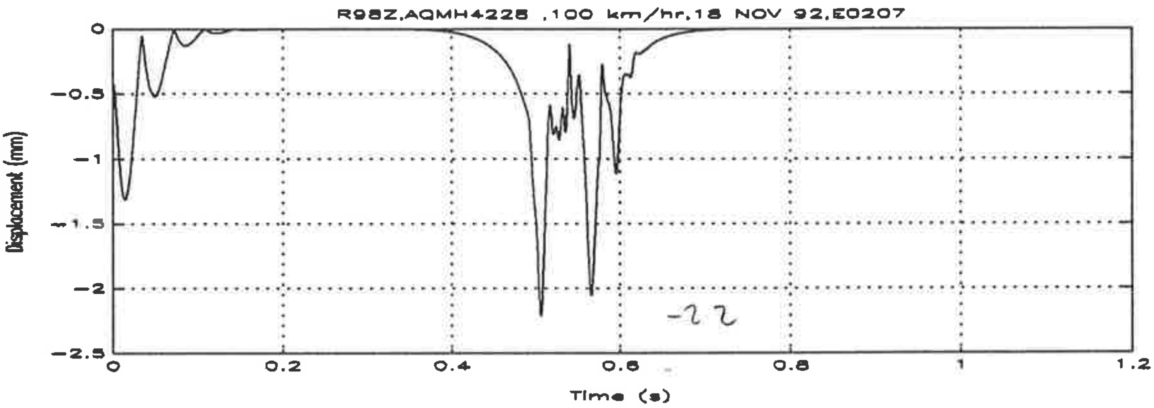

$\bar{x} = 2.59$

SD = 0.797

1.2
1.9
1.7 1.6
1.7 1.4
2.1 2.1
2.2 2.7
2.7 2.8
3.0 3.0
3.5
3.8

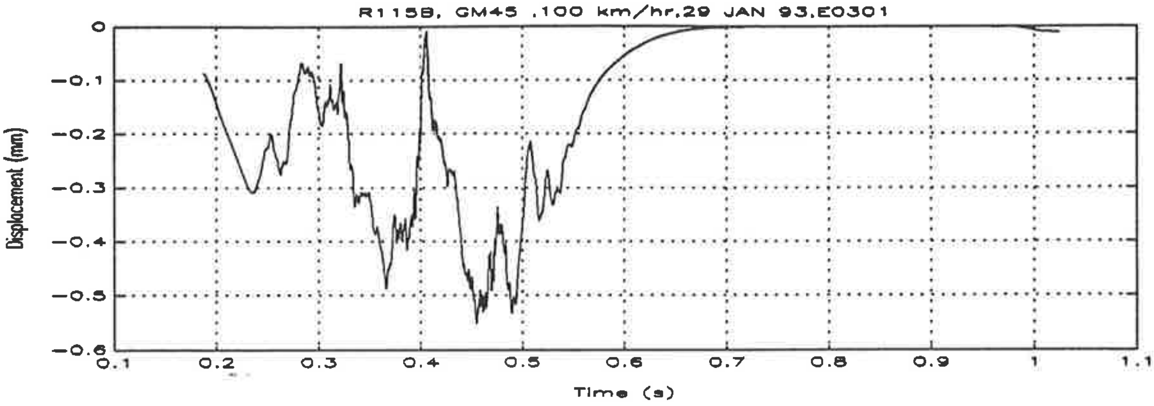
R115B, GM45 ,100 km/hr,29 JAN 93,E0301
Displacement (mm)
Time (s)

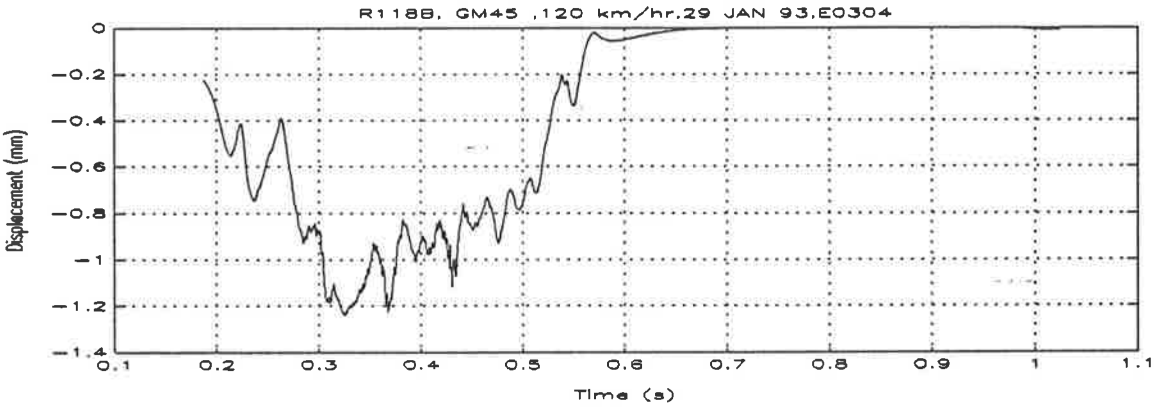
R118B, GM45 ,120 km/hr,29 JAN 93,E0304
Displacement (mm)
Time (s)

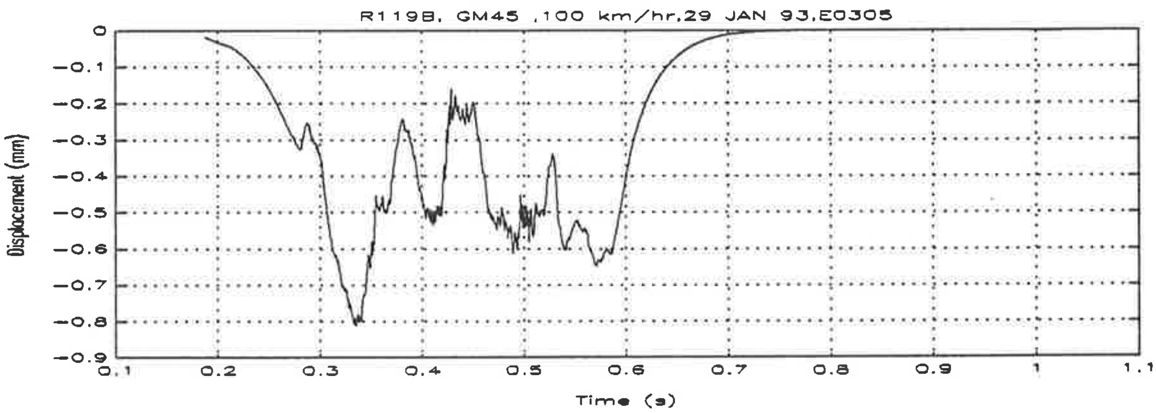
R119B, GM45 ,100 km/hr,29 JAN 93,E0305
Displacement (mm)
Time (s)

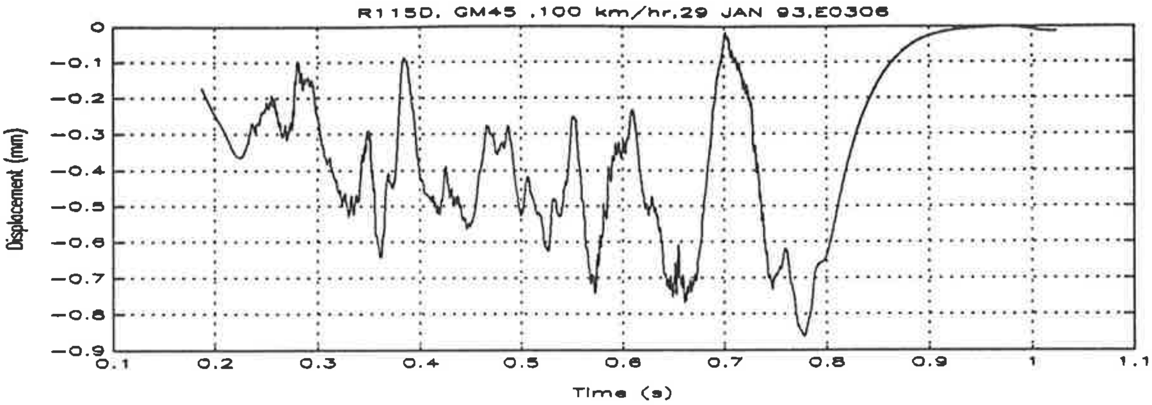
R115D, GM45 ,100 km/hr,29 JAN 93,E0306
Displacement (mm)
Time (s)

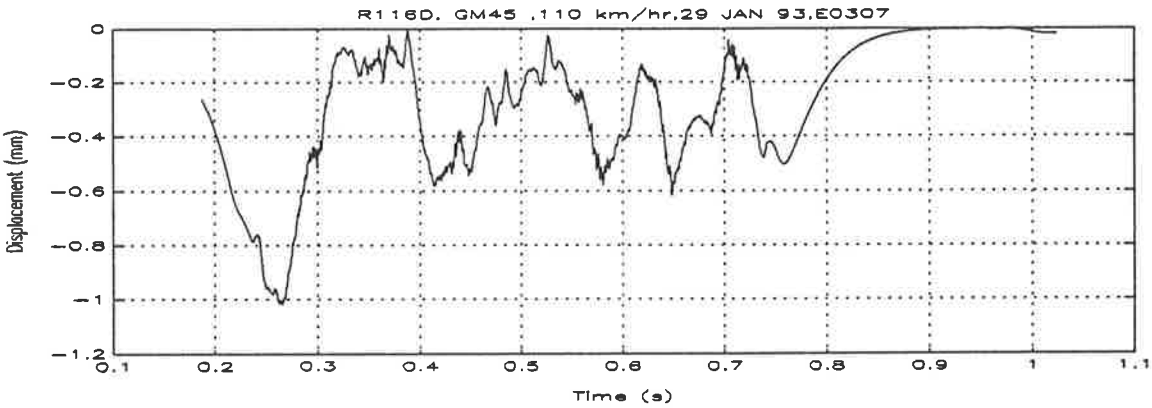
R116D, GM45 ,110 km/hr,29 JAN 93,E0307
Displacement (mm)
Time (s)

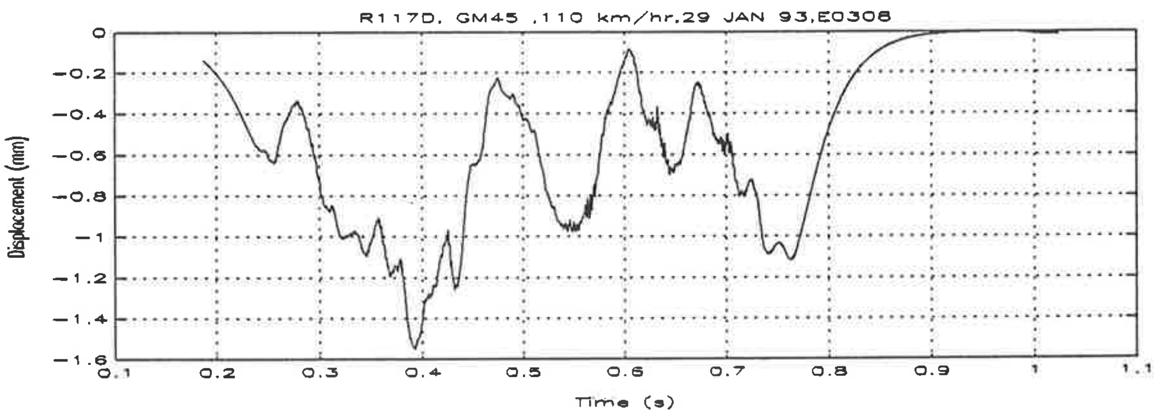
R117D, GM45 ,110 km/hr,29 JAN 93,E0308
Displacement (mm)
Time (s)

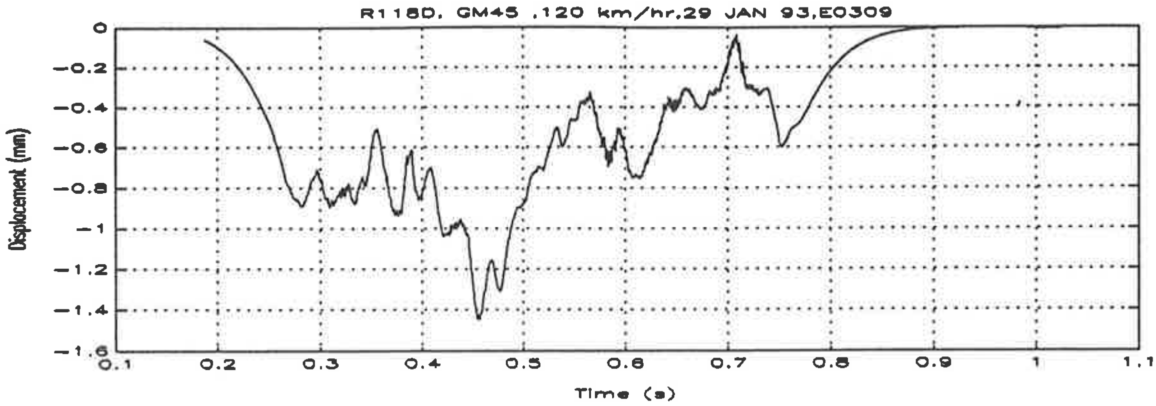
R118D, GM45 ,120 km/hr,29 JAN 93,E0309
Displacement (mm)
Time (s)

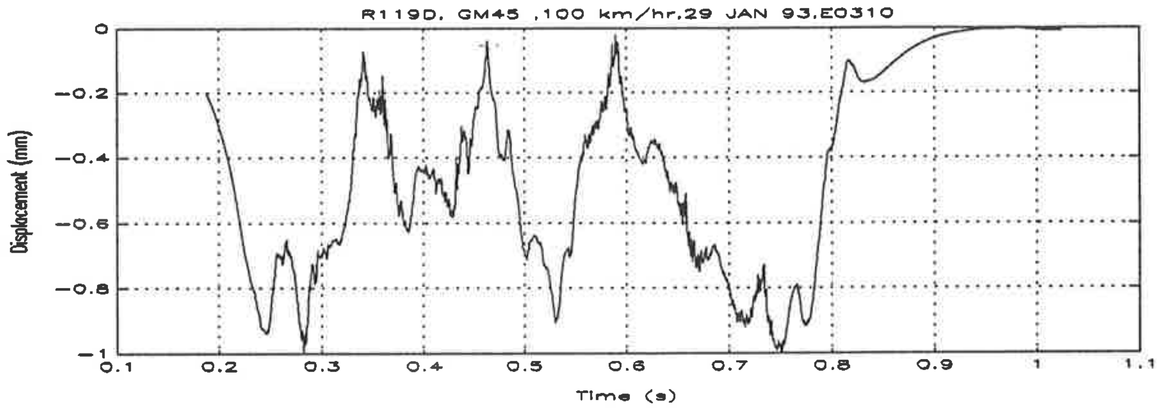
R119D, GM45 ,100 km/hr,29 JAN 93,E0310
Displacement (mm)
Time (s)

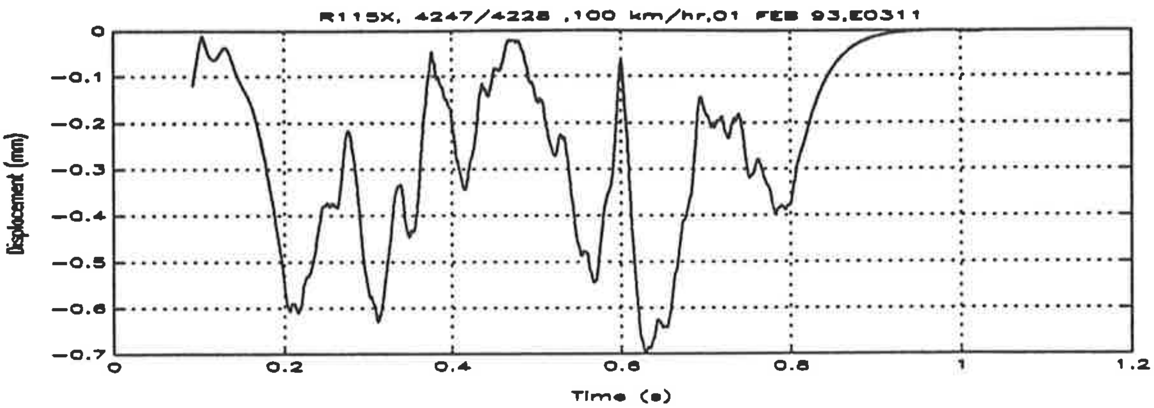
R115X, 4247/4228 ,100 km/hr,01 FEB 93,E0311
Displacement (mm)
Time (s)

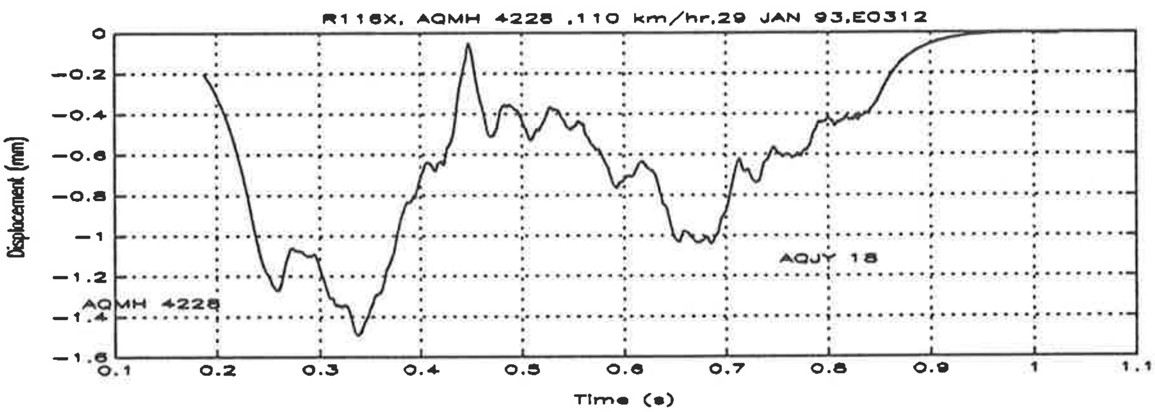
R116X, AQMH 4228 ,110 km/hr,29 JAN 93,E0312
Displacement (mm)
AQMH 4228
AQJY 18
Time (s)

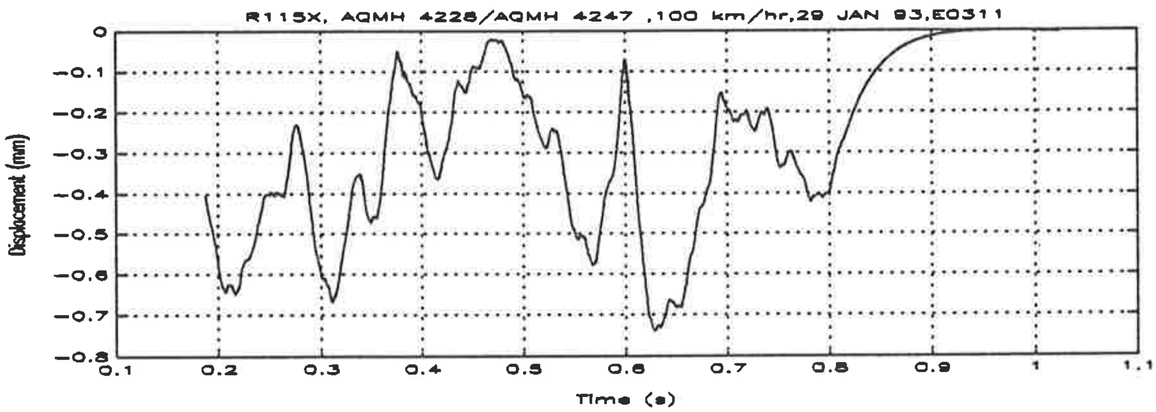
R115X, AQMH 4228/AQMH 4247 ,100 km/hr,29 JAN 93,E0311
Displacement (mm)
Time (s)

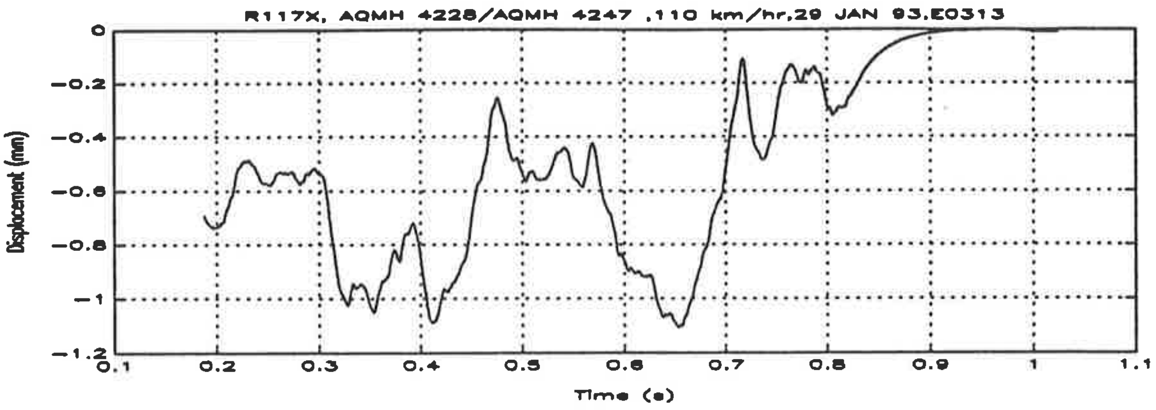
R117X, AQMH 4228/AQMH 4247 ,110 km/hr,29 JAN 93,E0313
Displacement (mm)
Time (s)

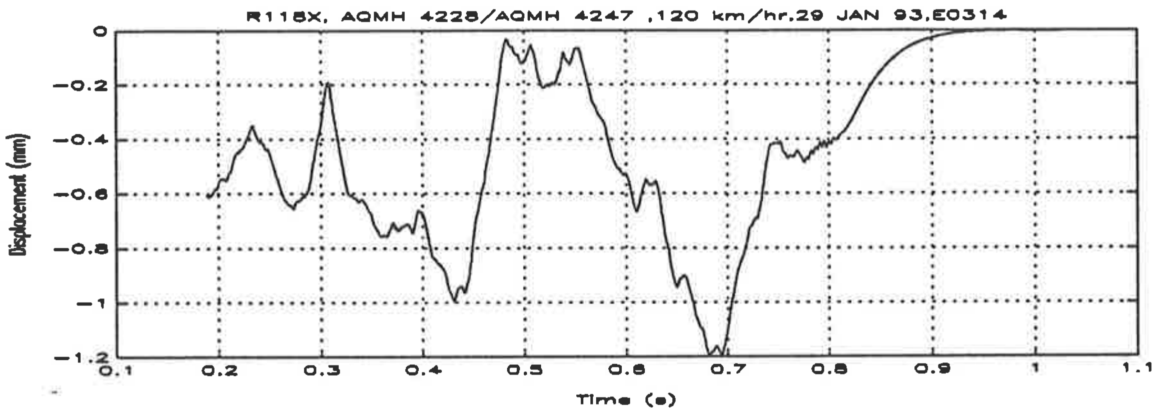
R118X, AQMH 4228/AQMH 4247 ,120 km/hr,29 JAN 93,E0314
Displacement (mm)
Time (s)

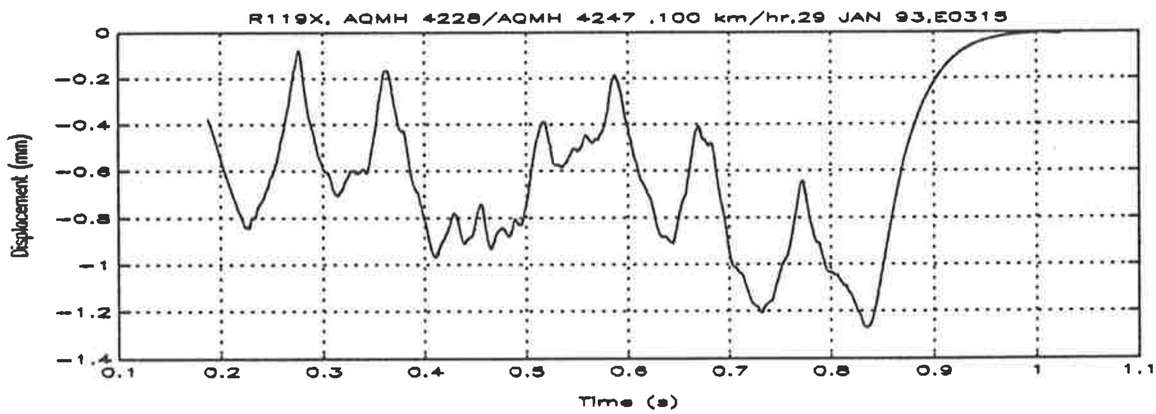
R119X, AQMH 4228/AQMH 4247 ,100 km/hr,29 JAN 93,E0315
Displacement (mm)
Time (s)

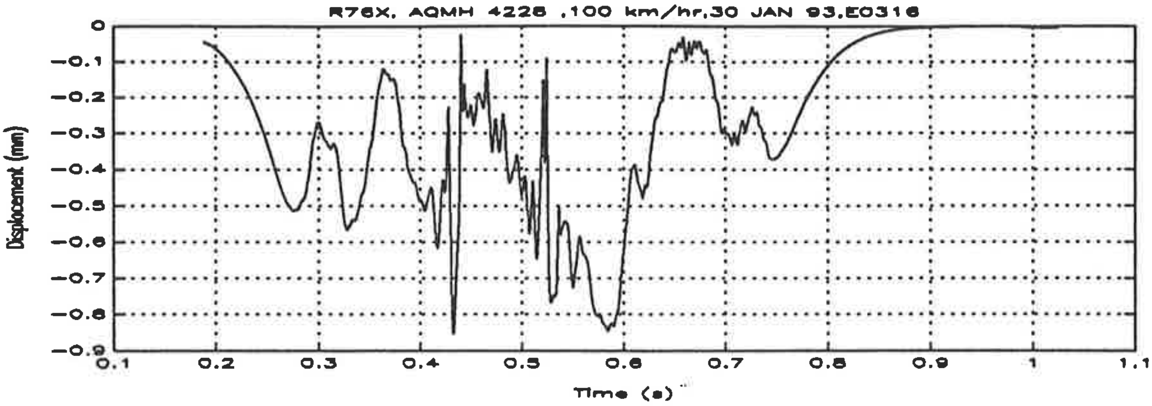
R76X, AQMH 4228 ,100 km/hr,30 JAN 93,E0316
Displacement (mm)
Time (s)

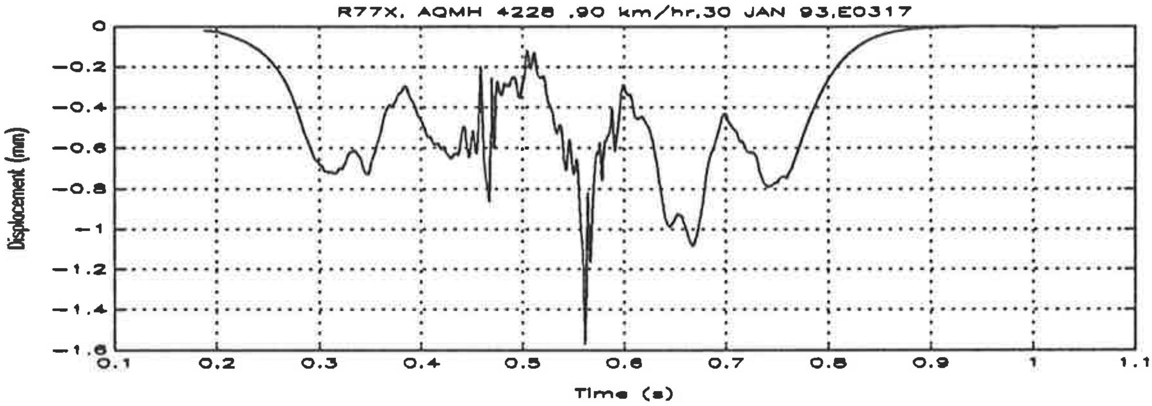
R77X, AQMH 4228 ,90 km/hr,30 JAN 93,E0317
Displacement (mm)
Time (s)

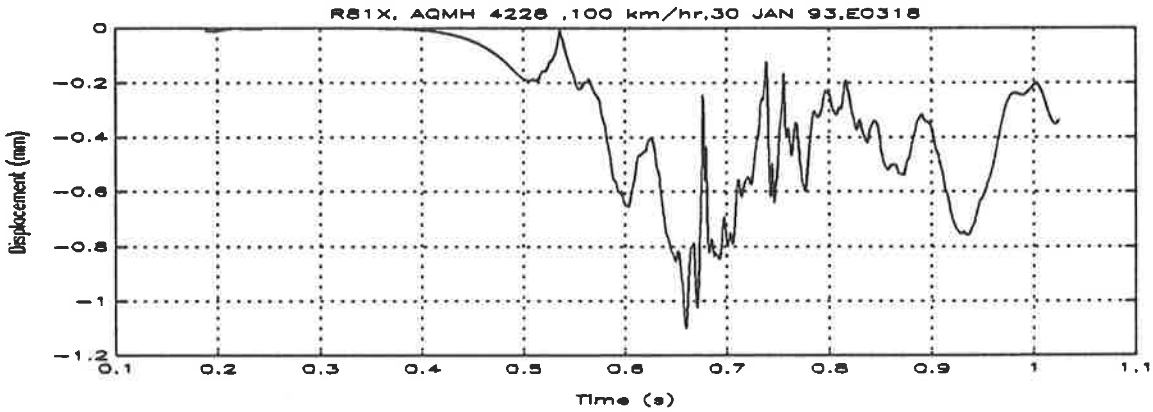
R81X, AQMH 4228 ,100 km/hr,30 JAN 93,E0318
Displacement (mm)
Time (s)

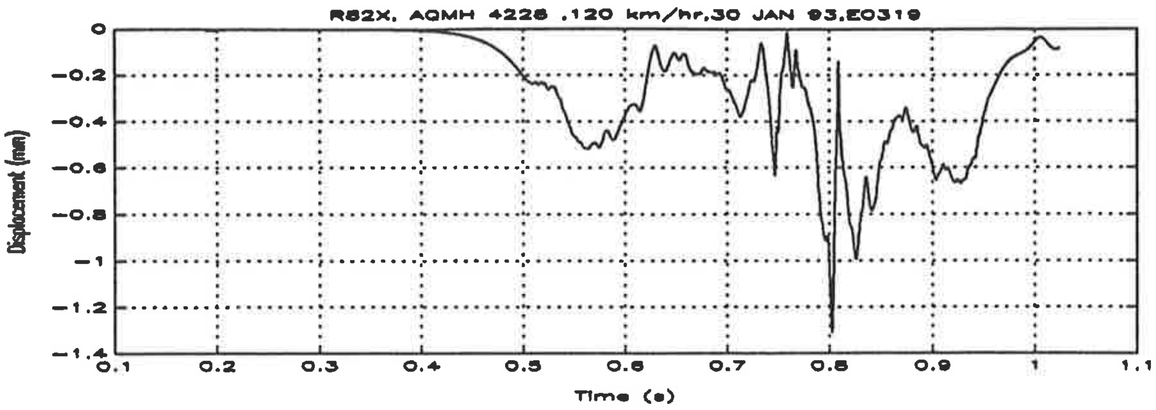
R82X, AQMH 4228 .120 km/hr,30 JAN 93,E0319
Displacement (mm)
0
-0.2
-0.4
-0.6
-0.8
-1
-1.2
-1.4
0.1
0.2
0.3
0.4
0.5
0.6
0.7
0.8
0.9
1
1.1
Time (s)

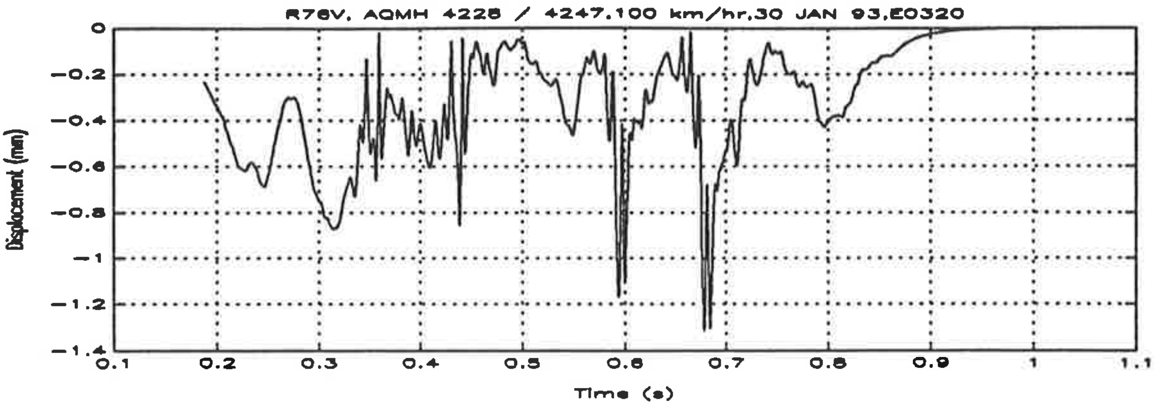
R76V, AQMH 4228 / 4247,100 km/hr,30 JAN 93,E0320
Displacement (mm)
Time (s)

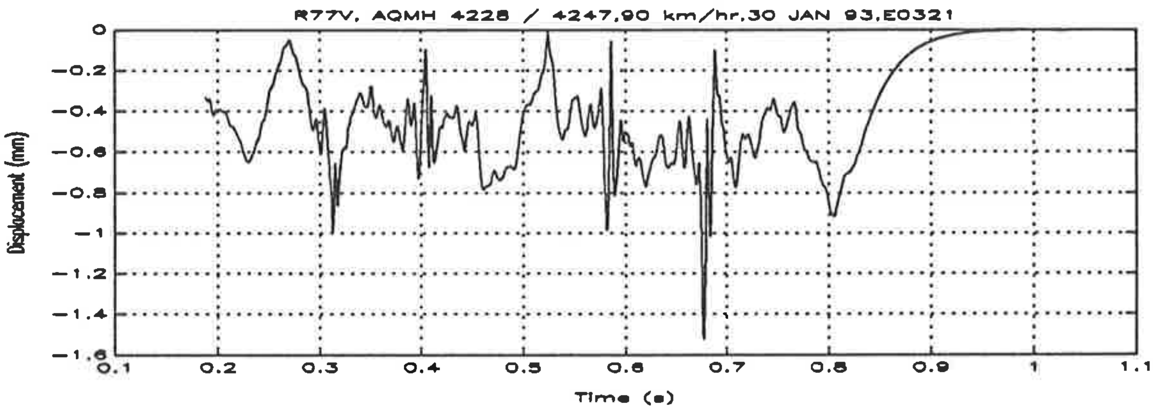
R77V, AQMH 4228 / 4247,90 km/hr,30 JAN 93,E0321
Displacement (mm)
Time (s)

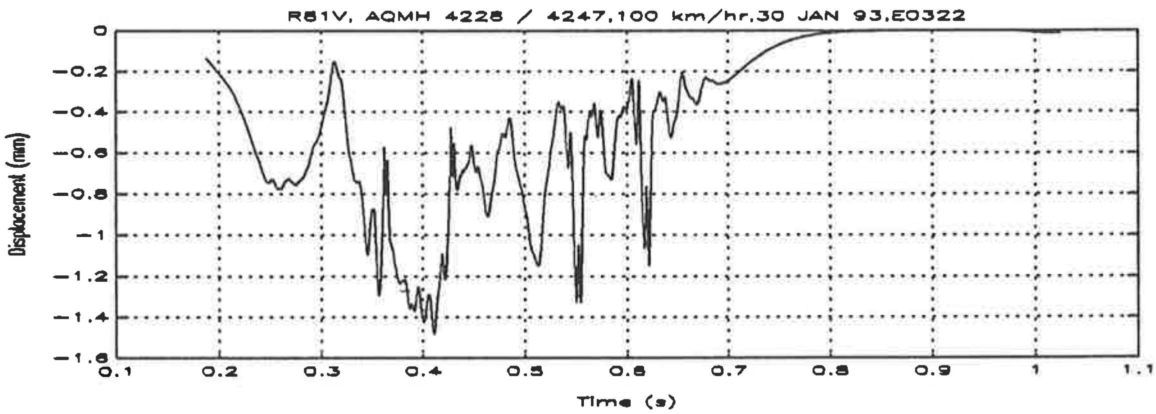
R81V, AQMH 4228 / 4247,100 km/hr,30 JAN 93,E0322
Displacement (mm)
Time (s)

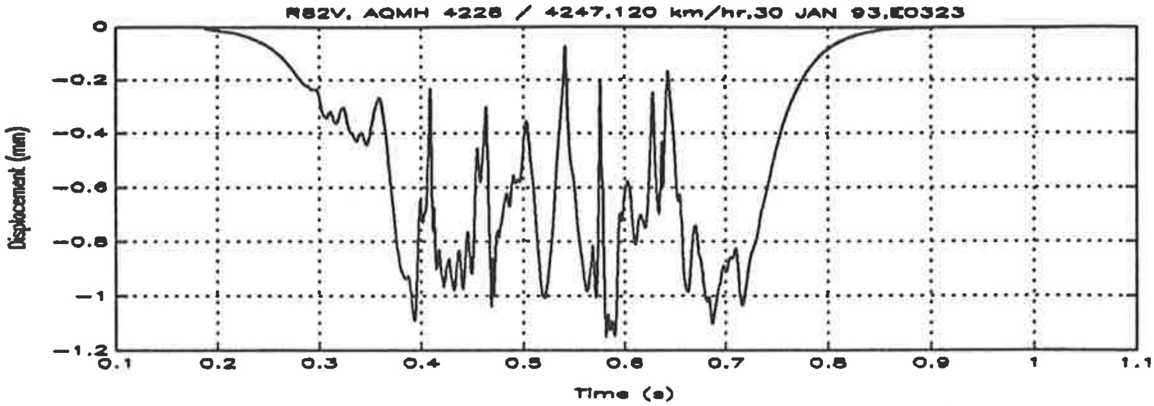
R82V, AQMH 4228 / 4247,120 km/hr,30 JAN 93,E0323
Displacement (mm)
0
-0.2
-0.4
-0.6
-0.8
-1
-1.2
0.1
0.2
0.3
0.4
0.5
0.6
0.7
0.8
0.9
1
1.1
Time (s)

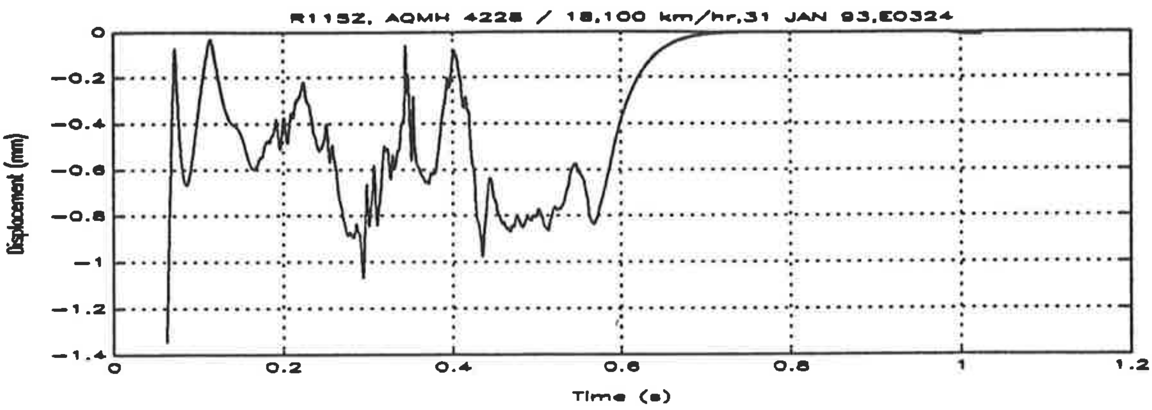
R115Z. AQMH 4228 / 18,100 km/hr,31 JAN 93,E0324
Displacement (mm)
Time (s)

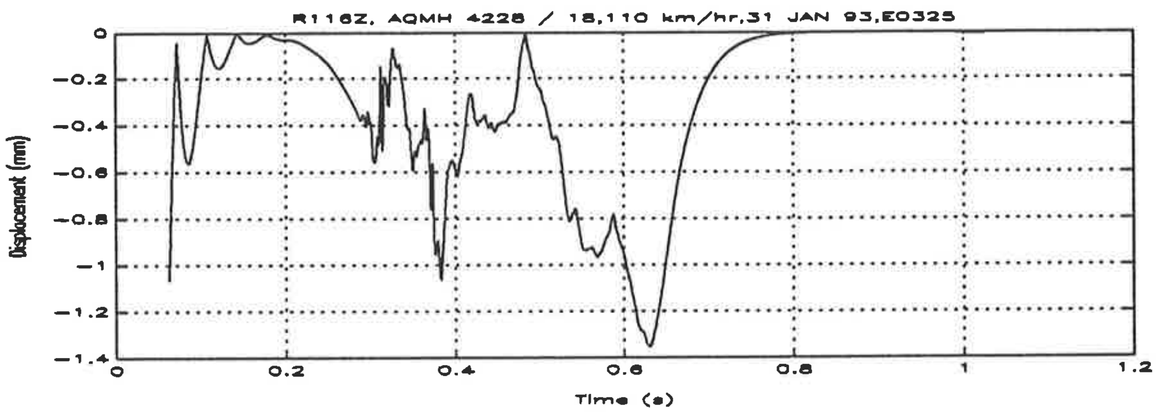
R116Z. AQMH 4228 / 18,110 km/hr,31 JAN 93,E0325
Displacement (mm)
Time (s)

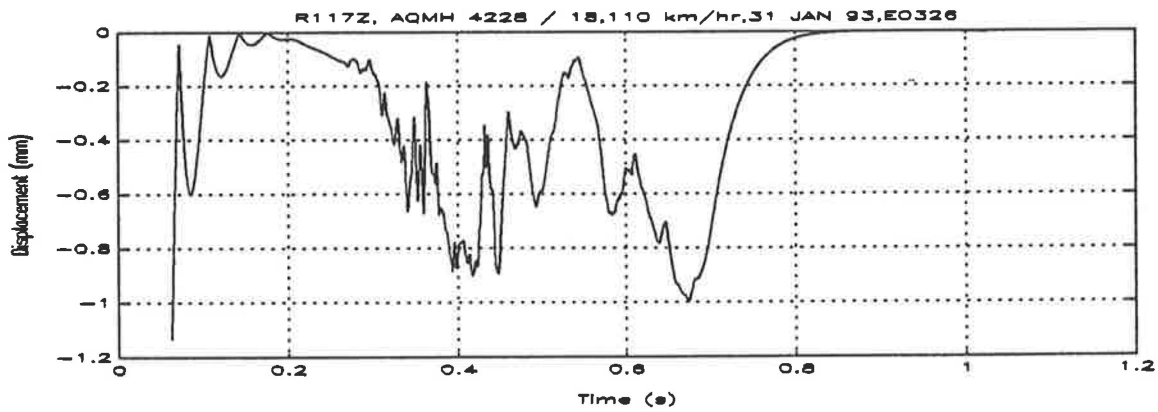
R117Z. AQMH 4228 / 18,110 km/hr,31 JAN 93,E0326
Displacement (mm)
Time (s)

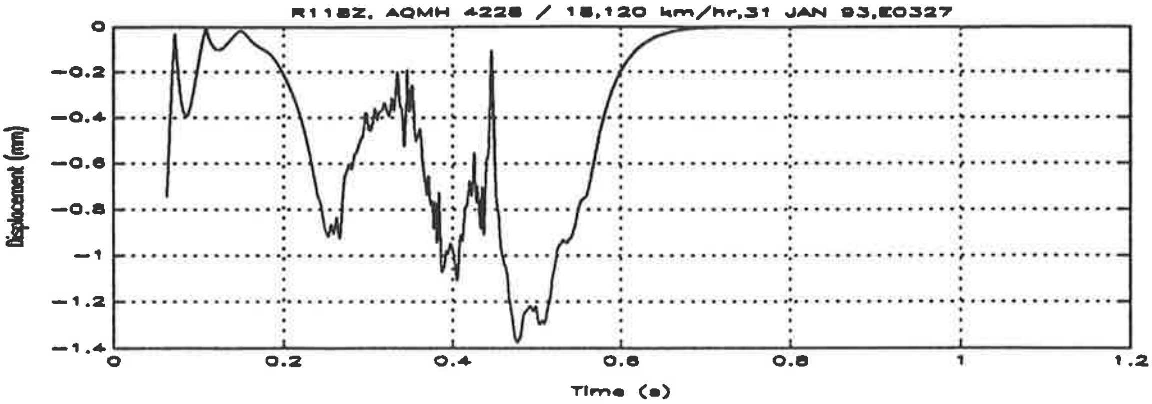
R118Z, AQMH 4228 / 18,120 km/hr,31 JAN 93,E0327
Displacement (mm)
0
-0.2
-0.4
-0.6
-0.8
-1
-1.2
-1.4
0
0.2
0.4
0.6
0.8
1
1.2
Time (s)

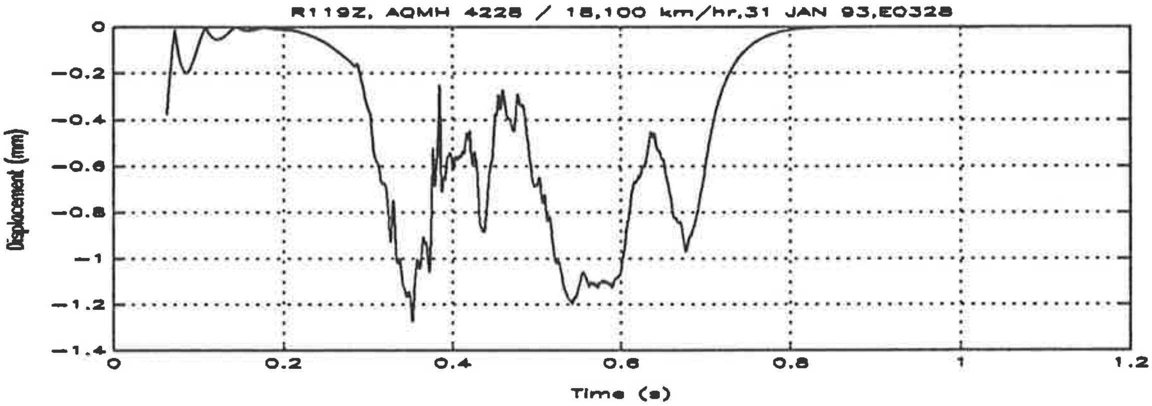
R119Z, AQMH 4228 / 18,100 km/hr,31 JAN 93,E0328
Displacement (mm)
0
-0.2
-0.4
-0.6
-0.8
-1
-1.2
-1.4
0
0.2
0.4
0.6
0.8
1
1.2
Time (s)

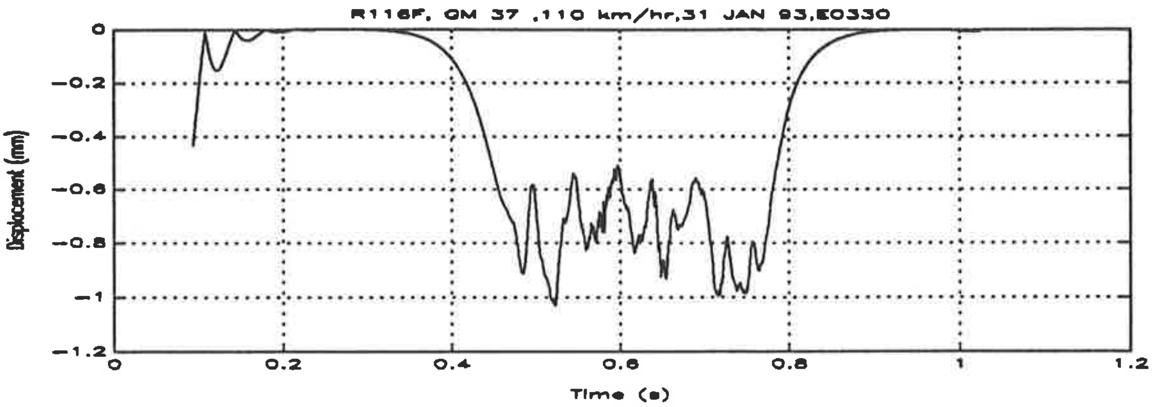
R116F, GM 37 ,110 km/hr,31 JAN 93,E0330
Displacement (mm)
Time (s)
0
-0.2
-0.4
-0.6
-0.8
-1
-1.2
0
0.2
0.4
0.6
0.8
1
1.2

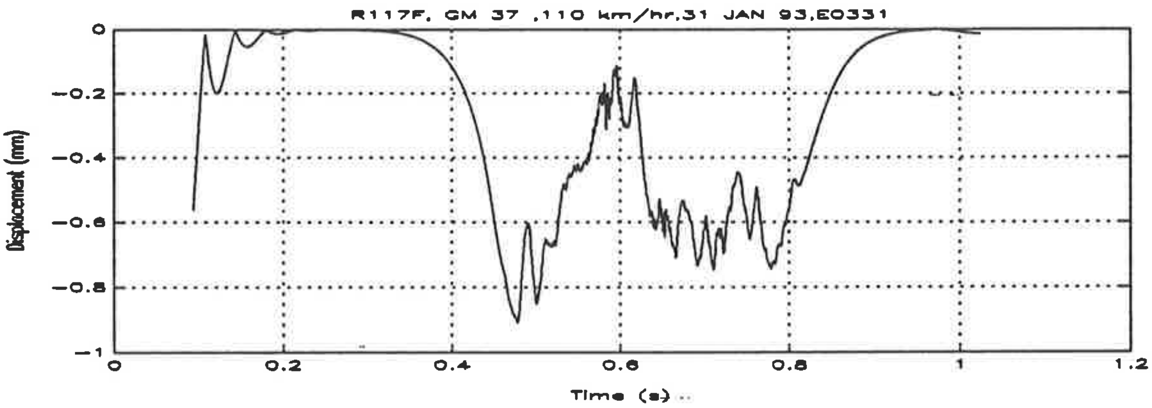
R117F, GM 37 ,110 km/hr,31 JAN 93,E0331
Displacement (mm)
Time (s)
0
-0.2
-0.4
-0.6
-0.8
-1
0
0.2
0.4
0.6
0.8
1
1.2

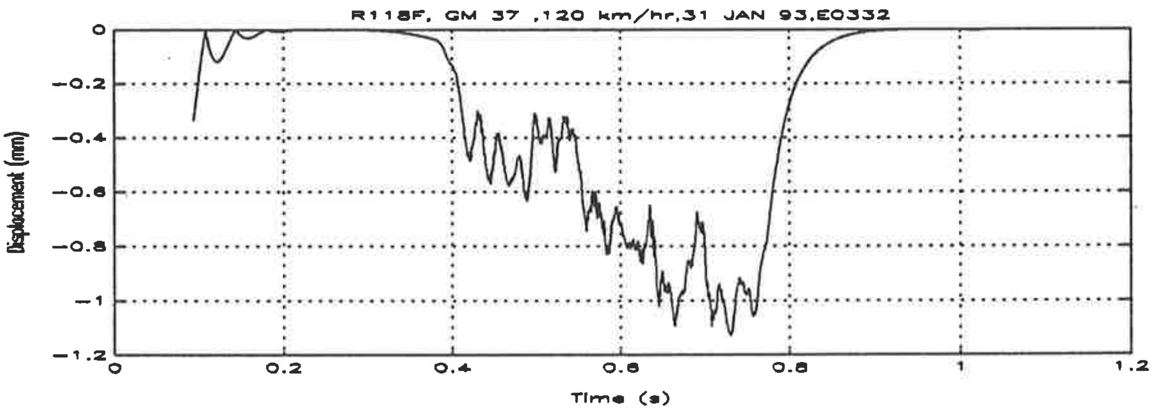
R118F, GM 37 ,120 km/hr,31 JAN 93,E0332
Displacement (mm)
Time (s)
0
-0.2
-0.4
-0.6
-0.8
-1
-1.2
0
0.2
0.4
0.6
0.8
1
1.2

[730e

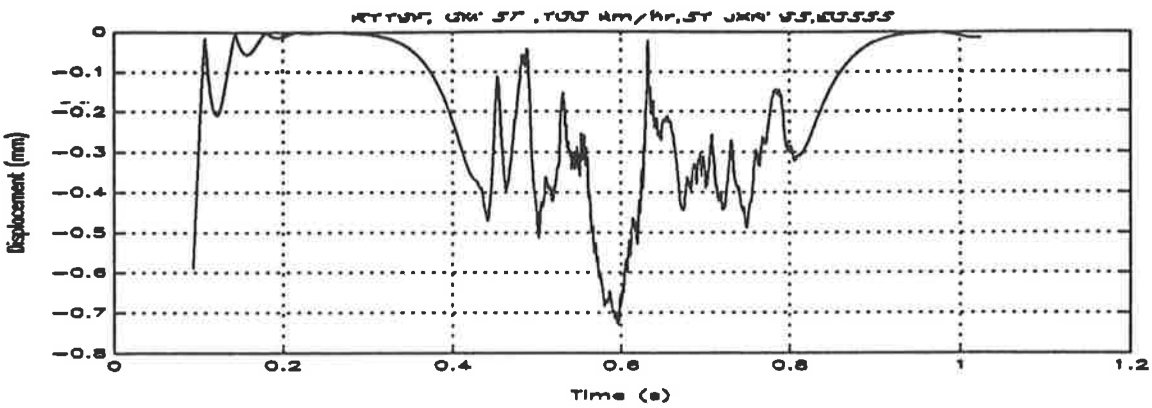

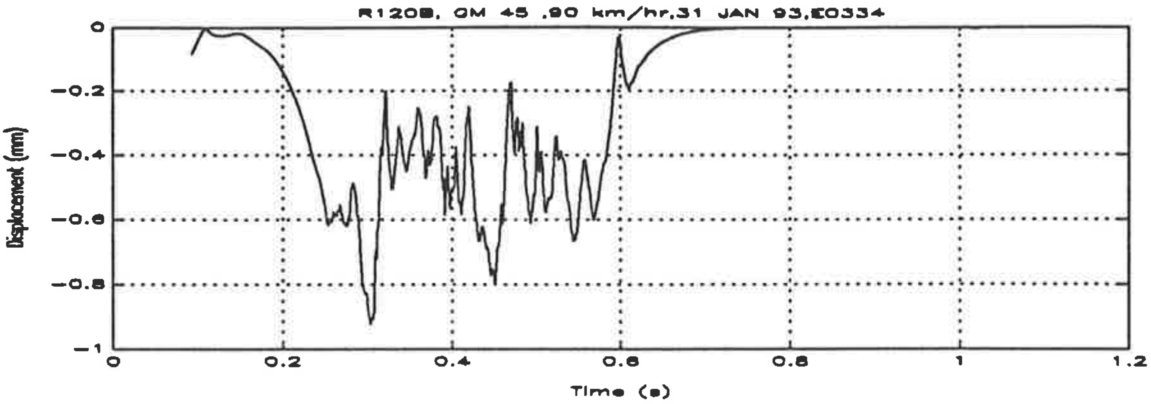
R120B, GM 45 ,90 km/hr,31 JAN 93,E0334
Displacement (mm)
0
-0.2
-0.4
-0.6
-0.8
-1
0
0.2
0.4
0.6
0.8
1
1.2
Time (s)

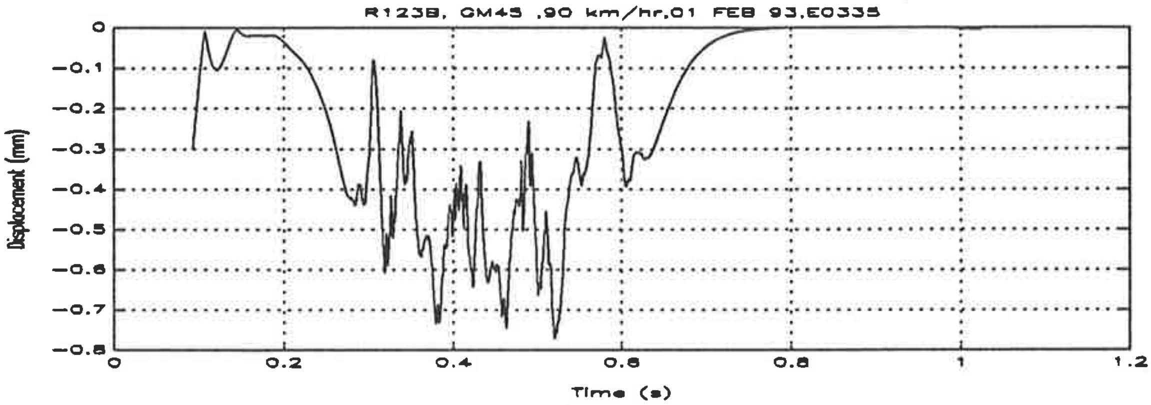
R123B, GM45 ,90 km/hr,01 FEB 93,E0335
Displacement (mm)
0
-0.1
-0.2
-0.3
-0.4
-0.5
-0.6
-0.7
-0.8
0
0.2
0.4
0.6
0.8
1
1.2
Time (s)

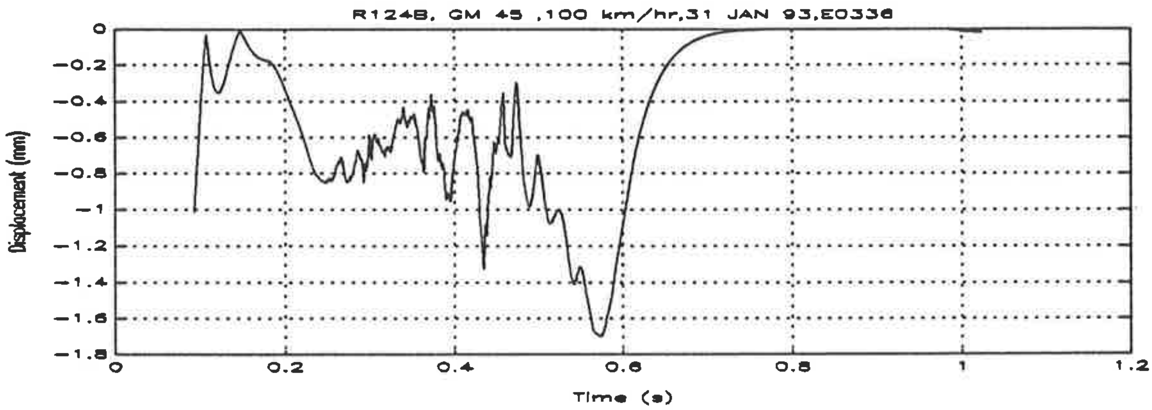
R124B, GM 45 ,100 km/hr,31 JAN 93,E0336
Displacement (mm)
0
-0.2
-0.4
-0.6
-0.8
-1
-1.2
-1.4
-1.6
-1.8
0
0.2
0.4
0.6
0.8
1
1.2
Time (s)

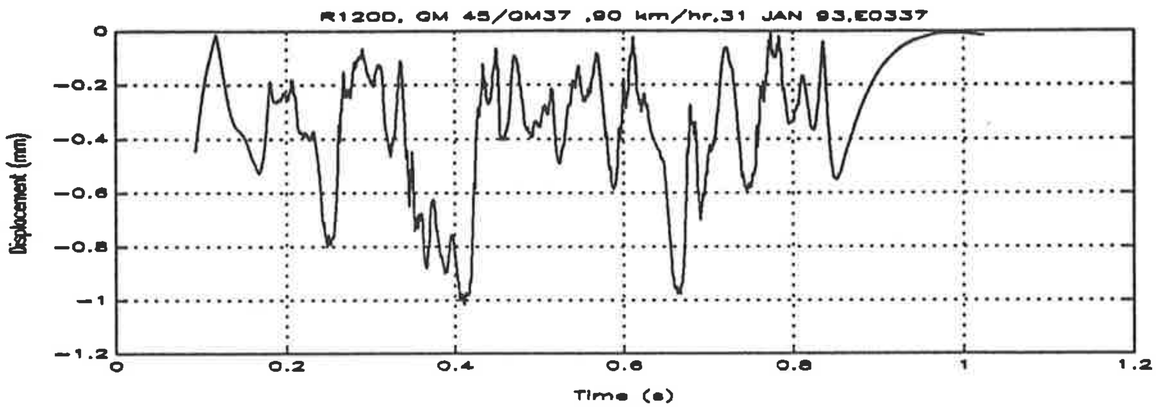
R120D, GM 45/GM37 ,90 km/hr,31 JAN 93,E0337
Displacement (mm)
Time (s)
0
-0.2
-0.4
-0.6
-0.8
-1
-1.2
0.2
0.4
0.6
0.8
1
1.2

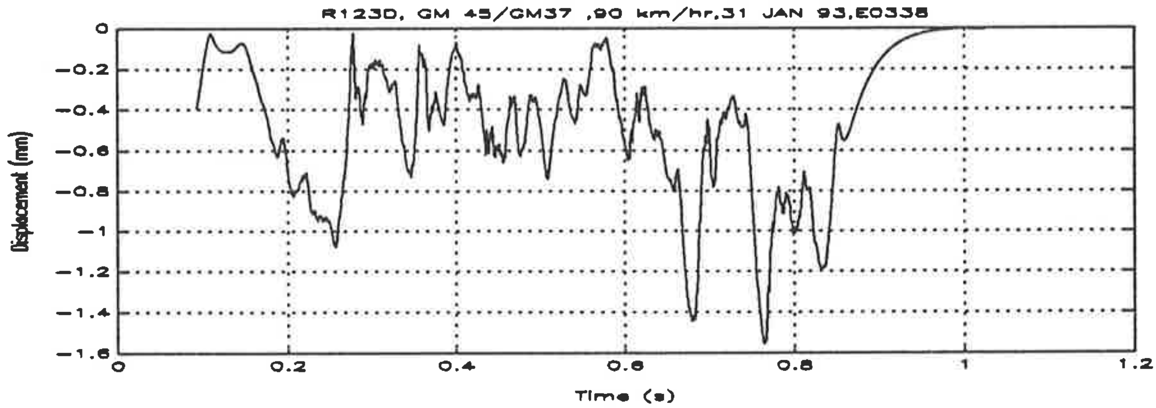
R123D, GM 45/GM37 ,90 km/hr,31 JAN 93,E0338
Displacement (mm)
Time (s)
0
-0.2
-0.4
-0.6
-0.8
-1
-1.2
-1.4
-1.6
0.2
0.4
0.6
0.8
1
1.2

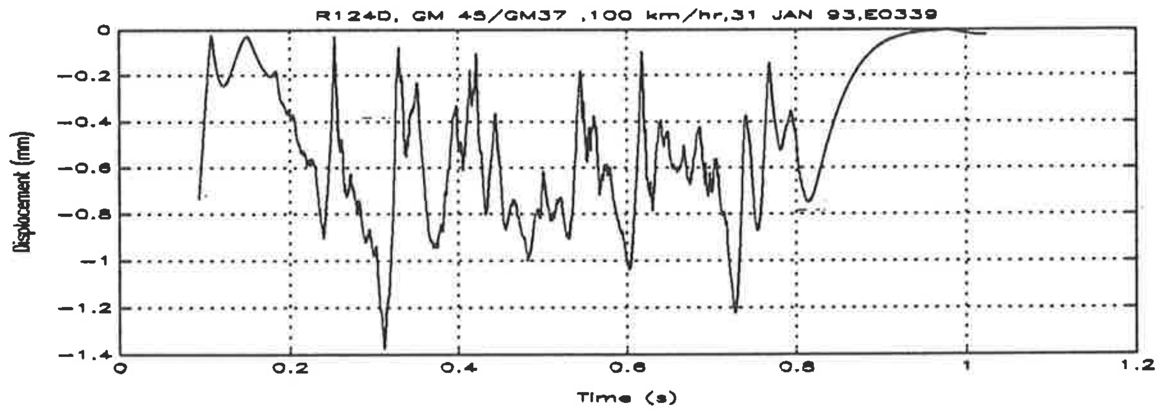
R124D, GM 45/GM37 ,100 km/hr,31 JAN 93,E0339
Displacement (mm)
Time (s)
0
-0.2
-0.4
-0.6
-0.8
-1
-1.2
-1.4
0.2
0.4
0.6
0.8
1
1.2

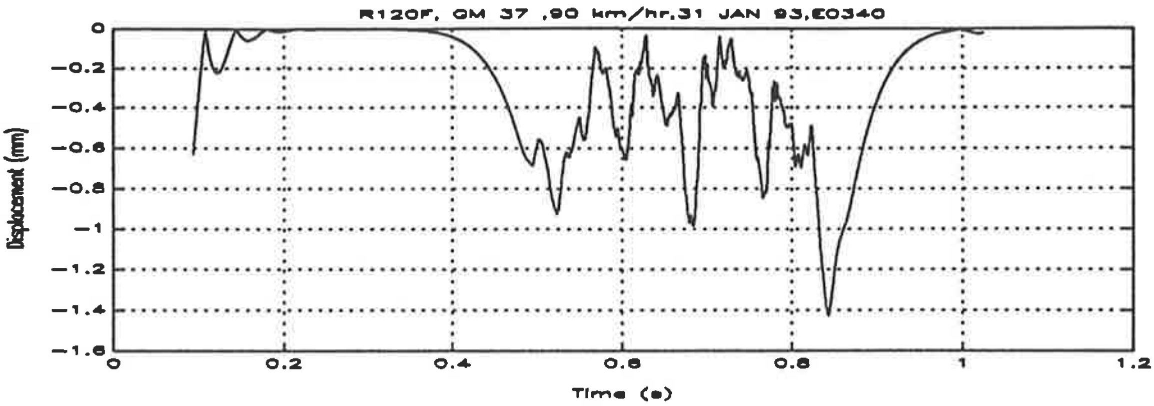
R120F, GM 37 ,90 km/hr,31 JAN 93,E0340
Displacement (mm)
Time (s)

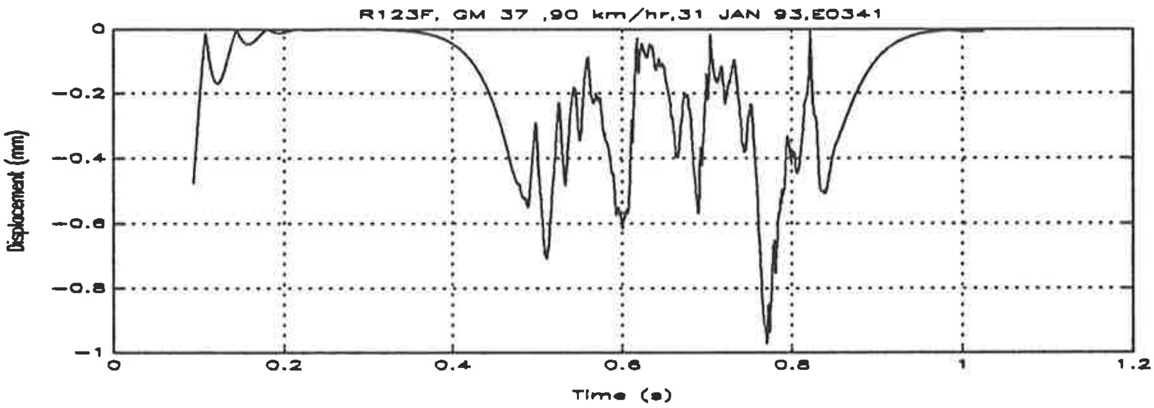
R123F, GM 37 ,90 km/hr,31 JAN 93,E0341
Displacement (mm)
Time (s)

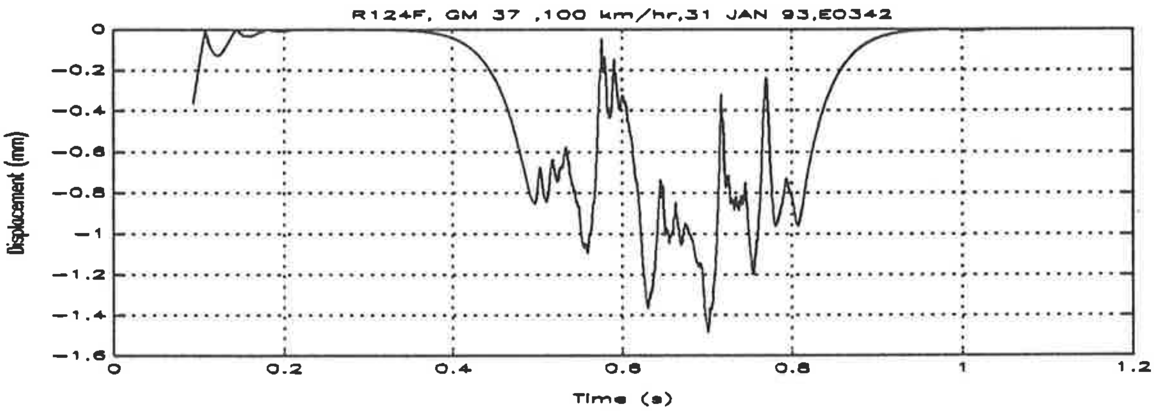
R124F, GM 37 ,100 km/hr,31 JAN 93,E0342
Displacement (mm)
Time (s)

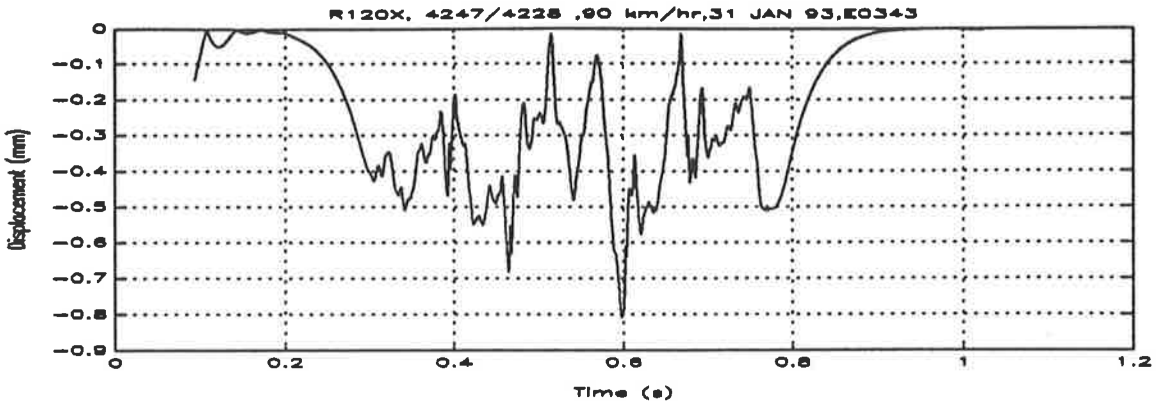
R120X, 4247/4228 ,90 km/hr,31 JAN 93,E0343
Displacement (mm)
0
-0.1
-0.2
-0.3
-0.4
-0.5
-0.6
-0.7
-0.8
-0.9
0
0.2
0.4
0.6
0.8
1
1.2
Time (s)

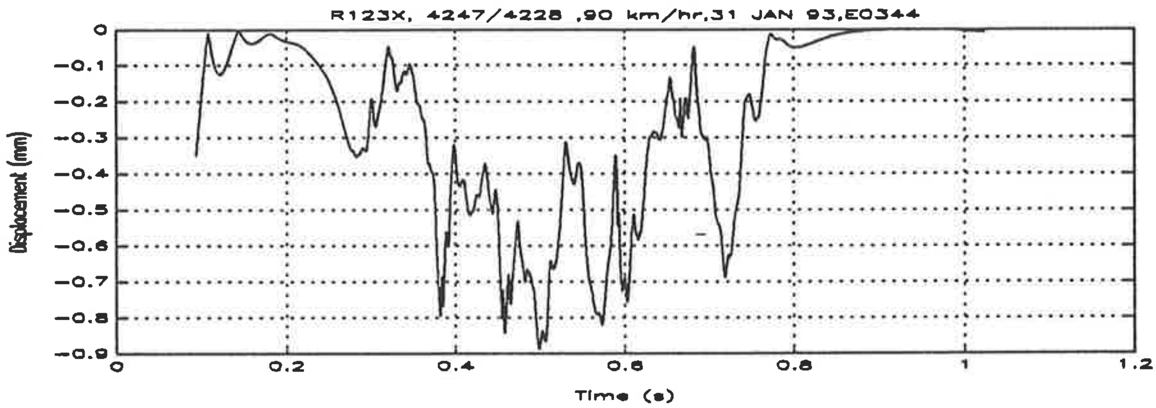
R123X, 4247/4228 ,90 km/hr,31 JAN 93,E0344
Displacement (mm)
0
-0.1
-0.2
-0.3
-0.4
-0.5
-0.6
-0.7
-0.8
-0.9
0
0.2
0.4
0.6
0.8
1
1.2
Time (s)

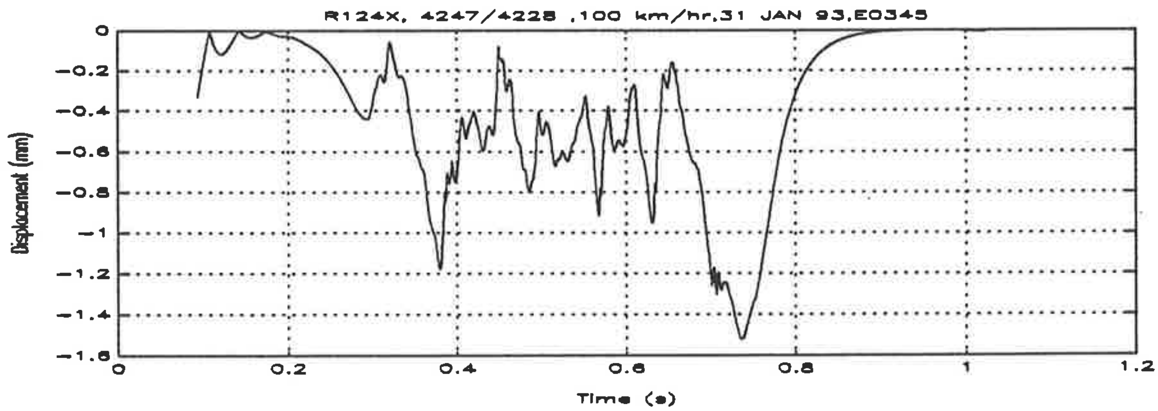
R124X, 4247/4228 ,100 km/hr,31 JAN 93,E0345
Displacement (mm)
0
-0.2
-0.4
-0.6
-0.8
-1
-1.2
-1.4
-1.6
0
0.2
0.4
0.6
0.8
1
1.2
Time (s)

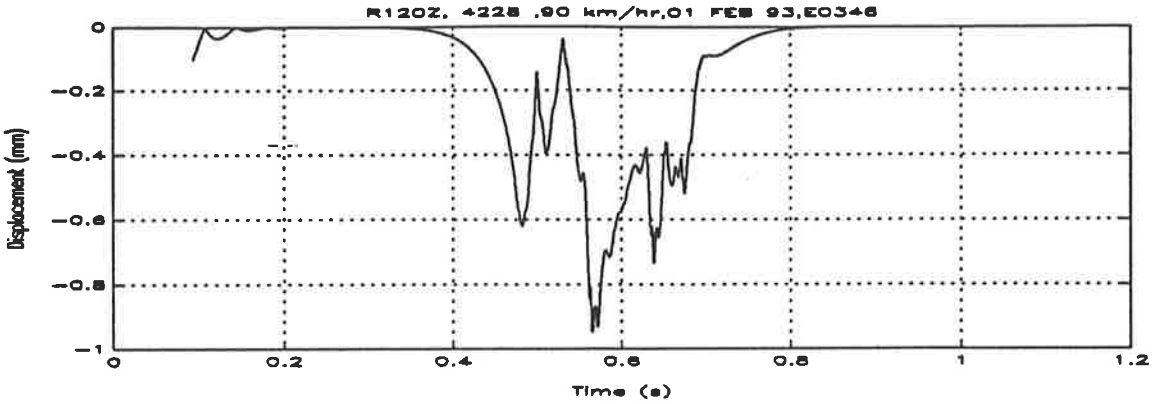
R120Z. 4228 ,90 km/hr,01 FEB 93,E0346
Displacement (mm)
0
-0.2
-0.4
-0.6
-0.8
-1
0
0.2
0.4
0.6
0.8
1
1.2
Time (s)

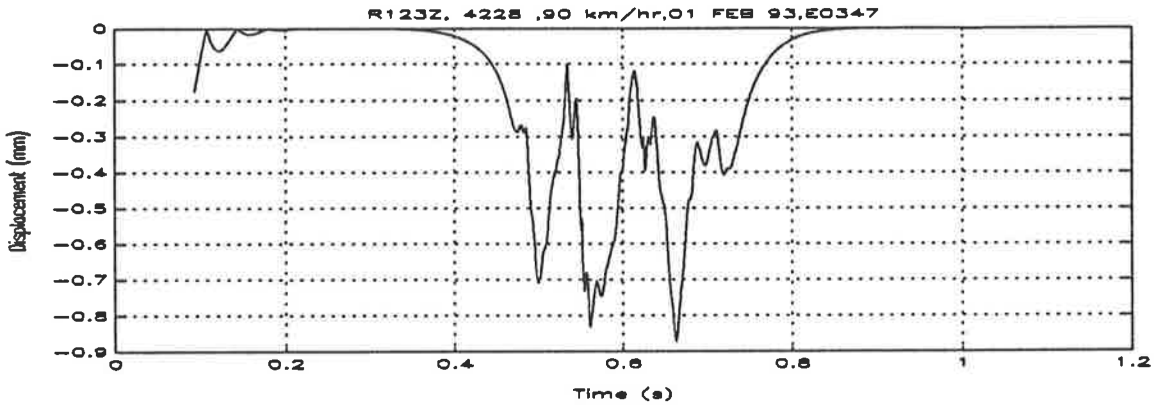
R123Z. 4228 ,90 km/hr,01 FEB 93,E0347
Displacement (mm)
0
-0.1
-0.2
-0.3
-0.4
-0.5
-0.6
-0.7
-0.8
-0.9
0
0.2
0.4
0.6
0.8
1
1.2
Time (s)

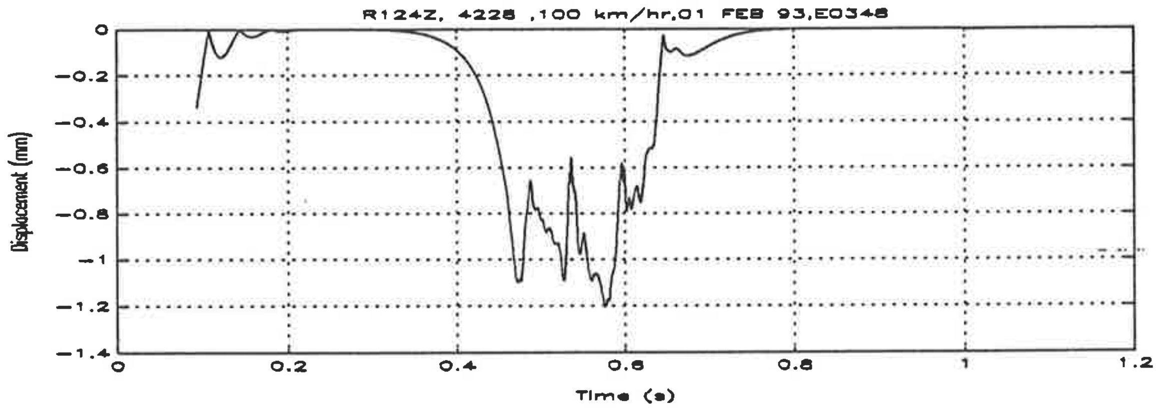
R124Z. 4228 ,100 km/hr,01 FEB 93,E0348
Displacement (mm)
0
-0.2
-0.4
-0.6
-0.8
-1
-1.2
-1.4
0
0.2
0.4
0.6
0.8
1
1.2
Time (s)

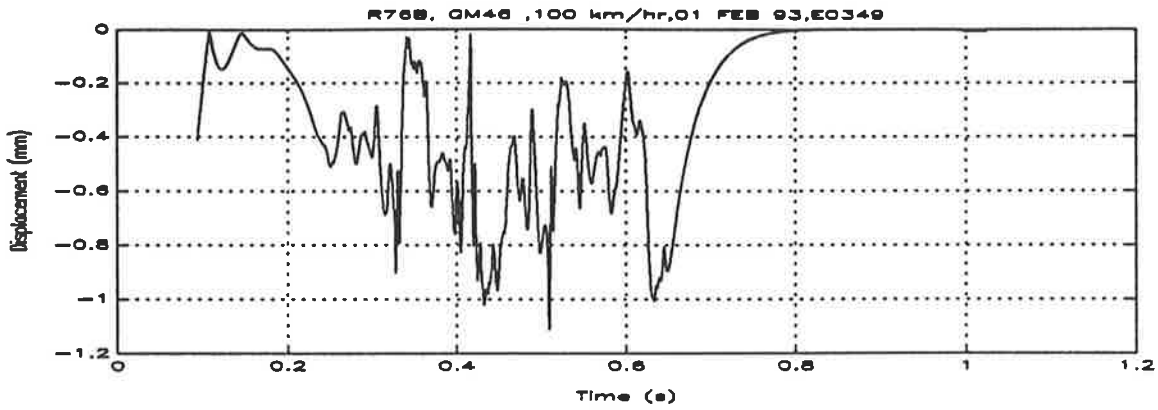
R76B, GM46 ,100 km/hr,01 FEB 93,E0349
Displacement (mm)
0
-0.2
-0.4
-0.6
-0.8
-1
-1.2
0
0.2
0.4
0.6
0.8
1
1.2
Time (s)

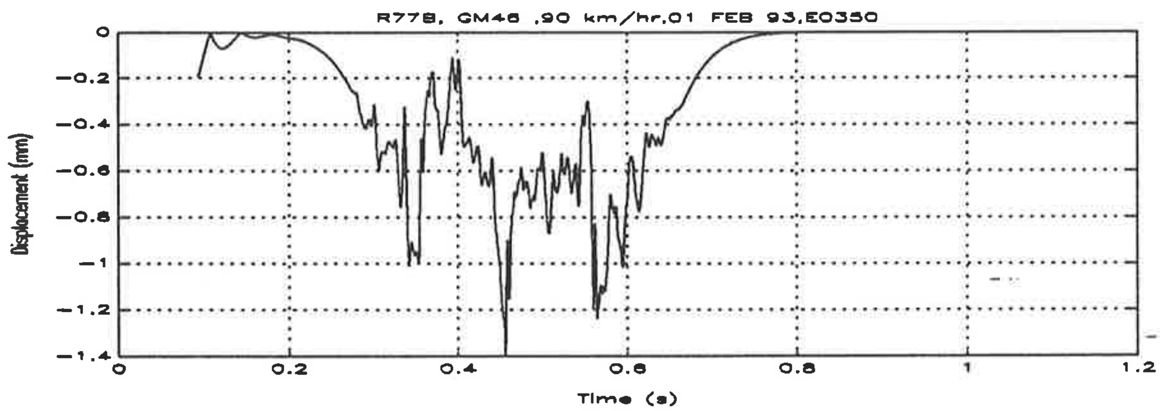
R77B, GM46 ,90 km/hr,01 FEB 93,E0350
Displacement (mm)
0
-0.2
-0.4
-0.6
-0.8
-1
-1.2
-1.4
0
0.2
0.4
0.6
0.8
1
1.2
Time (s)

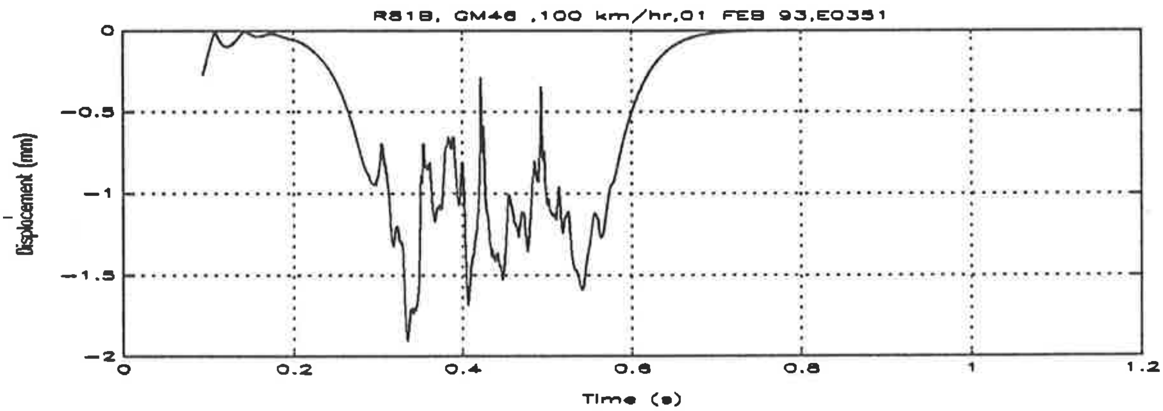
R81B, GM46 ,100 km/hr,01 FEB 93,E0351
Displacement (mm)
0
-0.5
-1
-1.5
-2
0
0.2
0.4
0.6
0.8
1
1.2
Time (s)

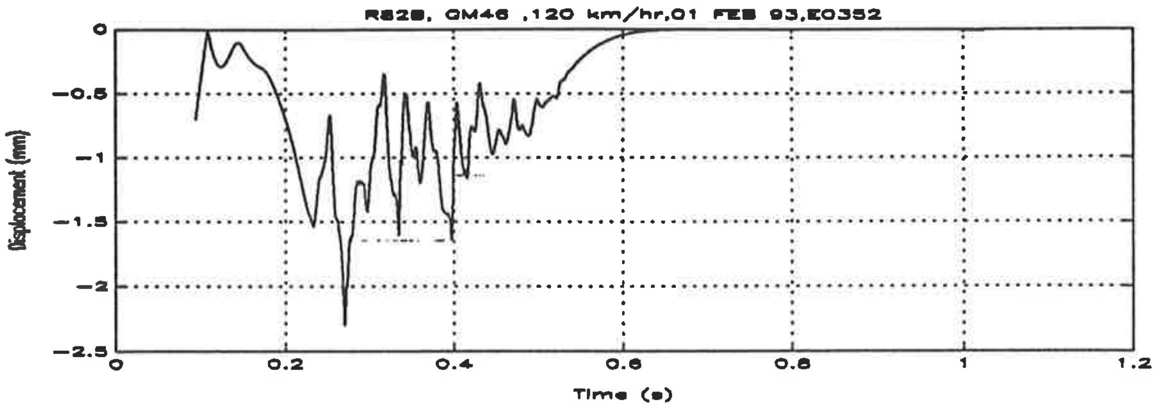

RS28, GM46 ,120 km/hr,01 FEB 93,E0352
Displacement (mm)
0
-0.5
-1
-1.5
-2
-2.5
0
0.2
0.4
0.6
0.8
1
1.2
Time (s)

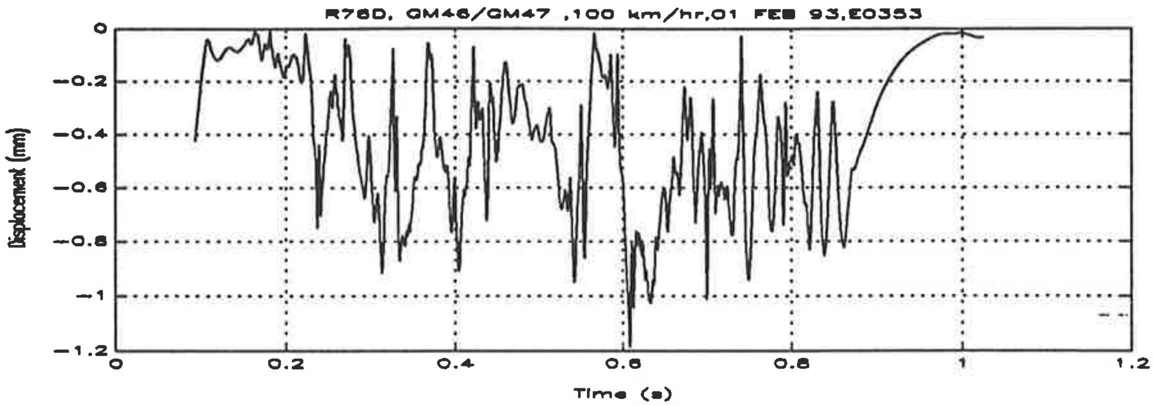
R76D, GM46/GM47 ,100 km/hr,01 FEB 93,E0353
Displacement (mm)
Time (s)

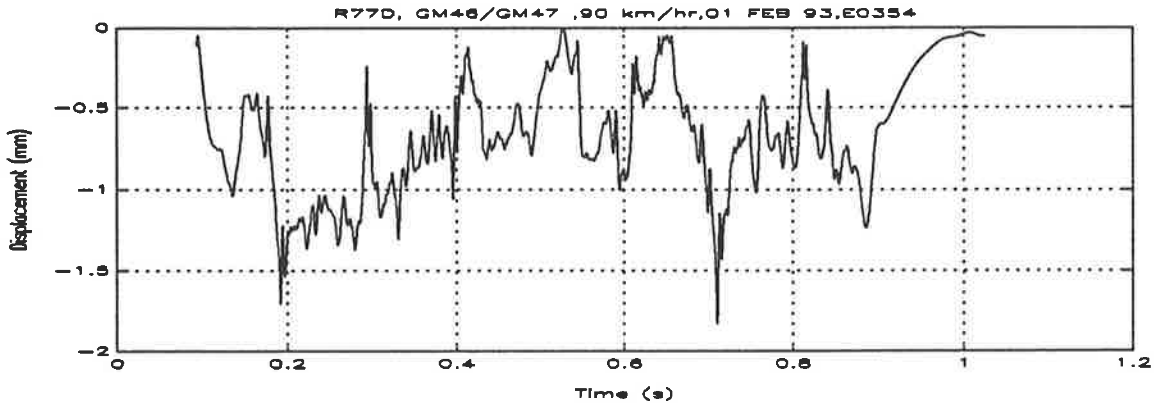
R77D, GM46/GM47 ,90 km/hr,01 FEB 93,E0354
Displacement (mm)
Time (s)

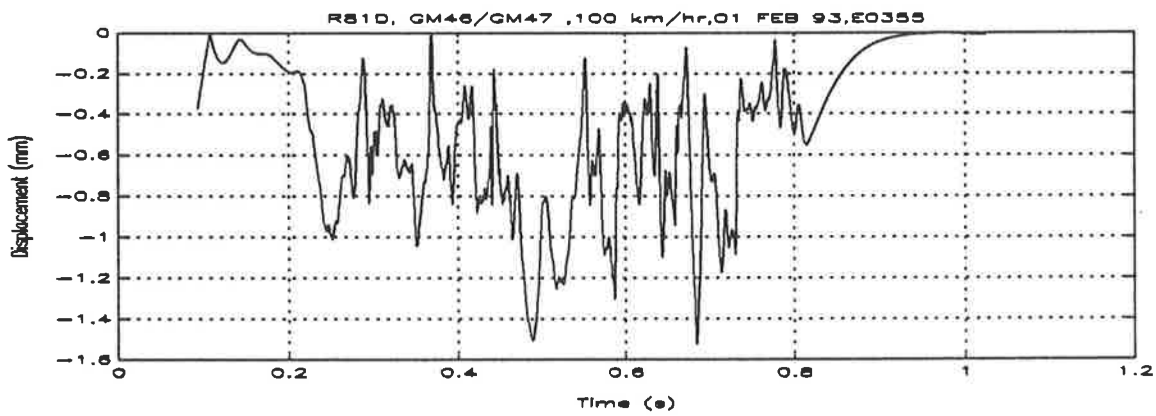
R81D, GM46/GM47 ,100 km/hr,01 FEB 93,E0355
Displacement (mm)
Time (s)

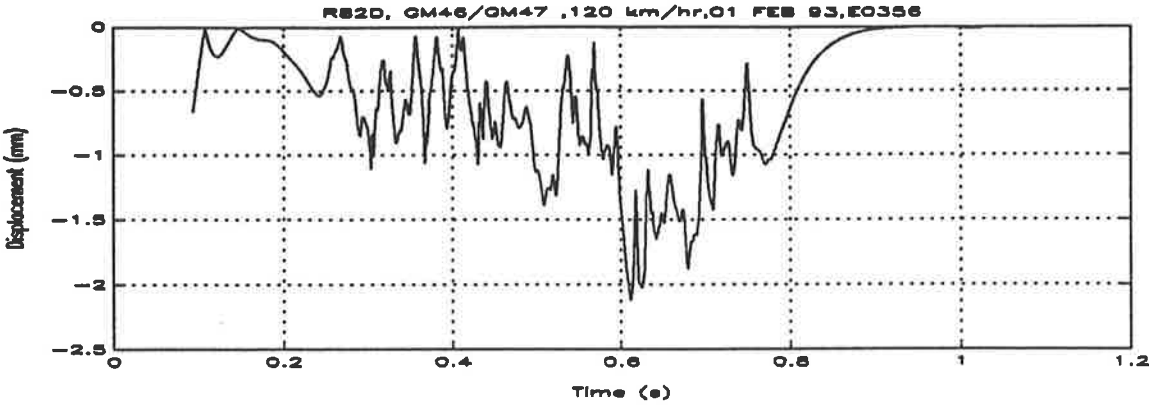
RS2D, GM46/GM47 ,120 km/hr,01 FEB 93,E0356
Displacement (mm)
0
-0.5
-1
-1.5
-2
-2.5
0
0.2
0.4
0.6
0.8
1
1.2
Time (s)

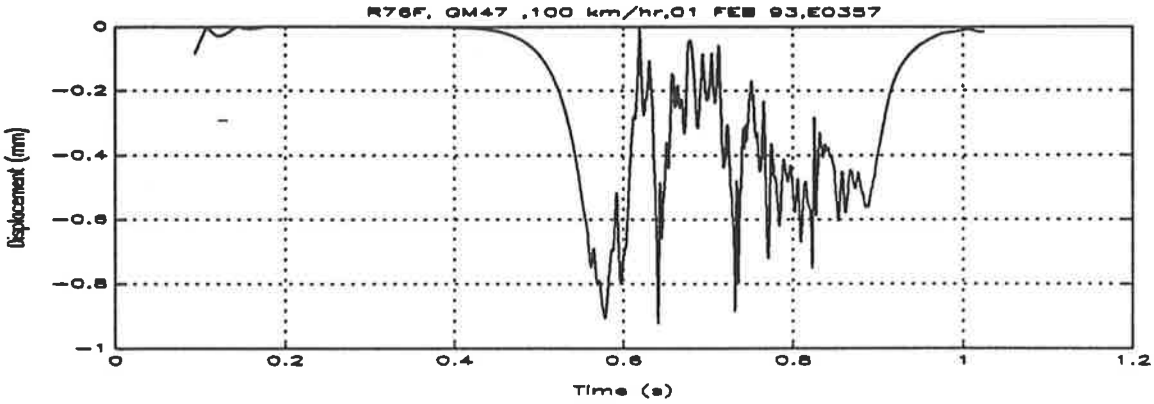
R76F, GM47 ,100 km/hr,01 FEB 93,E0357
Displacement (mm)
Time (s)

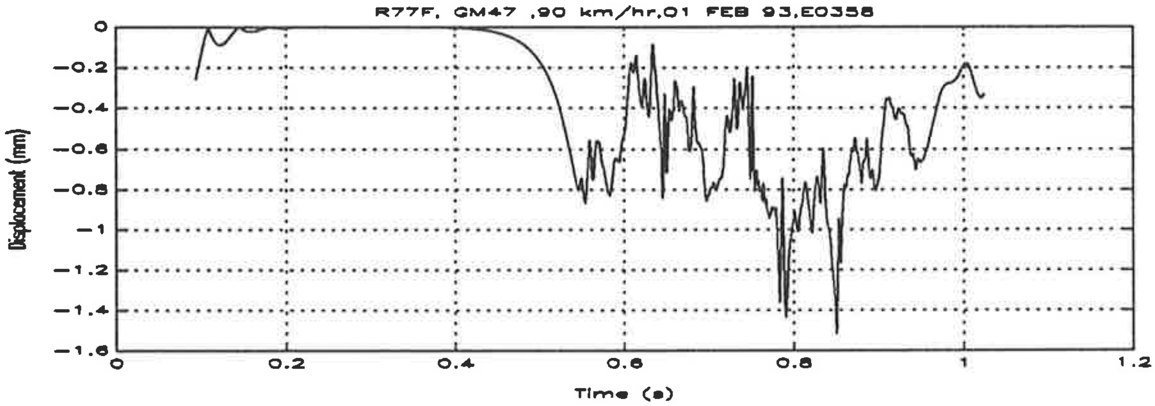
R77F, GM47 ,90 km/hr,01 FEB 93,E0358
Displacement (mm)
Time (s)

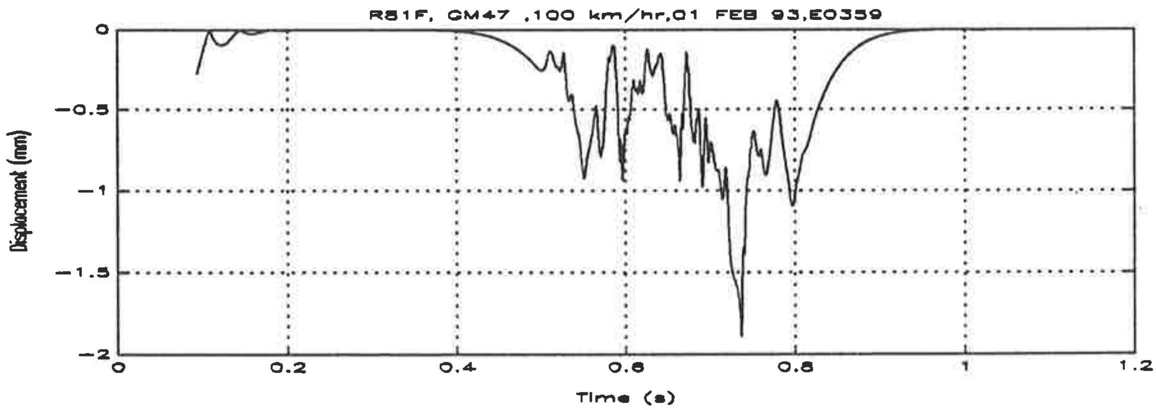
R81F, GM47 ,100 km/hr,01 FEB 93,E0359
Displacement (mm)
Time (s)

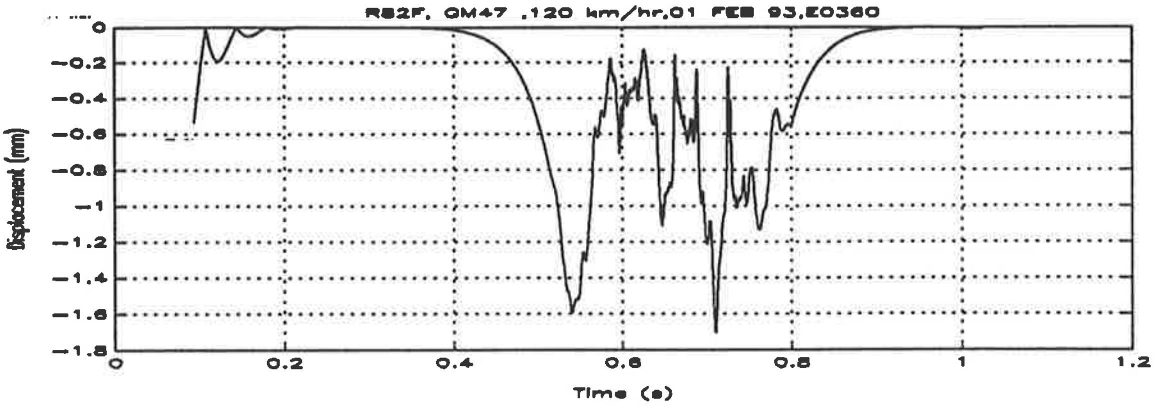
RS2F, GM47 ,120 km/hr,01 FEB 93,E0360
Displacement (mm)
0
-0.2
-0.4
-0.6
-0.8
-1
-1.2
-1.4
-1.6
-1.8
0
0.2
0.4
0.6
0.8
1
1.2
Time (s)

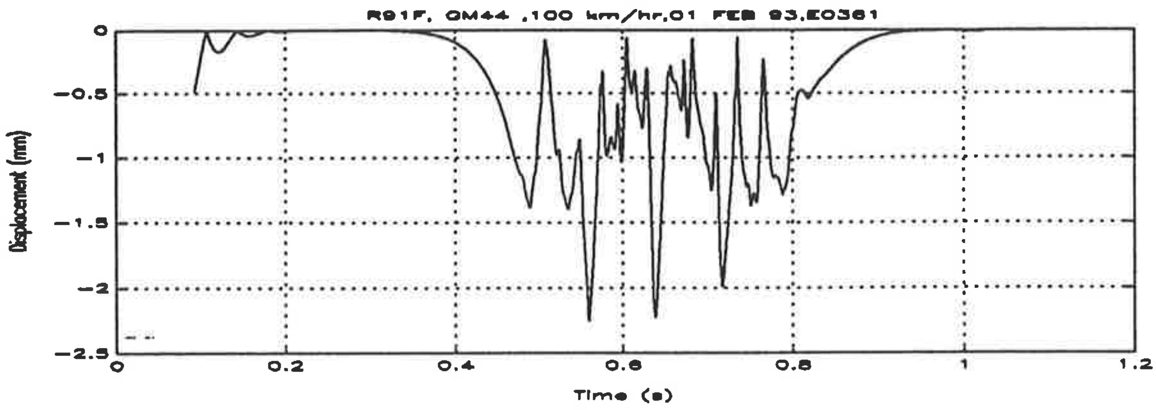
R91F, GM44 ,100 km/hr,01 FEB 93,E0361
Displacement (mm)
0
-0.5
-1
-1.5
-2
-2.5
0
0.2
0.4
0.6
0.8
1
1.2
Time (s)

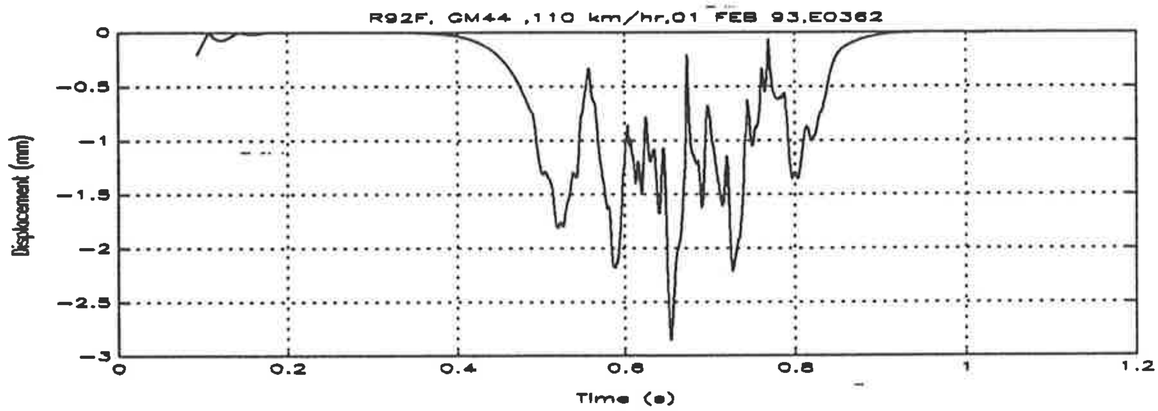
R92F, GM44 ,110 km/hr,01 FEB 93,E0362
Displacement (mm)
0
-0.5
-1
-1.5
-2
-2.5
-3
0
0.2
0.4
0.6
0.8
1
1.2
Time (s)

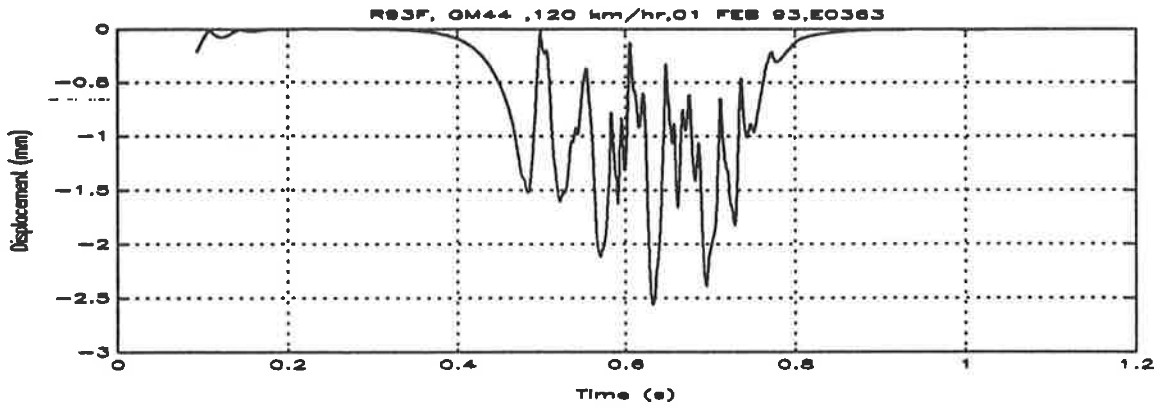
R93F, GM44 ,120 km/hr,01 FEB 93,E0363
Displacement (mm)
Time (s)

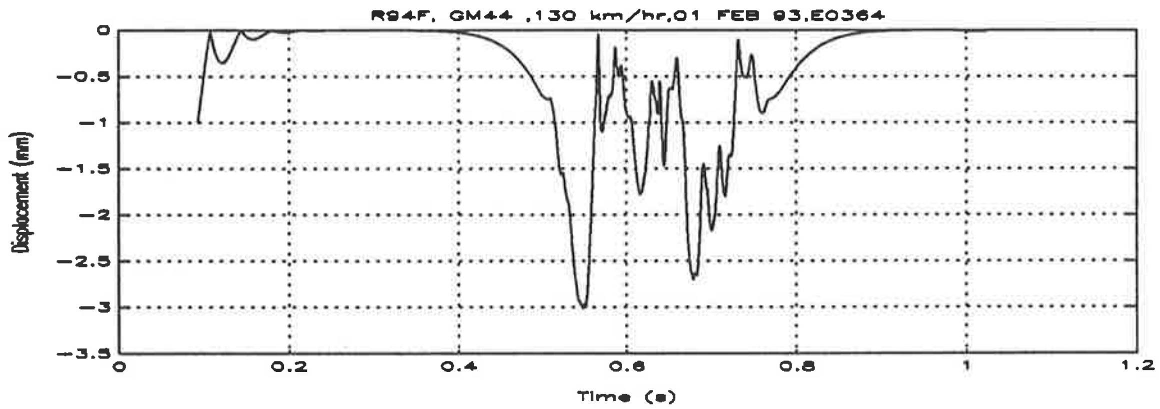
R94F, GM44 ,130 km/hr,01 FEB 93,E0364
Displacement (mm)
Time (s)

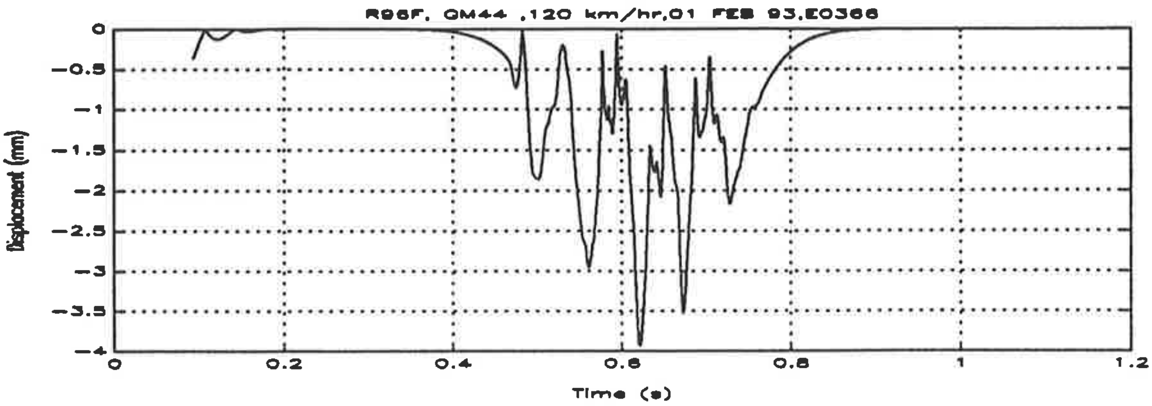
R96F, GM44 ,120 km/hr,01 FEB 93,E0366
Displacement (mm)
0
-0.5
-1
-1.5
-2
-2.5
-3
-3.5
-4
0
0.2
0.4
0.6
0.8
1
1.2
Time (s)

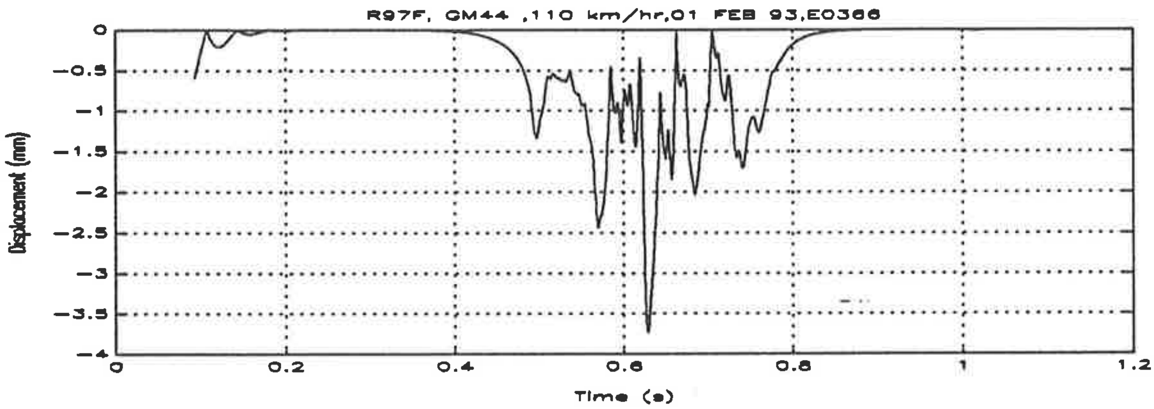
R97F, GM44 ,110 km/hr,01 FEB 93,E0366
Displacement (mm)
0
-0.5
-1
-1.5
-2
-2.5
-3
-3.5
-4
0
0.2
0.4
0.6
0.8
1
1.2
Time (s)

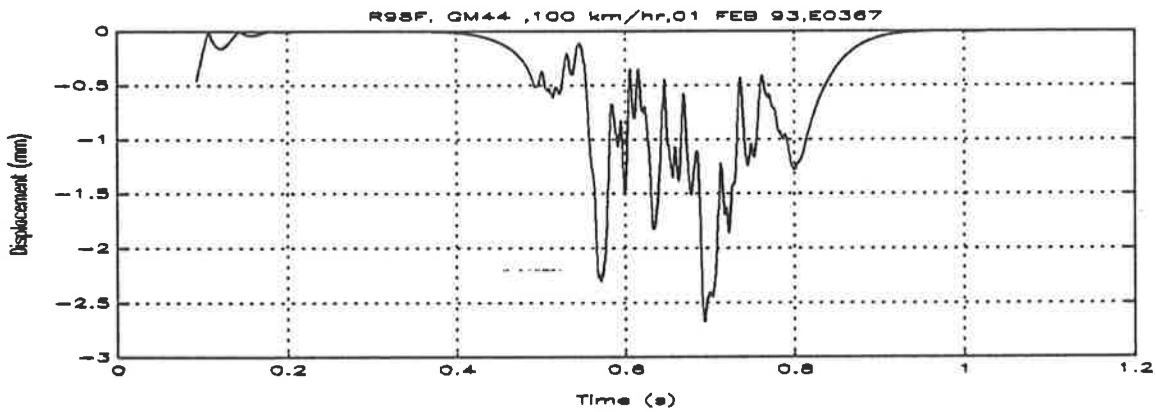
R98F, GM44 ,100 km/hr,01 FEB 93,E0367
Displacement (mm)
0
-0.5
-1
-1.5
-2
-2.5
-3
0
0.2
0.4
0.6
0.8
1
1.2
Time (s)

BIBLIOGRAPHY

1. **Stokes G.G.,**

   "Discussion of a differential equation relating to the breaking of railway bridges"

   Transactions of the Cambridge Philosophical Society, Vol 8, (1849).

2. **Ahlbeck D.**

   "Program IMPWHL user's manual"

   Battelle Columbus division

3. **Ahlbeck D.R.,**

   "The effects of railroad wheel profile roughness on impact loads and train resistance."

   Third Heavy Haul Railway Conference
   Vancouver, Canada, (1986)

4. **Ahlbeck D.R., Hadden J.A.,**

   "Measurement and Prediction of Impact loads from worn railroad wheel and rail surface profiles"

   Journal of Engineering for Industry
   Vol 107, (1985)

5. **Cai Z., Raymond G.P.**

   "Theoretical model for dynamic wheel/rail and track interaction"

   International Wheelset Congress,
   Sydney, Australia, (1992)

6. **Cai Z., Raymond G.P.,**

   "Responses of railway track to dynamic and static loading"

   5th International Heavy Haul Railway Conference
   Beijing (1992)

7. **Clark R.A. , Dean P.A., Elkins J.A., Newton S.G.,**

   "An investigation into the dynamic effects of railway vehicles running on corrugated rails"

   Journal Mechanical Engineering Science
   Vol 24 No 2 (1982)

8. **Grassie S.L.,**

   "User's manual for programs for dynamic response of corrugated track"

   Internal Australian National document

9. **Grassie S.L.,Gregory R.W.,Harrison D., Johnson K.L.**

   "The dynamic response of railway track to high frequency vertical excitation "

   Journal Mechanical Engineering Science
   Vol 24 , No 2 (1982)

10. **Grassie S.L.,**

"The dynamic response of railway track with unsupported sleepers"

Proc Institution of Mechanical Engineers
Vol 199,No D2, (1985)

11. **Hempelmann K., Ripke B., Dietz S.,**

"Modelling the dynamic interaction of wheelset and track"

Railway Gazette International
September (1992)

12. **Ishida M., Miura S.**

"Relationship between rail surface irregularity and dynamic wheel load"

International Wheelset Congress,
Sydney, Australia, (1992)

13. **Jenkins H.H., Stevenson J.E., Clayton E.A., Morland G.W., Lyon D.**

"The effect of track and vehicle parameters on wheel/rail vertical dynamic forces"

The Railway Engineering journal,
Vol 3, No 1 (1974)

14. **Lyon D.**

"A track dynamics program for the calculation of track forces due to dipped rail joints, wheel flats and rail welds"

British Railways Board
Research Department, Track Group
Track and Structures section (1972)

15. **Newton S.G., Clark R.A.,**

"An investigation into the dynamic effects on the track of wheelflats on railway vehicles"

Journal Mechanical Engineering Science
Vol 21 No 4 (1979)

16. **Williams M.A.,**

"Rail Track / Vehicle Interaction study"

Master of Engineering Thesis
University of Adelaide, (1974).

17. **Shelley S.J.,**

"SIMCAR users manual"

University of Adelaide / ROA (1984)

18. **Wanming Z., Kaiwen W., Maohai F., Junmaio Y.**

"Minimizing dynamic interaction between track and heavy haul freight cars"

5th International Heavy Haul Railway Conference
Beijing (1992)

19. **Esveld C.**

"Measuring and Rectifying Rail Roughness and Bad Welds"

Third Heavy Haul Railway Conference
Vancouver, Canada, (1986)

20. **Tunna.,**

"Wheel/rail forces due to wheel irregularities"

9th International wheelset congress, Montreal, September 1988.

21. **Jeffs T., Marich S.,**

"Ballast characteristics in the laboratory"

Conference on Railway Engineering
Perth, (1987)

22. **Dahlberg T.,**

"Structural response to moving forces determined by reciprocity relations"

Vehicle Systems Dynamics, 19 (1990), pp 113-130

23. **Thomson W.T,**

"Theory of Vibration"

3rd edition
Allen and Unwin, ISBN 0-04-445069-9

24. **Nashif A.D., Jones D.I., Henderson J.P.,**

"Vibration damping"

Wiley Interscience ISBN 0471867721

25. **Grassie S.L.**

"Resilient railpads: their dynamic behaviour in the laboratory and on track "

Proc Institution of Mechanical Engineers
Vol 203 pp 25-32 (1988)

26. **Maree J.S.,**

"Aspects of resilient rail pads"

5th International Heavy Haul Railway Conference
Beijing (1992)

27. **Ford R.,**

"Modal analysis of a concrete railway sleeper"

Research Note AVG/RN881122-1
Acoustics and Vibrations group
School of Mechanical and Industrial Engineering
The University of New South Wales. (1988)

28. **Lucas J.C.,**

"The Total track structure and its response to its environment"

4th International Rail Track and Sleeper conference
Adelaide (1981).

29. **Kohoutek M.E.,**

"Dynamic performance of concrete and timber sleepers"

9th International Rail Track Conference
Perth, (1992)

30. **Selig E.T., and Sluz A,**

"Ballast and subgrade response to train loads"

Transportation Research Review 694, (1978), pp 53-60

31. **Shenton M.J.**

"Ballast deformation and track deterioration"

Abstract from Track technology for the next decade
Thomas Telford Ltd.

32. **Office for Research and Experiments of the International Union of Railways.**

"Dynamic vehicle track interaction from the point of view of track maintenance"

Question D167 [1987]

33. **Frederick C.O.,**

"The effect of rail straightness on track maintenance"

Advanced Techniques in Permanent way design, construction and maintenance.
Madrid (1981)

34. **Frederick C.O.,**

"The effect of wheel and rail irregularities on the track"

1st International Heavy Haul Conference (1980)
Session 204 Paper G.2

35. **Reissberger K., Wenty R.,**

"Track quality - key to load bearing capacity and efficient maintenance"

5th International Heavy Haul Railway Conference
Beijing (1992)

36. **Generowicz B.S.,**

"A direct method of measuring degradation of crushed rock ballast under load"

4th International Rail Track and Sleeper conference
Adelaide (1981).

37. **Sato Y., and Odaka T., Takai H.,**

"Theoretical analysis on vibration of ballasted track"

Quarterly journal of RTRI
Vol 29, No 1, (1988)

38. **Koffman J.L., Bartlett D.L.,**

"An appreciation of the practical problems: A survey of the problems and their importance"

Proceedings of the Institution of Mechanical Engineers
1965-66 Vol 180 Pt 3F

39. **Eisenmann J., Leykauf G., Mattner L.,**

"Deflection and settlement behaviour of ballast"

5th International Heavy Haul Railway Conference
Beijing (1992)

40. **Ebershon W., Trevizo M.C., Selig E.T.,**

"Effect of low track modulus on track performance"

5th International Heavy Haul Railway Conference
Beijing (1992)

41. **Kearsley E.P., Van S.C.,**

"The effect of heavy haul traffic on track geometry deterioration"

5th International Heavy Haul Railway Conference
Beijing (1992)

42. **Cox S.J., Grassie S.L.**

"Understanding dynamics as an aid to developing track"

Third Heavy Haul Railway Conference
Vancouver, Canada, (1986)

43. **Mair R.I.,**

"Natural frequency of rail track and its relationship to rail corrugation"

The Institution of Engineers,Australia
Civil Engineering transactions (1977)

44. **Plunkett R.,**

"Measurement of damping"

From "Structural Dynamics"
Ruzika J.E.,
Colloquium on Structural Damping
ASME (1959)

45. **Janardhnam and Desai**

"Three dimensional testing and modelling of ballast"

ASCE Geotechnical Journal
Vol 109, No 6, (1983) , 783-796

46. **Tew G.P., Marich S.,**

"Achieving performance of steel sleepers through accurate design"

4th International Heavy Haul Railway Conference, Brisbane, (1989)

47. **Birks F.J., Tew G.P., Chitty G.B.,**

"Narrow gauge track with interspersed steel sleepers"

4th International Heavy Haul Railway Conference, Brisbane, (1989)

48. **Mair R.I., Jupp R.A., and Groenhout R.,**

"The characteristics and control of long pitch rail corrugation at heavy axle load"

BHP Melbourne Research Laboratories / 081/076/014 (1976)

49. **El-Sibaie M.,**

"On the component of track damping resistance and related damping measurements"

Applied Mechanics, Rail Transportation Symposium
AMD - Vol 96, RTD - Vol 2, (1988)

50. **Verhas H.P.,**

"Prediction of the propagation of train induced ground vibration"

Journal of Sound and Vibration (1979) 66(3), 371-376

51. **Miller G.F., Pursey H.,**

"Partition of energy between elastic waves in a semi infinite solid"

Proceedings of the Royal Society of London
Vol 233 A, (1956)

52. **Hooper L.E.**

"Application of state variable analysis methods to railway engineering"

Railway Engineering Conference,
Institution of Engineers, Australia,
(1981), Sydney.

53. **Mutton P.J., Jeffs T.,**

"Towards improving the performance of rail welds"

Proceedings of the 1992 Rail Track Conference

54. **Marich S., Poplawski A.,**

"Wheel Rail interaction at welds"

8th International Rail Track Conference
Sydney (1990)

55. **Johnson K.L.**

"One hundred years of Hertz contact"

Proc Institution of Mechanical Engineers
Vol 196, pp 363-378 (1982)

56. **Wilson E. L.**

"CAL-86 Computer assisted learning of structural analysis and the CAL/SAP development system"

Department of Civil Engineering
University of California
Berkeley, California (1986)

57. **DARE-P**

"Basic Features of DARE-P"

University of Adelaide (1985)

58. **Round D.J.,**

"The effect of rail straightness on track quality and deterioration"

Rail Technology, ISBN 0 9508596 0 5
Technical Print Services Ltd, Nottingham.
Proceedings of seminar at Nottingham University (1981)

59. **Meriam J.L.,**

"Dynamics, SI version"

Second edition, Wiley

60. **Mathsworks inc**

"386-Matlab users guide"

61. **Shigley J.E.,**

"Mechanical Engineering Design"

3rd edition, McGraw-Hill, ISBN 0-07-056881-2

62. **CTRAN**

Users guide, Thoroughbred Instruments

63. **Lynn P.A.,**

"The Analysis and Processing of Signals, Second Edition"

Macmillan Publishers, (1986)
ISBN 0-333-34030-2

64. **Lyon D.,**

"Dynamic measurements in the research and development of rail vehicles"

Vehicle Systems Dynamics, 16 (1987), pp 149-165

65. **Shugu.Z.**

"Dynamic test of heavy track structure"

Third Heavy Haul Railway Conference
Vancouver, Canada, (1986)